THE STUDY OF NUCLEAR REACTIONS

AT INTERMEDIATE ENERGY

THE STUDY OF NUCLEAR REACTIONS AT INTERMEDIATE ENERGY

by

Alan Capel Shotter

of

Linacre College

Oxford

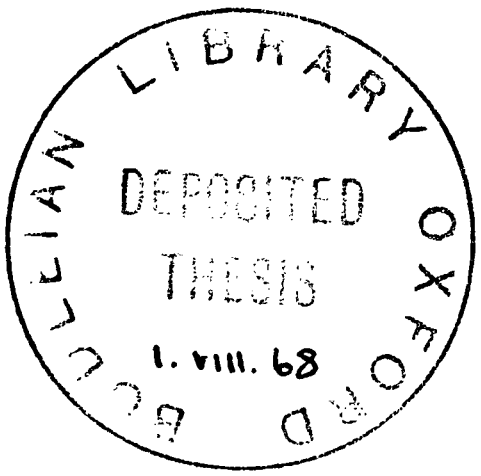

-o-o-o-o-o-o-o-o-o-

A thesis presented in the University of Oxford for the degree of Doctor of Philosophy

April 1968

-o-o-o-o-o-o-o-o-o-

TO MY MOTHER

AND THE MEMORY

OF MY FATHER

C O N T E N T S

FIGURES

The figures relevant to a particular chapter will be found at the end of that chapter; each chapter has its individual sequence of page numbers which will enable immediate location of figures. Alternatively, the position of any figure in the general sequence of pagination may be found by reference to the following table.

A B S T R A C T

Angular distributions were determined for inelastic proton scattering to ten residual states in Si^{28}. Measurements were carried out at 100 KeV steps in the incident energy range of 12 to 15 MeV. Since the purpose of the experiment was to search for intermediate structure in the inelastic reaction excitation functions, all determinations were made with a beam energy resolution of 100 KeV. The Van de Graaff accelerators of the University of Oxford were used for the experiment. The analysis of the 1000 proton spectra recorded in the course of the experiment was performed entirely by computers.

It was found that the angular distributions change rapidly with incident proton energy, and that the reaction excitation functions exhibit structure of the intermediate type. Cross-correlation analysis revealed that there is significant correlation between the structures associated with the different reaction excitation functions.

The experimental data were compared with the predictions of the doorway state theory of intermediate structure. It was found that both the characteristics of the

intermediate structure in the excitation functions and the existence of correlation between the structures of the different excitation functions are in accord with the predictions of this theory.

The experimental results were also considered in relation to the statistical theory of nuclear reactions. It was found that the experimental values of the mean squared deviation of the cross-sections associated with particular inelastic reactions were in reasonable agreement with the values calculated on the basis of this theory. In the experimental situation studied it was found that this theory also offers some explanation for the existence of correlation between the structures associated with the different excitation functions.

It was concluded that both the doorway state theory and statistical theory provide possible interpretations of the observed intermediate structure.

ACKNOWLEDGEMENTS

There are particular people without whose help and advice I could never have written this thesis; to these people I extend my sincere gratitude: to Professor D.H. Wilkinson, F.R.S., and Professor K.W. Allen, for extending to me the facilities of the Oxford University Nuclear Physics Laboratory; to my supervisor, Dr. P.S. Fisher, for his constant help and encouragement over the last three years; to Mr. H.R. Hyder, and the technical staff, for their willing support; to Mr. J. Takacs, for his advice on the design of beam energy modulation system; to Dr. D. Brink, for his kindness in discussing certain topics in connection with the statistical theory of nuclear reactions; to Dr. D.K. Scott, for his extreme willingness to help me in many different aspects of my research; to Dr. N.S. Chant, who could always be relied upon to give valuable advice on matters of computerisation; to Mr. R. Bastany, whose cheerfulness did not fail even in the face of the most laborious tasks; to Mr. L.G. Waine, who patiently trained me in the art of workshop practice; to Mr. J.M. Nelson, Dr. D.J. Skyrme, Mrs. P. Jones and Mr. J.M. Domingos, who

kindly assisted in running the experiments; to Mrs. E. Browne, for her time and care in typing this thesis. I would also like to extend my thanks to the Science Research Council for financial assistance during my three years of research. Finally, I owe a debt of gratitude to my parents who, throughout my education, have given me constant encouragement and support.

Oxford, April 1968.

C H A P T E R 1

INTRODUCTION

1.1 Early Developments in Nuclear Reaction Theory

Harkins and Gans (1934), following the work of Mott and Massey in their study of electron scattering, proposed a similar model for nucleon scattering from nuclei. However, experiments performed shortly after showed complete disagreement with this model (Tillman and Moon, 1935; Szilard, 1935; Fermi and Amaldi, 1935; Frisch et al., 1936; Halban and Preiswerk, 1936; Dunning, 1935); instead of the predicted slow energy variation of cross-section, rapid variations in the form of narrow resonances were observed. To understand these observations, Bohr (1936, 1937) proposed that the nucleon-nucleon interaction was not weak, as Harkins had assumed, but instead was strong enough for the energy of the incident nucleon to be quickly distributed amongst the target nucleons; since many degrees of freedom were involved, rapid energy variations of cross-sections were to be expected. This model, which became known as the compound nucleus model, was further considered by Breit (1936) and

found its mathematical expression in the work of several authors (Kapur and Peierls, 1938; Wigner, 1946; Wigner and Eisenbud, 1947). The model was extended by Feshbach et al. (1947, 1949) to the high energy regions where the number of resonances becomes so great that strong overlapping occurs between them; for this reason it was only possible to consider the energy variations of averaged cross-sections; the model became known as the continuum model. This model gave reasonable agreement with observations in the energy region 12 to 24 MeV; however, when applied to 90 MeV scattering experiments (Cook and Macmillan, 1949) a difficulty arose in that it predicted nuclear radii smaller than those calculated from the intermediate energy experiments. Further indications of the inadequateness of the continuum theory became obvious when scattering experiments (Fields, 1947; Miller et al., 1952) were performed in the energy region 1 to 3 MeV; instead of the predicted monotonic decrease of cross-section with energy, broad variations were observed. To explain these observations it was proposed (Weisskopf, 1952; Feshbach et al., 1953) that the nucleon-nucleon interaction was not so strong as originally thought, but instead somewhere intermediate between this and a weak non-local potential. Following an optical analogy, Fernbach et al., (1949)

and Feshbach et al., (1954) considered and developed a model in which the incident particle and target nucleus interacted through a complex non-local potential; it was shown that this model was in reasonable agreement with the experimental observations in the energy region 1 to 3 MeV. This model, although somewhat controversial, was in keeping with the spirit of the shell model of Mayer (1949, 1950) and Haxel et al., (1949, 1950).

Further evidence, that the incident particle did not necessarily share its energy amongst all the target nucleons, came to light when Butler (1951) found it was possible to explain the forward angle peaking in (d,n) reactions by the assumption that the incident particle interacted only with a few nucleons in the nuclear surface; similar conclusions were arrived at by McManus and Sharp (1952) and Austern et al., (1953) studying (p,n) and (p,p) reactions. Reactions of this type became known as direct reactions.

That the strong interaction and complex potential models were interrelated rather than contradictory was demonstrated by the work of Feshbach et al., (1953), with later extension by Wigner (1954), Scott (1954) and Lane et al., (1955). The interaction was considered to be composed of two parts: an average non-local potential, producing a

smooth variation of the cross-sections, and a residual interaction which caused sharp variations in the cross-sections by exciting the internal degrees of freedom of the target nucleus. Further understanding of the nucleon interaction in nuclear matter came from the work of Brueckner et al., (1954[a], 1954[b], 1955[a], 1960); these authors demonstrated that even though the nucleon-nucleon interaction was strong, a bound nucleon in a nucleus had similar properties to a free particle owing to the severe restrictions imposed on internal scattering by the Pauli exclusion principle. The work was further extended (Brueckner et al., 1955[b]) to the case of an unbound nucleon in nuclear matter and again the similarity to a free particle was demonstrated.

1.2 The Sequential Development of a Nuclear Reaction

Using a similar approach to that of Brueckner, Shaw (1959) attempted to determine the imaginary part of the scattering complex potential by calculating the probability that the incident nucleon suffered a hard collision (i.e., a collision in which energy is exchanged). He further considered the next stage to the reaction, to which there were three alternatives: (a) one or both collision particles

could escape from the nuclear interior, (b) the system could decay back to the entrance channel and (c) one or both collision particles could undergo further hard collisions. In the spirit of these calculations, which assumed for example that nuclear matter could be represented by an ideal Fermi gas, the author was able to predict the relative probabilities for these different alternatives. The first two mechanisms are closely similar to the direct reaction mechanism considered by Butler et al., while the last provides the possibility of forming more complicated states and ultimately the compound nucleus. It was still possible, of course, for the incident particle to travel through the nucleus without suffering a hard collision. Similar arguments about the sequential development of a nuclear reaction have been given in more pictorial terms by Weisskopf (1961).

The gross variation of cross-sections at low energies, 1 to 3 MeV, were explained (Feshbach et al., 1949; Feshbach et al., 1954) in terms of the optical model as being due to the incident particle resonating in the complex potential, and so Shaw has questioned whether or not smaller variations would result from a similar resonance of the reaction

particles created in the second reaction stage. (For a Fermi gas these particles are the incident and struck particles, and the hole left behind in the gas; this assemblage of particles is hereafter referred to as a 2p-1h state.) These ideas were further developed by Rodberg (1961) who observed that variations in cross-sections could also occur as a result of an interference of the 2p-1h states with the direct wave amplitude. A similar situation, in atomic physics, has been studied by Fano (1961) with the conclusions that the interference between a discrete state, in which no one particle has sufficient energy to escape, and the continuum states gives rise to characteristic asymmetrical peaks in the cross-section excitation functions, and that the ratio k of the actual transition probability to the probability of transition to the unperturbed continuum (i.e., absence of the discrete state) can be represented by

$$k = (q + e)^2 / (1 + e^2) \qquad (1.1)$$

where: q = coupling constant between the discrete and the continuum; $e = 2(E - E_D)/\Gamma$, in which E_D = energy of the discrete state and Γ is the escape width.

For large values of ℓ, this function varies rapidly in the energy region $E \approx \epsilon_\ell$. The mathematical structure for the nuclear situation is quite similar to this atomic case, since for both the interaction of the incident particle with the target is considered to be composed of an average non-local potential and a residual interaction. In general it would be expected that the second stage in the development of a nuclear reaction would produce the greatest interference with the direct reaction amplitude, since the later stages, being more complex in configuration, would have smaller coupling constants q.

1.3 The Strength Function and the First Reaction Collision

It was well known that the average variation of the low energy strength function for different elements originated from the interaction of the incident particle with the nuclear complex potential, and so it was suggested by Block (1963) that the fluctuation of the strength function about the average resulted from the next reaction stage 2p-1h interacting with the complex potential; pursuing these ideas he derived the following expression for the S wave neutron strength function

$$\langle \Gamma_{\downarrow} \rangle = 2\pi \sum_n (D_n/\Delta_n) |\langle \psi_n | V_n | \chi^+ \rangle|^2 \qquad (1.2)$$

where: χ^+ = incident channel wave function; ψ_n = wave function of a 2p-1h state of energy width Δ_n; D_n = average energy spacing of the compound states which can be created through the state ψ_n; V_n = residual interaction.

This formula can be understood by an argument put forward by Weisskopf. The number $|\langle \psi_n | V_n | \chi^+ \rangle|^2$ may be interpreted as the transition probability of the 2p-1h state decaying back to the 1p state χ^+, and therefore the average width of a compound state is expected to equal this probability multiplied by a factor which determines the probability that the 2p-1h state is realised in the compound state. Suppose there is only one state ψ_n within an energy interval of order Δ_n, then in this case only one term need be considered in the summation, and therefore the period of motion of the compound state (Breit, 1959) becomes $\hbar/D_n$; since the lifetime of the 2p-1h configuration is $\hbar/\Delta_n$ the relative probability of ψ_n in the compound state must be about D_n/Δ_n.
Inherent in this argument is the assumption that decay and formation of the compound states can only occur via the

2p-1h states; this is true if V_n is composed of two-particle interactions (Feshbach, 1958, 1962) which seems in fact to be the case in view of the success of energy level calculations using this interaction (Goldhammer, 1963). Successive applications of this two body operator to the wave function of the entrance channel will produce more and more complicated configurations (i.e., 2p-1h, 3p-2h, 4p-3h and so on) until finally the compound nucleus is formed. It is therefore because the 2p-1h state forms the entrance to this "alleyway" that it has been termed the "doorway state".

Using similar arguments, Shakin (1963) made a more detailed evaluation of the strength functions for the isotopes of lead and tin, and obtained reasonable agreement with experiment. His most important finding from this work was the appreciation that a small energy width associated with a cross-section resonance did not necessarily imply the formation of a complicated compound state, because he found that it was possible for the matrix elements determining the transition 1p to 2p-1h to vanish under certain circumstances, with the result that the width of the formation of a compound state was small, being determined only by higher order effects.

1.4 The Doorway State and Light Nuclei

Lemmer and Shakin (1964) studied the elastic scattering of neutrons from N^{15} by a method similar to that used in Shakin's earlier calculations, and they were able to obtain good agreement with experiment by assuming the compound state was no more complicated than the doorway state. The target was considered as a $p^{\frac{1}{2}}$ hole relative to the C^{16} core, and the compound states as particle-hole configurations. The calculation included energies up to 10 MeV and gave resonance widths from 0.6 KeV to 800 KeV. Similar calculations have been carried out for the reactions $C^{12}(n,n)C^{12}$ and $C^{13}(p,p')C^{13}$ (Lovas, 1966; Pfitner and Riedel, 1964). In the first of these calculations the author assumed the compound states were again no more complicated than the 2p-1h configurations; the second calculation was restricted to low enough energies to be able to assume the compound states were formed only by excitation of the neutron outside the C^{12} core, and therefore, in diagrammatic form, the reaction possibilities are :

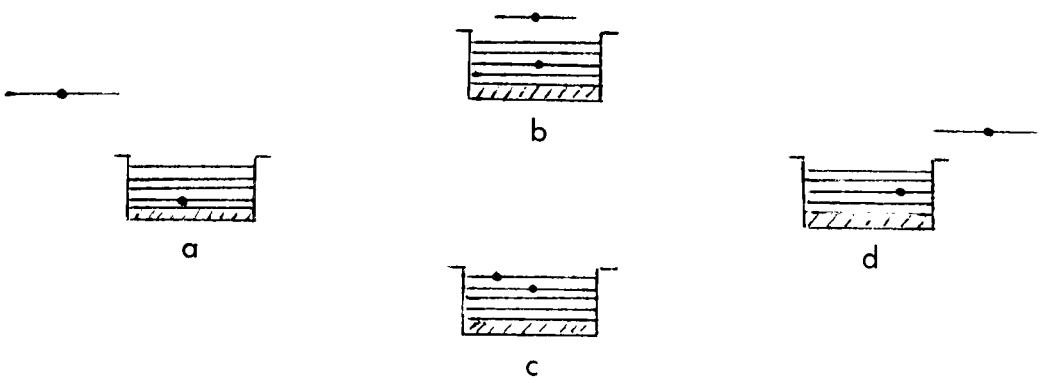

If the reaction followed the sequence a to c to d, then it would go through an intermediate or discrete state, and so, as first noted by Rodberg (1961), strong energy variations would be expected; if the reaction proceeded a to b to d, the cross-section variations would not be so strong, since the intermediate system would be unbound and therefore of short lifetime. It has also been possible to understand particular reaction cross-sections in $C^{12}(p,p')C^{12*}$, by assuming again the compound states are no more complicated than 2p-1h configurations (Meadsay et al., 1963; Kimmer and Fisher, 1964; Scott et al., 1967).

1.5 The Doorway State and Intermediate Structure

It has been generally concluded from the above work that the reaction mechanism for low energy particles bombarding light nuclei is particularly simple, involving no more than one or two particles. It has been possible to attempt precise calculations in these cases because the number of degrees of freedom is low; however, at higher energies or with heavier nuclei, the number rapidly increases, and for this reason it is no longer possible to attempt an exact calculation. A similar computational difficulty arises

in the calculation of bound energy levels with a realistic interaction; at low energies only a few outer shell parameters are involved, but at higher energies account must be taken of excitations from the inner shells; the greater number of permutations of the particles reflects in an exponential increase in the number of states. So even though simple excitations can explain reaction mechanisms at low energies, it is doubtful whether such simplicity exists at higher energies; indeed, because of the greater number of particles involved, it becomes more profitable to employ a statistical approach.

Early experiments performed in the intermediate energy range 10 to 20 MeV, and for intermediate nuclei A from 20 to 50, revealed the existence of rapid changes in reaction cross-sections over energy intervals of several hundred keV (Fischer et al., 1958; Bogata, 1959; Kawabe, 1959; Cohen et al., 1960; Goodman and Ball, 1960; Gupta et al., 1960; Kimura et al., 1961). It was observed by Izumo (1961) that such behaviour could not be explained in terms of the potential or compound nucleus model since the former only gave variations over several MeV, while the latter predicted resonances with widths of an order of magnitude

smaller than the observed structure. It was concluded that the observed variations were the effects caused by only a partial equilibrium of the reaction particles. Izumo was able to systematise the observations to some degree by using a phenomenological approach; this considered the target nucleus to be an inert core which provided a central potential for the incident particle and outer shell nucleons. This few-nucleon system had its own set of eigenstates, and if the incident energy were sufficient to excite a particular state the effects would be reflected in the cross-section. The width of the experimental cross-section variations can be understood from this model since the energy per particle is in general greater than for a particle in the true compound nucleus, and so the penetrabilities are therefore greater and the lifetime shorter. When the model was applied to different experiments, it was generally found that about six particles were involved in the reactions.

Recent experiments, using good energy resolution beams, (Colli, 1962[a], 1962[b]; Facchini, 1962) have demonstrated the existence of a narrower type of cross-section fluctuation. This structure has been interpreted by Ericson (1963, 1966) as resulting from an interference between neighbouring

compound nucleus levels; the structure is not to be identified with individual levels, but rather is to be considered as the result of an aggregation of many random quantities; the average fluctuation width can be associated with the average lifetime of the compound states. In many cases when the fluctuation cross-sections are mathematically averaged over several hundred keV, considerable residual structure still remains in the cross-sections (Lévi et al., 1966; Singh et al., 1966[b]; Kroepfl, 1967; Mehta and Divatia, 1967); this structure is similar to that considered by Izumo. Since this structure is intermediate between that expected for the complex potential and that for the compound nucleus model it has been termed intermediate structure. The partial equilibrium model of Izumo, because of its phenomenological nature, cannot give a detailed account of this structure; on the other hand, computational difficulties prevent a solution similar to the type used for light nuclei. Nevertheless, it still remains true that if the residual interaction is composed of two body forces, then the initial process in the reaction is the generation of a 2p-1h configuration. It has been known for some time that if the compound nucleus resonances are averaged over

several MeV, the average cross-section exhibits similar features to a particle scattering from a potential well. This, of course, is why a potential model is used at all, but also it shows that the interaction of the incident particle with the target is composed of an average potential plus a residual interaction, and this interaction is not sufficiently strong to smear out the cross-section resonances caused by the particle resonating in the average potential (Breit, 1959); stated in another way, the wave functions of the compound nucleus states still retain a small coherent component of the incident single partial wave function. So if the second reaction stage is a 2p-1h state, it is possible that the compound states to which this initial configuration decays, retain in a similar way the characteristics of the 2p-1h state; if this is so, then the cross-section would be expected to exhibit structure intermediate between the single particle giant resonances and fluctuations due to the compound nucleus. This explanation of the cause of intermediate structure has been proposed by Feshbach (1965[b], 1967[b]). A brief outline of this theory is given in the next section. Following this, another possible cause of intermediate structure is considered.

1.6 The Doorway State Theory of Intermediate Structure

(a) Projection operators in reaction theory

The wave function of a reaction, composed of an incident particle r_0 and a target nucleus with nucleons r_1, r_2 ..... r_N, may be expanded in the form

$$\Psi = \sum u(r_0)\, \phi(r_1, r_2 \ldots\ldots r_N). \qquad (1.3)$$

The sum is over all possible configurations of the target nucleons, and separates naturally into two component sums depending on whether $u(r_0)$ belongs to a bound or unbound particle. Feshbach (1958, 1962) has introduced projection operators P and Q to separate these two sums. $P\Psi$ and $Q\Psi$ are vectors in the unbound and bound subspaces of reaction space. Since all experimental measurable quantities are contained in $P\Psi$, the aim of the projection method is to obtain a Hamiltonian with $P\Psi$ as argument. If the total Hamiltonian is H, then

$$H(P + Q)\Psi = (P + Q)\Psi \quad . \qquad (1.4)$$

Operating on this equation separately by P and Q yields the equations

$$(H_{PP} - E)P\Psi = - H_{PQ} Q\Psi \qquad (1.5)$$

$$(H_{QQ} - E)Q\Psi = - H_{QP} P\Psi \qquad (1.6)$$

where: PHP is denoted by H_{PP} etc.

If these two equations are solved by the inverse operator method (Feshbach, 1965), the equation for $P\Psi$ becomes

$$(H_{PP} - E)P\Psi = \left[H_{PQ} \frac{1}{(H_{QQ} - E)} H_{QP} \right] P\Psi . \qquad (1.7)$$

The transition amplitude for the reaction can then be written as (Feshbach, 1966)

$$T = T_1 + \langle \psi_o^- | H_{PQ} \frac{1}{(E - H_{QQ} - W_{QQ})} H_{QP} | \psi_o^+ \rangle \qquad (1.8)$$

where: $\psi_o^{\pm}$ are solutions of the equation $(H_{PP}-E)\phi = 0$, and T_1 is the transition amplitude of this equation; and $W_{QQ} = H_{QP} \frac{1}{(E^+ - H_{PP})} H_{PQ}$.

From Eq. (1.8) it is evident that T may undergo strong variations when the incident energy is near an eigenvalue

of H_{QQ}.

(b) Projection operators and doorway states

To determine the effect of the first collision on the transition amplitude further projection operators are introduced; these are d and q, defined by

$$\Psi = 1\Psi + d\Psi + q\Psi \qquad (1.9)$$

and $Pd = dP = 0$; $Pq = qP = 0$; $dq = qd = 0$.

The projection operator d projects Ψ onto the 2p-1h states in space Q, and q projects onto the remaining more complicated states. If H_{pq} only consists of two body interactions then $H_{pq} = 0$, but $H_{pd} \neq 0$. The Hamiltonian H_{QQ} may be decomposed in the following way

$$H_{QQ} = H_{dd} + H_{qq} + H_{qd} + H_{dq}. \qquad (1.10)$$

H_{qd} provides the coupling between the doorway and more complicated states. The transition amplitude for elastic scattering may be decomposed in a similar way

$$T = T_1 + T_d + T_q \qquad (1.11)$$

where : $$T_d = \langle \psi_o^- | H_{Pd} \frac{1}{(E-H_{dd}-W_{dd})} H_{dP} | \psi_o^+ \rangle$$

$$T_q = \langle \psi_o^- | H_{Pd} OH_{dq} \frac{1}{(E-H_{qq}-H_{qd}OH_{dq})} H_{qd} OH_{dp} | \psi_o^+ \rangle$$

and $$0 \equiv \frac{1}{(E - H_{dd} - W_{dd})} .$$

In these equations T_d represents the transition amplitude for the formation and decay of the doorway states, while T_q corresponds to formation and decay of the complicated states via the doorway. Since the density of levels belonging to q is greater than d, T will have three types of energy variation: a slow variation T_1 due to the incident particle resonating in the potential well, a more rapid variation T_d due to the formation of 2p-1h configurations, and finally a strongly fluctuating component T_q due to the formation of the more complicated states.

The effects of the first collision are more easily seen if T is averaged over an energy interval which is large compared to the fluctuating component, but small enough to regard T_d as constant. If this is done it is

found that the average $[T_q]$ has a similar energy variation to T_d, the main reason being that the complicated states can only be formed via the doorway state. Since these two terms have similar structure they are combined into one; the average transition amplitude then becomes

$$[T_J] = T_1 + \left\langle \psi_o^- \middle| H_{Pd} \frac{1}{E - H_{dd} - W_{dd} - H_{dq} \frac{1}{(A_{qq}^{-1} + W_{qq})} H_{qd}} H_{dP} \middle| \psi_o^+ \right\rangle \tag{1.12}$$

where: $$A_{qq}^{-1} = \frac{1}{(E + h_{qq} - W_{qq})} .$$

From Eq. (1.12) it will be seen that the second term is identical to T_d if W_{dd} is replaced by $W_{dd} + \bar{T}_{dd}$, where

$$\bar{T}_{dd} = H_{dq} \frac{1}{(A_{qq}^{-1} + W_{qq})} H_{qd}. \tag{1.13}$$

The physical meaning of this term is not too difficult to understand, because the width associated with T_d alone only takes account of the doorway state decaying back into the entrance channel, but the combination of $[T_q]$ with T_d

has introduced, into T_d, the possibility of the doorway state decaying to the more complicated states.

For an energy region influenced by only one doorway state, Eq. (1.12) becomes quite simple, since for this case $\bar{W}_{dd}$ and W_{dd} are both diagonal, and so

$$[T] = T_1 + \frac{\langle \Psi_o^- | H_{Pd} | \Psi_d \rangle \langle \Psi_d | H_{dP} | \Psi_o^+ \rangle}{(E - E_d - \Delta_d^{\uparrow} + \frac{i}{2} \Gamma_d^{\downarrow} + \frac{i}{2} \Gamma_d^{\uparrow} - \Delta_d^{\downarrow})} \tag{1.14}$$

where: $W_{dd} = \Delta_d^{\uparrow} - \frac{i}{2} \Gamma_d^{\uparrow}$ (escape to 1p states)

$\bar{W}_{dd} = \Delta_d^{\downarrow} - \frac{i}{2} \Gamma_d^{\downarrow}$ (decay to 3p-2h etc.)

and $\Gamma_d^{\downarrow} = \frac{2\pi}{\Delta E} \sum_q | \langle \phi_q | H_{qd} | \Psi_d \rangle |^2$

where the sum is over q states within the average interval ΔE.

From Eq. (1.14) it is evident that if the incident energy is in the proximity of the 2p-1h state, then the intermediate average transition amplitude will be in a state of resonance. Under these circumstances the average absorption cross-section for $\ell = 0$ and zero channel spin,

becomes

$$\sigma_A = \frac{\pi}{k^2} \frac{\Gamma_d^{\uparrow} \Gamma_d^{\downarrow}}{(E - E_d)^2 + \frac{1}{4}(\Gamma_d^{\uparrow} + \Gamma_d^{\downarrow})^2} . \qquad (1.15)$$

The strength function, being simply related to σ_A, will exhibit similar structure.

For simplicity the above equations have been restricted to elastic scattering; however, reactions are easily included in the formalism by respectively replacing ψ_o^+, ψ_o^- by ψ_f^+, ψ_i^-, where these are the inelastic wave functions satisfying the equation

$$(H_{pp} - E) \psi_f^+ = 0.$$

By following the same procedures, and again assuming one doorway, the intermediate averaged inelastic transition matrix becomes

$$[T_{fi}] = (T_{pot})_{fi} + \frac{\langle \psi_f^- | H_{Pd} | \psi_d \rangle \langle \psi_d | H_{Pd} | \psi_i^+ \rangle}{(E - E_d - \Delta_d^{\uparrow} - \Delta_d^{\downarrow} + \frac{i}{2}(\Gamma_d^{\uparrow} + \Gamma_d^{\downarrow}))} \qquad (1.16)$$

where: $(T_{pot})_{fi}$ includes the direct reaction and

potential scattering amplitudes; the escape width $\Gamma_d^{\uparrow}$ is given by

$$\Gamma_d^{\uparrow} = 2\pi \sum_f |\langle \psi_d | H_{dP} | \psi_f^+ \rangle|^2 . \qquad (1.17)$$

The sum is over all possible open channels, including the elastic, to which the doorway state ψ_d can decay.

(c) Experimental predictions from the theory

The result shown in Eq. (1.16) is of paramount importance, for it shows that if the assumptions about the sequential development of a nuclear reaction are correct, then similar intermediate structure would be expected to occur in different reaction channels. There are three reservations to this statement: firstly, the width of the structure $\Gamma_d^{\uparrow} + \Gamma_d^{\downarrow}$ must be sufficiently small for the resonance to be observable above the direct component $(T_{pot})_{fi}$; secondly, the resonance position $E_d + \Delta_d^{\uparrow} + \Delta_d^{\downarrow}$ may differ slightly from channel to channel since $\Delta_d^{\uparrow}$ depends upon ψ_f^-; and lastly, it is the resonance positions which are correlated not the amplitudes, therefore a particular resonance need not necessarily be present in

all reaction channels. Another general result from Eq. (1.16) is that differential cross-sections for particular reaction channels, measured at different angles, should exhibit similar structure.

1.7 Intermediate Structure and the Statistical Theory

There is much evidence that the statistical theory of nuclear reactions (e.g., Allan, 1961; Erba et al., 1961) is in reasonable agreement with experimental data with regard to orders of magnitude and average energy dependence of cross-sections. Therefore it has been suggested (Egelstaff, 1956; Ericson, 1960; Agodi et al., 1962) that the statistical theory should also be capable of explaining the fluctuations of a cross-section about its average.

It has been demonstrated by Blumberg and Porter (1958) that if the matrix elements of the Hamiltonian operator, which defines the eigenstates of the compound nucleus, follow normal distributions, then the distribution of level widths and level spacings are those proposed by Porter and Thomas (1956) and Wigner (1956) respectively. The fact that these distributions are supported by experimental

evidence has been taken to indicate the validity of the randomness hypothesis (Feshbach, 1960). From these distributions it should be possible to determine the associated cross-section fluctuations.

In the light of the above, analyses of cross-section fluctuations have been carried out by several authors; in particular Tsukada and Tanaka (1963) and Monahan and Alwyn (1967) investigated fluctuations of total neutron cross-sections on the assumption that the cause of the fluctuations was variation of widths and level spacings; Agodi and Pappalardo (1963) considered similar cross-sections but assumed that the fluctuations arose purely from level spacing variations. Ericson (1963) has shown that, at high energies, where the density of levels is high, strong fluctuations can occur in cross-sections even when the fluctuations caused by level-parameter variations are negligible. The fluctuations in such cases are caused by interference between the amplitudes associated with the resonances of the compound nucleus.

If cross-sections are averaged over a sufficiently large energy interval the associated fluctuations will ultimately disappear, but for a smaller energy interval some residual structure will remain. This therefore presents

an interesting question: can the recently observed intermediate structure be explained in terms of this residual statistical fluctuation? This question forms the subject of Chapter 5 of this thesis.

1.8 Recent Experimental Examples of Intermediate Structure

Other than the examples considered in the first part of this chapter, further experimental evidence of intermediate structure and doorway states has come from several different types of experiment. A brief outline of some of these experiments is given below.

Analogue States

Analogue resonances probably provide the clearest examples of intermediate structure. Since their discovery in 1964 (Fox et al., 1964) several hundred cases have been found. The most noticeable characteristic of these resonances is that they have very small widths, the accepted reason being that the doorway state is inhibited from decaying to the more complicated configurations because its isotopic spin differs from that of its immediate neighbouring states.

Thermal Neutron Capture

Ikegami and Emery (1964) observed that there exists an anticorrelation between the yields of (n,γ) and (d,p) reactions, and that this could be explained in terms of the doorway state concept.

Neutron Evaporation Spectra

Energy studies (Wood et al., 1965) of evaporated neutrons from (p,n) reactions often reveal a high energy "tail" in the neutron spectrum which is unexplainable in terms of the classical statistical theory (Weisskopf, 1937). Griffin (1966) sees the reaction as a successive creation of particle-hole states, and the "tail" as the result of an emission of neutrons before the establishment of equilibrium amongst the nucleons.

Distribution of Level Strengths in (d,p) Reactions

Bolsterli et al., (1966), considering $Ca^{40}(d,p)Ca^{41}$, have studied the proton groups which are produced by mechanisms other than stripping. It was discovered that there exists a coherence of reaction strength between these proton groups over a period of 100 KeV, this was interpreted

as the result of 2p-1h states sharing their strength between the states of higher seniority.

Phase Shift Analysis

Recently Singh et al., (1966[b]) carried out a phase shift analysis for the reaction $Mg^{26}(\alpha,\alpha)Mg^{26}$. They found that the scattering amplitude varied in a systematic way over periods of several hundred KeV, and this they have interpreted in terms of the doorway state concept. (The behaviour of the scattering amplitude in the proximity of a doorway state resonance has been discussed by Monahan, 1966.)

Photo Capture in Light Nuclei

If the giant resonance of a (p,γ) reaction is experimentally studied with good energy resolution, it is found that the resonance is composed of a fine structure of a type proposed by Ericson (1963). When the cross-sections are averaged, the fluctuations decrease in amplitude, but a broader, intermediate structure is sometimes evident (Singh et al., 1965). This structure has been interpreted in terms of the doorway state concept (Gillet et al., 1967).

1.9 Statement of Thesis Problem

Many experimental examples of intermediate structure have been taken to imply the existence of doorway states; however, few experiments have been undertaken to test the main predictions of the doorway state theory. These predictions are (Section 1.6.e):

1. Excitation functions corresponding to different reaction channels should exhibit structure of width intermediate between the widths of compound nucleus fluctuations and single particle resonances.

2. There should be some correlation between the intermediate structures belonging to different reaction channels.

3. For a particular reaction channel, the differential cross-section excitation functions should exhibit intermediate structure; there should also be some correlation between the intermediate structures associated with excitation functions measured at different scattering angles.

It is the purpose of this thesis to test these predictions, for a particular nucleus, by measuring the

excitation functions of inelastically scattered protons for as many reaction channels as possible; further, to determine the significance of any conclusions which may be drawn from these tests, an attempt is made to interpret the experimental results by means of the theory based on the hypothesis that the reaction mechanism is of a statistical nature.

The nucleus chosen for this work was Si^{28}. The reasons for this choice were that Si^{28} belongs to a mass region in which the total neutron cross-sections of nuclei, in the incident energy range of 4 to 12 MeV, undergo considerable fluctuations (Tsukada and Tanaka, 1963; Carlson and Barschall, 1965; Fasoli et al., 1966), and, of this mass region, Si^{28} is unique in having a doubly closed subshell, which therefore may be expected to simplify calculations of the second reaction stage. The reaction was investigated in the incident proton energy range of 12 to 15 MeV, since in this range, the compound nucleus excitation energy is within those values corresponding to incident neutron energies of 4 to 12 MeV.

Since the purpose of the experiment was to search for intermediate structure, it was decided, in order to reduce the amount of data analysis, to determine the cross-section

excitation functions by measuring the reaction angular distributions at energy intervals of 100 KeV and with a beam energy resolution of 100 KeV.

C H A P T E R 2

EXPERIMENTAL METHODS

2.1 Introduction

The University of Oxford Van de Graaff accelerators were used as the source of high energy protons for this experiment.

Since the intrinsic resolution of these machines is a few KeV it was necessary to devise a convenient method of obtaining cross-section averages over 100 KeV. The most obvious way of doing this is to use a thick target; however, this suffers from the disadvantage that the scattered particles entering the detection system also have an energy spread of 100 KeV. A spread of this amount becomes a serious concern if states in Si^{28} above an excitation energy of 6 MeV are to be resolved; the situation is even more serious if contaminants are present in the target. Because of this disadvantage another method was used in which the current of the final analysing magnet was modulated in such a way that the energy stabilisation loop of the accelerator in turn modulated the acceleration voltage, and consequently

the energy of the accelerated particles. This energy spread of the incident beam produced, to a first order of approximation, a similar energy spread for all the scattered particles from the target. To compensate for this spread a small variable voltage, synchronized to the energy of the accelerator, was subtracted from the analogue pulses, corresponding to the reaction particles, so that the resultant pulses remained constant.

2.2 The Accelerator

The Oxford accelerator complex consists of two electrostatic generators (Rutherford Lab., 1962, 1966), a single stage and tandem Van de Graaff (Fig. 2.1). Each machine may be used separately or coupled together in such a way that the single stage accelerator acts as an injector into the tandem. The injector can accelerate several microamps of negative ions up to an energy of 10 MeV; the transmission of this beam through the tandem is about 30 per cent. Since the centre terminal of the tandem operates up to 6 million volts, the combined machines can produce proton beams of energies up to 22 MeV. With coupled operation the proton beam has an energy resolution of several keV

which is principally determined by the voltage ripple of the accelerator voltage terminals, and the finite widths of the analysing slits before and after the bending magnets. Energy stabilisation of the accelerator is achieved by comparing the amount of beam current striking the two sides of a vertical slit placed after the final analysing magnet. If, due to an energy change, the beam passes asymmetrically through this slit, the net pick-up current is used, after suitable amplification, to operate a servomechanism which restores the beam energy.

2.3 The Experimental Beam Line

The layout of the experimental beam line is shown in Fig. 2.2. The beam control system of the accelerator is designed to produce a horizontal focus at the position of a vertical slit a distance of 2R from the centre of the analysing magnet, where R is its radius of curvature. The beam emerges from the magnet to again form a horizontal focus at a second slit which acts both as an analyser and a probe for the energy stabilisation system. The beam is finally focused onto the target by a doublet magnetic quadrupole focusing in the horizontal and vertical planes.

Magnetic deflectors are incorporated in the line to facilitate steerage of the beam. Viewing boxes, containing retractable quartz scintillators, were installed before and after the scattering chamber. These scintillators were of great value in helping to align the beam at the start of an experiment.

The beam, after passing through the scattering chamber, was stopped on a small block of uranium three metres from the target. The beam pipe over the last two metres was electrically isolated so that it could be used as a Faraday cup.

2.4 The Scattering Chamber

A schematic diagram of the scattering chamber is shown in Fig. 2.3. The chamber is totally constructed of duralumin; it has a diameter of 24" and a depth of 8"; the beam entrance and exit ports are welded into place. The design incorporated a rotating base plate, sealed against external pressure, in order that the counter angles could be changed without breaking the vacuum (Fig. 2.4). A well, secured to this plate, enabled introduction of electrical leads and liquid nitrogen pipes into the chamber. In this way,

everything associated with the counters remained static relative to the rotating base plate - an important consideration when many counters are to be used. Six targets could be mounted on a frame supported by a steel rod which passed through a vertical O-ringed shaft; in this way a change of target position was possible without breaking the vacuum. The chamber was rigidly secured to a table, which, once aligned with the help of its four adjustable legs, could be solidly clamped to the floor.

The layout of the counters on the rotating table is shown in Fig. 2.5. Since four counters were used, four positions of the rotating table were required to give an angular distribution of sixteen points. The rotating table was driven by an electrical motor operated from the counting area; the angular position of the table was relayed by closed circuit television.

The design of the counter mounts is shown in Fig. 2.6. The mounts were guided by stainless steel rods pinned accurately along the radii of the rotating table.

2.5 The Chamber Collimator

The purpose of the chamber collimator was to allow

passage of the primary beam but to prevent passage of the scattered protons from the slits associated with the analysing magnet.

The design of the chamber collimator is shown in Fig. 2.7, and a schematic diagram of its working principles is shown in Fig. 2.8. The size of the first aperture was made equal to the expected size of the final focused beam spot. The subsequent apertures reduced the secondary scattering from the first aperture. The collimator was electrically isolated so that the pick-up current from the various apertures could be monitored. With this collimation system it was found possible to record spectra that were reasonably free from spurious background at scattering angles as small as 10^{o}.

2.6 Counters

The choice of detector was mainly influenced by the requirement that it should be capable of stopping a 15 MeV proton. This required a detector with a sensitive thickness of 2 mm. The main types of semiconductor particle detectors belong to the following categories: diffused junction, surface barrier and lithium drifted detectors.

In the case of the first two it is difficult to produce reliable counters of the required thickness; however, it is possible to manufacture lithium drifted detectors with sensitive layers several millimetres thick. The resolution of these lithium drifted counters can be improved if they are cooled.

For these reasons, lithium drifted detectors which could be cooled to liquid nitrogen temperature were used in this experiment.

2.7 The Counter Cooling System

The way in which the counters were cooled is illustrated in Figs. 2.4 and 2.6. The counters were clamped to copper plates which were cooled by contact with a metal pipe conveying liquid nitrogen. The pipe was a continuous piece of copper tubing bent into shape after annealing; to achieve good thermal contact the pipe was hard soldered to the copper cold-plates. External connection to the pipe was made through the vacuum seal shown in Fig. 2.9. This consists of a stainless steel cylinder with thin walls and base, the inlet pipe being hard soldered to the base and further supported by a thermally insulated plug. Linkage with

the pipe inside the chamber was made by means of a copper sleeve. The main consideration in the design of the vacuum seal was to prevent the O-ring from freezing. This can normally be achieved by making the cylinder long and wide, but owing to restricted space this was not possible. An alternative method incorporating a heating element wound on the cylinder was used instead. It was empirically found that a dissipation of ten watts was sufficient to keep the O-rings at room temperature.

Liquid nitrogen was passed through the pipes by connecting the inlet seal to a flask of pressurised liquid nitrogen. Since this seal was connected to the rotating part of the chamber, it was necessary to make connection to the flask by means of a heavily lagged flexible tube; lagging was necessary to prevent atmospheric moisture from icing the surface and so rendering the tube inflexible. Originally air pressure was used to pressurise the flask of nitrogen but this proved unsuccessful because of ice formation at the air inlet. A more successful method was the use of a self-pressurising container; such vessels are manufactured by Unilear (Western Germany) and have an internal pressure of 22 lbs./ sq. in., which for this application was found

sufficient. The flow of nitrogen was adjusted until the liquid phase just emerged from the outlet pipe of the chamber; under these conditions about eight litres of liquid nitrogen were consumed per hour.

Cu-Cd thermal junctions were used to determine the temperature of the counter mounts. It was found that liquid nitrogen temperatures could be attained in 15 to 20 minutes by using a pressure of 15 lbs./ sq. in. to force the nitrogen through the system. To use a time any shorter than this seemed unwise owing to the increased thermal stress and strain in the counters.

In some earlier designs of the cooling system, flexible stainless steel pipes were used to convey the nitrogen inside the chamber. This design had the advantage over the rigid pipe system in that the counter mounts could be moved radially; however, this design feature proved unsuccessful because the flexible pipes became porous after several hours of use at liquid nitrogen temperature.

2.8 Energy Modulation

To modulate the energy of the beam, use was made of the energy stabilisation system of the Tandem accelerator

(Section 2.2). The principle of the method was to modulate the current slowly in the final analysing magnet so as to cause the beam always to pass slightly off-centre through the stabilising slits and so produce a net current pick-up which, in turn, caused the stabilisation system continuously to change the acceleration voltage of the tandem and therefore the energy of the protons.

The generator energising the analysing magnet was controlled by the output signal of a differential amplifier. In this amplifier a comparison was made of the voltage the magnet current developed across a standard resistance, and a reference voltage which was produced by dividing the output voltage V_o of a stabilised supply across precision potentiometers (Fig. 2.10). Changing the value of the potentiometers produced a net output from the amplifier which caused the generator to change the magnet current until a null condition was restored in the amplifier.

To modulate the magnet current a small triangular varying signal was superimposed on the reference voltage. In order to do this, a standard resistance of low impedance and a voltage ramp generator of high impedance were inserted in the reference circuit as illustrated in Fig. 2.10. The circuit of the ramp generator is shown in Fig. 2.11; it is

no more complicated than a transistor emitter follower with a varying base voltage which is produced by periodically driving the spindle of a ten-turn potentiometer.

The response of the magnet current to a sudden increase in reference voltage is shown in Fig. 2.12. Over a period of about 15 seconds the current remains constant, and then changes to its new value with an approximate exponential increase which has a time constant of about five seconds. For a small voltage change saturation effects do not occur, but instead the current immediately starts to rise exponentially to its new value. For a reference voltage modulated by a triangular waveform, the occurrence of a finite time constant results in a distortion of the magnet current modulation waveform; this distortion is mainly a rounding of the turnover points (Fig. 2.13). It is important to ensure this distortion is not too severe, otherwise the accelerator spends more time at the extreme cycle energies and this results in a distortion of the energy resolution function (Fig. 2.14). To gain a better understanding of the effects of the finite time constant, a calculation was carried out to investigate the response of a system with a time constant C to the passage of a triangular signal $V_o(t)$. If the

triangular period is T, then $V_o(t)$ may be expanded in the form

$$V_o(t) = \sum_{n=1}^{\infty} \frac{8}{\pi^2 n^2} \cos(2\pi nt/T) \qquad (2.1)$$

and the response waveform may be expanded as

$$V_f(t) = \sum_{n=1}^{\infty} \frac{8 \cos((2\pi nt/T) + \psi)}{\pi^2 n^2 \sqrt{(1 + (2\pi Cn/T)^2)}} \qquad (2.2)$$

where: $\tan \psi = 2\pi nC/T$.

From this equation it is evident that the square root factor damps the higher order terms - the terms which determine the sharpness of the turnover points. It will also be noted that for small values of C/T and n, $\tan \psi \approx \psi$, and so $\cos((2\pi nt/T) + \psi)$ becomes $\cos(2\pi n(t+C)/T)$; so in this approximation the response waveform is delayed by a time C compared to the initiating signal. The effect of this is considered later (Section 2.10).

From these considerations it would seem that the most favourable situation would occur when the cycle period is made as long as possible. However, owing to the fact that the beam intensity fluctuated, several energy sweeps were

required in order to produce a rectangular-shaped resolution function. Since the time of an experimental run was limited by other circumstances to about 10 minutes, a compromise between these two requirements was met by setting the cycle time to 100 seconds, in which case $\frac{C}{T} = \frac{1}{10}$, and the beam energy was swept twelve times.

2.9 The Energy Compensator

If the energy of the incident beam is modulated so also is the energy of the scattered particles; in this circumstance it is therefore not possible to exploit the full resolution characteristics of the particle counters. This section describes an electronic method which overcomes this disadvantage.

The kinematics of the problem are considered in Appendix 1. The results of these kinematic calculations are displayed in Fig. 2.16. A fraction f is plotted, where f is defined by

$$\Delta E(\theta,Q) = (1 + f(\theta,Q))\Delta E \qquad (2.3)$$

where: ΔE = energy spread of incident beam; $\Delta E(\theta,Q)$ = energy spread of protons scattered into angle θ, from a state of excitation energy Q.

for each counter.

The method used to calibrate the relationship between the amplitude of the bias voltage modulation ΔV_B and the resistance R1 is described in Section 2.11(b) of this chapter. From this calibration the appropriate value of R1 could be determined from the argument that for a proton of energy E, with corresponding analogue voltage V, the voltage variation ΔV_B for 100 KeV energy modulation is given by

$$\Delta V_B = V(1 + f(\epsilon,\omega))/10E. \qquad (2.4)$$

2.10 Control Linkage between the Modulator and Compensator

To retain the intrinsic resolution of the counters the energy modulation and compensation must be in phase. However, as discussed in Section 2.8, the phase of the potentiometer R2 (Fig. 2.11), controlling the energy, is advanced in relation to the energy of the accelerator. It is therefore necessary for R2 to be in advance of the potentiometer controlling the compensator. The method by which this was achieved is illustrated in Fig. 2.16. The two control potentiometers were independently driven by the low geared electric motors M1 and M2; the rotational direction of M2

was controlled by a microswitch S1, which was operated by a cam attached to the motor spindle of M2. The microswitch not only reversed the direction of M2 but also triggered an electronic circuit which reversed, after a pre-set time, the motor M1. A schematic diagram of this delay circuit is shown in the upper half of Fig. 2.18. In the following paragraph a brief description of this circuit is given.

Suppose the states of the relays RL3 and RL4 are as shown in Fig. 2.18, i.e., RL4 is energised by the current from the -30 V supply to the earthed point of S1, and RL3 is de-energised. When S1 is actuated RL4 remains energised but one plate of the condenser C1 is earthed. This condenser begins to charge with a time constant of R1 x C1. When the potential on the base of T1 is high enough, T1 begins to conduct and so energises RL1. The contacts of this relay connect the earth directly to one terminal of RL1, discharge C1 and energise RL3. If RL3 is energised, RL4 and RL1 are de-energised. The result is that after a certain time-lag, determined by the time constant R1 x C1, RL4 is de-energised and RL3 is energised. If the microswitch S1 is again actuated the circuit action is similar to the above, but the result is that RL4 is energised and RL3 de-energised.

The contacts of the relays RL3 and RL4 respectively connect to M1 the electrical power for clockwise and anticlockwise rotation.

The speeds of the electric motors were found to be slightly temperature dependent, and so, in order to keep the relative speeds the same, a variac P4 was inserted in the electrical supply-line of M1. Indication of the position of P1 relative to P2 was provided by the meter M1. It was found necessary to adjust P4 after about twelve hours of continuous running.

2.11 Calibration of the Energy Modulator and Compensator

(a) Energy Modulation. Since the energy of the accelerated particles was modulated by varying the current of the final analysing magnet, the relationship between the magnet's magnetic field and current was required. This calibration was carried out by measuring the magnetic field with a nuclear magnetic resonance probe, and by measuring the current by the voltage V1 it produced when passed through a low impedance standard resistance (Fig. 2.10). The results of this calibration are displayed in Figs. 2.19 and 2.20. It is to be noted that the magnetic hysteresis is quite

small - the variation in current, for a particular field, amounting to no more than 3 per cent. The relationship between the magnetic field and current can be approximately represented by the linear equation

$$V1 = 0.064\ E^{\frac{1}{2}} \pm 3\% \qquad (2.5)$$

From this equation the current variation, in terms of V1, can be determined for a particular energy modulation ΔE.

It will be recalled from Fig. 2.10 that the method used to vary the magnetic current involved modulation of the reference voltage V_R. Since the potentiometer R2, of the δV_R modulation unit (Fig. 2.11), varied between fixed limits, the relationship between R3 and $\Delta V1$ was required. This was determined by using a high impedance digital voltmeter to measure the voltage variation $\Delta V1$ for different settings of R3. This relationship was found to be linear, and when used with Eq. (2.5) gave the relationship between R3 and ΔE as

$$R3 = 9.4\ E^{\frac{1}{2}} / \Delta E. \qquad (2.6)$$

This relation was experimentally verified in the following

way. Inelastic proton spectra were recorded for the two end cycle values of potentiometer P2. By examining these two spectra the shifts in the centroids of corresponding peaks were measured. Then by using the f correction factor of Fig. 2.16, the value of ΔE was deduced from the average shift. The values of ΔE determined by this method were found to be in reasonable agreement with Eq. (2.6).

(b) Compensator. The calibration of the compensator (Section 2.9) involved a determination of the relationship between the bias variation ΔV_B and the resistance R1. To do this, the potentiometer P1 was set at an end cycle position, and analogue pulses generated by a Hg oscillator were passed through the compensator circuit and then analysed by a kicksorter. This was repeated for the other end cycle position of P1. From the difference in the centroids of the two peaks, the change in the bias voltage ΔV_B, caused by a cycle of P1, could be determined. To obtain the required relationship this procedure was repeated for different values of R1.

2.12 Examples of Energy Regulation and Compensation

The lower portion of a spectrum of inelastically

scattered protons from Si^{28}, corresponding to a pure incident energy of 13 MeV, is shown in Fig. 2.21. A similar spectrum, but with the incident energy modulated by an amplitude of 100 KeV, is shown in Fig. 2.22. Finally, Fig. 2.23 shows the improvement of this spectrum when the analogue pulses were processed by the compensator. It is clear that there is such improvement. In particular, the three topmost groups are well separated in Fig. 2.23 but merge together in Fig. 2.22; similarly, the three groups halfway down the spectrum are well resolved in Fig. 2.23 but unresolved in Fig. 2.22.

It will be noted that for the spectrum in which the beam energy is modulated, but for which there is no energy compensation, there is a reduction of the peak amplitudes - as there must be since the area of a peak remains constant for a particular beam charge. A formula which relates the peak reduction ratio to the incident beam energy spread is derived in Appendix 2. If the energy is spread by 2Δ, and the peak profiles are Gaussian with a R.M.S. deviation of σ, then the peak reduction ratio is

$$r = Y_\sigma/Y_0 = \sigma^{\frac{1}{2}}EHP(s)/2.s \qquad (2.7)$$

where: $s = \Delta/\omega$; erfP(s) = error function; Y = peak height.

The function r is plotted in Fig. 2.15. The Gaussian shape that best fits the peaks in Fig. 2.21 has a value of ω of 21.4 KeV. (This corresponds to a F.W.H.M. resolution of 36 KeV.) The peak reduction ratio for corresponding peaks in Figs. 2.21 and 2.22 is 0.39, and so by referring to Fig. 2.15 this gives an s value of 2.25, and the energy spread of the scattered particles as

$$2 \cdot \omega \cdot s = 97 \text{ KeV.}$$

Since the incident beam energy was actually spread by 100 KeV, and the counter was at 45°, the calculated and experimental values of the beam spread are in reasonable agreement. The reduction ratio between Fig. 2.21 and Fig. 2.23 is 0.95, which gives an effective energy spread of 12 KeV. From this, it may be inferred that the energy compensation is about 90 per cent. The reason why it is not 100 per cent is probably associated with the distortion of the modulation waveform (Fig. 2.13).

2.13 The Experimental Counting Electronics

Independent amplification systems were used for each of the four counters employed in the determination of the angular distributions. The electronic system for the most forward angle counter is shown schematically in Fig. 2.24. A similar diagram for the remaining counters is shown in Fig. 2.25. The reason why the forward counter had a different electronic system from the rest can be appreciated from the following comments. This counter, due to Coulomb scattering, had the highest counting rate of all the counters, and so while it could be counting at the maximum permissible rate the backward counters would probably be counting very inefficiently. Overall efficiency was therefore determined by the maximum counting rate the forward counter could accept. This rate was limited by two factors: the deadtime generated in the analogue to digital converters (hereafter A.D.C.), and the deterioration in resolution due to baseline jitter. The deadtime limitation was particularly severe, because, of all the analogue signals, those corresponding to elastic scattering had the greatest amplitude, and therefore, the greatest A.D.C. conversion time. To avoid this limitation it was decided to intercept these signals

before they entered the A.D.C. This was done by using an electronic gate which only allowed passage of those analogue signals which were accompanied by a logic pulse. The logic pulses were generated for all analogue signals except those corresponding to elastic scattering.

The reason for the use of a double delay line clipped amplifier for the forward counter is that, at comparable counting rates, it has less base line jitter than an E.C. amplifier. However, E.C. main amplifiers were used for the remaining counters, since for these counters the counting rates at maximum never exceeded several hundred events per second.

Each counter amplifier system used separate A.D.C.s; these A.D.C.s were linked into an on-line I.D.H.7 computer (Murray and Macefield, 1967). After an analogue signal had been processed by the A.D.C., the digitized signal was stored in a memory buffer until the computer was free to transfer the information to its memory. The different buffers had a descending order of transfer priority. An analogue signal was rejected if it arrived at the A.D.C. during the period of an A.D.C. conversion time or the waiting time of a buffer. To determine the number of rejected events, the prompt analogue signals from each main amplifier were fed into

discriminators which generated logic pulses if the input signals were above a discrimination threshold. The logic pulses from each discriminator were split and fed into two scalars. One of these scalars was inhibited by a D.C. level from the computer during the conversion and buffer waiting time. It is shown in Appendix 3 that the ratio t of the actual number of signals to the number recorded by the computer is

$$t = \frac{N(1)}{N(2)}$$

where: N(1) = number of counts recorded by the uninhibited scalar; N(2) = number of counts recorded by the inhibited scalar.

This result is independent of the analogue signal amplitudes, and therefore, if the number of events recorded by the computer in a particular channel is $\bar{N}(c)$, the actual number of events is $t \cdot \bar{N}(c)$.

2.14 Control Electronics

The beam charge integrator, which also recorded the instantaneous current, was used to control the experiment

(Fig. 2.26). When the beam charge reached a pre-set value the computer and scalars were automatically stopped. If during an experiment the beam fell below a certain value the beam threshold control unit automatically stopped the computer, scalars, and the electric motors controlling the energy modulation and compensation. When the beam rose again above the threshold the apparatus reverted to an operative state. Had the experiment not been stopped following the disappearance of the beam, it was most unlikely that the beam would have returned at the same energy as it left. The beam threshold control unit consisted simply of a Schmidt trigger circuit operating a relay. A slave output from the beam integrator which was proportional to the instantaneous current provided the input for the trigger circuit.

2.15 Beam Monitoring

The beam was stopped on a block of uranium positioned at the end of an electrically insulated two-metre section of beam pipe. In some earlier experiments an electrostatic electron suppressor was fitted to the entrance of this Faraday cup pipe. This suppressor was later rejected since it was found to cause a fluctuation of 7 per cent in the

ratio of the integrated beam charge to the number of events recorded by a counter. The reason for the fluctuation was believed to be connected with the ionisation of the residual gas caused by the incident beam. In later experiments a collimator, electrically connected to the Faraday cup, was employed to restrict the escape of electrons.

The beam charge was monitored by a charge integrator manufactured by Elcor Incorporated.

2.16 Targets

To avoid unnecessary contamination, self-supporting silicon targets were used for this experiment. The method by which these were produced is as follows.

First of all, a glass slide was covered with a sodium chloride substrate by evaporation of the salt in a vacuum. Silicon, evaporated by an electron gun, was then deposited on this slide; after evaporation the slide was allowed to cool before exposure to air. The usual method of flotation was used to remove the silicon from the slide, the salt acting as the release agent. Owing to the extreme brittleness of the silicon films, the success rate of making the films was quite low. In fact, to produce a film of a thickness

greater than 150 µgm was considered a near impossibility; this was not only due to the handling problems but also because the film tended to break up if the thickness exceeded this value during evaporation. This break-up was tentatively attributed to thermal strains within the film.

The thickness of the target was mainly dictated by the energy spread it caused for the low energy scattered protons. The criterion adopted was that for a 2 MeV proton this spread should be no more than 20 KeV; this gives a silicon target thickness of 150 µgm. The targets used in the experiment had a thickness of about 100 µgm.

The thickness of a target was measured by two methods: direct weighing and alpha particle attenuation. The direct method involved weighing a dummy slide before and after the silicon evaporation. The alpha particle attenuation method involved measuring the reduction in air range of alpha particles after they had passed through the target.

Subsequent analyses of the proton spectra from the targets revealed the presence of considerable quantities of oxygen and carbon; since their presence considerably complicated the data analyses, several attempts were made to eliminate these contaminants, but without success. The cause of the trouble was thought to be fundamental in that

during evaporation the pressure of the residual gas was not low enough; the pressure used in the evaporation was 10^{-6} mm. Use of a better pump, e.g., an ion pump, and provision for baking the apparatus would be an obvious improvement, but unfortunately at the time of this experiment these facilities were not available.

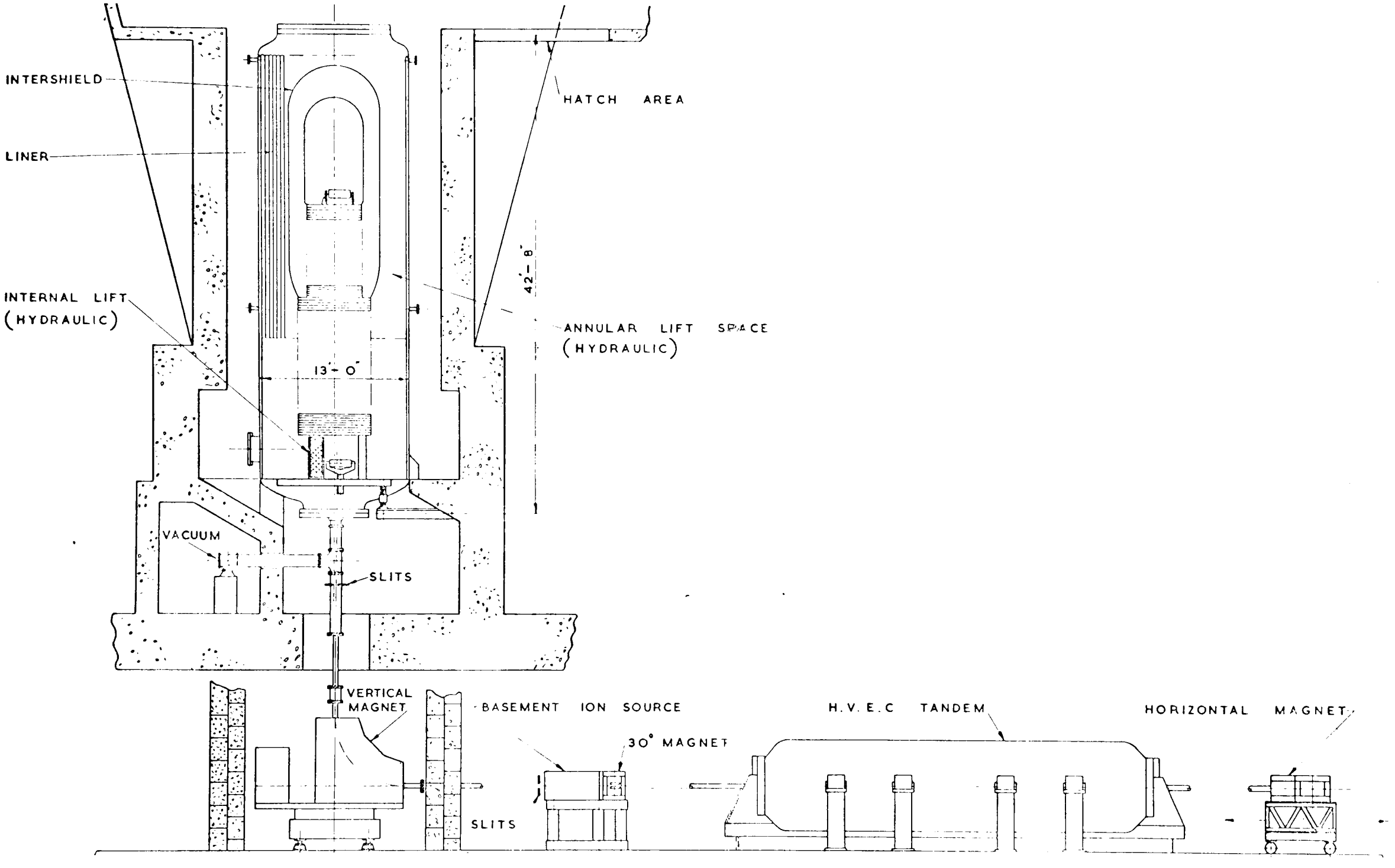

OXFORD ELECTROSTATIC ACCELERATOR

FIGURE 2.1

EXPERIMENTAL BEAM LINE

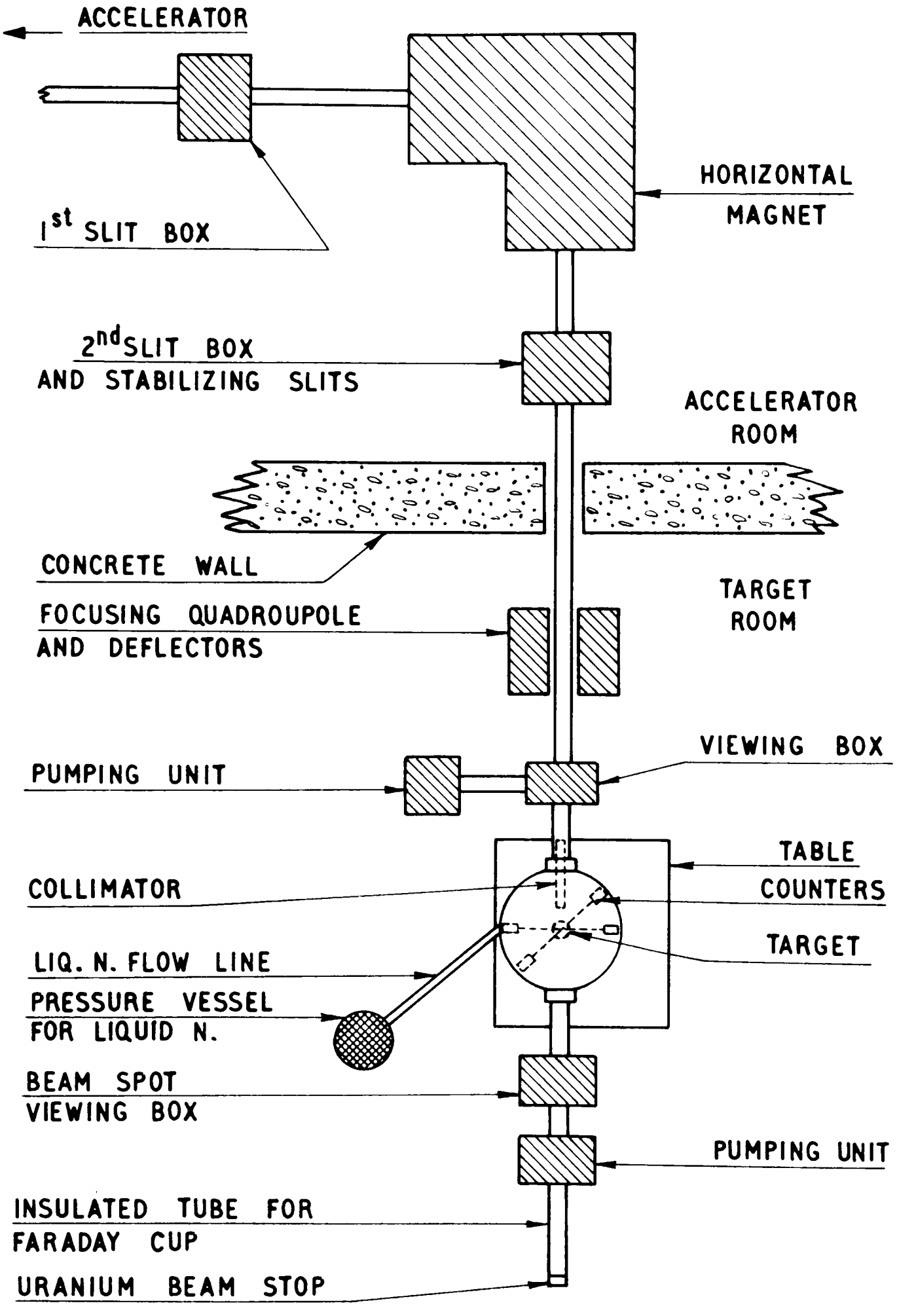

FIGURE 2·2

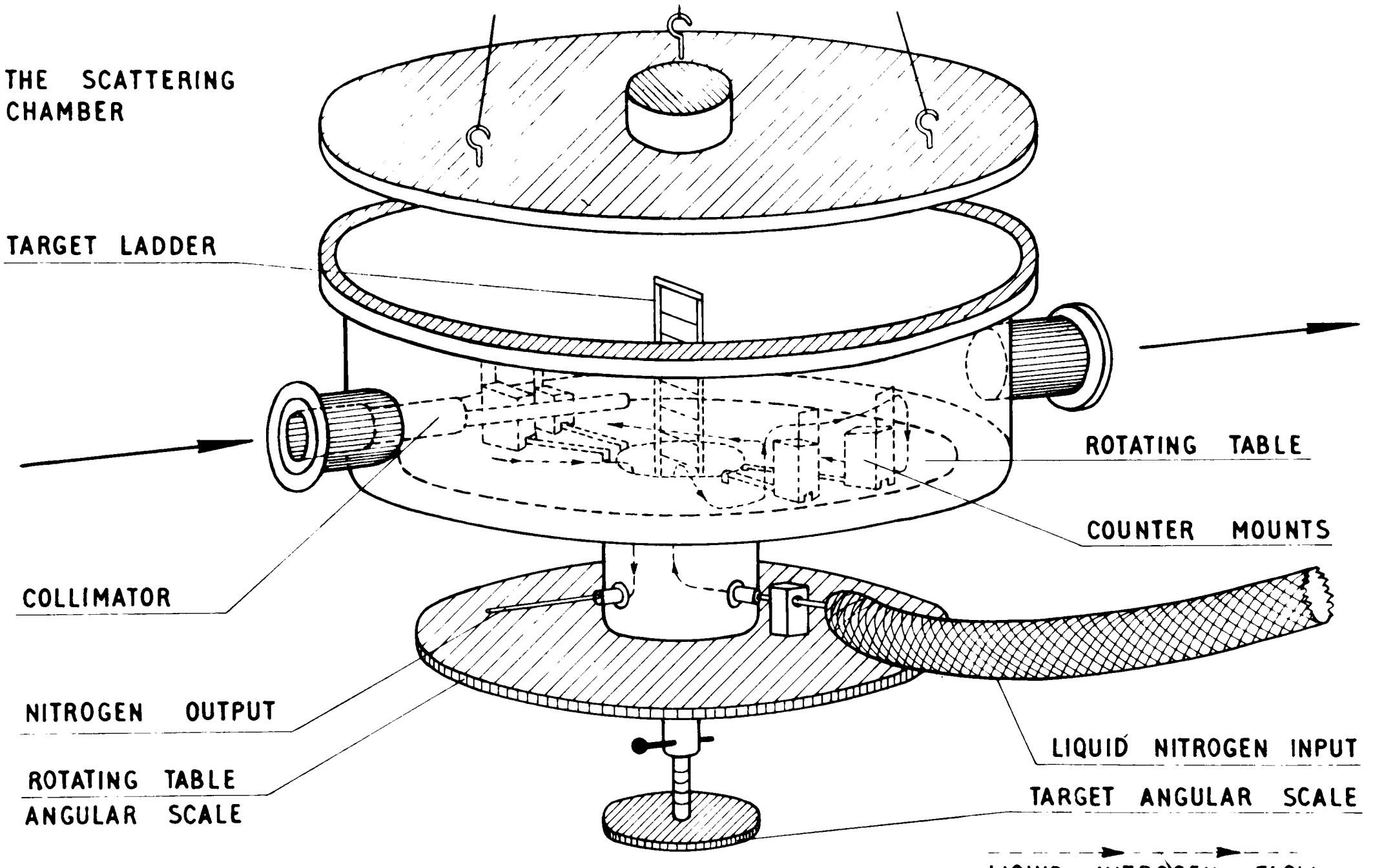
THE SCATTERING CHAMBER
TARGET LADDER
ROTATING TABLE
COUNTER MOUNTS
COLLIMATOR
NITROGEN OUTPUT
ROTATING TABLE ANGULAR SCALE
LIQUID NITROGEN INPUT
TARGET ANGULAR SCALE
LIQUID NITROGEN FLOW

FIGURE 2·3

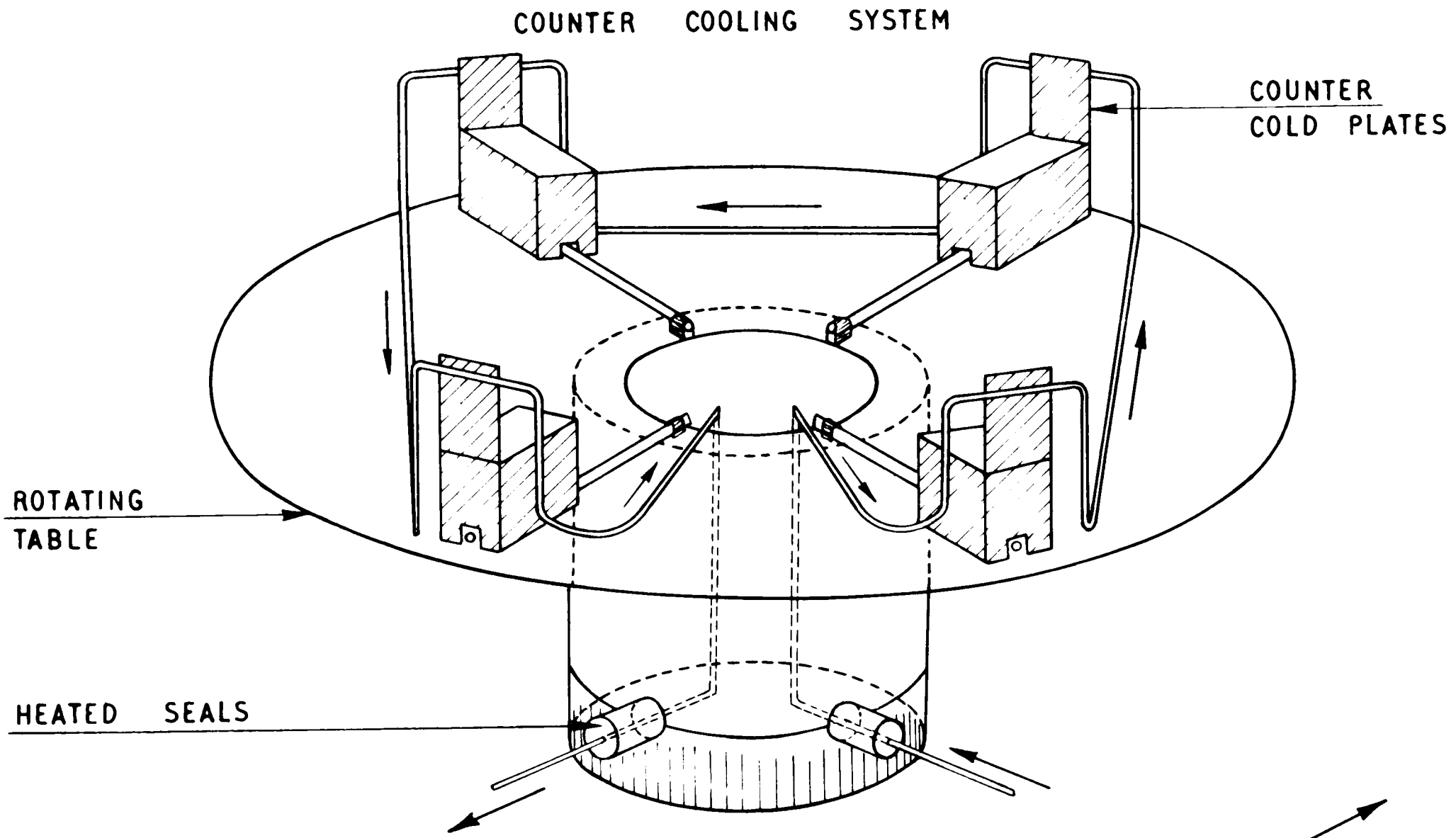
COUNTER COOLING SYSTEM
COUNTER
COLD PLATES
ROTATING
TABLE
HEATED SEALS
INDICATES
DIRECTION OF
LIQ. N. FLOW

FIGURE 2·4

COUNTER ARRAY

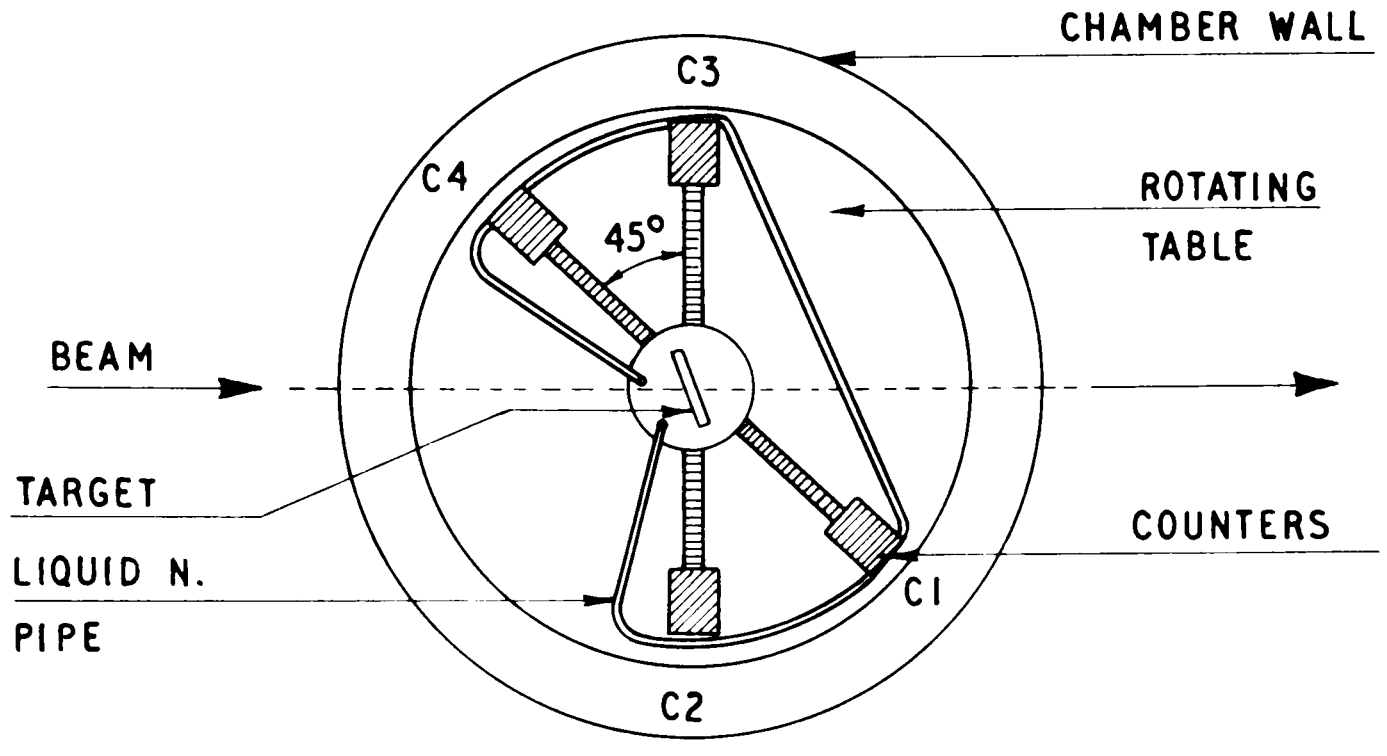

FIGURE 2·5

COUNTER MOUNT

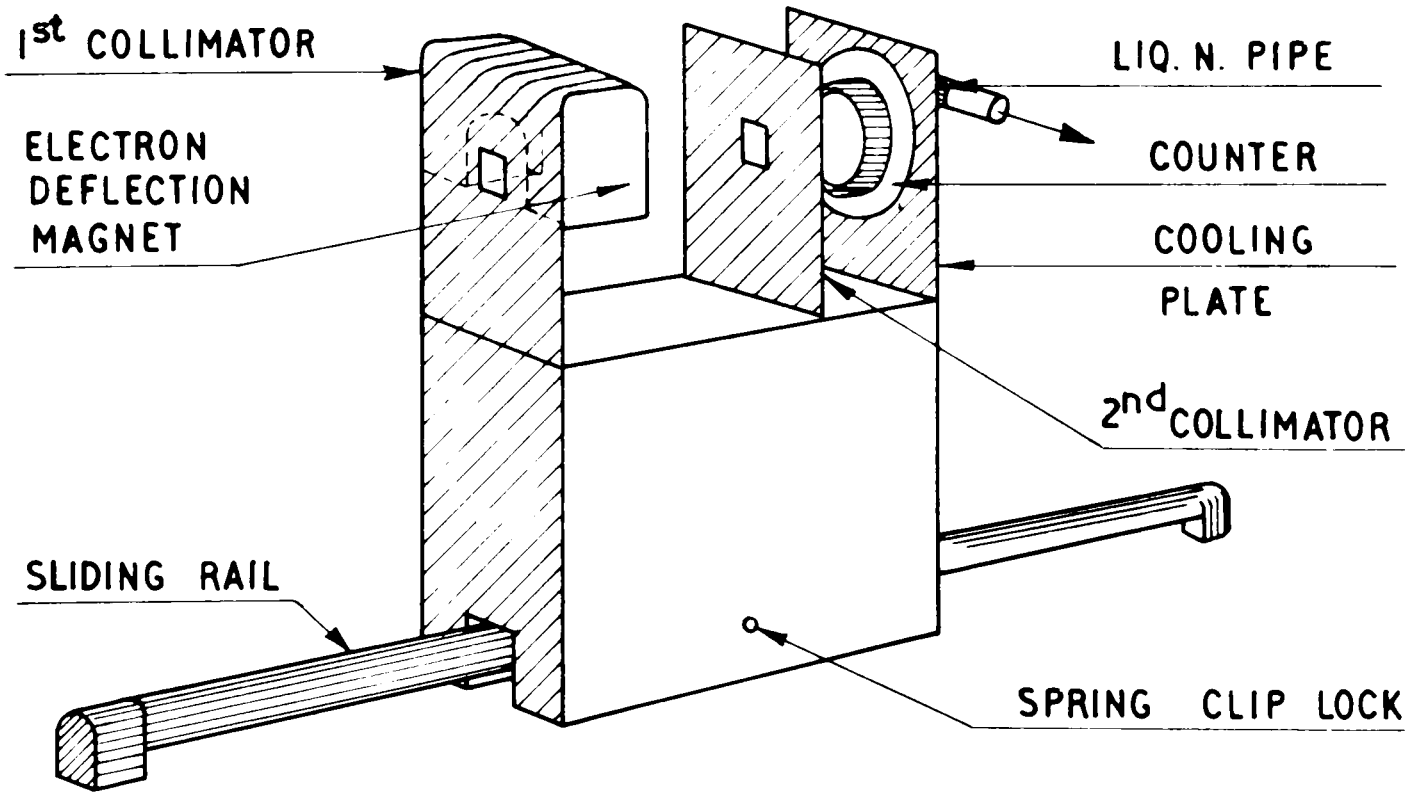

FIGURE 2·6

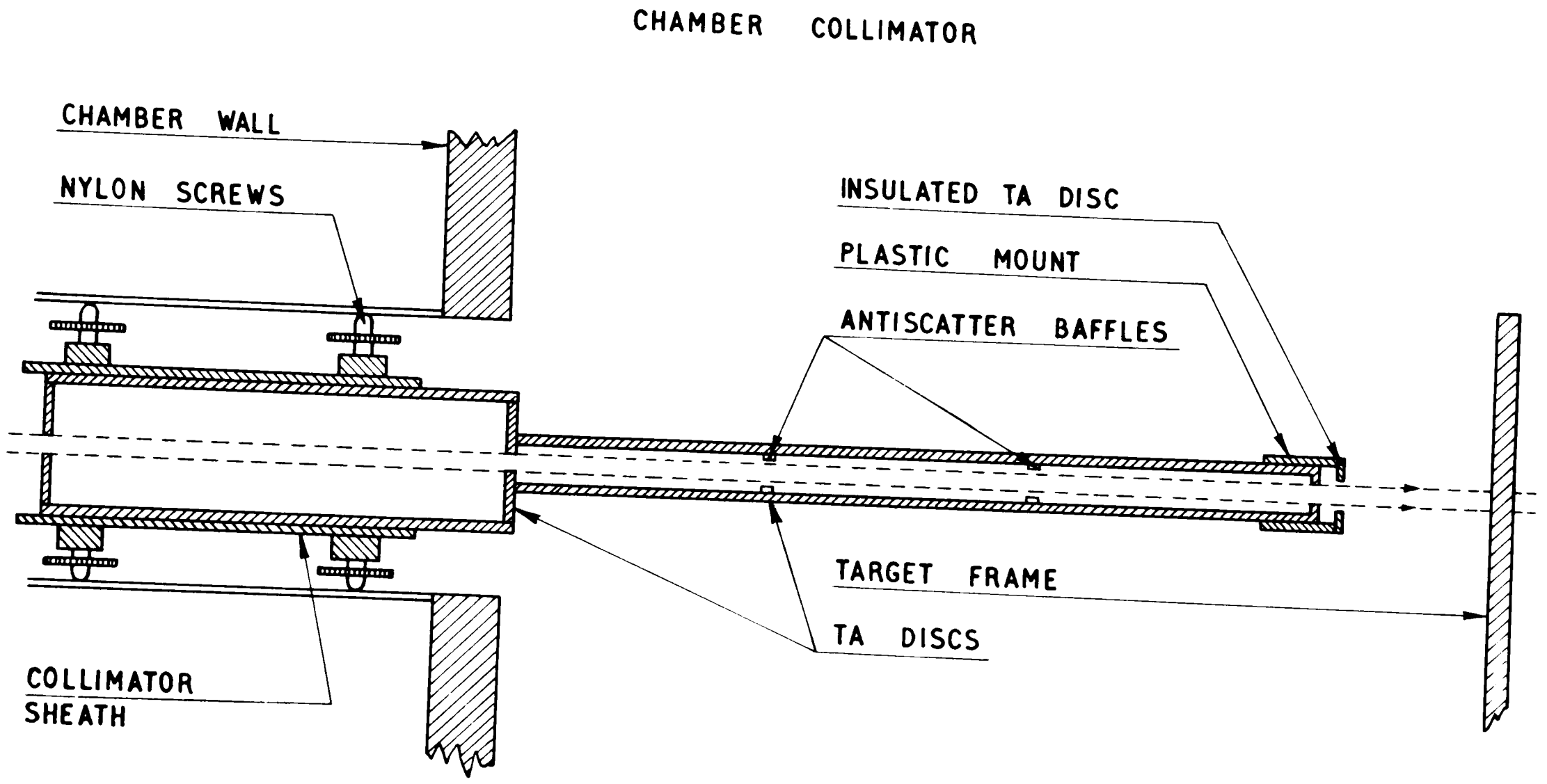
CHAMBER COLLIMATOR
CHAMBER WALL
NYLON SCREWS
INSULATED TA DISC
PLASTIC MOUNT
ANTISCATTER BAFFLES
TARGET FRAME
TA DISCS
COLLIMATOR SHEATH

FIGURE 2·7

PRINCIPLE OF BEAM COLLIMATION

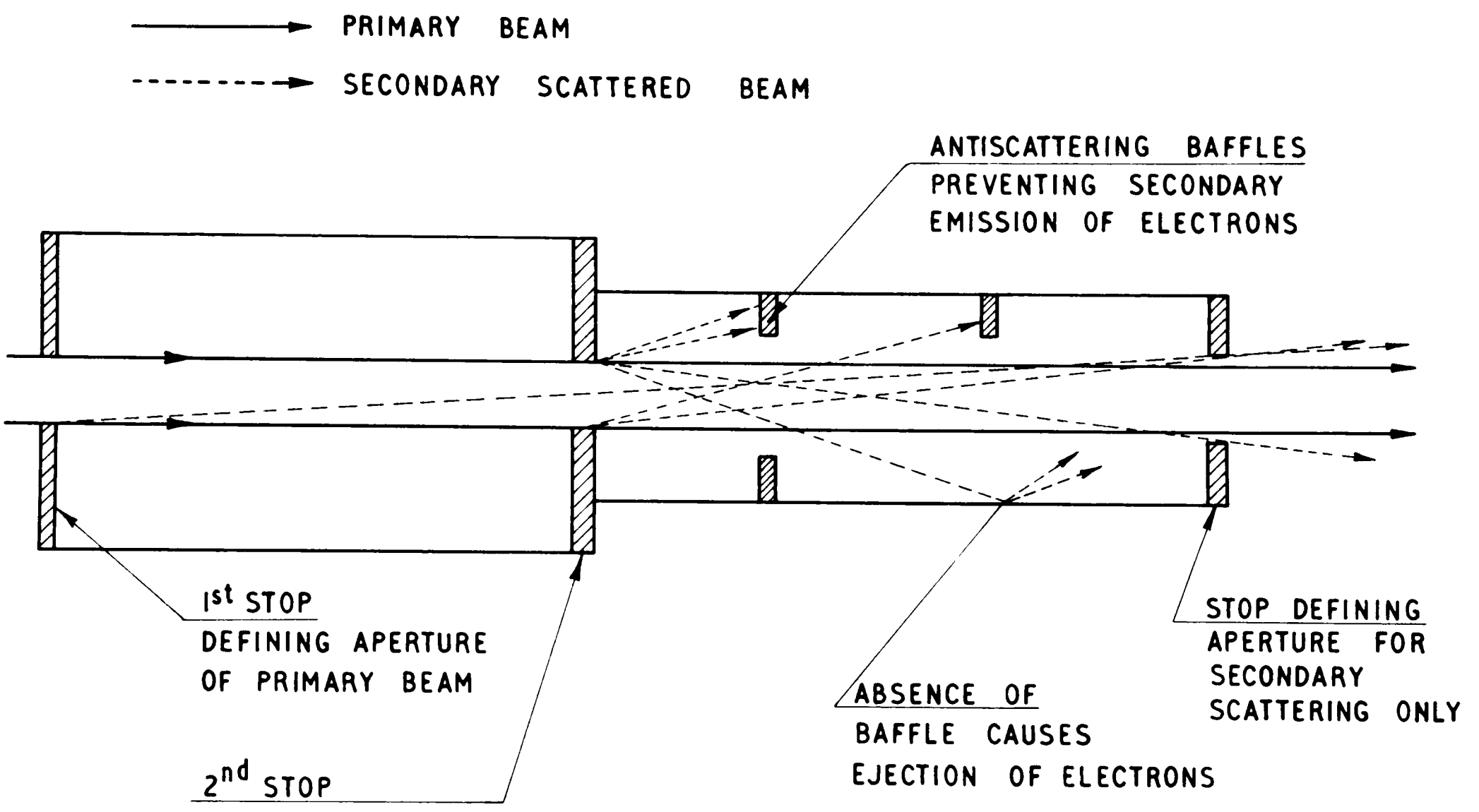

FIGURE 2·8

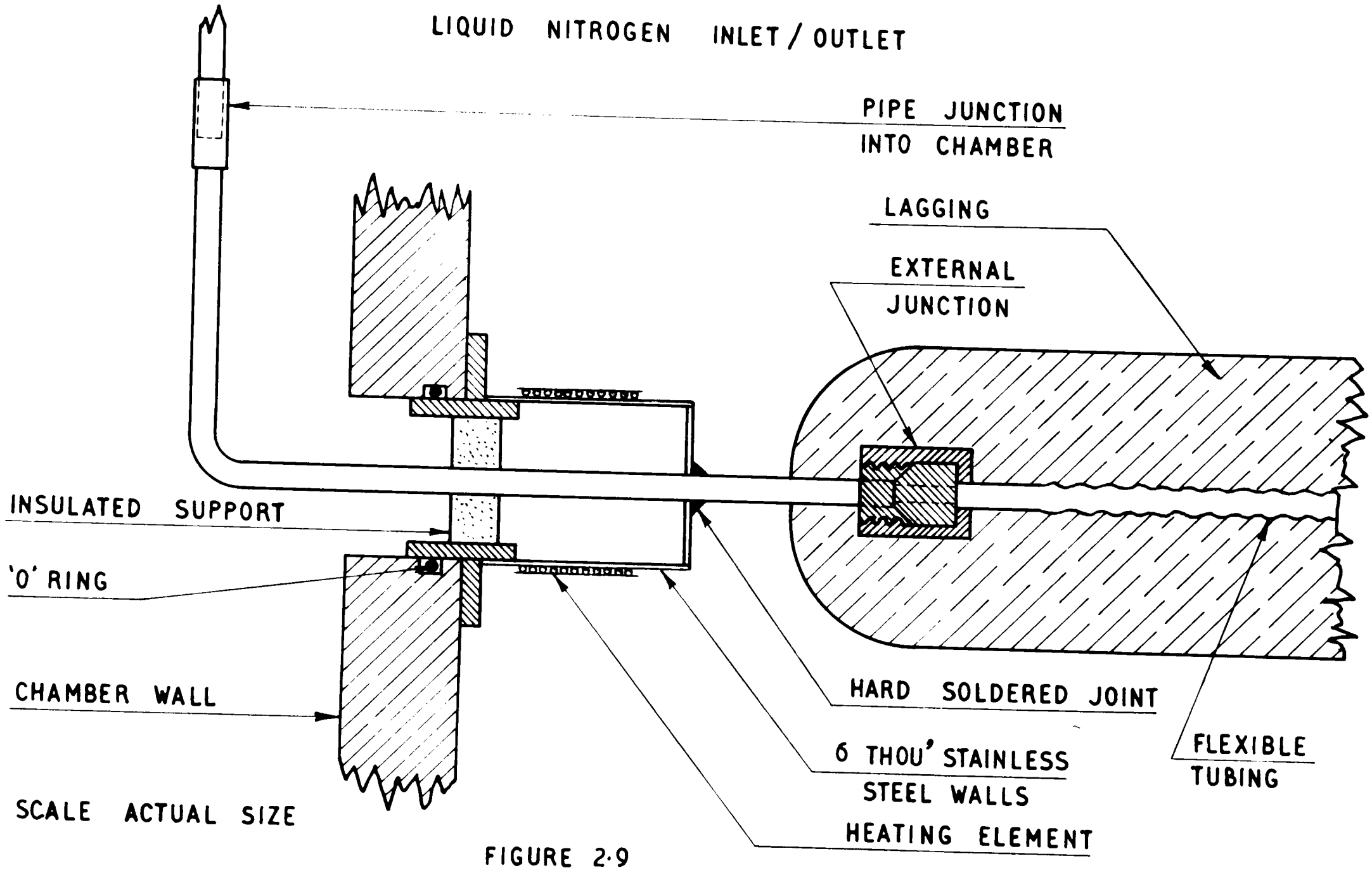
LIQUID NITROGEN INLET / OUTLET
PIPE JUNCTION INTO CHAMBER
LAGGING
EXTERNAL JUNCTION
INSULATED SUPPORT
'O' RING
CHAMBER WALL
SCALE ACTUAL SIZE
HARD SOLDERED JOINT
6 THOU' STAINLESS STEEL WALLS
HEATING ELEMENT
FLEXIBLE TUBING

FIGURE 2·9

MAGNET CURRENT CONTROL UNIT

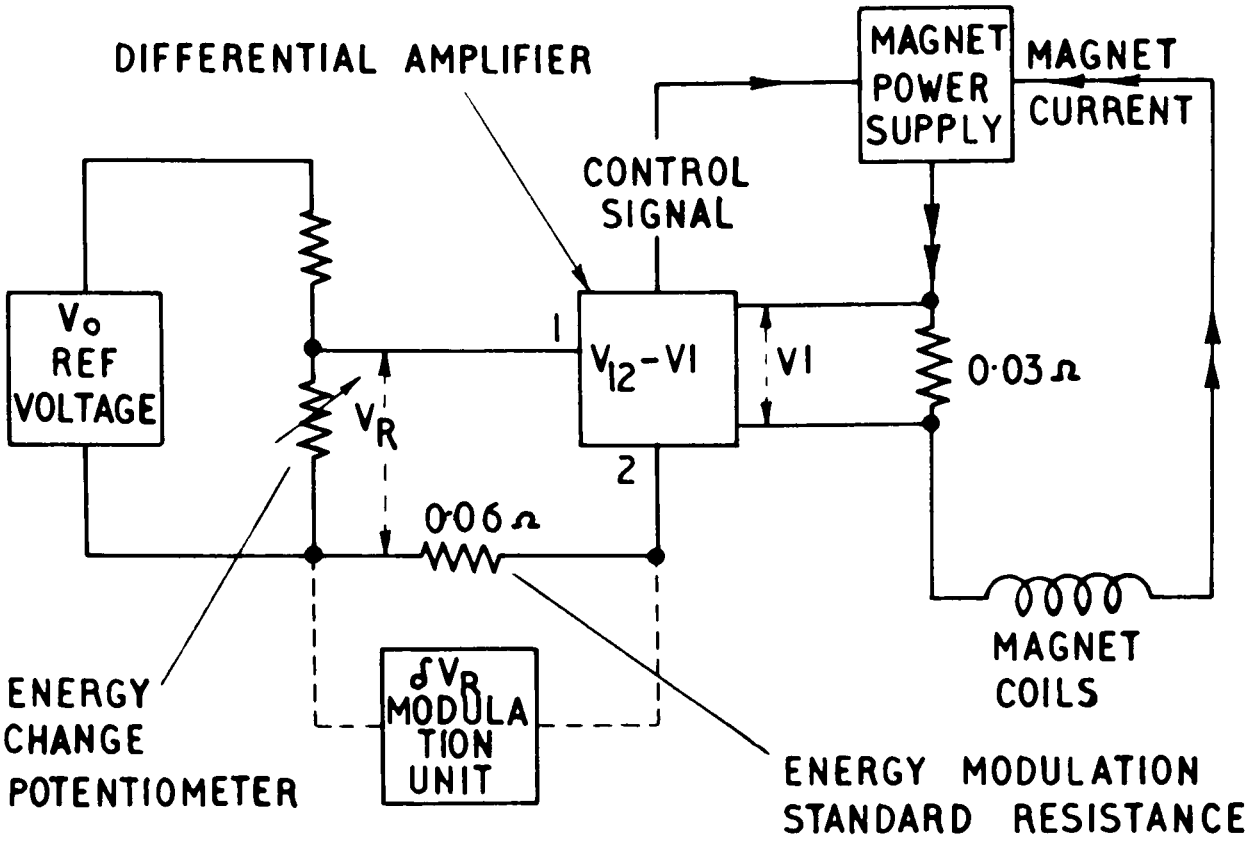

FIGURE 2·10

δV_R MODULATION UNIT

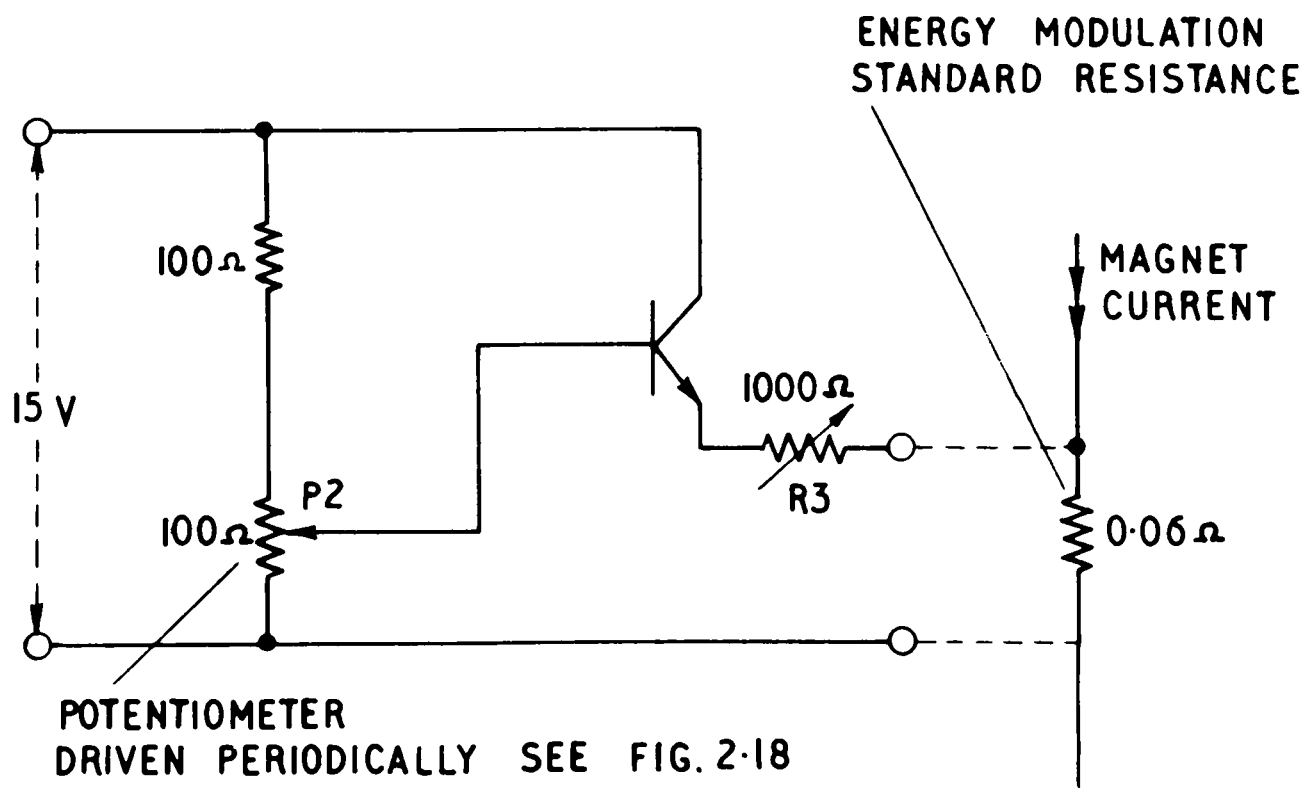

FIGURE 2·11

RESPONSE OF MAGNET TO STEP IN REFERENCE VOLTAGE

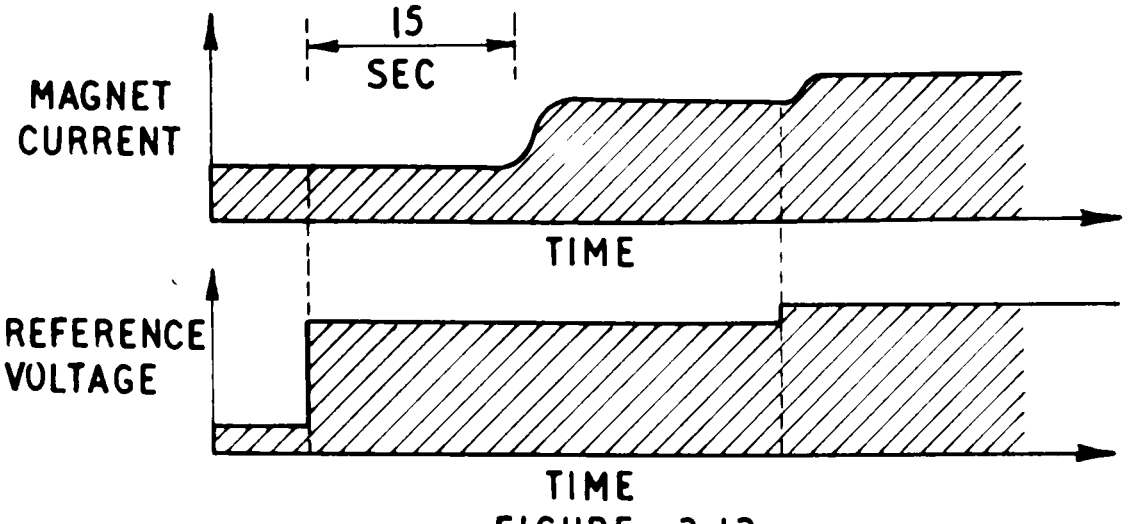

FIGURE 2·12

RESPONSE OF MAGNET TO MODULATION

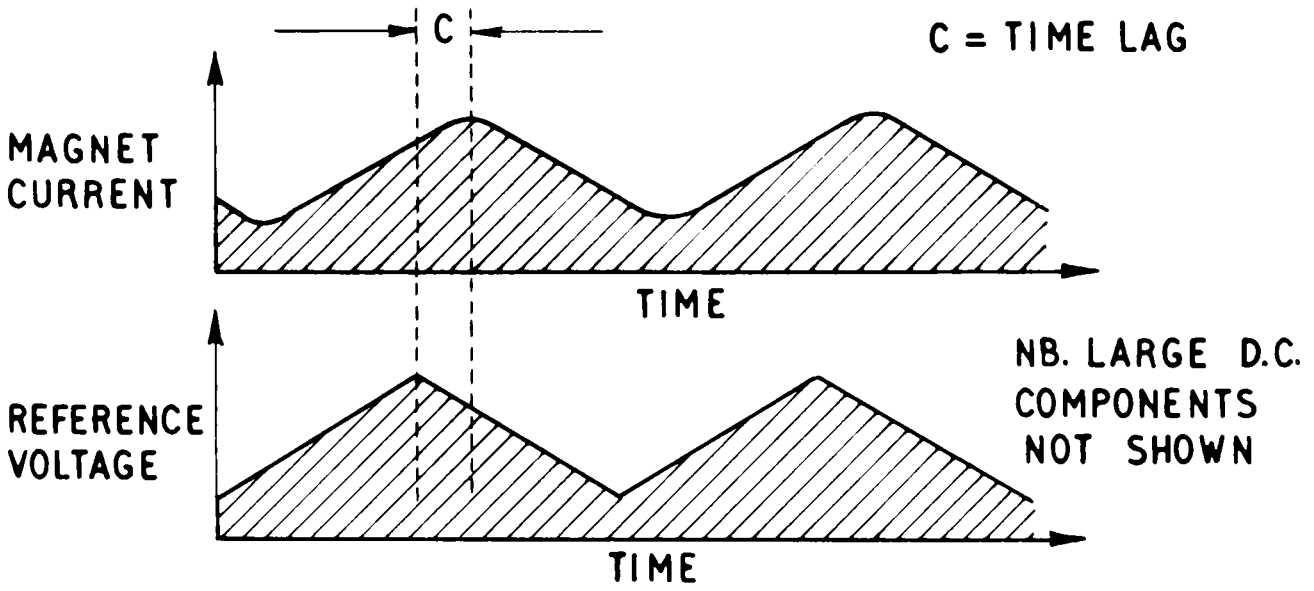

FIGURE 2·13

RESOLUTION FUNCTION

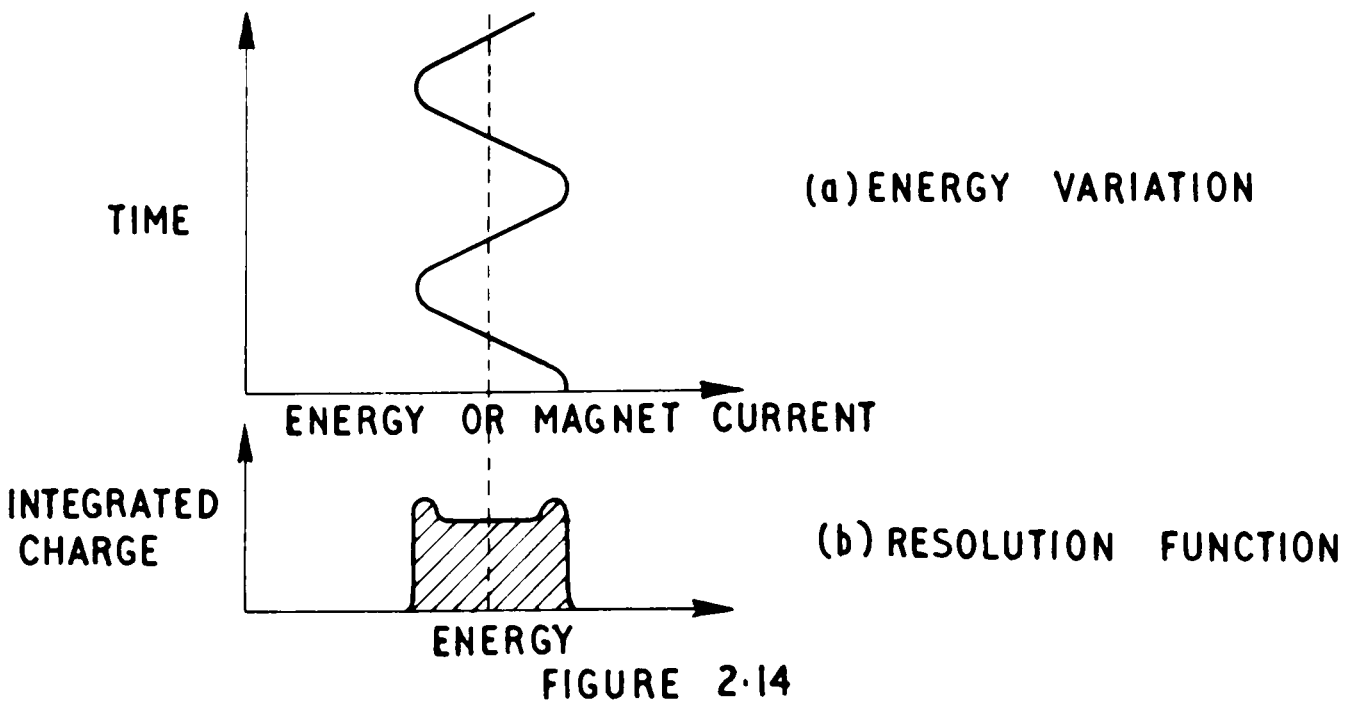

FIGURE 2·14

GRAPH OF Y_S/Y_o

$$\frac{Y_S}{Y_o} = \frac{ERF\ (S)}{S} \cdot \frac{1}{1{\cdot}13}$$

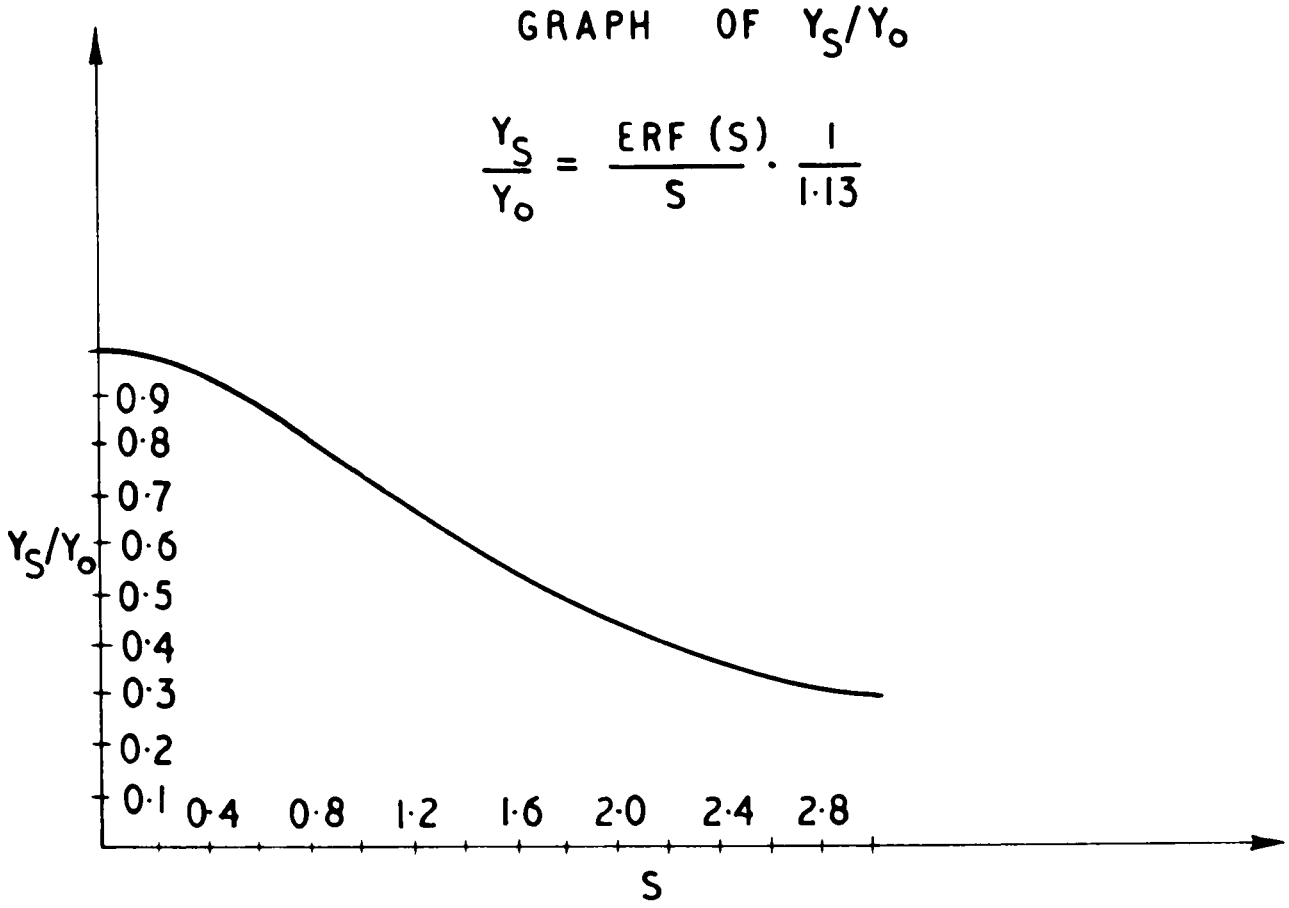

FIGURE 2·15

KINEMATIC RATIO f AS FUNCTION OF ANGLE AND Q VALUE

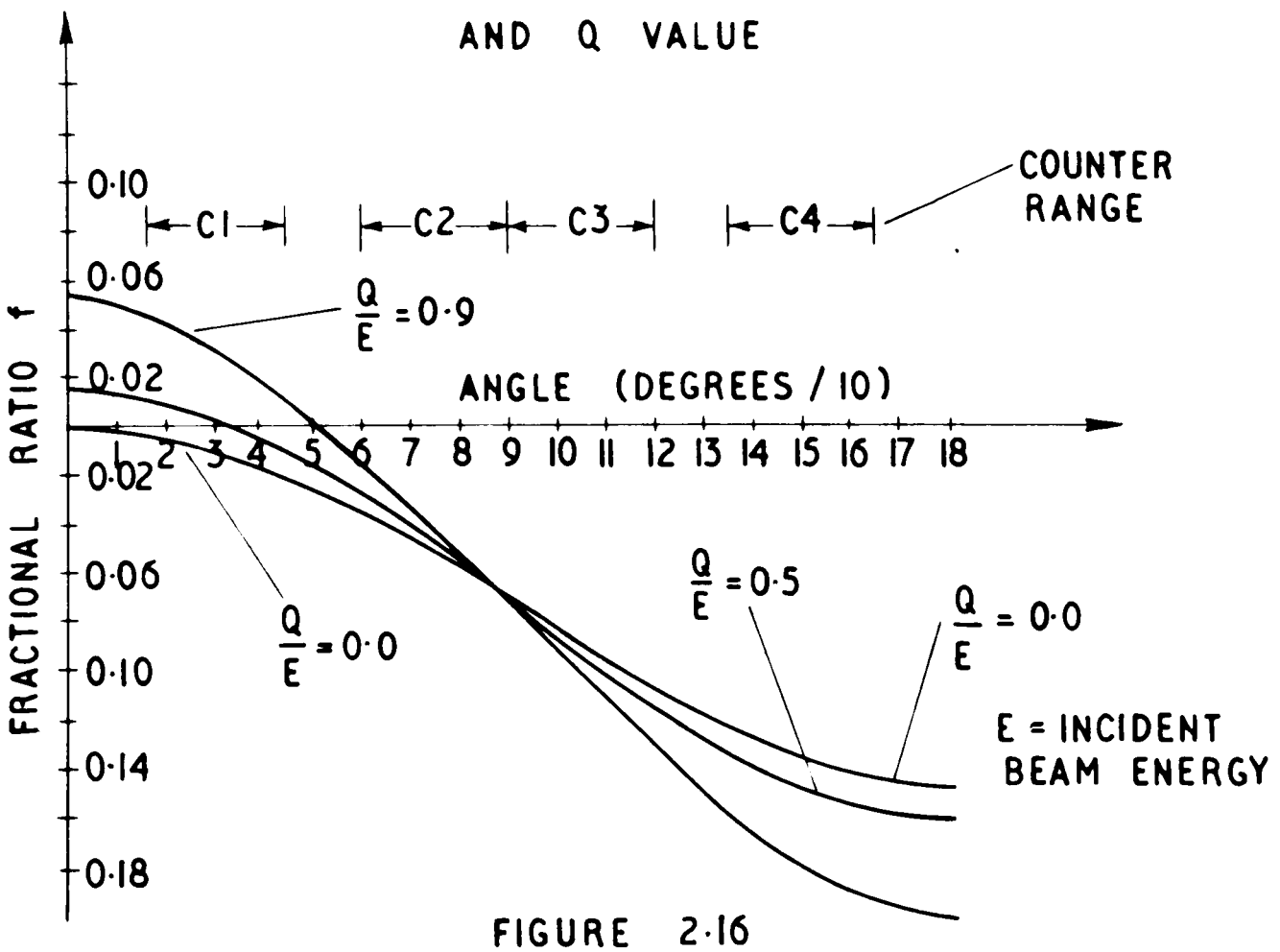

FIGURE 2·16

ELECTRONIC COMPENSATOR

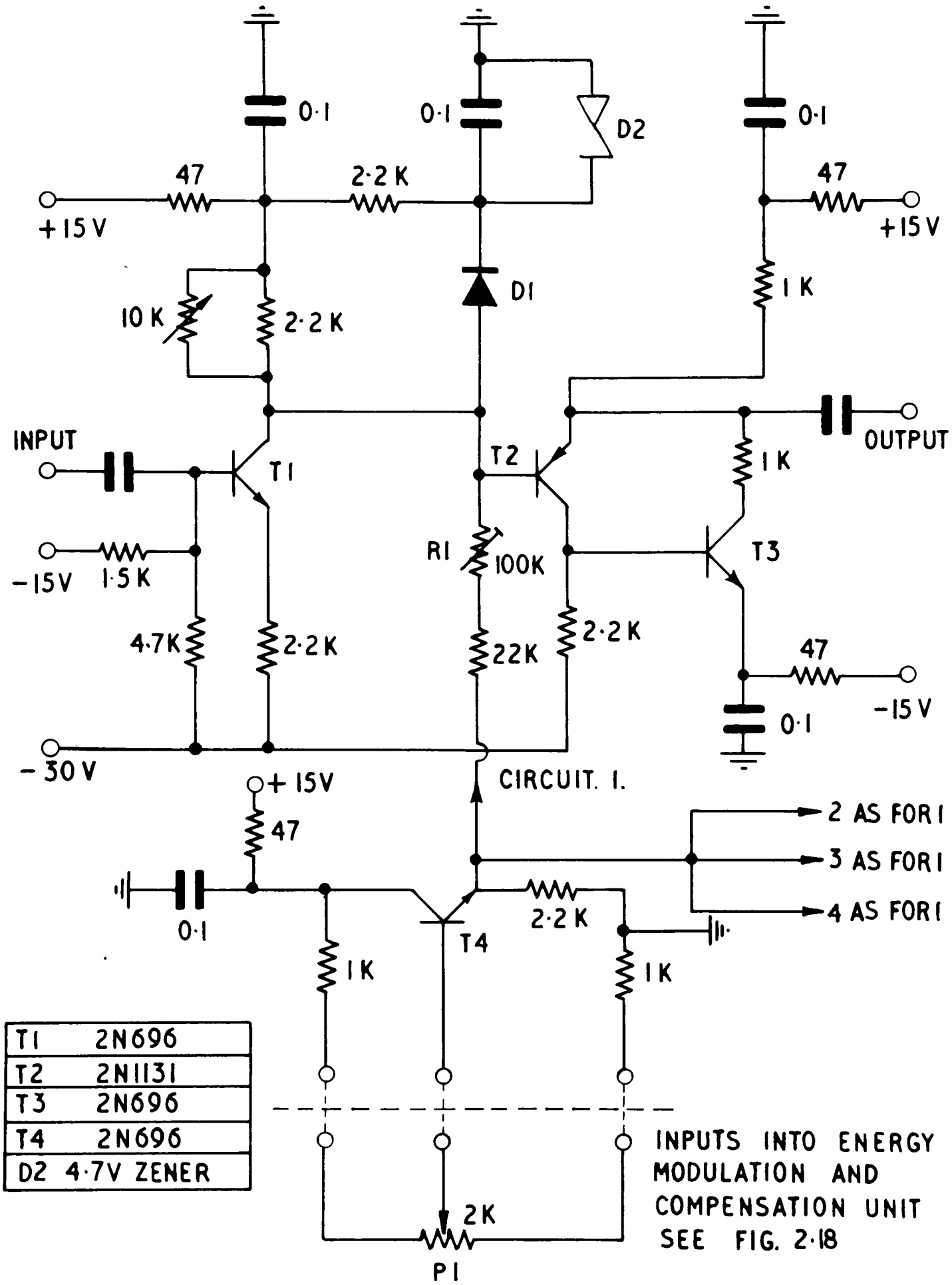

T1	2N696
T2	2N1131
T3	2N696
T4	2N696
D2	4·7V ZENER

FIGURE 2·17

ENERGY MODULATION AND COMPENSATION CONTROL UNIT

P3 TIME DELAY CONTROL
P4 MOTOR SPEED CONTROL
S1 MICROSWITCH OPERATED BY M2
S2 TO SWITCH P4 IN POWER LINE FOR M1 OR M2
S3 TO STOP M2 AT MID-POINT OF CYCLE (FOR AN ENERGY CHANGE)
S4 M1 STOP/START
S5 M1 AND M2 STOP/START
30V S/S 30V SUPPLY IF FINITE BEAM; ZERO IF NO BEAM
RL RELAY COIL; RC RELAY CONTACT
MT METER INDICATING ROTATION POSITION OF M1
NEON INDICATES ROTATION DIRECTION OF M1

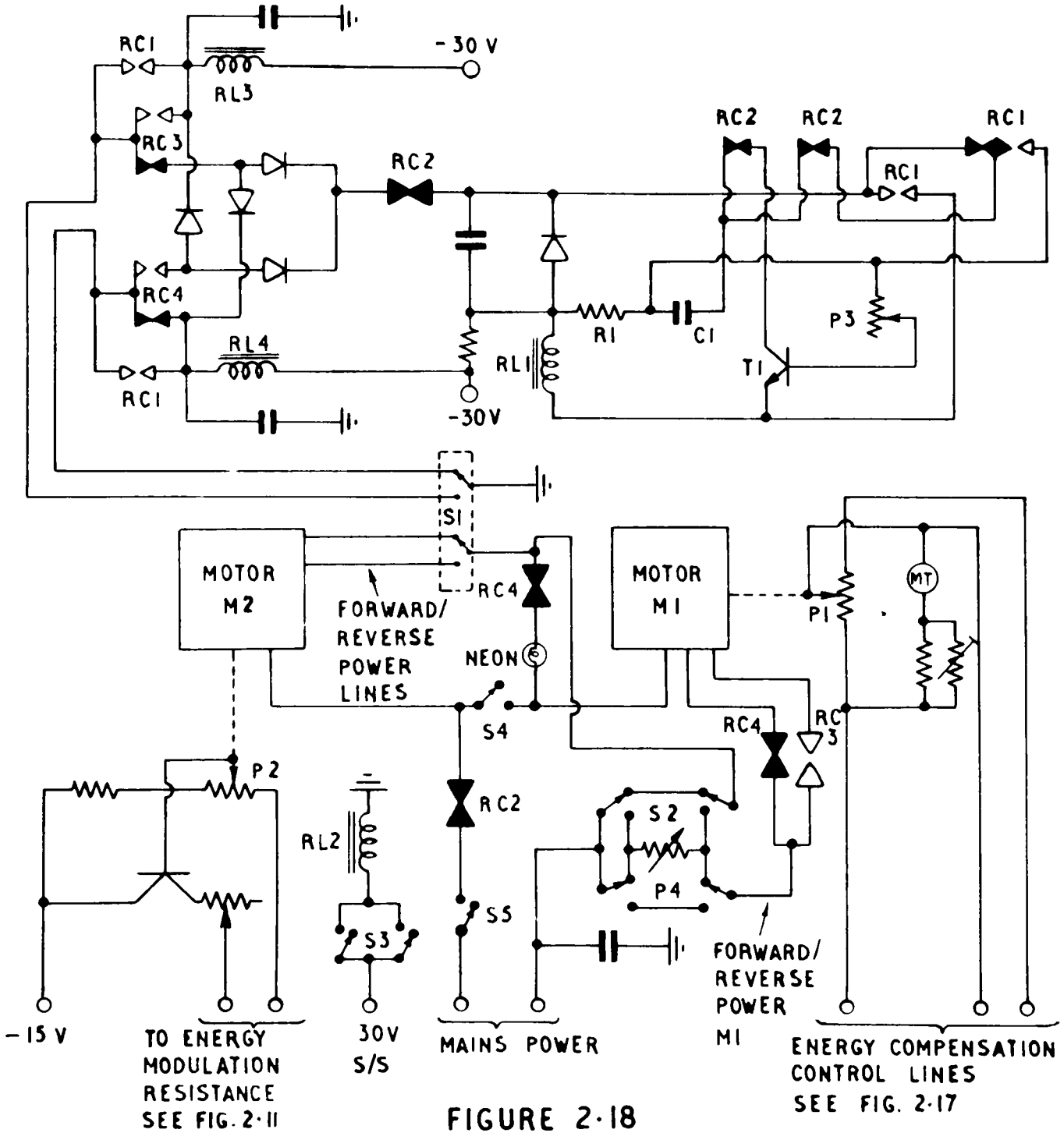

FIGURE 2·18

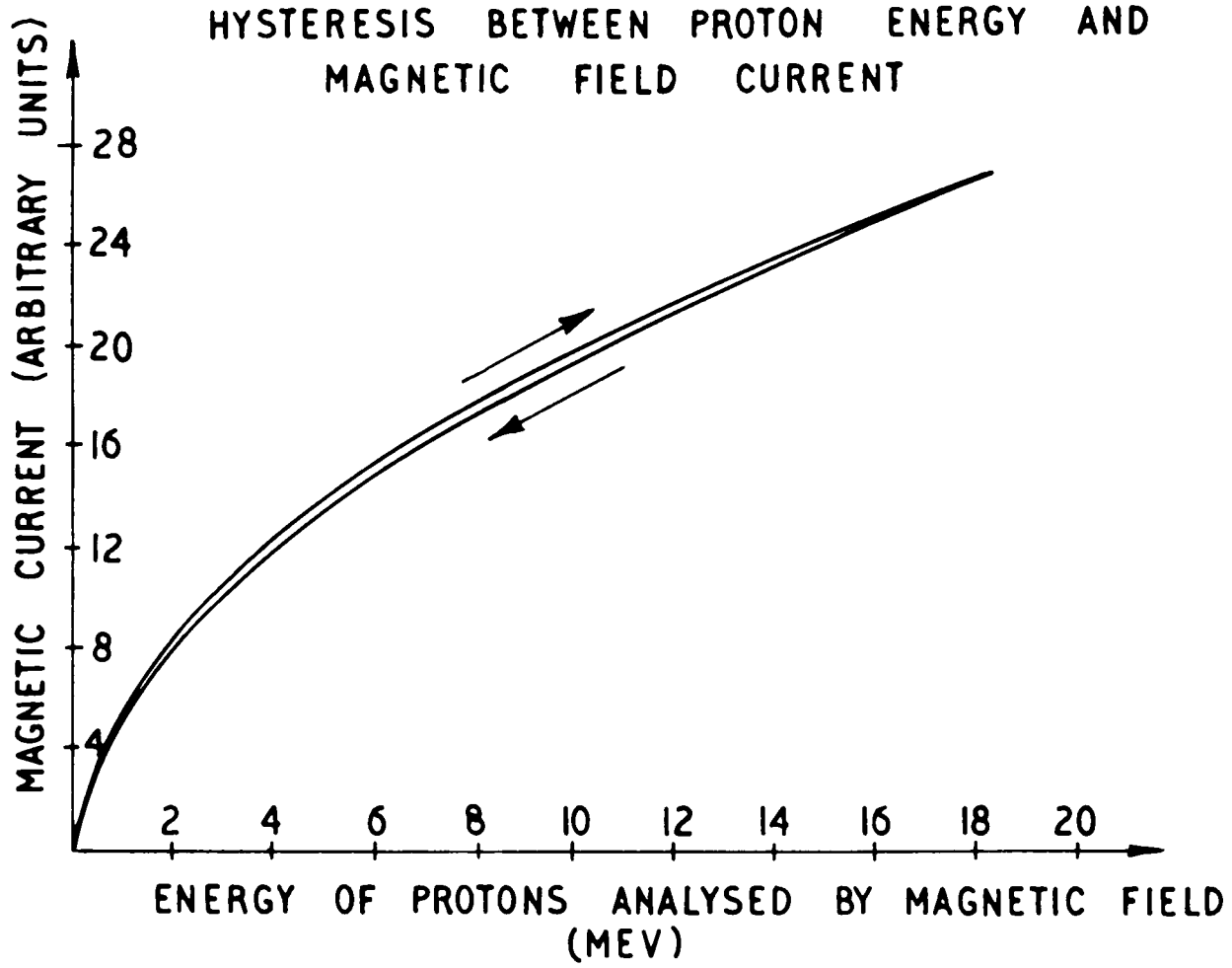

FIGURE 2·19

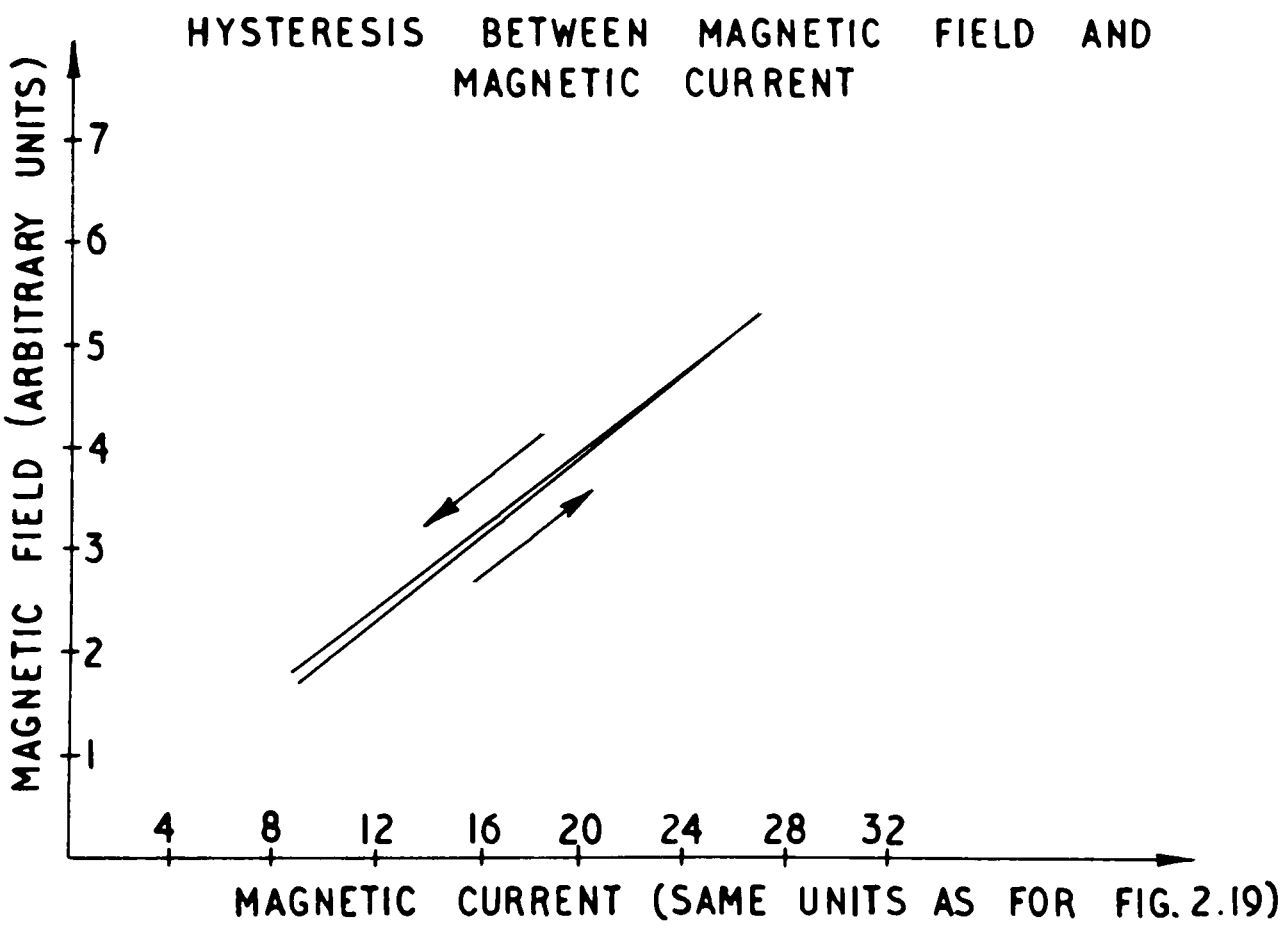

FIGURE 2·20

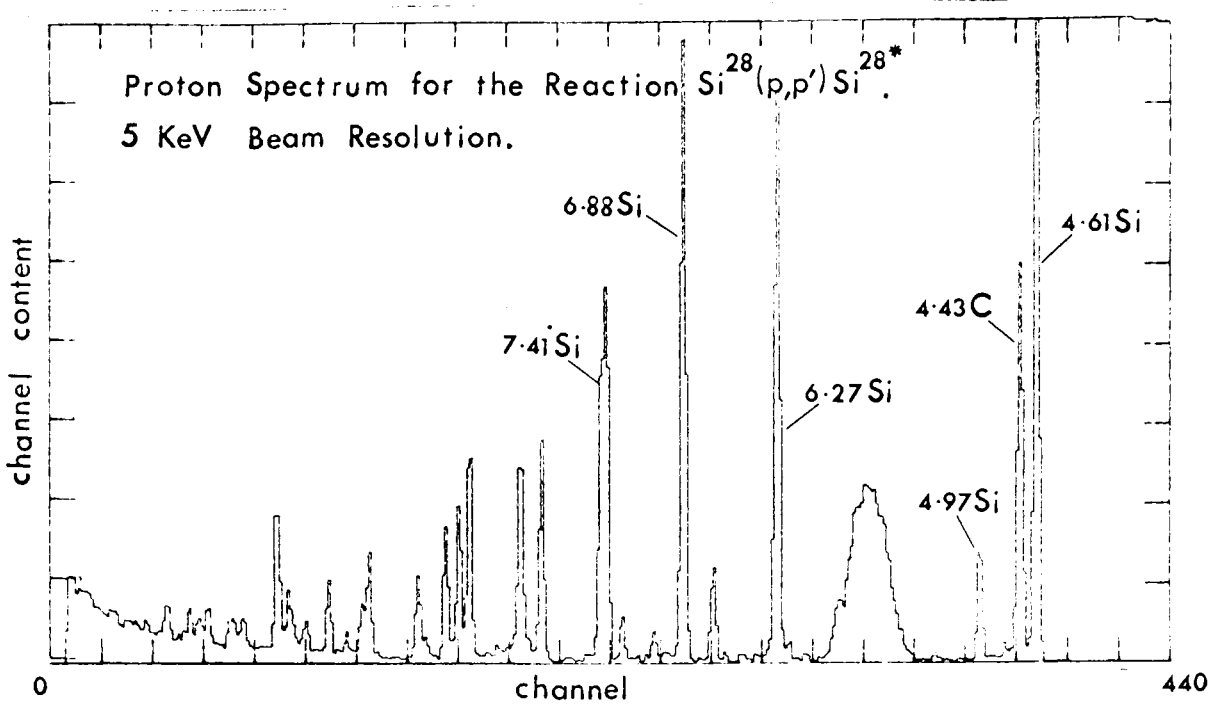

FIGURE 2.21

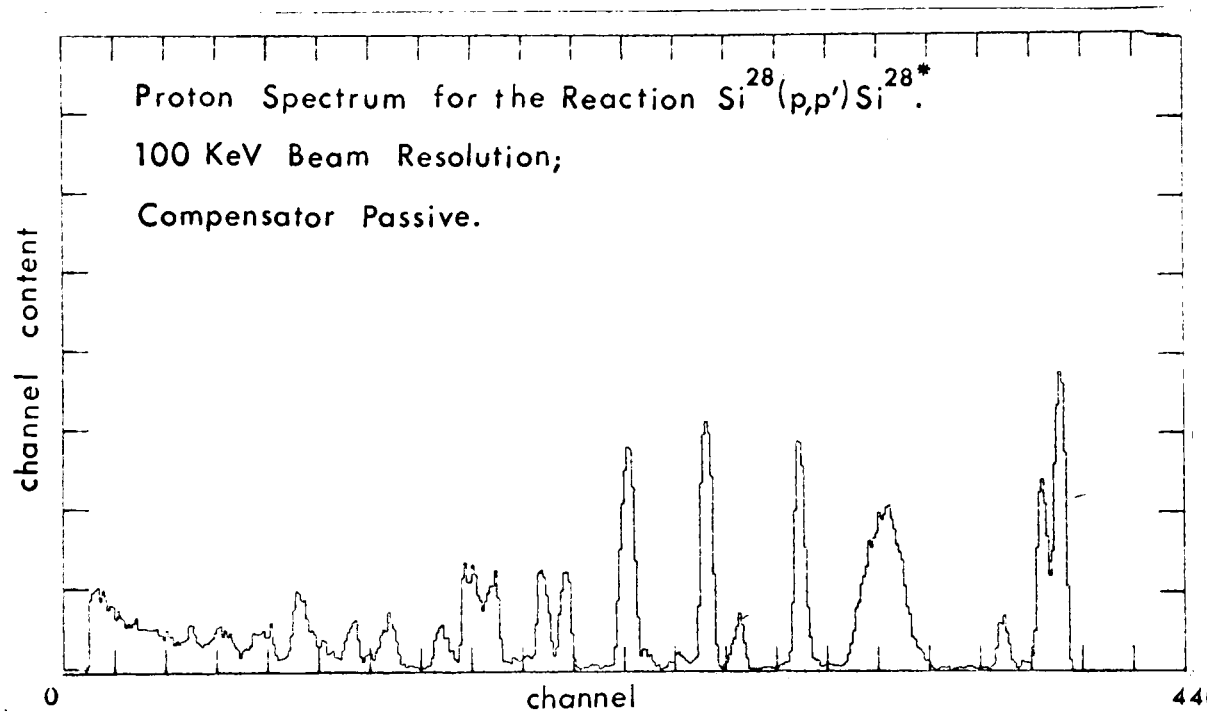

FIGURE 2.22

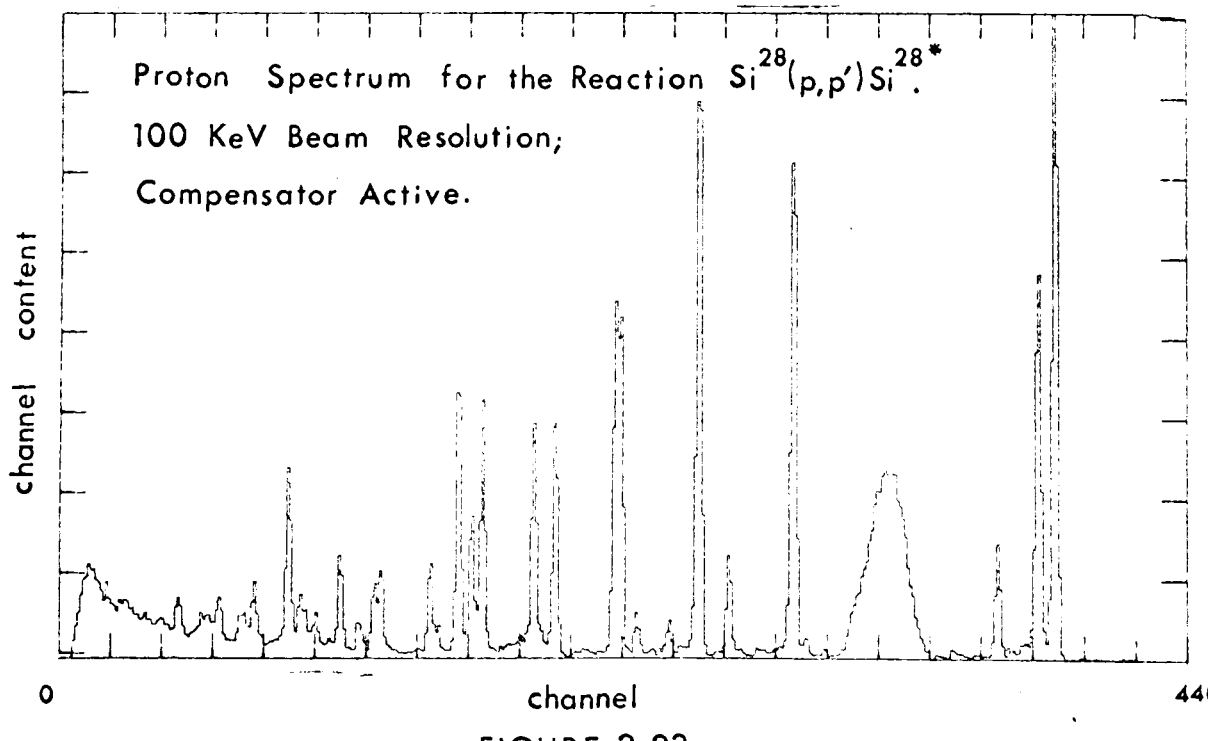

FIGURE 2.23

ELECTRONIC SYSTEM FOR FORWARD COUNTER

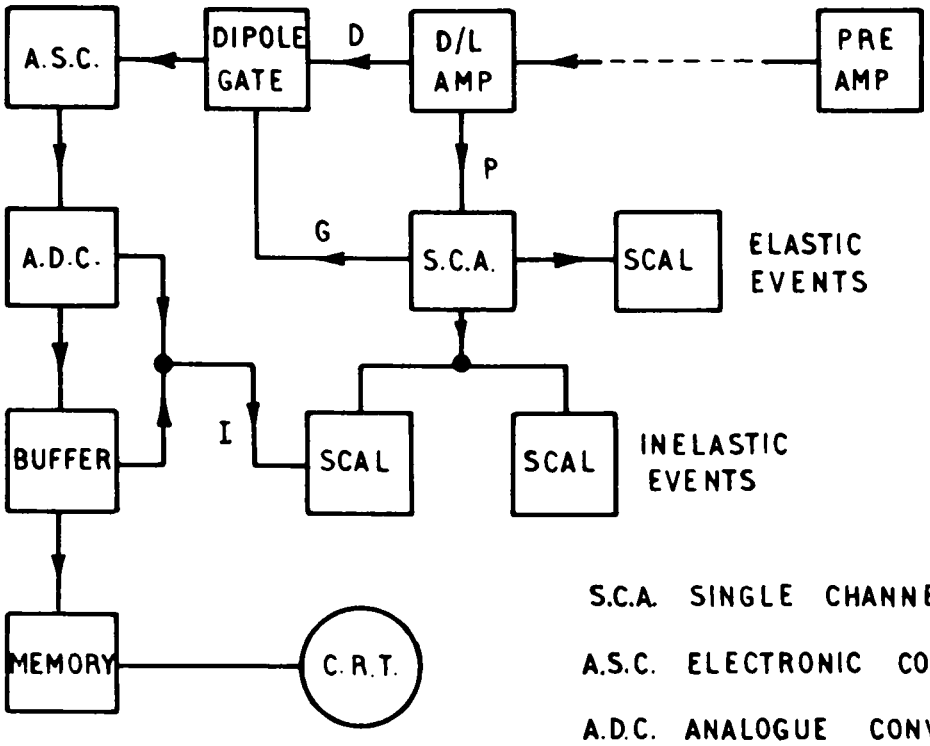

S.C.A. SINGLE CHANNEL ANALYSER

A.S.C. ELECTRONIC COMPENSATOR

A.D.C. ANALOGUE CONVERTER

P PROMPT PULSE

D DELAYED PULSE

G GATING PULSE

FIGURE 2·24

ELECTRONIC SYSTEM FOR BACKWARD COUNTERS

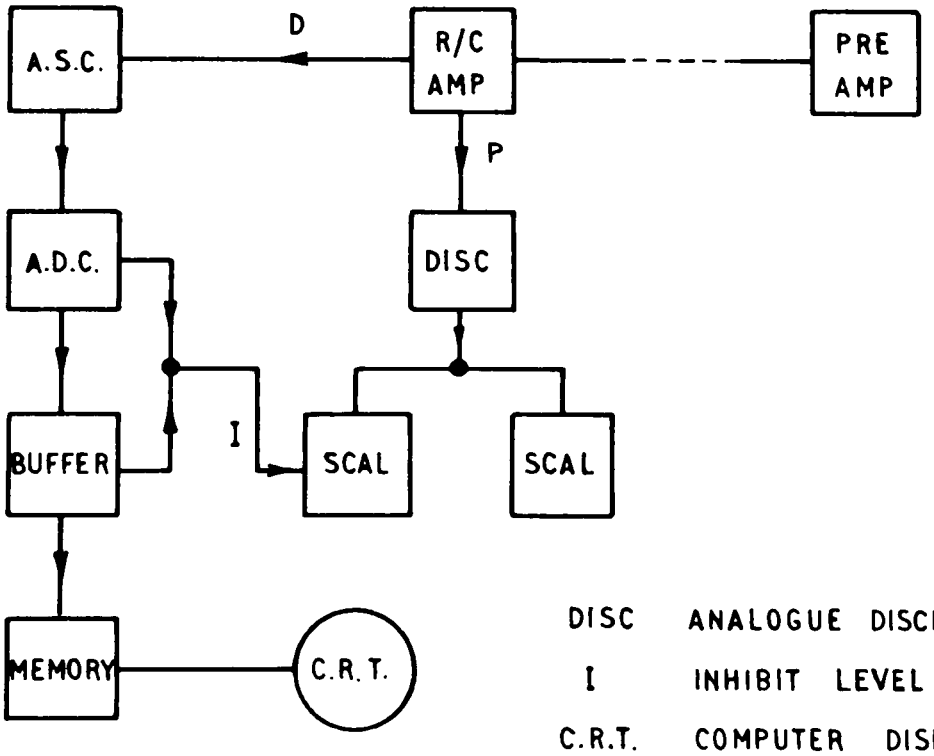

DISC ANALOGUE DISCRIMINATOR

I INHIBIT LEVEL

C.R.T. COMPUTER DISPLAY

FIGURE 2·25

EXPERIMENTAL CONTROL SYSTEM

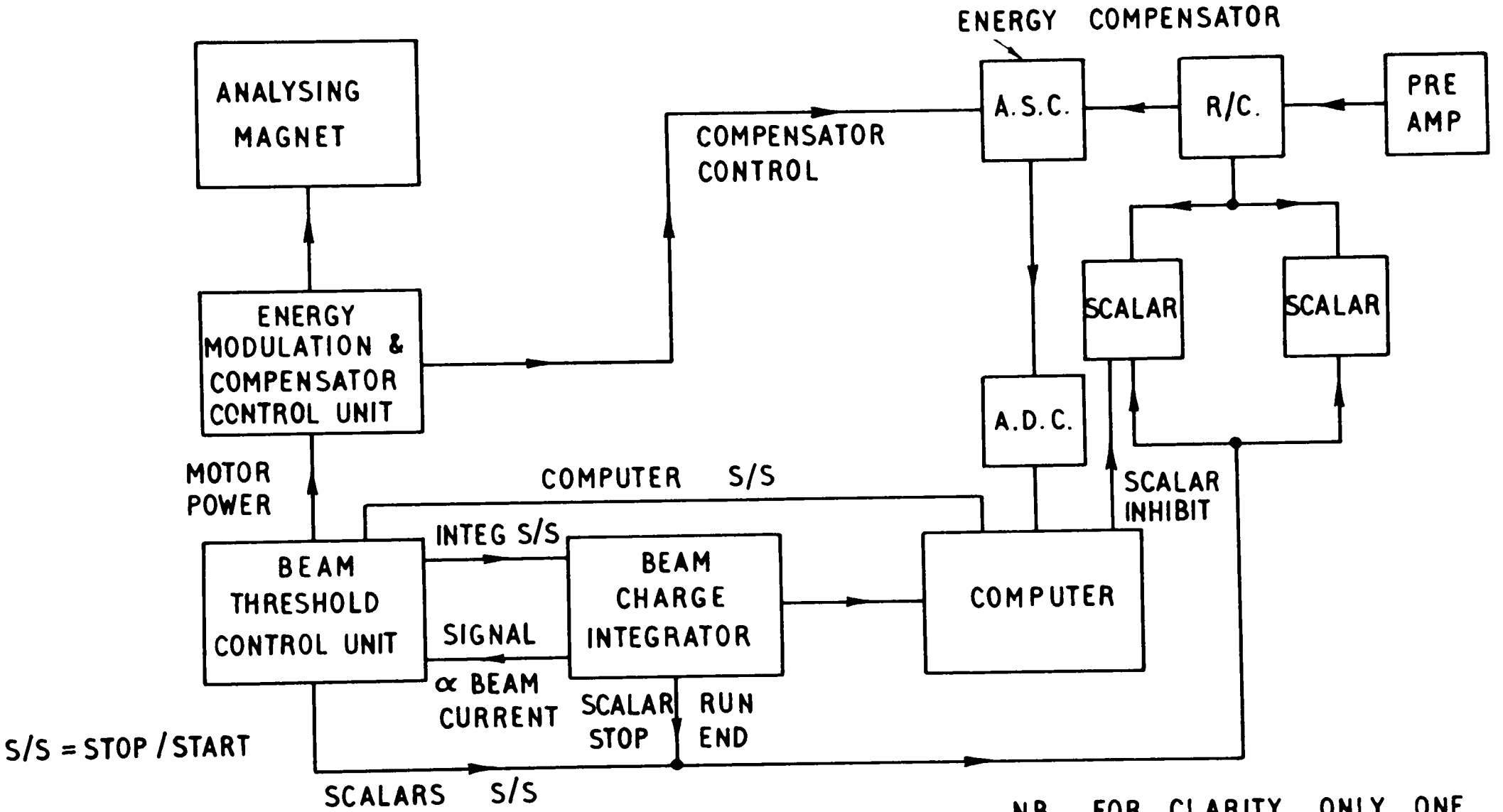

FIGURE 2·26

C H A P T E R 3

EXPERIMENTAL PROCEDURE AND REDUCTION OF DATA

3.1 Optimisation of Beam Conditions

The beam-spot size and position were roughly checked on the retractable scintillator positioned in front of the scattering chamber. With the scintillator retracted, the beam was finally focused and deflected for maximum beam transmission to the Faraday cup and minimum current to both the first aperture of the chamber collimator and to a dummy metal target with a 2 mm. diameter hole.

3.2 Adjustment of the Experimental Equipment

The counters and their associated electronics were tested, before the beam was passed through the chamber, by using an Am^{241} alpha particle source to provide the appropriate signals. The source was attached to one of the target mounts in the target ladder (Fig. 2.3). When the counters were cooled to liquid nitrogen temperature, the recorded half-width of the line corresponding to the 5.5 MeV alpha particle was between 25 and 35 KeV.

To determine the range of linearity of the amplification systems, signals from a Hg pulse generator were injected into each pre-amplifier, and the analogue signals from the associated main amplifiers were analysed by a kicksorter. By varying the amplitudes of the input signals, the range of linearity could be established. Under running conditions, it was ensured that the signals corresponding to the elastically scattered protons were within the region of linearity.

After setting R3 to a value corresponding to the required amplitude of energy modulation, the actual experimental modulation was determined by a similar method to that described in Section 2.11a. The correct compensator bias settings were estimated from the calibration curve of ΔV_B and R1 (Section 2.11b).

In some early experiments, it was discovered that the electronic noise level of the counter-amplification systems increased by a significant amount when the beam passed through a target. It was considered that the main cause of the increase was ejection of electrons from the target material. (Classically, the greatest energy which a 10 MeV proton can transfer to a static electron is 5 KeV.) In later experiments, to prevent these electrons from being

intercepted by the counters, an electron deflection system was positioned before each counter. These deflection systems consisted of two collimating slits 3 cm. apart, with a permanent magnet between them (Fig. 2.6). The magnet had a maximum field strength of 500 gauss, which was sufficient to prevent a 5 KeV electron from traversing the second collimator. When the deflection systems were used, the energy resolution of the proton spectra improved from 50 KeV to 35 KeV.

3.3 Experimental Running Procedure

The counters were fixed at a distance of 10 cm. from the target. The aperture widths of the counter collimators were 2 mm. With this geometry, the angular energy spread of the scattered protons, within the solid angle defined by the collimators, never exceeded 10 KeV.

The experimental beam current varied between 75 and 150 nA depending upon the angular position of the most forward-angled counter. The time for an experimental run varied from between four to eight minutes. For each incident energy, four experimental runs were performed, corresponding to different positions of the rotating table; in this way,

sixteen points were determined for each angular distribution. The smallest scattering angle was 15°; in general, the spectra recorded at this angle were reasonably free from spurious scattering; an example of such a spectrum is shown in Fig. 3.1.

All the proton spectra were analysed with a dispersion of 800 channels; the spectra were stored on magnetic tape. Angular distributions were recorded at 100 KeV intervals within the incident energy range of 12 to 15 MeV. For all the experimental runs, the amplitude of the energy modulation was set at 100 KeV.

3.4 The Experimental Spectra

A typical experimental spectrum is shown in Fig. 3.2. It is evident that the target contained considerable amounts of oxygen and carbon. The possible reaction products, corresponding to an incident proton energy of 14.5 MeV, are listed below. The numbers in parentheses are equal to the C.M. kinetic energy of the light reaction products which leave the residual nucleus in the ground state; the energies are expressed in MeV.

Si^{28}	O^{16}	C^{12}
$Si^{28}(p,p')Si^{28*}$	$O^{16}(p,p')O^{16*}$	$C^{12}(p,p')C^{12*}$
$Si^{28}(p,2p)Al^{27*}$ [2.4]	$O^{16}(p,2p)N^{15*}$ [1.9]	
$Si^{28}(p,He^4)Al^{25*}$ [6.4]	$O^{16}(p,He^4)N^{13*}$ [8.8]	$C^{12}(p,He^4)B^{9*}$ [6.4]

The particle energy spectrum shown in Fig. 3.2 was recorded at a scattering angle of 155^0, for an incident proton energy of 14.5 MeV. It shows inelastic groups from silicon, carbon and oxygen, but there is little observable evidence for the other reactions; this result is not unexpected, since the more complicated reactions have smaller penetration factors than those corresponding to the inelastic proton reactions. The proton groups from all the known states in Si^{28}, up to an energy of 10 MeV, are present in the spectra. There is also evidence of the recently discovered 6.68 MeV state of Si^{28} (Lévesque, 1966).

3.5 Reduction of the Experimental Data

In the course of this experiment about one thousand proton spectra were recorded. Since each spectrum was composed of about forty lines, and with some lines only

partially resolved, hand analysis of the spectra was considered unpractical. A computer was therefore programmed to perform the data reduction. The computer programme included the following procedures :

1. Automatic determination and subtraction of the spectrum background.

2. Determination of the spectrum regions containing one or more peaks.

3. Determination of the number of peaks within a peak region.

4. Fitting of a standard shape to each peak within a peak region.

5. Determination of the probable error associated with each peak yield.

6. Identification of the Q value (energy of residual nucleus) associated with each peak.

7. Normalisation of the yields for electronic dead time and counter normalisation.

The different procedures will be described in the following sections.

The programme was written for the S.R.C. Atlas computer at Harwell. The programme execution time for a complete spectrum reduction was about 20 seconds.

3.6 The Spectrum Analysis Programme

(a) Peak Detection Routine

The start of a peak, or peak region, is taken to be determined if positive results are obtained for either of two sets of tests. Denoting the channel content, of channel I, as N(I), these tests are :

$$\text{1st Set.} \quad N(I+1) - N(I) > + \sqrt{N(I+1) + N(I)} \quad \underline{\text{and}} \quad N(I+2) - N(I+1) > + \sqrt{N(I+2) + N(I+1)} \tag{3.1}$$

$$\text{2nd Set.} \quad N(I+1) - N(I) > + 3\sqrt{N(I+1) + N(I)} \quad \underline{\text{and}} \quad N(I+2) \geqslant N(I+1) \quad \underline{\text{and}} \quad N(I+3) \geqslant N(I+2) \; . \tag{3.2}$$

The first test of the first set determines whether the difference in channel content between two adjacent channels

is greater than the standard error for the difference; if so, I is increased by unity and the test is performed a second time. A peak is therefore only detected if it is statistically significant above the background. The second set deals with those cases in which the peak rises sharply in one channel, and then remains reasonably constant over two or three channels. In a spectrum region devoid of any true peaks, it is still possible for a positive result to be recorded for either of the two sets of tests. The combined probability of this happening is 0.025, and so for a typical spectrum of 800 channels, about eight spurious peaks would be recorded; however, most of these peaks are rejected in the remaining parts of the programme.

To determine the end of a peak, or peak region, the following tests are performed :

$$\begin{aligned} &\text{1st Test.} && N(I) < N(IN) \\ &\text{2nd Test.} && N(I) - N(IN) < + \sqrt{N(I) + N(IN)} \end{aligned} \qquad (3.3)$$

where: N(IN) = channel content of the peak starting channel.

The second test determines if the difference between the channel contents of the starting channel and the current channel I is smaller than the error for the difference.

(b) Background Subtraction Routine

This routine first determines the non-peak regions of the spectrum, by utilising the peak detection routine to find the peak regions. In principle it is then possible, by using the least squares technique, to fit a polynomial to the non-peak regions. However, if the shape of the spectrum background is complicated, this procedure becomes unattractive because of the high order required for the polynomial. (The difficulty arises from the ill-behaviour of the inversion matrix (McCracken and Dorn, 1964).) To avoid this complication, the spectrum is divided into several parts, and a low order polynomial is fitted to each. Generous overlap is allowed between neighbouring segments, to ensure the polynomials join smoothly onto one another.

(c) Peak Fitting Routine

This routine first utilises a modified version of the peak detection routine to calculate the peak regions for the background subtracted spectrum. It is necessary to modify the peak detection routine, as outlined in part (a) of this section, because the R.H.S. of Eq. (3.1) should be calculated from the original spectrum, while the L.H.S. should be

calculated from the background subtracted spectrum.

The routine examines each peak region in turn to determine the number of peaks within the region. This is achieved by finding the number of times the first derivative of the spectrum curve becomes zero with negative second derivative.

The routine then proceeds to fit a Gaussian shape peak to each experimental peak within a region. The principle of the fitting procedure is to minimise the sum of the squares of the difference between the experimental and calculated channel contents; i.e., χ^2 is minimised, where χ^2 is given by

$$\chi^2 = \sum_{I=I_1}^{I_2} \frac{\left(NX(I) - \sum_i T_i \exp(-(EI_i-I)^2/DEV) \right)^2}{N(I)} \qquad (3.4)$$

where: I_1 = starting channel of peak region; I_2 = end channel of peak region; i = peak identifier; NX(I) = channel content for background subtracted spectrum.

The minimisation of χ^2 is carried out by an iteration procedure in which the amplitudes (T_i), channel positions

(EI_i) and widths (DEV) of the lines are iterated. The starting values of the different parameters are set equal to the associated experimental values. For example, the amplitudes (T_i) are initially set equal to the experimental channel contents of the peak channels. The widths (DEV) of the fitted lines for the different peak regions are allowed to vary, since the value of the experimental width may differ from spectrum to spectrum, due to a possible variance in the degree of energy compensation. However, all the line widths within a region are varied in a similar way.

A Gaussian shape was used in the fitting routine mainly because of its mathematical simplicity. It was not considered an advantage to use any other shape, since the actual experimental shape, due to incomplete energy compensation, varied for the different spectra. It was found that a Gaussian shape gave a reasonable fit, since the minimum value of χ^2, divided by the number of degrees of freedom, was generally of the order of unity.

(d) Error Routine

The yields associated with each experimental peak are calculated from the fitted Gaussian. The errors of the yields

are compounded of three parts: the background subtraction error, the statistical counting error and the fitting error. The error routine estimates the background error and counting error for a particular peak by first calculating a quantity E, given by

$$E = \sum_{I} \frac{(N(I) - NT(I))^2}{(\sum_{I} 1)^2} \qquad (3.5)$$

where: NT(I) = channel content of the fitted background; the sum extends over the neighbouring non-peak regions surrounding the peak region. The routine then calculates the combined error ER by the relation

$$ER = \left(\sum_{I}^{peak} N(I) + 12 \cdot DEV \cdot E\right)^{\frac{1}{2}} \qquad (3.6)$$

where: $2\sqrt{3 \cdot DEV}$ = number of significant channels in a peak.

The error associated with the fitting procedure is difficult to estimate, and for this reason the error routine gives no account of it. However, since χ^2_{min} is generally

of the correct order for a good fit, the error of the fitting procedure is likely to be smaller than EH.

(e) Kinematic Identification Routine

This routine identifies the Q values associated with the spectrum peaks. The first operation in the routine calibrates the energy-channel relationship by calculating the reaction energy associated with two peaks of well known Q values. From this calibration, the proton energies corresponding to the remaining peaks are easily calculated, and thus their Q values. The input data needed for this routine includes: proton incident energy, the counter angle and the peak centroids of the two calibration lines.

3.7 Analysis of the Angular Distributions

(a) Data Handling

The output data from the spectrum analysis programme was transferred onto fortran cards. Each card contained information about one particular proton group. This included: the yield value, the yield error, the counter angle, the Q value corresponding to the residual state and the energy of

the incident proton. These cards were then sorted into groups, corresponding to the different Q values and incident energies. The programme written to analyse these angular distributions is described in the following subsection.

(b) The Angular Distribution Programme

The first procedure in this programme converts the differential cross-sections from the laboratory frame of reference to the centre of mass frame. The conversion formulae are listed below.

Angle conversion:

$$\tan \theta_L = \sin \theta_c / (\sin \theta_c + \gamma). \qquad (3.7)$$

Differential cross-section conversion:

$$\sigma_c(\theta)/\sigma_L(\theta) = (1 + \gamma \cos \theta_c) / (1 + 2 \gamma \cos \theta_c + \gamma^2)^{3/2} \qquad (3.8)$$

where: $$\gamma^2 = \left(\frac{m_1}{m_2}\right)^2 \frac{E}{(E - Q(m_2/(m_1 + m_2)))} .$$

In these formulae c refers to centre of mass frame and L to the laboratory frame; E is equal to the incident energy,

and m_1, m_2 denote the mass of the incident particle and target nucleus.

The next procedure in the programme fits a series of Legendre polynomials to the experimental angular distribution. The fitting procedure determines the coefficients B_L of the expansion

$$Y(\theta) = \sum_{L=0}^{M} B_L P_L (\cos \theta). \qquad (3.9)$$

To determine the coefficients the principle of least squares is utilised; the quantity η^2 is minimised, where η^2_M is given by

$$\eta^2_M = \sum_{i=1}^{N} ((YE_i - Y_M(\theta_i)) \cdot w_i)^2 \qquad (3.10)$$

where: YE_i = experimental yield at angle θ_i; w_i is the weight of the experimental point, which is taken to equal the inverse of its standard error.

The routine determines the best value of M for a particular set of experimental points by calculating for different values of M the quantity μ^2_M

$$\mu^2_M = \eta^2_M / (N - M - 1). \qquad (3.11)$$

The best value of N is indicated when μ_N^2 becomes independent of N (Wilks, 1962). To avoid unnecessary computation, the method of orthogonal polynomials is used to calculate the different values of μ_N^2 (Ralston, 1965).

The errors in the coefficients B_L are calculated by expressing B_L in terms of the experimental quantities.

PROTON SPECTRUM FOR THE REACTION $Si^{28}(p,p')Si^{28*}$

E_p = 13·9 MeV ; SCATTERING ANGLE = 15°

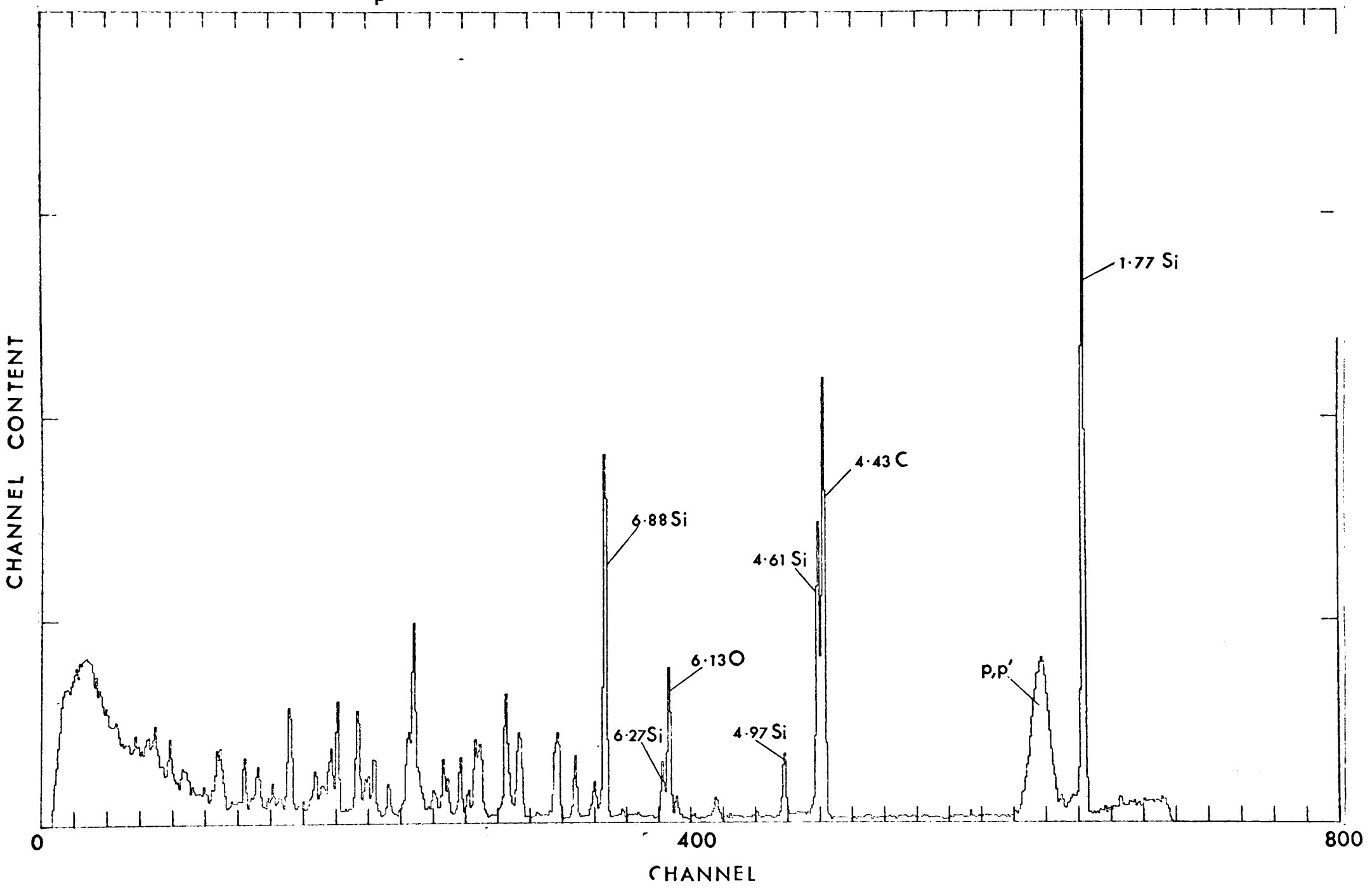

FIGURE 3.1

PROTON SPECTRUM FOR THE REACTION $Si^{28}(p,p')Si^{28*}$

E_p = 14·5 MeV ; SCATTERING ANGLE = 155°

Peak.	State (MeV)
1	0·0 Si
2	0·0 O
3	0·0 C
4	1·77 Si
5	4·61 Si
6	4·97 Si
7	4·43 C
8	6·27 Si
9	6·68 Si
10	6·88 Si; 6·13 O
11	7·38, 7·41 Si
12	6·92 O
13	7·80 Si; 7·12 O
14	7·93 Si

Peak.	State (MeV)
16	8·26 Si
17	8·33 Si
18	8·41 Si
19	8·59 Si
20	8·90 Si; 7·66 C
21	8·94 Si
22	9·17 Si
23	9·31 Si
24	9·41 Si
25	8·88 O
26	9·70 Si
27	9·76 Si
28	9·93 Si
29	10·18 Si; 9·59 O

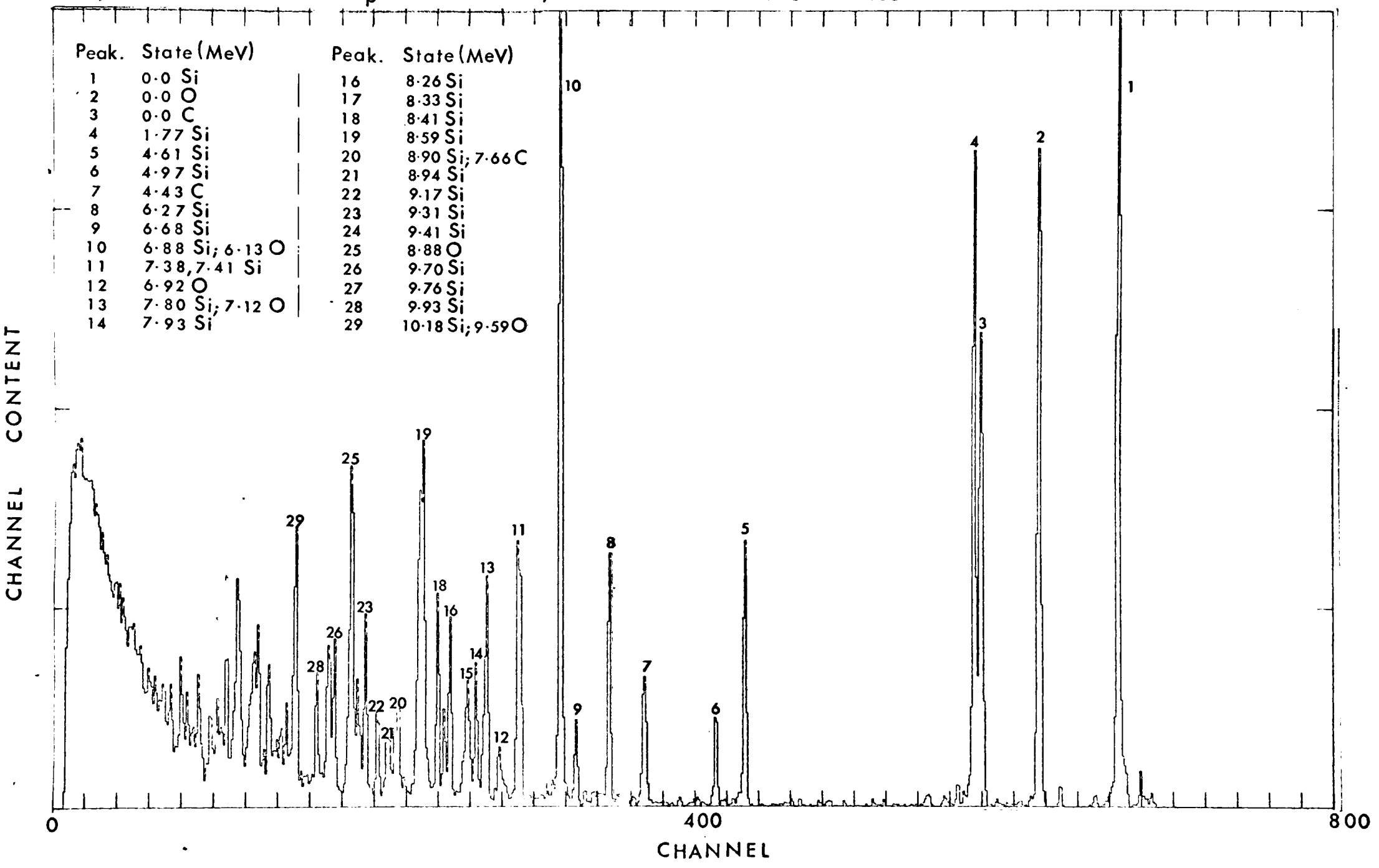

FIGURE 3.2

C H A P T E R 4

EXPERIMENTAL RESULTS

4.1 Angular Distributions

From the experimental spectra, angular distributions were determined for inelastic scattering from all states in Si^{28}, except the 6.69 state, up to an energy of 8 MeV, and for incident proton energies between 12.1 MeV and 14.9 MeV in 100 KeV steps. Angular distributions were also determined for the sum of the yields of all states above 8 MeV in Si^{28}.

The experimental angular distributions are shown in the figures of Appendix 8. To produce these figures a computer was programmed to print, on a lineprinter output, the experimental yields, the associated error bars and the fitted curve through the experimental points; these graphs were then photographically reduced in size. The axes of these graphs refer to the centre of mass scattering system; the y axes, except for the elastic scattering state, represent the yields by a linear scale; for the elastic state the y axes represent the yields by a logarithmic scale. In all cases the y axes are divided by ten markers; the highest

marker coincides with the highest experimental point. The relative normalisation of the top marker, for graphs corresponding to the same state, is represented by the value of N shown on each graph. To determine the absolute differential cross-section associated with a plotted point the following formula should be used

$$\frac{d\sigma}{d\Omega} = 1.6 \cdot \frac{Y}{10} \cdot N \cdot 10^{-3} \text{ mb. steradian}^{-1} \qquad (4.1)$$

where: N is equal to the number shown on the graph; Y is equal to the value of the yield expressed in terms of the y axis markers, the topmost marker being taken as a value of 10.

For the majority of cases the yield values plotted in these graphs were taken directly from the output of the spectrum analysis programme (Section 3.6). For those cases where a particular peak of interest was unresolved from a contamination peak, the programme only gave the sum yield for the two peaks. In this circumstance an estimate of the yield was made by subtracting from the sum yield the value of the contamination yield at an angle where the peak was resolved. If this procedure appeared to be dubious in any way (e.g., by the yield of the contamination line changing

rapidly with angle, or the contamination yield being comparable to the yield of interest) the data was rejected.

In the absence of interference from contaminants the angular distributions are represented by sixteen experimental points. However, due to a counter break-down, the angular distributions corresponding to the incident energy E = 13.6 meV are only represented by twelve experimental points.

The total cross-section corresponding to each angular distribution was determined by using the best fitted curve y(θ) through the experimental points in the following formula

$$\sigma = \int_0^{2\pi}\int_0^{\pi} y(\theta) \sin\theta \, d\theta \, d\varphi. \qquad (4.2)$$

The total cross-sections for inelastic scattering to different states in Si^{28} are shown in Fig. 4.1.

The coefficients of the expansion of y(θ) in terms of Legendre polynomials are shown, for the different angular distributions, in Figs. 4.2, 4.3; in the graphs the ratio B_L/B_0 is plotted as a function of energy, where

$$\frac{d\sigma}{d\Omega} = \sum_L B_L P_L(\cos(\theta)). \qquad (4.3)$$

4.2 Errors of the Experimental Quantities

The errors associated with the experimental yields consist of several components:

(a) Beam monitoring errors

(b) Beam averaging errors

(c) Errors of normalisation between the different counters

(d) Spectrum analysis errors.

To investigate the consistency of beam monitoring several long experimental runs were performed under identical conditions (no energy modulation or compensation). It was found that the experimental yields for the different runs were consistent to within 3 per cent. Part of this variation was probably due to a slight non-uniformity in the target thickness.

Since the experimental beam intensity fluctuated, it was possible for the shape of the energy averaging function to vary from run to run. To check the goodness of averaging between different experimental runs, part of the experimental energy range was investigated with good resolution and the yields then mathematically averaged over intervals of 100 KeV.

The values found in this way were consistent to within 5 per cent of the values found directly from the experimental energy modulation method.

Since four counters were used to determine the angular distributions, the normalisation between the different counters was required. To determine these normalisations, experimental spectra were recorded from the counters for different positions of the rotating table, in such a way that one or both pairs of counters were at the same scattering angle but on opposite sides of the scattering chamber. From the proton yields the relative normalisations between the different counters could be deduced to within 3 per cent.

For absolute determination of the nuclear cross-sections the solid angles which the counters subtended with the target were required; these angles were measured directly to within 10 per cent.

The spectrum analysis errors are discussed in Section 3.6. d. It was usually found that these errors were within 5 per cent.

From these estimations it was concluded that the relative magnitudes of the yields were uncertain to within 8 per cent; the absolute yields, due to the solid angle and target thickness errors, were uncertain to within 20 per

cent. In some cases the errors of the relative yields were increased to as much as 20 per cent due to contamination from other proton groups.

The relative total cross-section errors were computed from the angular distribution yield errors by assuming them to be independent. The average errors for the different cross-sections are indicated in Fig. 4.1.

4.3 Fine Structure Experiments

To determine the coherence width associated with the differential cross-sections for inelastic scattering from Si^{28}, an experiment was performed in which the inelastic scattering yields were measured at one particular angle with an incident beam resolution of 5 KeV. The incident energy was varied in 10 KeV steps from 12.5 MeV to 13.3 MeV. The differential cross-sections for inelastic scattering from six states of Si^{28} are shown in Fig. 4.4.

The method of peak counting was used to determine the coherence width Γ associated with the measured excitation functions. This method was introduced by Brink and Stephen (1963) who calculated the relation between Γ and the average number of maxima K per unit energy interval for an

N channel reaction to be

$$\Gamma = 0.5\, b_N/K \qquad (4.4)$$

where: $b_1 = 1$, $b_2 = 0.78$, $b_3 = 0.75$ and $b_\infty = 0.707$.

There appears to be some uncertainty as to the exact value of the constant in this equation, since for one-channel reactions Stephen (1963) has derived the relation

$$\Gamma = 0.587/K.$$

Van der Woude (1966) investigated the peak counting method by studying synthetic excitation functions; he concluded that the value of the constant only deviates a few per cent from 0.5, and the average number of maxima per unit interval is nearly independent of the number of channels participating in the reaction and the amount of direct interaction involved. In these studies $w(\Gamma/D)$ is generally taken to be much greater than unity (generally in the region of 100). However, in the present experimental situation this value is of the order of 7. How a low value of $w(\Gamma/D)$ affects eq. (4.4) is uncertain, but it is of note that a

recent study by Dallimore and Hall (1965) gives some evidence of the validity of the fluctuation theory when $\pi(\Gamma/D) \approx 6$.

For the above reasons Eq. (4.4) was used to calculate Γ but with the assumption that the variation of b_y with E could be ignored. The number of peaks in each curve of Fig. 4.4 is about the same, the average number being 7.5 peaks. Using this value, Eq. (4.4) gives a value for Γ of 50 ± 4 KeV. (The quoted error is obtained from the work of Van der Woude (1966) who concluded that for an excitation curve of interval length 15 Γ the standard error of Γ computed by the peak counting method is 20 per cent of Γ.) This value of Γ is within the scatter of values for other nuclei in this mass region. The aggregates of the experimental values of Γ for the compound nuclei Si^{29} (Cassagnou et al., 1963; Cadioli et al., 1964; Naqib et al., 1965; Rössle, 1965), Al^{27} (Häusser et al., 1964; Allardyce et al., 1965; Allardyce et al., 1966) and Si^{28} (Allardyce et al., 1964; Bizzeti et al., 1964; Rauch and Rössle, 1964; Sommer, 1964; Budd et al., 1965; Singh et al., 1965) are within the region 40 ± 20 KeV.

4.4 Correlation between the Inelastic Reaction Cross-sections

This section gives the results of an investigation which was carried out to determine whether there is a significant correlation between the structures of the experimental excitation functions commented upon in Section 4.1.

(a) The Cross-correlation Function

Several workers analysing reaction cross-section data have used the cross-correlation function to determine if there is correlation between different reaction excitation functions. If any two excitation functions are denoted by σ_i and σ_j then the cross-correlation function is defined by

$$R_{ij}(\epsilon) = \frac{\langle (\sigma_i(E+\epsilon) - \langle \sigma_i(E+\epsilon) \rangle)(\sigma_j(E) - \langle \sigma_j(E) \rangle) \rangle}{\langle \sigma_i(E+\epsilon) \rangle \langle \sigma_j(E) \rangle} \qquad (4.5)$$

where: $\langle x \rangle$ = energy average of x over the experimental energy range.

In the absence of correlation between excitation functions which are of infinite energy range the value of $R_{ij}(\epsilon)$ is zero; for any experimental situation, however, it is possible to obtain a finite value of $R_{ij}(\epsilon)$ due to

the limited statistical sampling. It is therefore of great importance to be able to estimate the finite energy range of data (F.E.D.) error associated with $R_{ij}(e)$. This problem, together with its related aspects, has been considered by several authors (Hall, 1964; Dallimore and Hall, 1965; Dearnaley et al., 1965; Gibbs, 1965[a]; Gibbs 1965[b]; Halbert and Böhning, 1965). Hall (1964) originally calculated the errors by assuming the excitation functions to be composed of n independent points, where $n\Gamma$ is the experimental energy range and Γ the coherence width of the excitation functions. The F.E.D. error for $R_{ij}(e)$ (expressed as a standard deviation) was calculated to be

$$ER = 1/(nN_iN_j)^{\frac{1}{2}} \qquad (4.6)$$

where: N is the fluctuation damping coefficient arising from the effective number (N) of equally contributing independent reaction channels.

It has been pointed out, however, that the assumption of no correlation between points Γ apart in an excitation function is invalid (Dallimore and Hall, 1965; Gibbs, 1965[a]; Gibbs, 1965[b]). Dallimore and Hall (1965) investigated the F.E.D. errors by synthesising artificial excitation

functions from a sum of Breit-Wigner amplitudes; they concluded that the P.T.D. error for $R_{ij}(e)$ should be

$$\Delta R = (\pi/2nN_iN_j)^{\frac{1}{2}} . \qquad (4.7)$$

The question of the effective number of channels N associated with total reaction cross-section excitation functions has been discussed by Ericson (1963). He has argued that if a reaction between two states c and c' only takes place by a compound nucleus mechanism, then the effective number of channels associated with the total reaction cross-section is

$$N = \frac{\left(\sum_c \frac{(2J+1)\, T(c\, l\, s)\, T(c'l's')}{(\Gamma_{J\pi}/D_{J\pi})} \right)^2}{\sum_c \frac{(2J+1)^2\, T^2(c\, l\, s)\, T^2(c'l's')}{(\Gamma_{J\pi}/D_{J\pi})^2}} \qquad (4.8)$$

where: $T(c\, l\, s)$, $T(c'l's')$ are the transmission coefficients for the reaction particles in the entrance and exit channels respectively; the sum over c includes the sum over the quantum numbers J, π, l, l', s and s' (see Section A5.1).

Before the Eqs. (4.7) and (4.8) could be applied to the experimental situation studied in this thesis they had to be extended to the case of energy averaged excitation functions. The following considerations suggested the way in which this might be done. It has been shown by Lang (1965) that if an excitation function, having coherence width Γ, is measured with a Lorentz-type energy averaging function, having a F.W.H.M. value of Δ, then the coherence width of the resulting excitation function is

$$\Gamma_{\Delta} = \Gamma + \Delta \qquad (4.9)$$

This suggests that the value of n to use in Eq. (4.7) should equal the ratio of the experimental energy range to the width Γ_{Δ}. Lang also shows that the variance of the fluctuations of an excitation function decreases by the factor $\Gamma/(\Gamma + \Delta)$ when the excitation function is measured with a Lorentz averaging function. This then suggests that the damping coefficient associated with the energy averaged excitation function is $N(\Gamma + \Delta)/\Gamma$ compared with N for the original excitation function.

The energy averaged cross-sections determined by this experiment (Fig. 4.1) were measured with a rectangular

shape averaging function and not with a Lorentz shape function; the effect of a rectangular shape averaging function on N and n is considered in Appendix 4.

(b) Experimental Results

The cross-correlation functions $R_{ij}(e)$ for different combinations of experimental excitation functions (Fig. 4.1) are shown in the graphs of Figs. 4.5, 4.6; in these figures the y-axis normalisations are the same for all the graphs in any column. The value of the argument e could only be varied in discrete steps of 100 KeV since the experimental excitation functions were measured at 100 KeV intervals. The errors indicated on the side of each graph are the probable P.M.D. errors calculated from Eq. (4.7) with the appropriate values of N and n. The P.M.D. errors for the combinations which include the elastic scattering excitation function are not shown because of the uncertainty in the value of N for the elastic scattering reaction.

If the different excitation functions (Fig. 4.1) are uncorrelated, then in any one graph of Figs. 4.5, 4.6 there should be approximately the same number of points lying within the error bar as there are outside. The interpretation of the results involving the excitation

functions corresponding to inelastic scattering to the lower energy states of Si^{28} is made more complicated by the possible presence of a direct reaction mechanism; this causes the values of $R_{ij}(e)$ to be depressed. Nevertheless, there are at least four different excitation functions which, when correlated with the 1.77 MeV state excitation function, give $R_{ij}(e)$ values greater than the associated F.R.D. error over an interval of 300 KeV. The two main conclusions which can be drawn from Figs. 4.5, 4.6 are:

(1) Of the forty possible different combinations of the experimental excitation functions, only six cases have negative $R_{ij}(e)$ values for $e = 0$.

(2) For the majority of the combinations which exclude the 6.27 MeV and 6.88 MeV state excitation functions, the values of $R_{ij}(e)$ are positive for a region of several hundred KeV centring around $e = 0$, and, for many of these cases, the values within this region are consistently greater than the calculated F.R.D. error.

Both these conclusions are contrary to what would be expected in the absence of correlation between the excitation functions. It may be concluded that there is some evidence of correlation between the excitation functions

corresponding to inelastic scattering to the 0.0, 1.77, 4.61, 4.97, 7.4, 7.8 and 7.93 MeV states of Si^{28}.

Further evidence of correlation between the experimental excitation functions may be educed from Fig. 4.1; this figure shows graphs of the experimental reaction cross-sections, together with composite graphs summing several of these reaction cross-sections. It is clear that there is correlation between the structures of the single and compounded excitation functions - a result which is contrary to that which would be expected if the reaction cross-sections were uncorrelated.

4.5 Correlation between Differential Reaction Cross-sections

One of the predictions of the doorway state theory of intermediate structure (see Section 1.9) is that there may be a correlation of structure between differential cross-section excitation functions measured at widely different angles. Experimental differential cross-sections for inelastic scattering to the 4.61 MeV and 4.97 MeV states of Si^{28} are shown in Fig. 4.7. From this figure it will be seen that there is some similarity between the structures of the excitation functions corresponding to different scattering angles.

Some angular correlation would be expected if the reaction mechanism were of a statistical nature. Brink, Stephen and Tanner (1964) have calculated the expected correlation by assuming that the outgoing reaction waves are emitted by uncorrelated sources on the nuclear surface. They conclude that if α is the angle between two outgoing directions, then strong correlations should only exist between the differential cross-sections when

$$2KR \sin(\alpha/2) < 1 \qquad (4.10)$$

where: R = radius of nucleus; K = wave number of the emitted waves.

In the present experimental situation this statistical model gives an upper limit of about 18° for the angle between the outgoing particles, for which the corresponding differential cross-sections should be correlated. From the experimental data (Fig. 4.7) it seems that the correlations extend over a much wider angle than this model predicts.

INELASTIC REACTION CROSS SECTIONS
Si (P, P') Si'

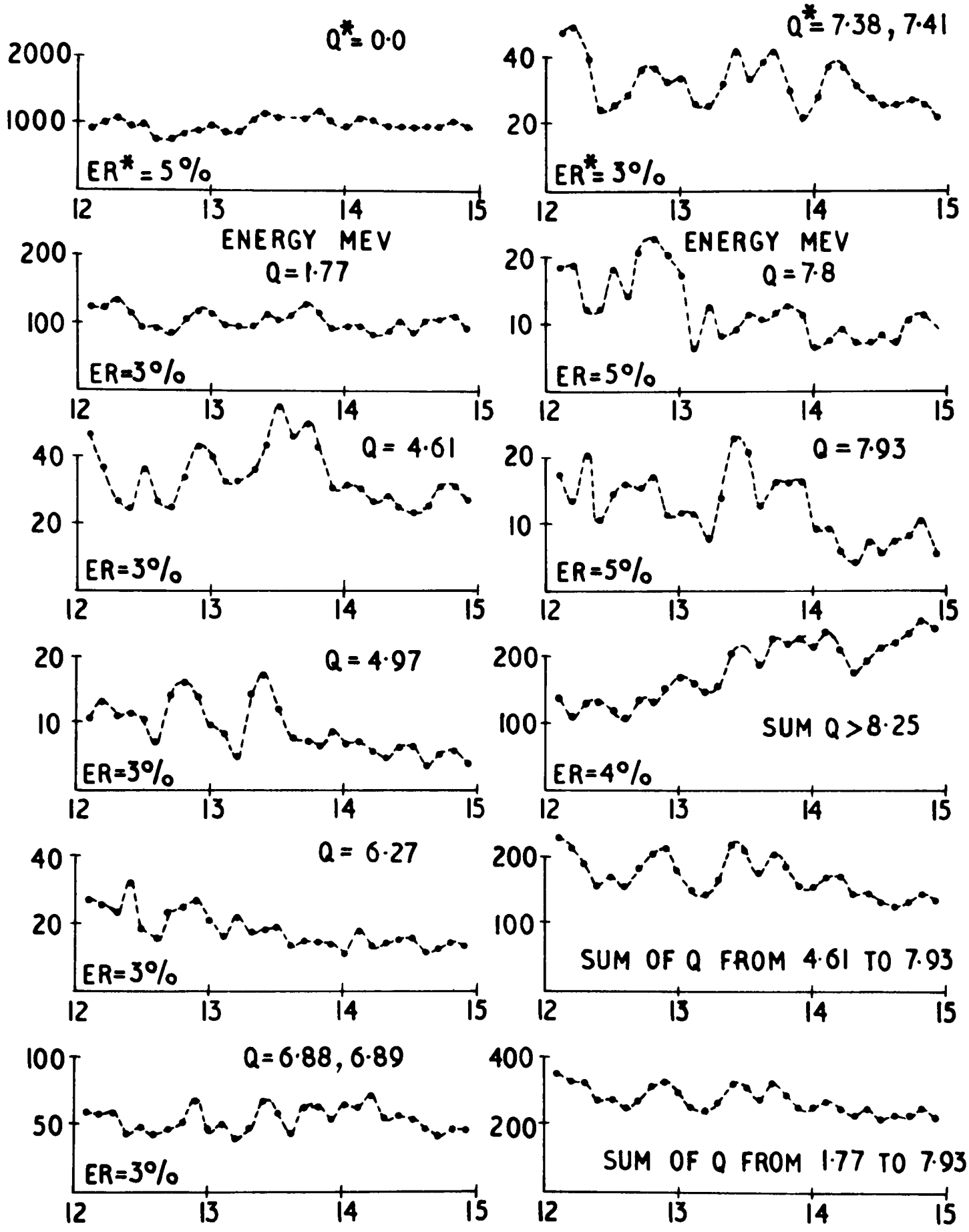

*ER = AVERAGE STANDARD ERROR OF CROSS SECTIONS

*Q=EXCITATION ENERGY OF RESIDUAL STATE IN Si(28)

N.B. UNITS OF Y AXIS ARE IN mb.

FIGURE 4·1

NORMALIZED LEGENDRE COEFFICIENTS (B_L / B_0)
FOR THE ANGULAR DISTRIBUTIONS $Si(P,P')Si^1$

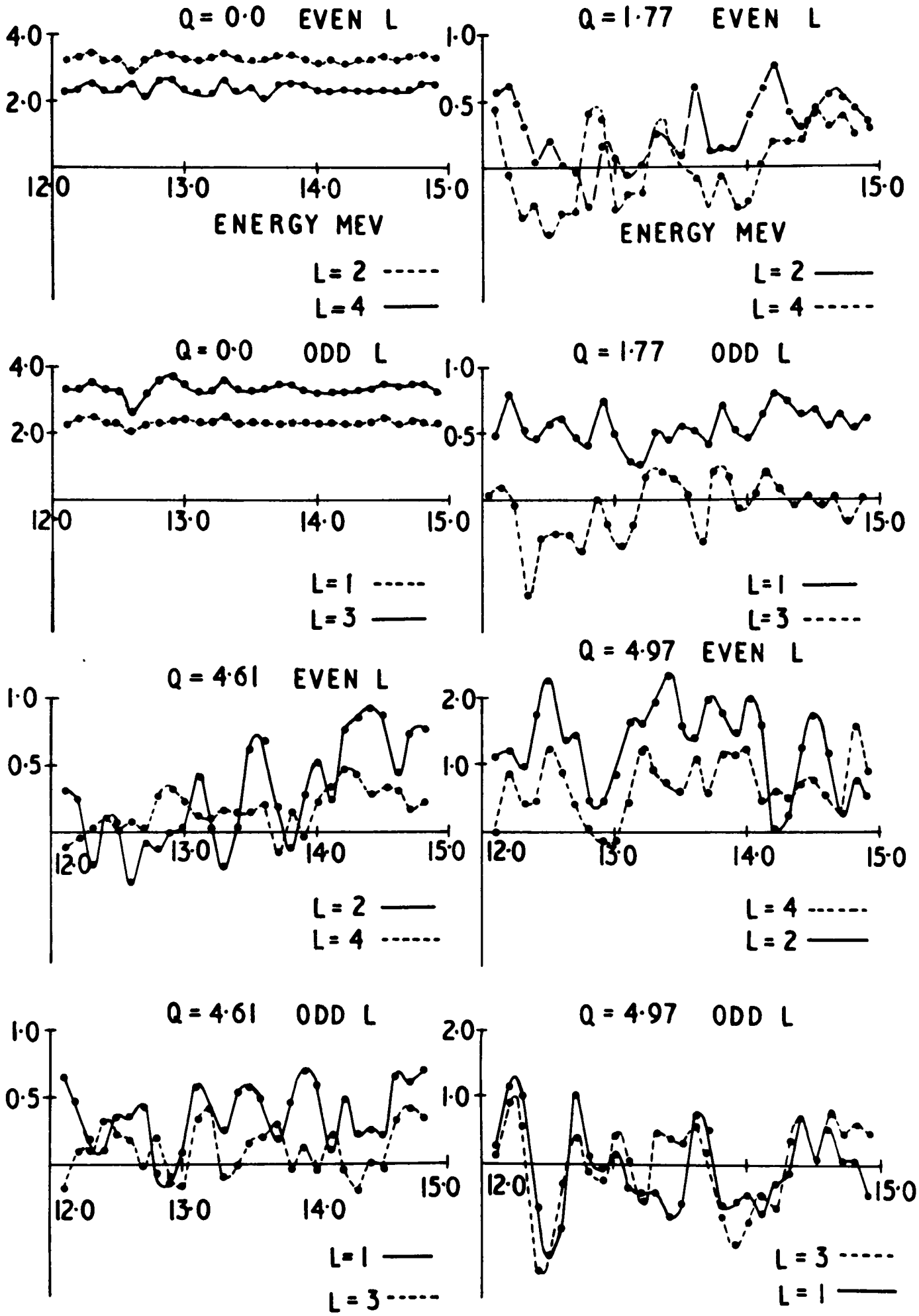

FIGURE 4·2

NORMALIZED LEGENDRE COEFICIENTS (B_L/B_0)
FOR THE ANGULAR DISTRIBUTIONS Si (p, p') Si

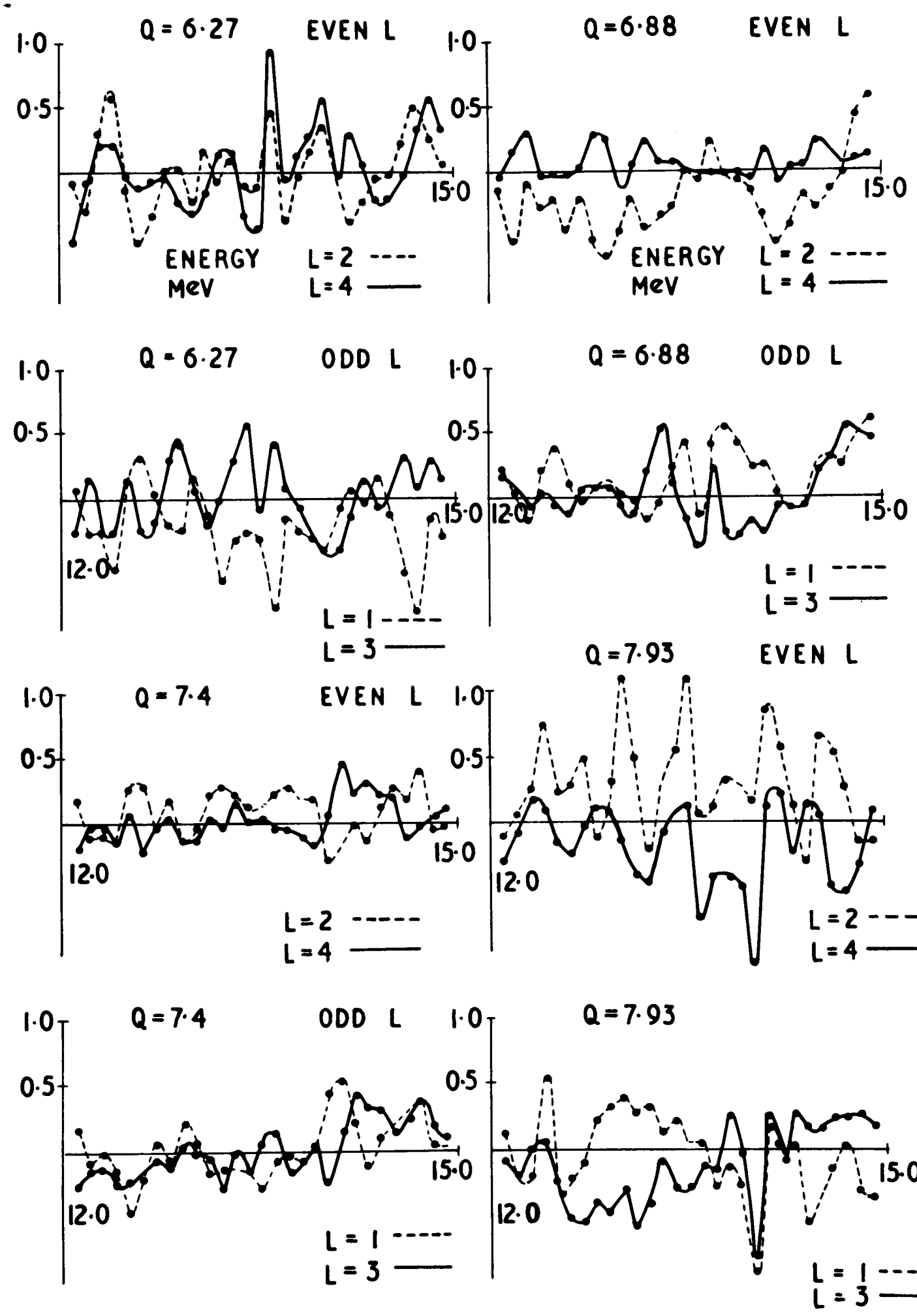

FIGURE 4·3

DIFFERENTIAL CROSS SECTIONS $Si(P, P^1)Si^1$
SCATTERING ANGLE 146° ENERGY RESOLUTION 5 KEV

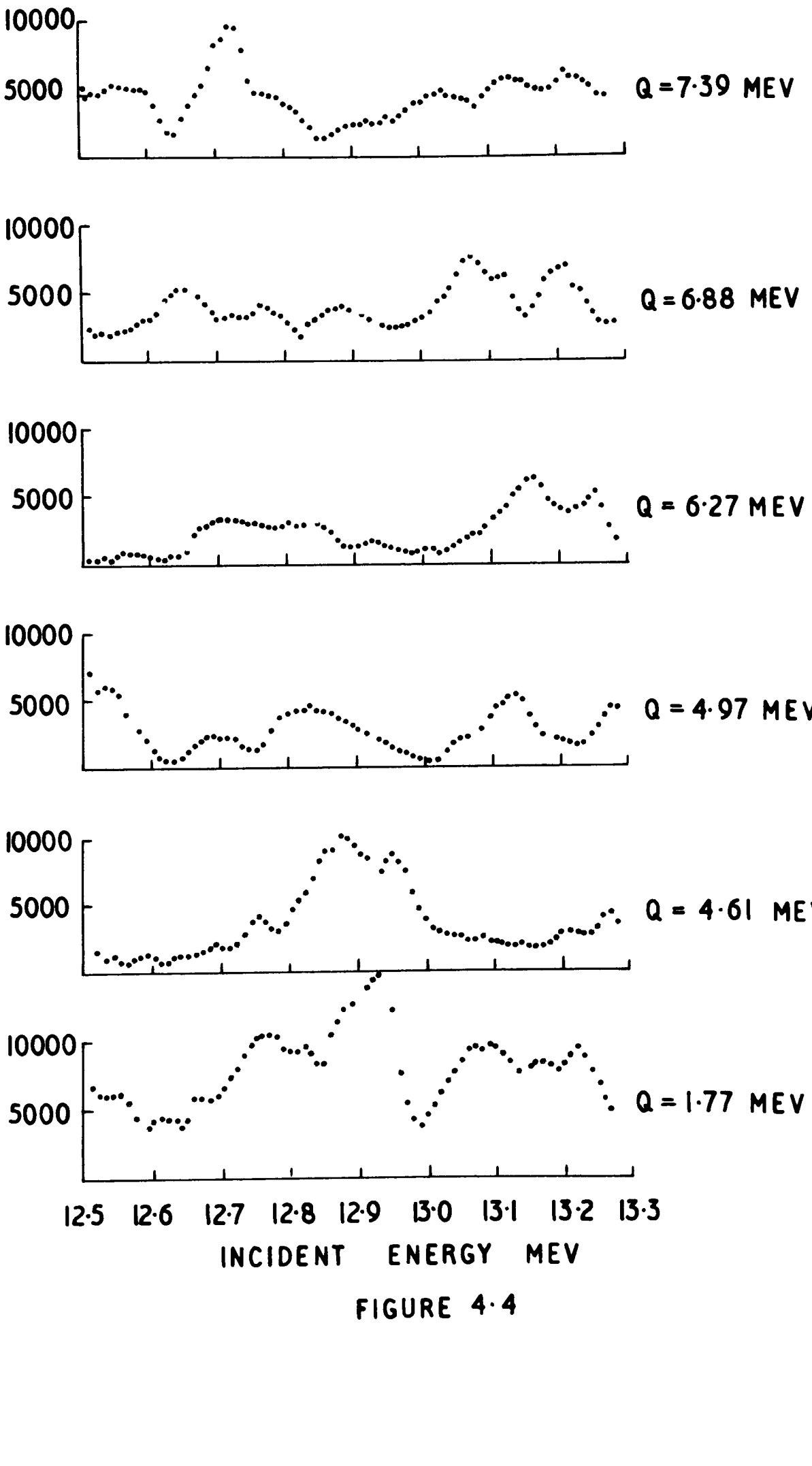

FIGURE 4·4

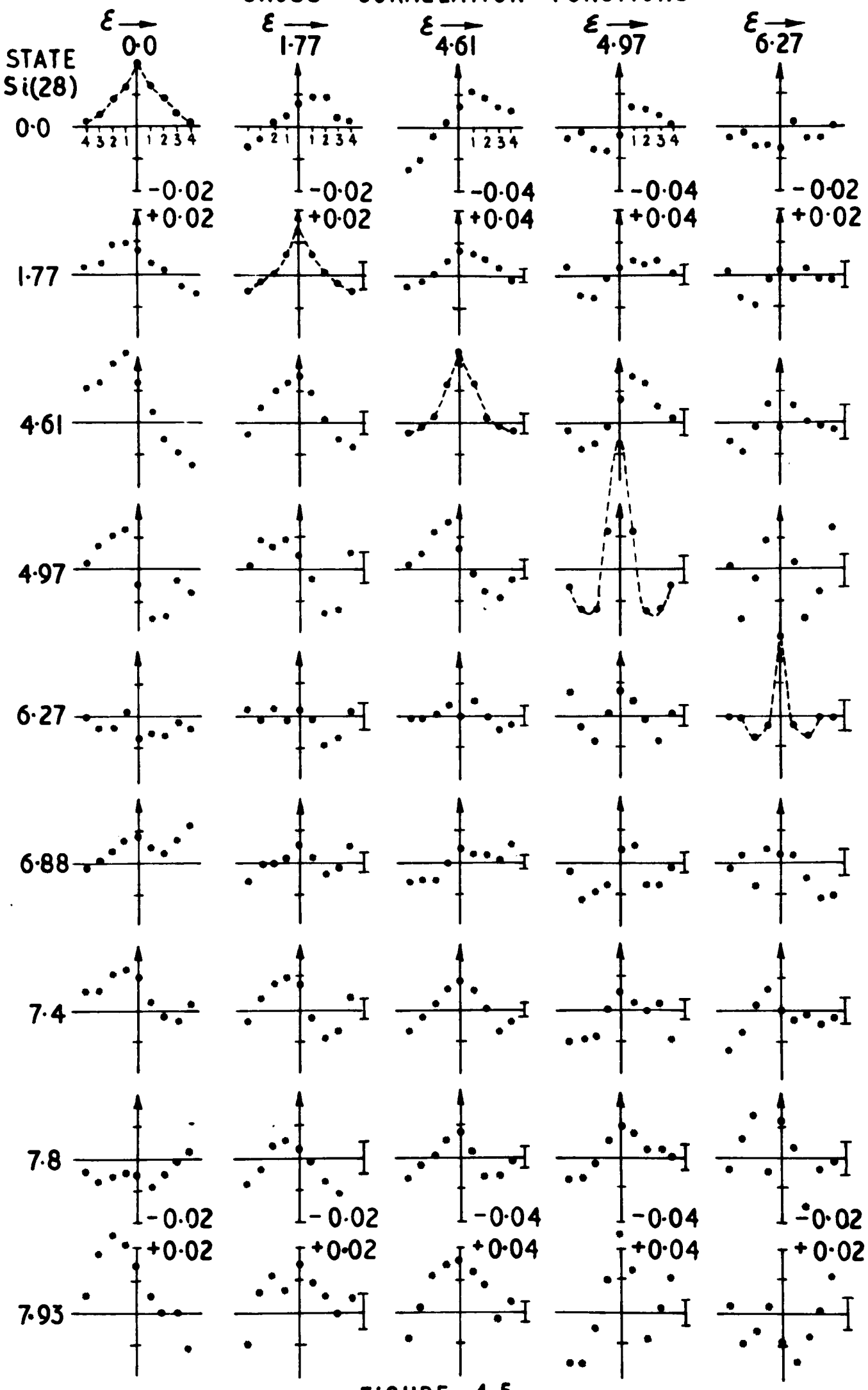
CROSS CORRELATION FUNCTIONS
STATE Si(28)
ε 0·0
ε 1·77
ε 4·61
ε 4·97
ε 6·27
0·0
1·77
4·61
4·97
6·27
6·88
7·4
7·8
7·93
-0·02
+0·02
-0·04
+0·04
-0·02
+0·02

FIGURE 4·5

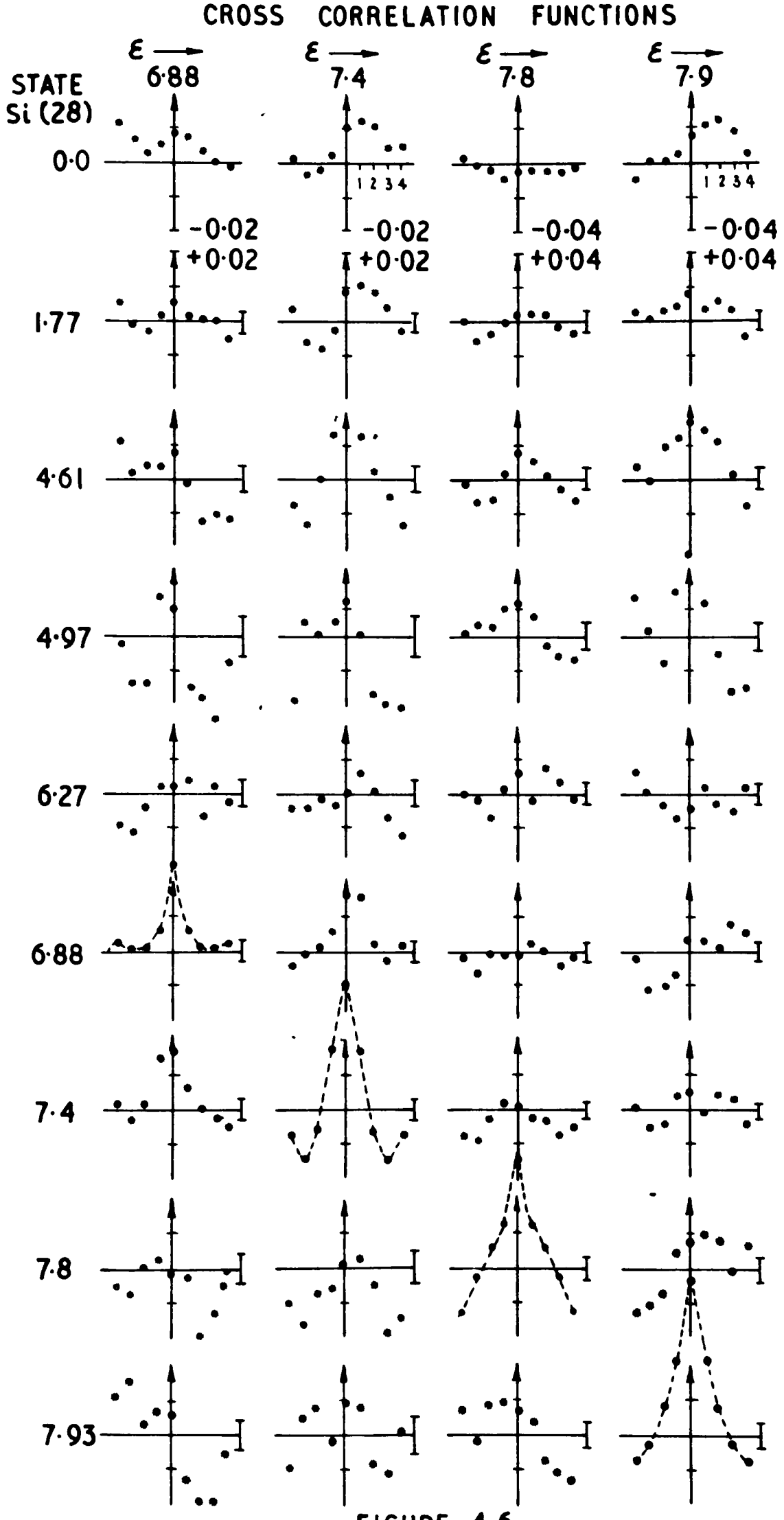
CROSS CORRELATION FUNCTIONS
STATE Si (28)
ε → 6·88
ε → 7·4
ε → 7·8
ε → 7·9
0·0
1·77
4·61
4·97
6·27
6·88
7·4
7·8
7·93
-0·02
+0·02
-0·02
+0·02
-0·04
+0·04
-0·04
+0·04
1 2 3 4
1 2 3 4

FIGURE 4·6

DIFFERENTIAL CROSS SECTIONS

Si (P, P') Si'

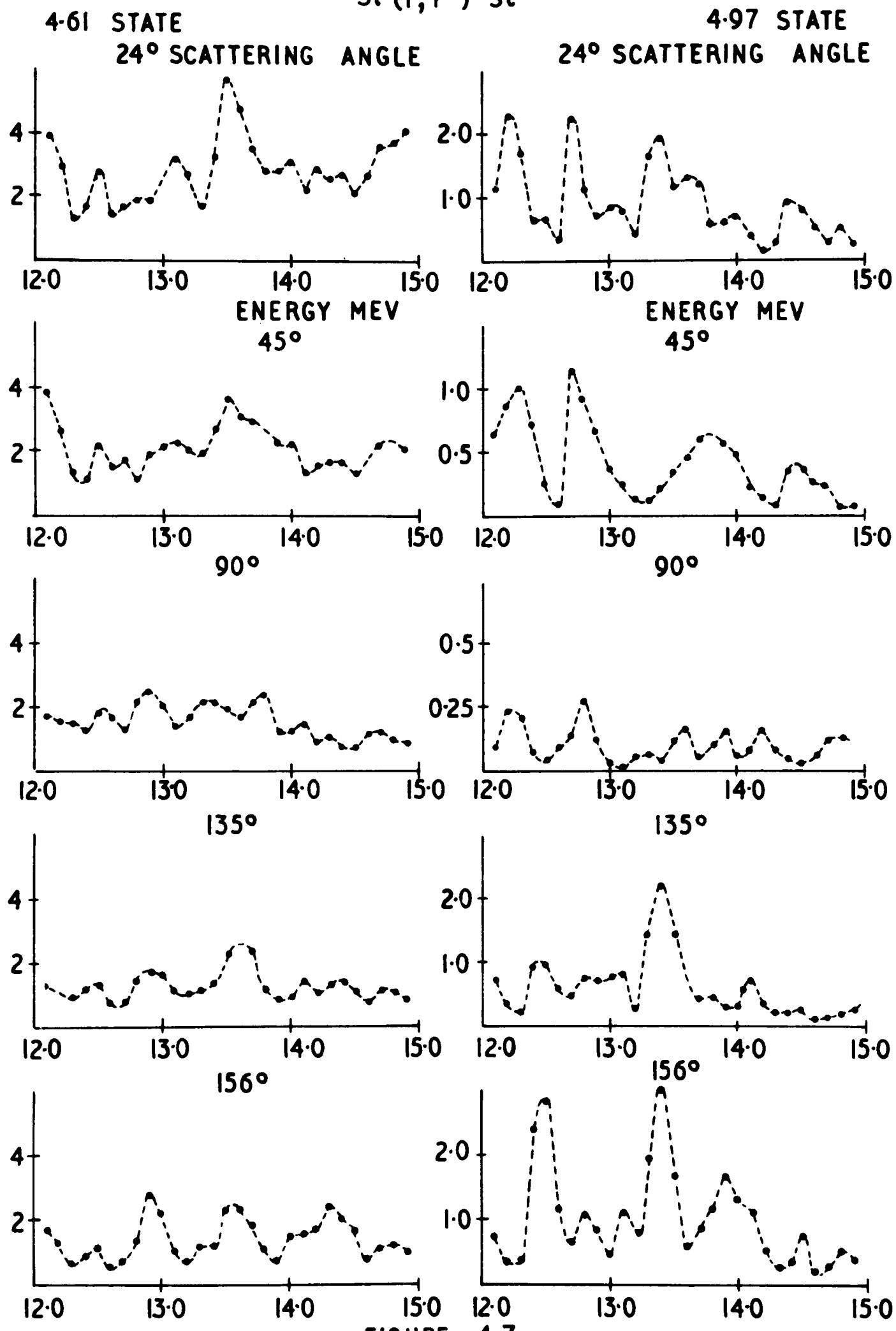

FIGURE 4·7

C H A P T E R 5

THE EXPERIMENTAL RESULTS AND THE STATISTICAL MODEL

5.1 Introduction

In this chapter a comparison is made between the experimental reaction data and the predictions from the hypothesis that the reaction mechanism is wholly of a statistical nature.

The statistical theory of the reaction mechanism is considered in Appendix 5. Using assumptions about the random nature of the widths and energy spacings of the compound nucleus levels which enter into the theory, it is shown that for a reaction between two states a and a', in which the direct reaction component is small, the total cross-section variance defined as

$$\mathrm{var}\,(\sigma(a|a')) = \langle (\sigma(a|a') - \langle \sigma(a|a') \rangle)^2 \rangle \qquad (5.1)$$

is given by

$$\mathrm{var}\left(\sigma(a|a')\right) = \sum_{J\pi\beta} \langle \sigma(aa',\beta J\pi)\rangle^2 \left(1 + \frac{1}{\pi(\Gamma(J\pi)/D(J\pi))}\right)$$

$$+ \sum_{J\pi} \left\langle \sum_{\beta} \sigma(aa',\beta J\pi)\right\rangle^2 / (\pi\Gamma(J\pi)/D(J\pi)) \qquad (5.2)$$

where: the angle brackets denote an average over energy; β denotes the quantum numbers ℓ, s, ℓ', s' (see Section A5.1); $\sigma(aa',\beta J\pi)$ are the partial reaction cross-sections (see Eq. (5.4)); $\Gamma(J\pi)$,$D(J\pi)$ are the average widths and energy spacings of the compound nucleus levels having quantum numbers J and π.

The first term in this equation mainly originates from interference between the reaction amplitudes of the different compound nucleus resonances which are associated with the same set of quantum numbers J, π and β. The structure of the second term results from the fact that the partial cross-sections $\sigma(aa',\beta J\pi)$, for different β, are associated with the same set of compound nucleus levels (J,π); a random grouping of these levels will therefore have a similar

effect on all the partial cross-sections. The first term in the equation remains finite when $(\Gamma/D) \gg 1$, but the second term becomes negligible; for this reason only the first term is considered in most analyses. For the experimental situation studied in this thesis, however, $(\Gamma/D) \approx 1$, and so for this reason both terms of Eq. (5.2) are considered in this chapter.

The cross-sections determined by this experiment were measured with a finite energy resolution, and so before the values calculated from Eq. (5.2) could be compared with the experimental data, it was necessary to investigate the reduction of cross-section variances caused by finite energy resolution. This reduction has been considered by Lang (1965), and his results for a box shape resolution function (as used in this experiment) are considered in Appendix 4. It is shown, in this appendix, that the ratio of the variance for a cross-section measured with a box shape resolution function of energy width 2Δ to the cross-section variance measured with good energy resolution is given by

$$\frac{(\mathrm{var}\,(\sigma(a|a'))\,)_{\Delta}}{(\mathrm{var}\,(\sigma\,(a|a'))\,)_{\Delta=0}} = R(\Gamma/\Delta) \qquad (5.3)$$

where the function R is plotted in Fig. A4.1.

5.2 Calculation of the Cross-section Variance

In using Eq. (5.2) to calculate the cross-section variance, the values of the averaged partial cross-sections were required; these values were computed by using the following statistical model formula (Hauser and Feshbach, 1952; Preston, 1962) :

$$\langle \sigma(a|a') \rangle = \sum_{J\pi\beta} \langle \sigma(aa', \beta J\pi) \rangle$$

$$= \sum_{J\pi} g(J) \sum_{\beta} \left\langle \frac{T(a\ l\ s)T(a'\ l'\ s')}{\sum_{\beta}(\Gamma(J\pi)/D(J\pi))} \right\rangle \qquad (5.4)$$

where: $T(a\ l\ s)$, $T(a'\ l'\ s')$ are the transmission coefficients for protons in the entrance and exit channels respectively; $g(J) = \frac{\pi \lambda^2 (2J+1)}{(2I+1)(2i+1)}$, in which I = spin of the target nucleus and i = spin of the incident particle.

The functional dependence of $(\Gamma(J\pi)/D(J\pi))$ upon J for the compound nucleus P^{29} is discussed in Appendix 7, with the conclusion that the function is likely to vary

between two limited forms, each distinguished by a different value of the spin cut-off parameter of the residual nucleus Si^{28}. These two functions, corresponding to Si^{28} spin cut-off parameters (hereafter S.C.P.) of 2.0 and 2.25, are shown in Fig. A7.3.

The values of the transmission coefficients used in Eq. (5.4) were deduced from those calculated by Moldner and Linder (1964) who used the optical model parameters of Perey (1963). These coefficients are plotted in Fig. 5.1.

In the use of Eqs. (5.2), (5.4) to calculate the cross-section variances, it was assumed that the factors containing the average product of the transmission coefficients could be replaced by the value of the product corresponding to the central energy of the experimental range.

In using Eq. (5.3) to calculate the variance for averaged cross-sections the function $R(\Gamma/\Delta)$ was assumed to be independent of J and π; the value of Γ was set equal to the value found from the high resolution experiment (see Section 4.3), and the value of Δ was taken to equal 50 KeV.

The experimental values of the cross-section variances were determined by fitting a smooth curve through the experimental points, and then calculating the mean squared

deviation of the points from this curve. The calculated and experimental values of the variances, corresponding to Si^{28} S.C.F.'s of 2.0 and 2.25, are shown in Figs. 5.2, 5.3 for the different inelastic reactions.

The two states at 6.88 and 6.89 MeV were experimentally unresolved, and so the experimental value of the variance corresponds to the sum of these two cross-sections. For this reason the corresponding calculated value (see Appendix 5) was computed from the equation

$$\mathrm{var}\left(\sum_n \sigma(a|a_n)\right) = \sum_{n\beta Jw} \langle \sigma(aa_n,\beta Jw)\rangle^2 \left(1+\frac{1}{\pi(\Gamma(Jw)/D(Jw))}\right) + \sum_{Jw}\left\langle\sum_{n\beta}\sigma(aa_n,\beta Jw)\right\rangle^2 / (\pi\Gamma(Jw)/D(Jw)) \qquad (5.5)$$

where: the sum over n just includes the 6.88 and 6.89 MeV states.

The states at 7.38 and 7.41 MeV were similarly unresolved, and so in this case also Eq. (5.5) was used to calculate the variance.

The errors indicated in Figs. 5.2, 5.3 were calculated

from the finite range of data error formulae given by Hall (1964) and Dallimore and Hall (1965).

5.3 Discussion of the Results

It is evident from Figs. 5.2, 5.3 that the calculated values of the cross-section variances for inelastic scattering to different residual states in Si^{28} are consistently greater than the experimental values. Some understanding of the reason for this can be gained from a study of Figs. 5.4, 5.5. In these figures the experimental values of the averaged total reaction cross-sections, corresponding to a centre of mass incident energy of 13 MeV, are plotted against the values calculated from Eq. (5.4). The points of each graph, excluding the 1.77 MeV state, form a more or less linear trend. (The large deviation of the 1.77 MeV state from the linear trend is probably the result of a direct mechanism in the reaction process. This effect may also be present, to some extent, in the other reactions.) It is clear that, for both values of the Si^{28} S.C.P., the calculated values of the averaged cross-sections are greater than the corresponding experimental values. One possible reason for this discrepancy is

incorrect normalisation of the ($\Gamma(Jw)/D(Jw)$) ratios (see Appendix 7). The calculated values of the averaged cross-sections are inversely proportional to this normalisation, and so the slopes of the lines drawn in Figs. 5.4, 5.5 suggest that the renormalisation factors for the corresponding ($\Gamma(Jw)/D(Jw)$) ratios should be 1.75 and 1.65.

Using the renormalised values of ($\Gamma(Jw)/D(Jw)$) the variances for the different cross-sections were recalculated; these values are shown in Figs. 5.6, 5.7 for the two spin parameters. These figures show that there is closer agreement between the experimental and calculated values than in the figures considered earlier. The renormalisation argument therefore appears to be consistent in that, at the same time, both the averaged cross-sections and the cross-section variances can be brought into reasonable agreement with the experimental data. In Section 5.7 further evidence is presented to support this argument.

The reason for the large experimental variance associated with the 1.77 MeV state is probably interference between the direct and compound reaction amplitudes. The following expression, used to estimate the corresponding increase in variance $var_{DC}(\sigma)$, was suggested by the work of several authors (Ericson, 1963; Brink and Stephen, 1963;

Hateliff, 1964) :

$$\mathrm{var}_{DC}(\sigma(a|a')) = 2\pi(\Gamma/\Delta) \sum_{J\pi\beta} \sigma_D(aa',\beta J\pi)\,\sigma_C(aa',\beta J\pi) \qquad (5.6)$$

where: σ_D = direct reaction component of the cross-section;
σ_C = compound nucleus component of the cross-section.

In order to evaluate this expression the ratio between σ_D and σ_C was estimated by using Fig. 5.4; assuming that this ratio is independent of the quantum numbers J, π and β, the value of $\mathrm{var}_{DC}(\sigma)$ is about 100 mb^2. This value, in spite of this crude assumption, is not inconsistent with the plotted point in Fig. 5.6.

Figures 5.6, 5.7 show that there is only a small difference between the calculated values of the variances corresponding to the two Si^{28} S.C.P.s; therefore, the calculations discussed in the rest of this chapter are only concerned with a Si^{28} S.C.P. of 2.0.

5.4 The Variance of Compounded Excitation Functions

If the reaction cross-sections for inelastic scattering to different residual states in Si^{28} (Fig. 4.1) are completely

uncorrelated, then the variance of a compounded excitation function, produced by adding several of the reaction cross-sections together, should be equal to the sum of the variances of the associated reaction cross-sections, i.e., if

$$\sigma_c = \sum_n \sigma(a \mid e_n) \tag{5.7}$$

then

$$\mathrm{var}(\sigma_c) = \sum_n \mathrm{var}(\sigma(a \mid a_n)) \tag{5.8}$$

where: n labels the inelastic reaction channel.

To test the validity of this last equation (Eq. (5.8)) several compounded excitation functions were generated, each corresponding to a different combination of the experimental reaction cross-sections, and the variances of these compounded excitation functions were determined in a similar way to that outlined in Section 5.2. These values, together with the variances computed from Eq. (5.8) (using the calculated values of the cross-section variances

plotted in Fig. 5.2), are shown in Fig. 5.8. The slopes of the lines drawn in Figs. 5.2, 5.8 are the same. If Eq. (5.8) is correct, then in Fig. 5.8 the plotted points should be distributed about the line; it is evident from this figure that the experimental values are greater than those calculated from Eq. (5.8).

If some correlation exists between the individual reaction cross-sections (Fig. 4.1) then the experimental variance of a compounded excitation function will be greater than the value computed from Eq. (5.8). The distribution of points in Fig. 5.8 therefore suggests that there is some correlation between the individual reaction cross-sections. On the basis of the doorway state theory of intermediate structure such correlation is not unexpected (see Section 1.6.c). However, when $(\Gamma/D) \approx 1$, as in the present experimental situation, some correlation is also to be expected from the statistical theory of the reaction mechanism. The correlation in this case is due to the fact that the different reaction channels a_n are associated with the same sets of compound nucleus levels (J,π), and so a random grouping of these levels will affect all the reaction cross-sections in a similar way. The

increase in the variance of a compounded excitation function caused by this random grouping effect is further considered in the following paragraphs.

It is shown in Appendix 5 (see Eq. (A5.34)) that, on account of the random grouping effect, the variance of a compounded excitation function should be computed from the equation

$$\mathrm{var}(\sigma_c) = \sum_n \mathrm{var}(\sigma_n) + \sum_{Jwnn'} \left(\frac{\langle \sum_\beta \sigma\,(\alpha\alpha_n, \beta Jw) \rangle \langle \sum_\beta \sigma\,(\alpha\alpha_{n'}, \beta Jw) \rangle}{w\,\Gamma\,(Jw)/D(Jw)} \right)_{n \neq n'} \tag{5.9}$$

Comparison of this equation with Eq. (5.8) shows that the random grouping effect enhances the value of $\mathrm{var}(\sigma_c)$; it is of note that the second term of Eq. (5.9) becomes negligible when $(\Gamma/D) \gg 1$.

The points in Figs. 5.8, 5.9 correspond to the same compounded excitation functions but the calculated variances for Fig. 5.9 have been computed from Eq. (5.9). The line drawn in Fig. 5.9 has the same slope as the line in Fig. 5.8. It will be noted from these figures that the second term in Eq. (5.9) is sufficient to increase the calculated variances so that the plotted points are distributed about the line.

Figures 5.10, 5.11 are similar to Figs. 5.8, 5.9, but the calculated variances have been computed by using the renormalised values of ($\Gamma(Jw)/D(Jw)$) (see Section 5.3). Even in this case, where the relative magnitude of the second term of Eq. (5.9) is smaller than in the previous case, the distribution of points in Fig. 5.11 is not inconsistent with Eq. (5.9).

From these results it was concluded that, given the set of assumptions from which Eq. (5.9) is derived, a significant part of the correlation between the reaction cross-sections (Fig. 4.1) can be associated with the random grouping of the compound nucleus levels.

5.5 The Legendre Coefficients

The Legendre coefficients of a reaction angular distribution are defined by the equation

$$\frac{d\sigma\,(a|a')}{d\Omega} = \sum_L B_L\,(a|a')\,P_L(\cos\theta) \quad . \qquad (5.10)$$

These coefficients, plotted as a function of incident proton energy, are shown in Figs. 4.2, 4.3 for the different reactions investigated in this experiment. In the following paragraphs the nature of the B_L coefficients is discussed.

The coefficients may be expressed in terms of the [illegible] scattering matrix S in the following form (see Section A5.1 and Blatt and Biedenharn, 1952; Huby, 1954) :

$$B_L(a|a') = \frac{\lambda^2}{4(2I+1)(2i+1)} \sum (-1)^{s'-s} \bar{Z}(\ell_1 J_1 \ell_2 J_2; sL)\bar{Z}(\ell_1' J_1 \ell_2' J_2; s'L)$$

$$\mathrm{Re}(S(a\ell_1 s \mid a'\ell_1' s' \mid J_1 \pi_1) S^*(a\ell_2 s \mid a'\ell_2' s' \mid J_2 \pi_2)) \qquad (5.11)$$

where: ℓ = orbital angular momentum of the incident particle; ℓ' = orbital angular momentum of the emergent

particle; s = channel spin; J and w are the quantum numbers of the compound system; the sum is taken over all angular momenta and parity quantum numbers but not over a, a', I or i; the $\overline{Z}$ coefficients are defined in Appendix 6.

To elucidate the structure of Eq. (5.11) the summation of the equation is separated into two components

$$B_L(a \mid a') = \frac{\lambda^2}{4\,(2I+1)(2i+1)} \cdot \left[\sum_c \bar{\omega}(c,c,L) \mid S(c) \mid^2 + \sum_{c_1 c_2} (\bar{\omega}(c_1,c_2,L) \mathrm{Re}\, S(c_1)S^*(c_2))_{c_1 \neq c_2} \right]_{aa'} \qquad (5.12)$$

where: $c_1 \equiv (l_1, l_1', s, s', j_1, w_1)$; $\bar{\omega}$ is defined by

$$\bar{\omega}(c_1,c_2,L) = (-1)^{s'-s}\, \overline{Z}(l_1 J_1 l_2 J_2; sL)\, \overline{Z}(l_1' J_1 l_2' J_2; s'L).$$

The first term in Eq. (5.12) is non-zero only for even L coefficients (this is a direct result of parity considerations for the vectors (l_1, l_2, L) and (l_1', l_2', L)); the second term appears in both even and odd coefficients.

but not for L = 0. The second term, however, may be further separated into two parts which are associated with either odd or even L coefficients. This may be understood from the following relations for non-vanishing $\bar{Z}$ coefficients :

$$\left.\begin{array}{l} l_1 + l_2 + L \\ l'_1 + l'_2 + L \end{array}\right\} \text{ must both be even}$$

and so, for odd L, either

l_1 is even, l_2 is odd

or

l_1 is odd, l_2 is even,

and for even L, either

l_1 is even, l_2 is even

or

l_1 is odd, l_2 is odd.

Similar relations hold in the case of l'_1 and l'_2.

The above relations divide the possible combinations

of c_1 and c_2 into two categories: (a) those which have non-zero values of $\bar{\omega}(c_1,c_2,L)$ for even L, and zero values for odd L; (b) those which have non-zero values for odd L, and zero values for even L. Therefore, the same combinations of c_1 and c_2 are associated with all the even L (B_L) coefficients, although, due to the other angular momentum addition equations governing the $\bar{Z}$ coefficients, some combinations for a particular L may give zero contribution. Since the same combinations appear in all the even L coefficients it is likely that there is some correlation between these coefficients. Similar conclusions hold for the odd L (B_L) coefficients.

It has been shown (Ericson, 1963) that, if it is assumed that the direct component of the scattering matrix is zero and the compound nucleus component is completely random for the different channels c, then there is zero cross-correlation between the odd and the even B_L coefficients.

The experimental values of the B_L coefficients shown in Figs. 4.2, 4.3 are not inconsistent with the above conclusions, since there is some evidence of correlation between the even L coefficients and between the odd L coefficients, the effect being particularly strong for inelastic scattering to the 4.97 MeV state. For the 4.97 MeV state

there also appears to be little or no correlation between the even and odd L coefficients.

5.6 Variance of the Legendre Coefficients

By using the same assumptions that were employed in the derivation of Eq. (5.2), it is shown in Appendix 6 that the variance of the B_L coefficients defined as

$$\mathrm{var}(B_L) = \langle (B_L - \langle B_L \rangle)^2 \rangle \quad , \tag{5.13}$$

is given by

$$\mathrm{var}(B_L(a \mid a')) = \left[\sum_{c} \omega^2(c,c,L) \langle \sigma(c) \rangle^2 \right.$$

$$+ \sum_{c_1 c_2} \left(\omega^2(c_1,c_2,L) \langle \sigma(c_1) \rangle \langle \sigma(c_2) \rangle \right)_{c_1 \neq c_2}$$

$$+ \sum_{Jw} \sum_{c_1 c_2}' (\omega(c_1,c_1,L)\omega(c_2,c_2,L) + \omega^2(c_1,c_2,L))$$

$$\left. \cdot \frac{\langle \sigma(c_1) \rangle \langle \sigma(c_2) \rangle}{w\Gamma(Jw)/D(Jw)} \right] \tag{5.14}$$

where: $\sum'$ indicates that the summation is only over sets c associated with particular values of J and π.

Comparison of the terms in Eq. (5.2) with those of Eq. (5.14), in association with Eq. (5.12), suggests they are similar in origin. The first term of Eq. (5.14) is analogous to the first term of Eq. (5.2), and arises mainly from interference between the compound resonances associated with a particular set of quantum numbers c. The second term in Eq. (5.14) arises from an interference between compound resonances associated with different sets of the quantum numbers c; this interference is represented by the second term in Eq. (5.12). The third term in Eq. (5.14) is analogous to the second term of Eq. (5.2), and arises from the contribution of the single resonance states to the variance; this term becomes negligible when $(\Gamma/D) \gg 1$.

Owing to the many different combinations of c_1 and c_2, Eq. (5.14) is difficult to apply to a general experimental situation; however, some simplification occurs if the target and residual nuclei have zero spin. Such a situation arises in the case of inelastic scattering to the 4.97 MeV state of Si^{28}. For this reason Eq. (5.14) has been specifically applied to this situation.

5.7 Variance of the Legendre Coefficients for the Reaction $Si^{28}(p,p')Si^{*28}$, Q = 4.97 MeV

Whether or not a particular reaction channel contributes significantly to the terms of Eq. (5.14) depends upon the associated channel transmission coefficients. For the reaction studied in this section the following table lists the most important channels:

TABLE 5.1

c	s	ℓ	J	π	ℓ'	s'
1	½	0	½	+	0	½
2	½	1	½	-	1	½
3	½	1	3/2	-	1	½
4	½	2	3/2	+	2	½
5	½	2	5/2	+	2	½
6	½	3	5/2	-	3	½
7	½	3	7/2	-	3	½
8	½	4	7/2	+	4	½
9	½	4	9/2	+	4	½

The pairs of the channels which have non-zero $\omega(c_1,c_2,L)$ coefficients, and which therefore contribute to the second term in Eq. (5.14), are tabulated in Table 5.3 (see end of chapter) for the different L coefficients.

The partial reaction cross-sections occurring in Eq. (5.14) were computed by using Eq. (5.4) with the values of $(\Gamma(J\pi)/D(J\pi))$ corresponding to a Si^{28} S.C.F. of 2.0, and for a centre of mass energy of 13 MeV. The values of $\omega(c_1,c_2,L)$ were computed from the 3-j and 6-j coefficients tabulated by Rotenberg et al. (1959). To calculate var(B_L) for the averaged angular distributions investigated in this experiment, it was assumed that Eq. (5.3) was true for the B_L as well as for the B_0 coefficients. The calculated values of the terms occurring in Eq. (5.14) are listed in Table 5.2 below for the different L coefficients.

TABLE 5.2

L	Term in Eq.(5.14) $(mb/strd)^2$ 1st	2nd	3rd
1		95	
2	29	104	7
3		134	
4	14.2	124	3.3

It will be noted in Table 5.2 that the value of the last

term of Eq. (5.14) is small compared to the values of the other terms.

The calculated variances are compared with the experimental values in Fig. 5.12; the line drawn in this figure has the same slope as the line drawn in Fig. 5.2. It will be observed that, as was found for the variances of the total reaction cross-sections (Section 5.3), the calculated values of the variances are greater than the experimental values. A similar difficulty was described in Section 5.3 and it was suggested that the reason was an incorrect normalisation of the ratios ($\Gamma(Jw)/D(Jw)$). The variances of the B_L coefficients were therefore recalculated with the renormalised values determined from the total reaction cross-sections. These recalculated values are plotted in Fig. 5.13. It is evident that there is better agreement between the calculated and experimental values, although due to the large experimental errors it is difficult to draw any firm conclusions.

The renormalisation argument therefore appears to be consistent in that, at the same time, the average total reaction cross-sections, variances of reaction cross-sections and the variances of the B_L coefficients can be brought into reasonable agreement with the experimental results.

TABLE 5.3

L	(c_1, c_2)
1	(1,2)(1,3)(2,4)(3,4)(3,5)(4,6)(5,6)(5,7)(6,8)(7,8)(7,9)
2	(1,4)(1,5)(2,6)(3,6)(3,7)(2,3)(4,5)(4,8)(5,8)(5,9)(6,7)(7,9)
3	(2,3)(3,4)(3,5)(4,6)(4,7)(5,6)(5,7)(6,9)(6,8)(7,8)(7,9)(2,8)(3,8)(3,9)(1,6)(1,7)
4	(1,5)(1,9)(2,7)(3,6)(3,7)(4,5)(4,8)(4,9)(5,6)(5,9)(6,7)(8,9)

(This table is referred to on page 113.)

TRANSMISSION COEFFICIENTS
FOR PROTONS IN Si

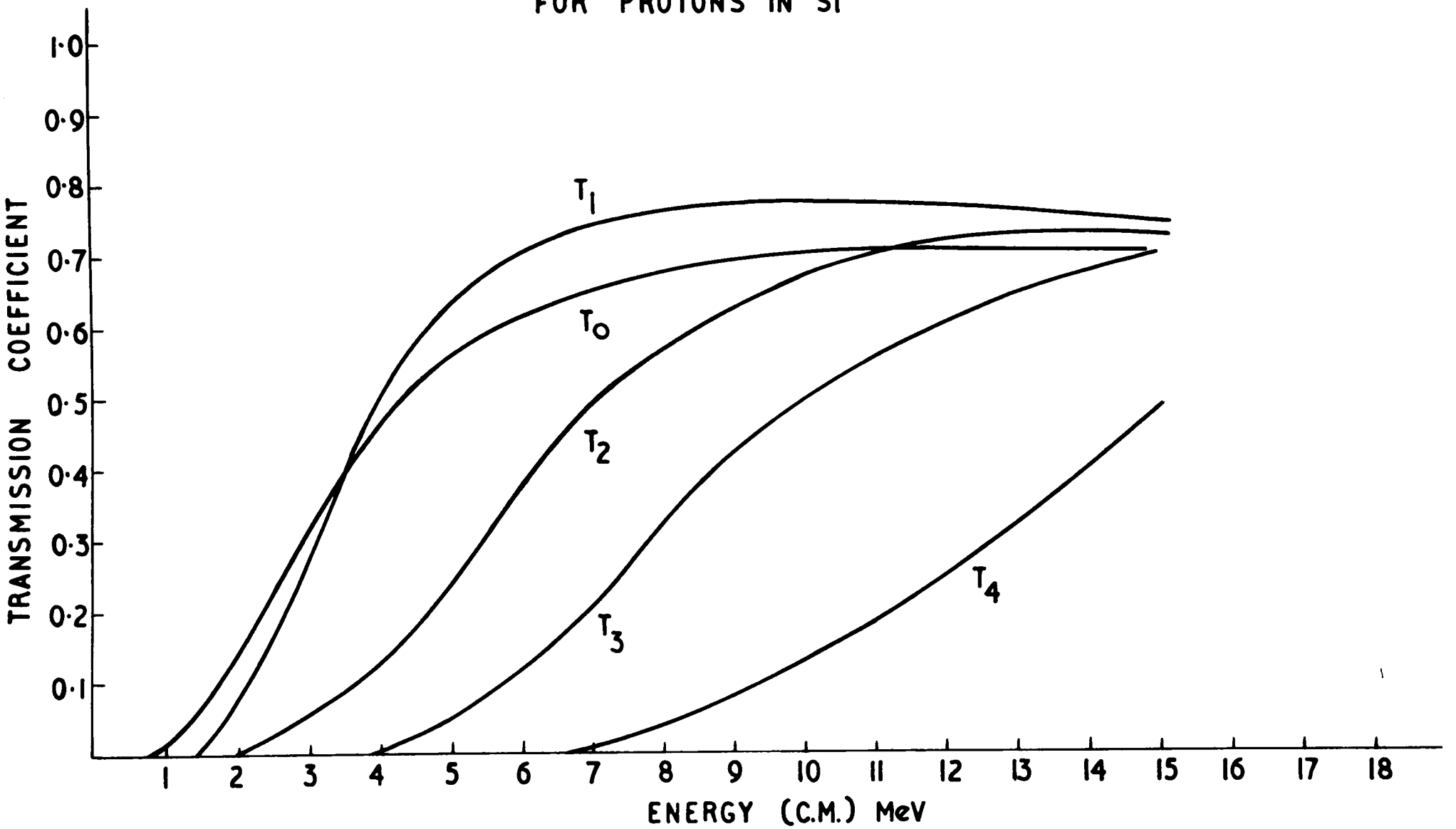

FIGURE 5·1

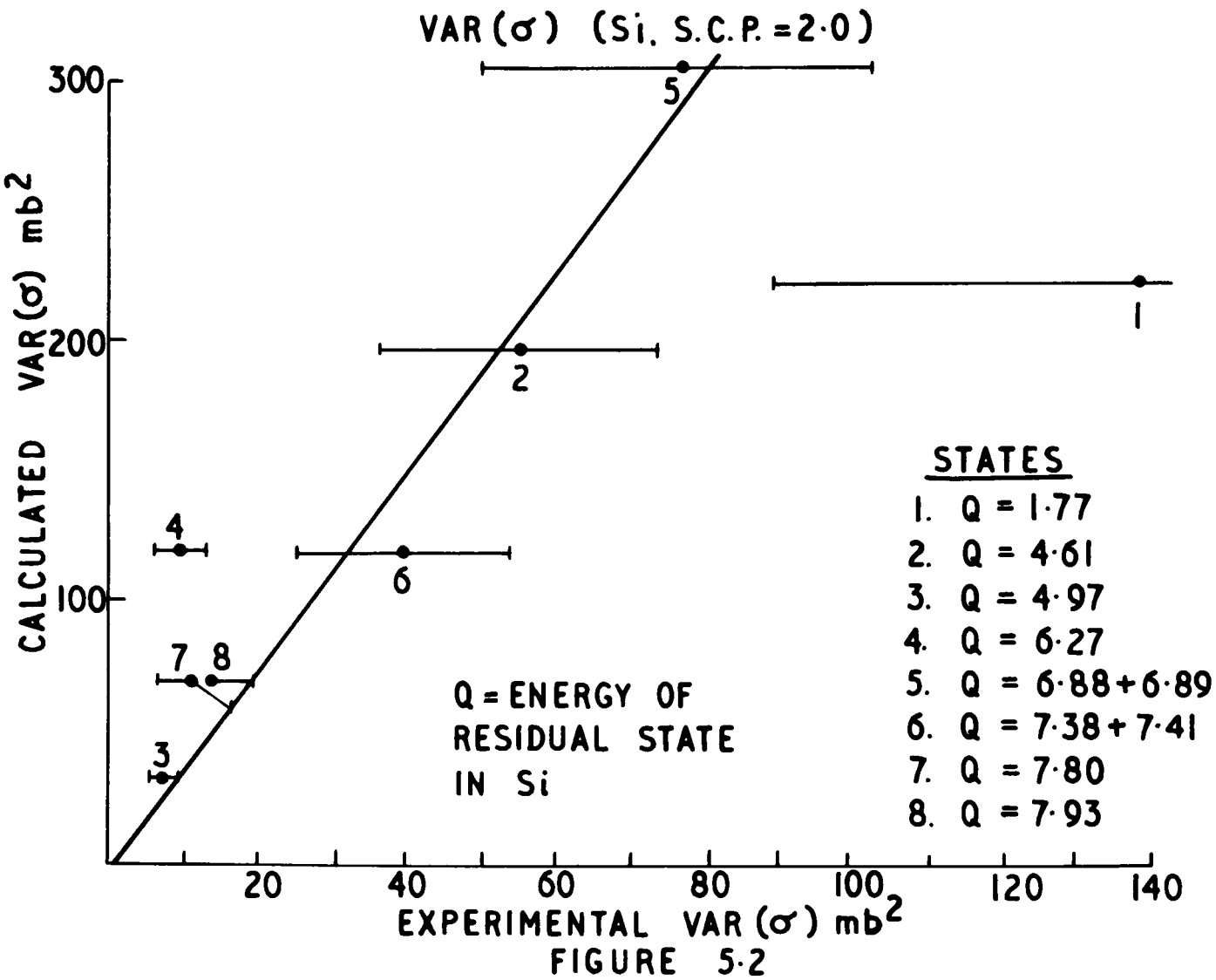

FIGURE 5·2

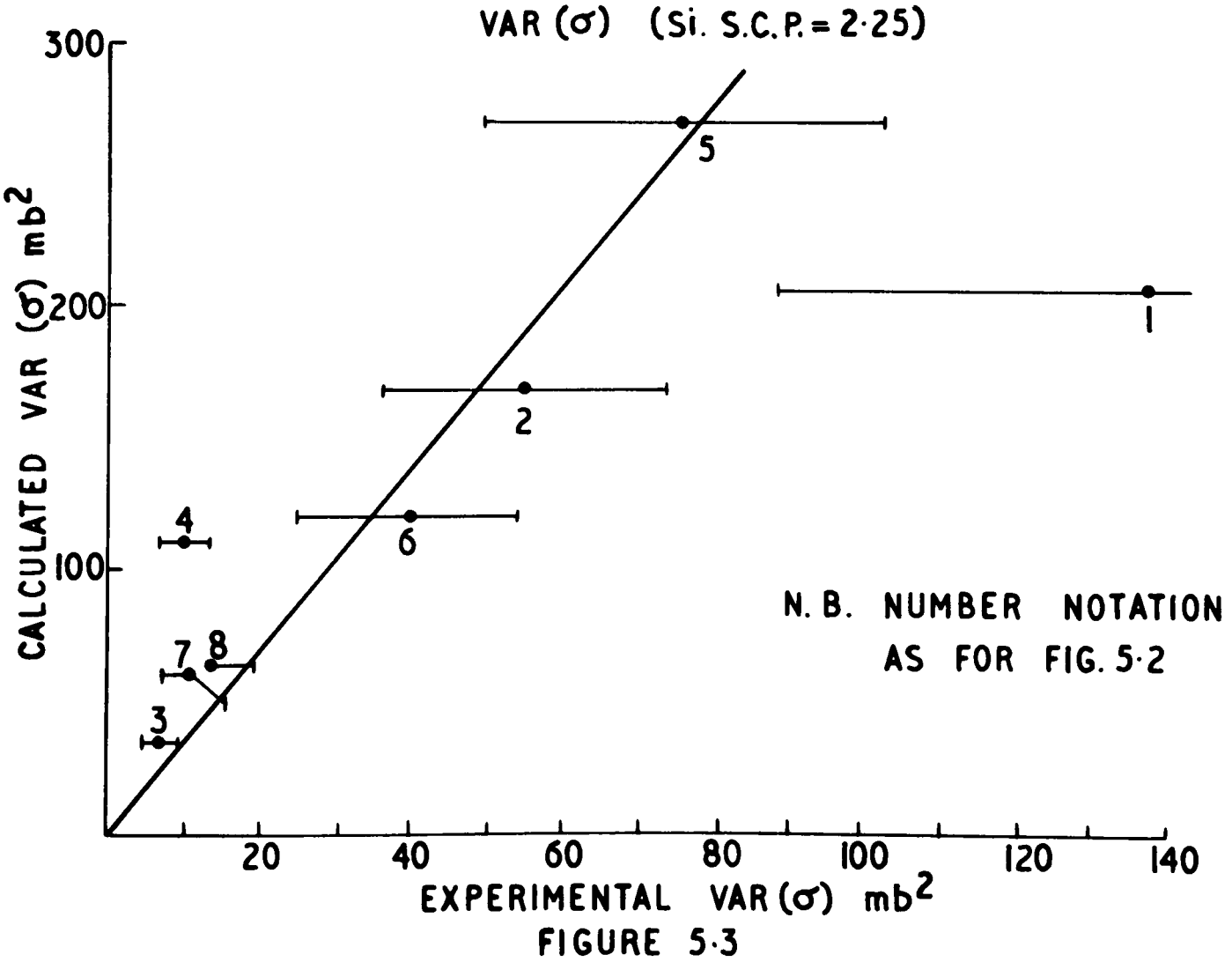

FIGURE 5·3

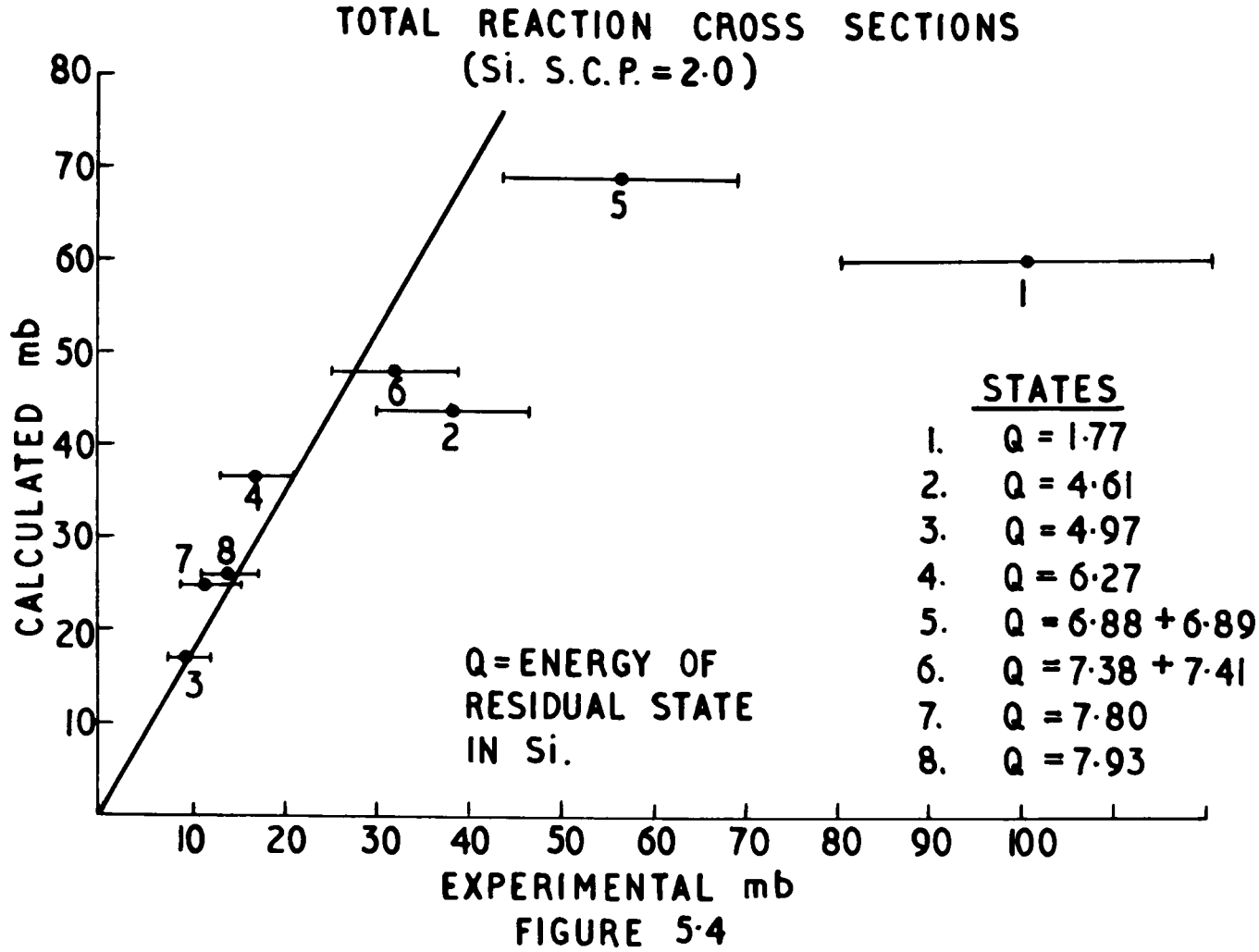

FIGURE 5·4

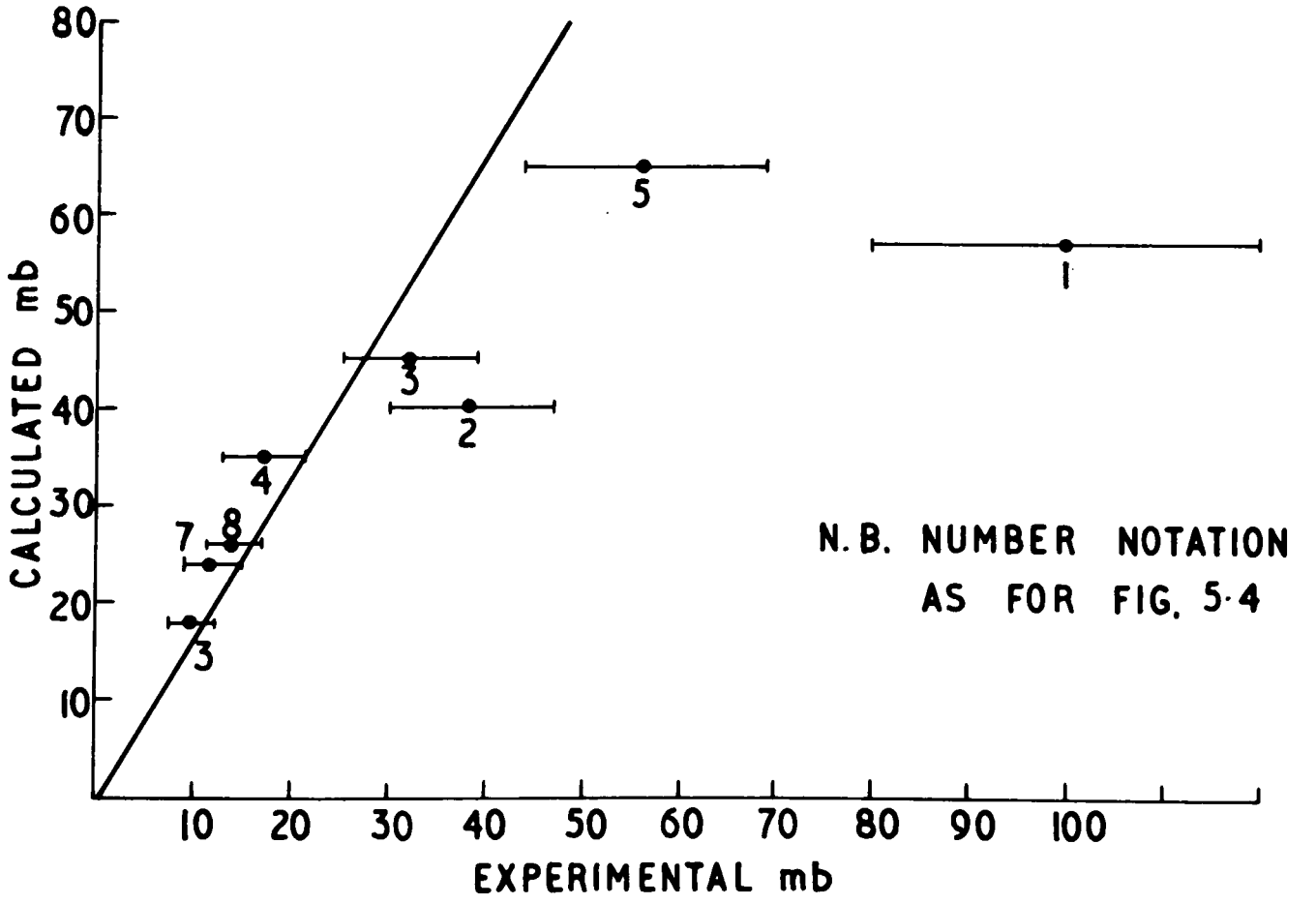

FIGURE 5·5

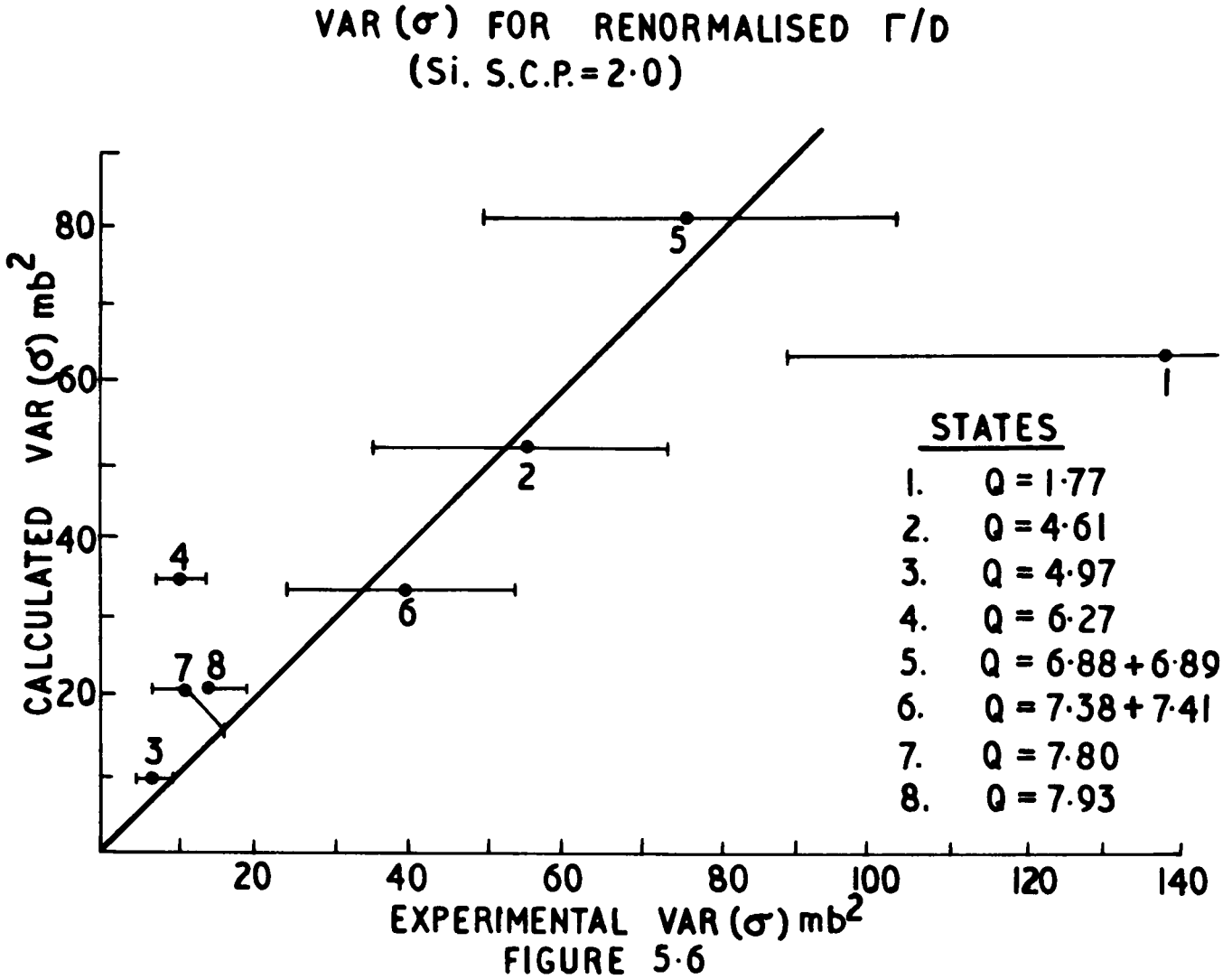

FIGURE 5·6

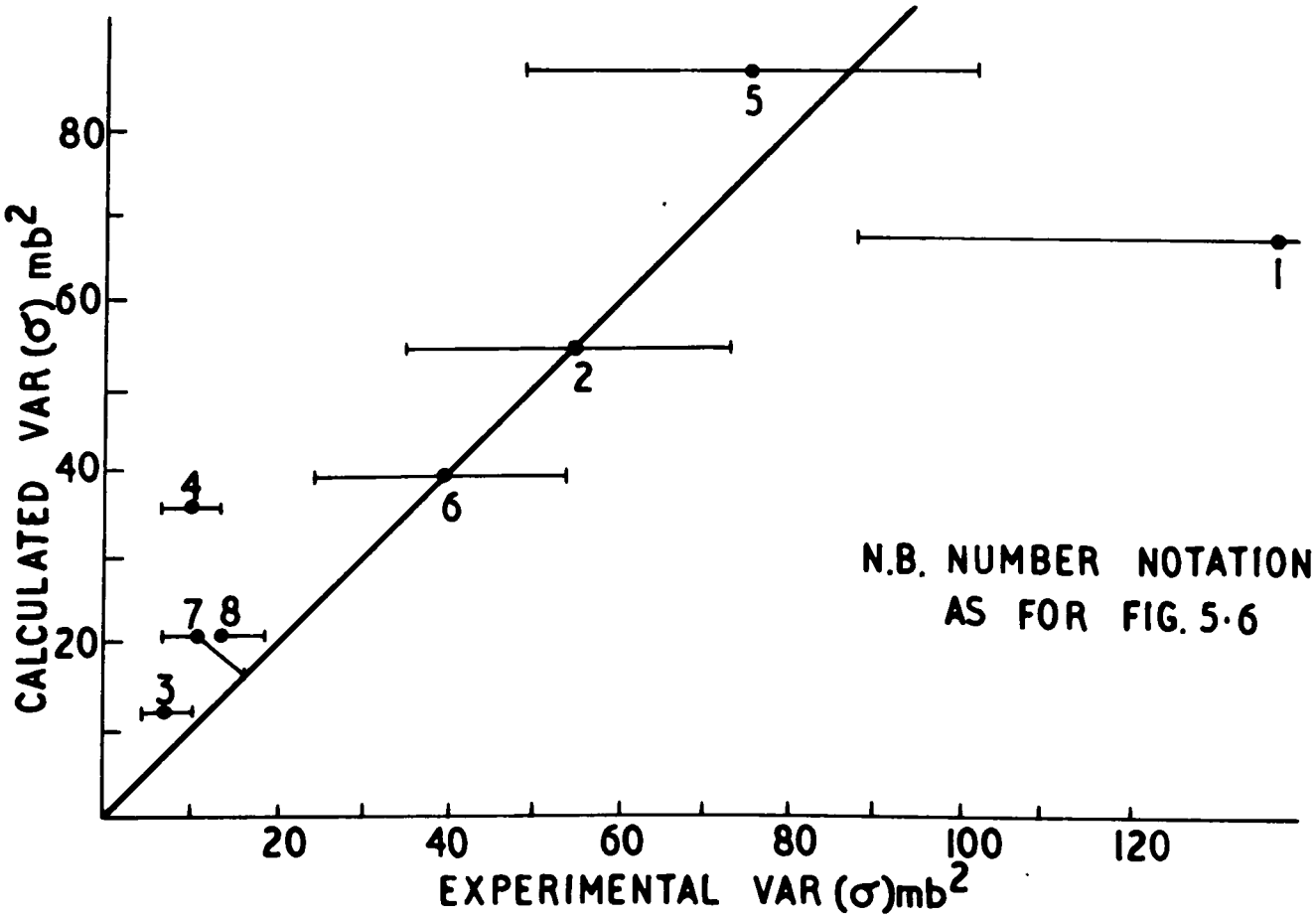

FIGURE 5·7

VAR (σ) FOR SUMMED CROSS SECTIONS

σ(R) = SUM OF CROSS SECTIONS FOR STATES WITH Q VALUES:
4·61, 4·97, 6·27, 6·88†, 7·41†, 7·8, 7·93 MeV

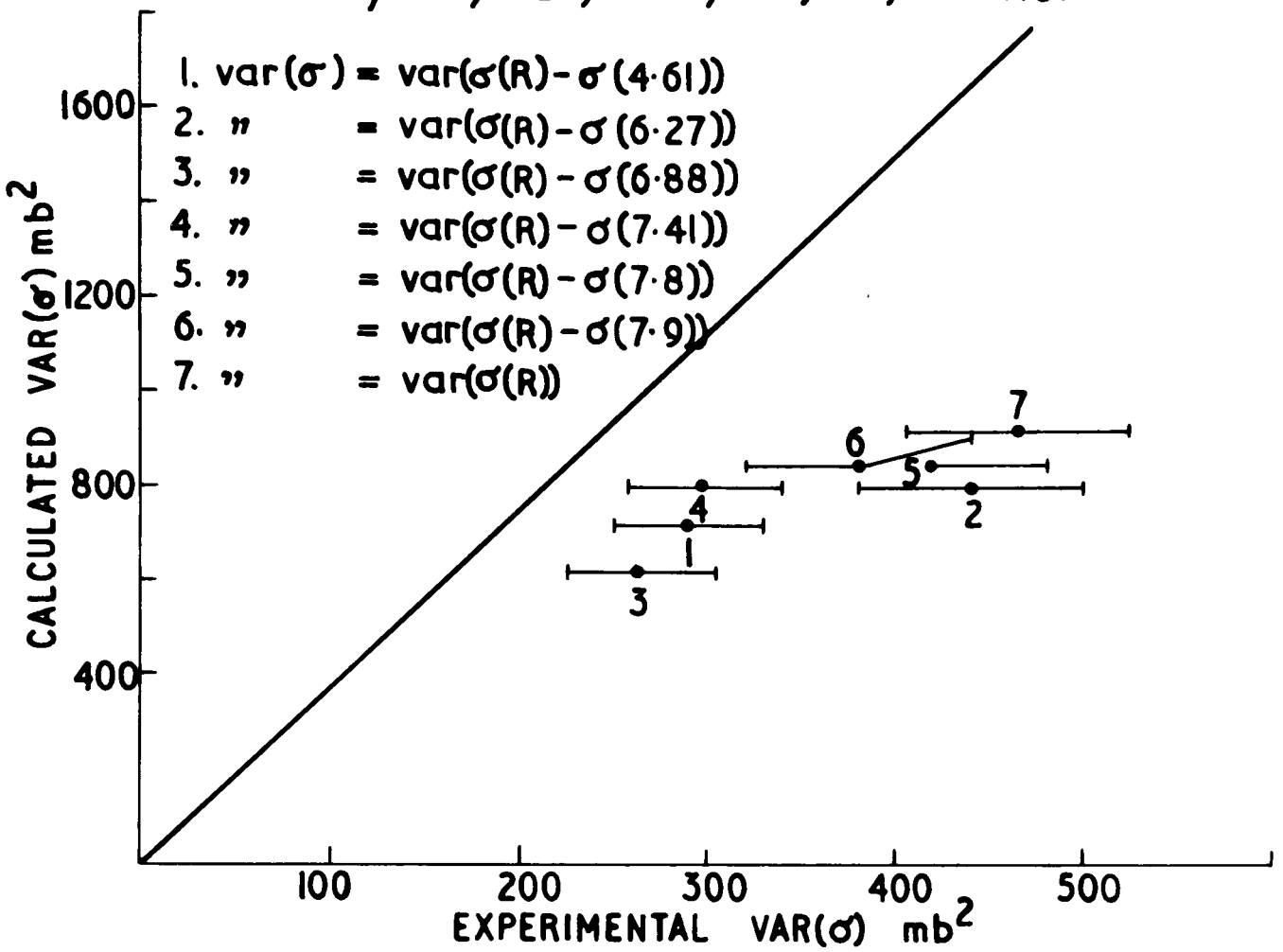

FIGURE 5·8

VAR (σ) FOR SUMMED CROSS SECTIONS

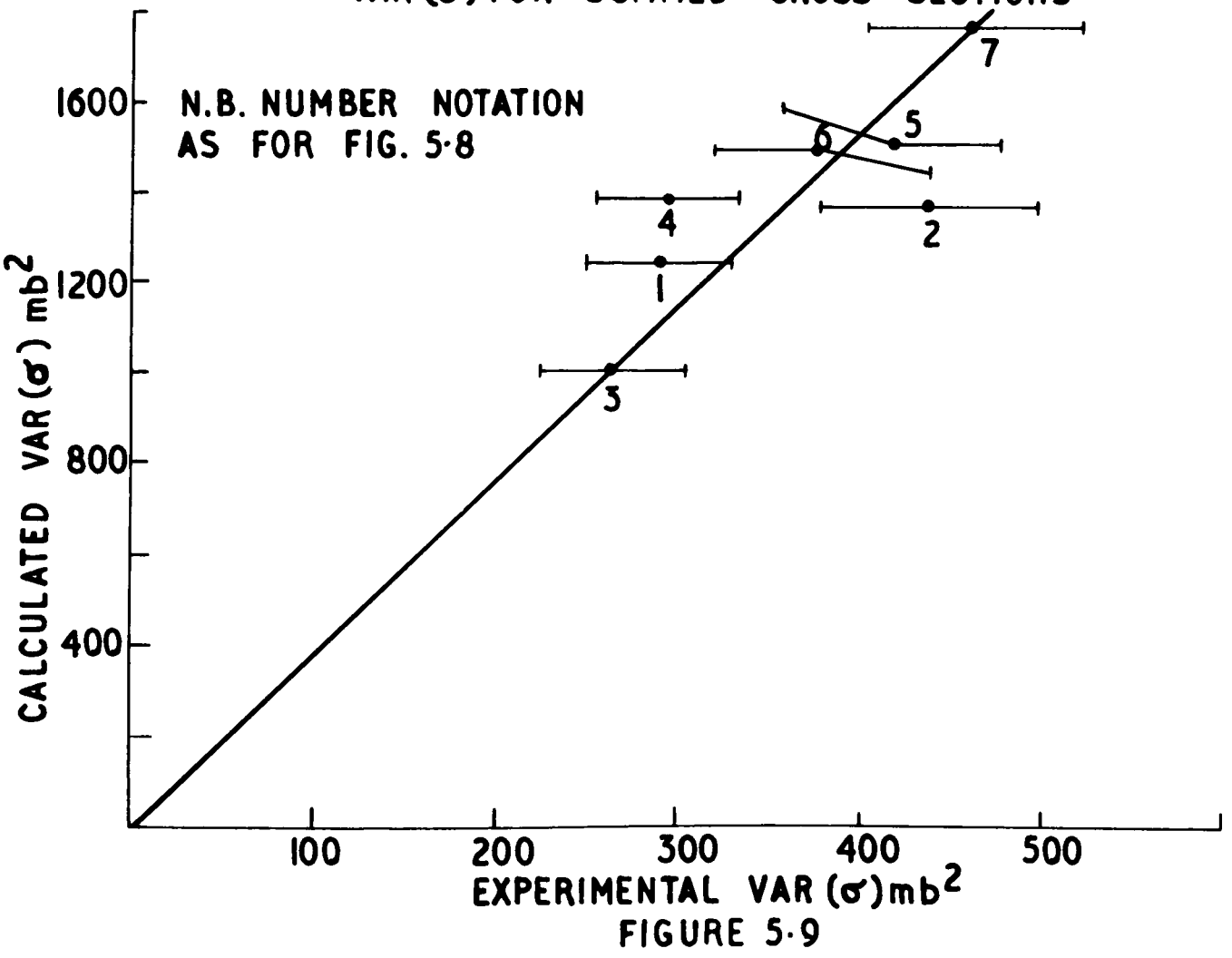

FIGURE 5·9

VAR (σ) FOR SUMMED CROSS-SECTIONS

σ(R)=SUM OF CROSS SECTIONS FOR STATES WITH Q VALUES:
4·61, 4·97, 6·27, 6·88,† 7·41†, 7·8, 7·93 MeV

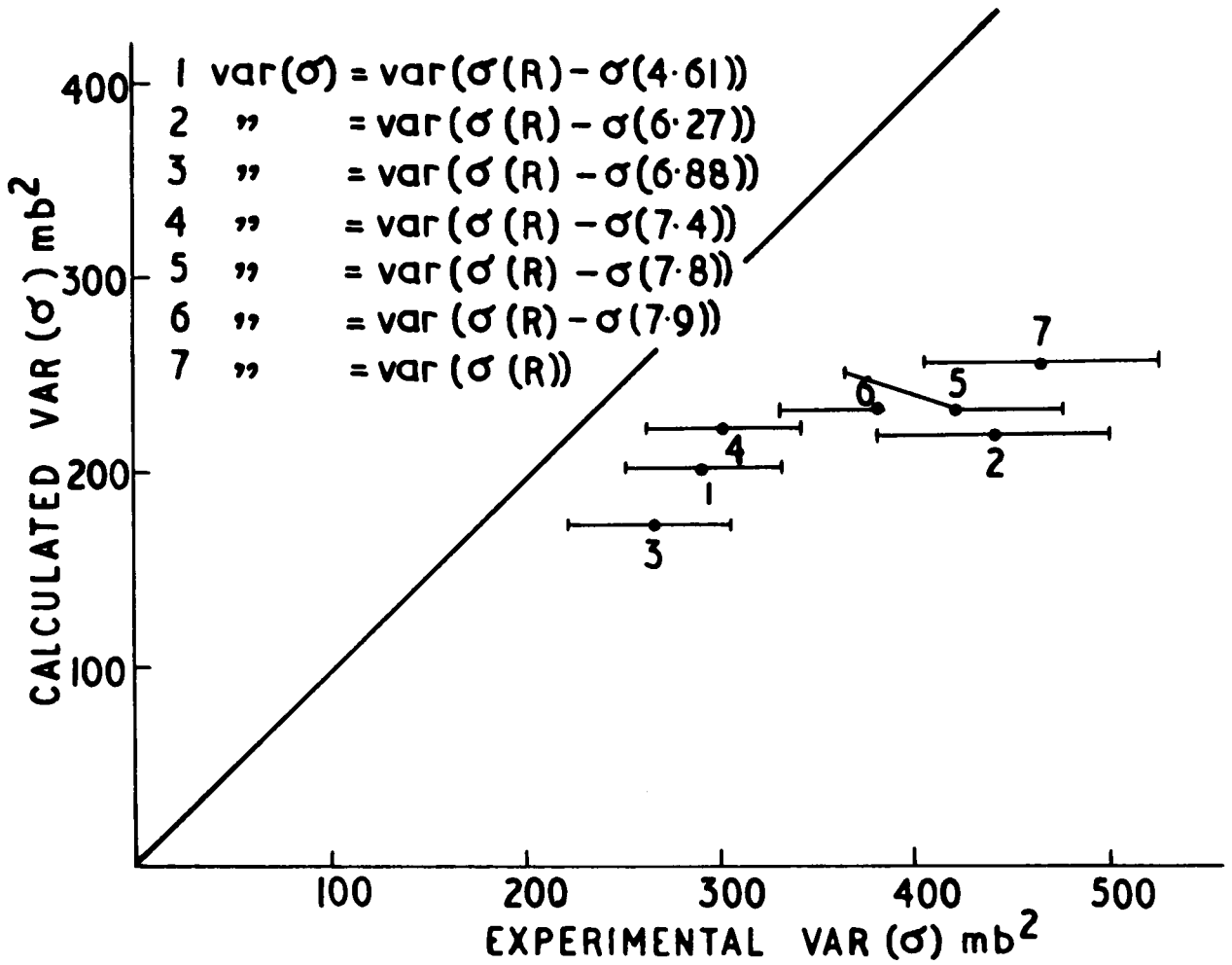

FIGURE 5·10

VAR (σ) FOR SUMMED CROSS SECTIONS

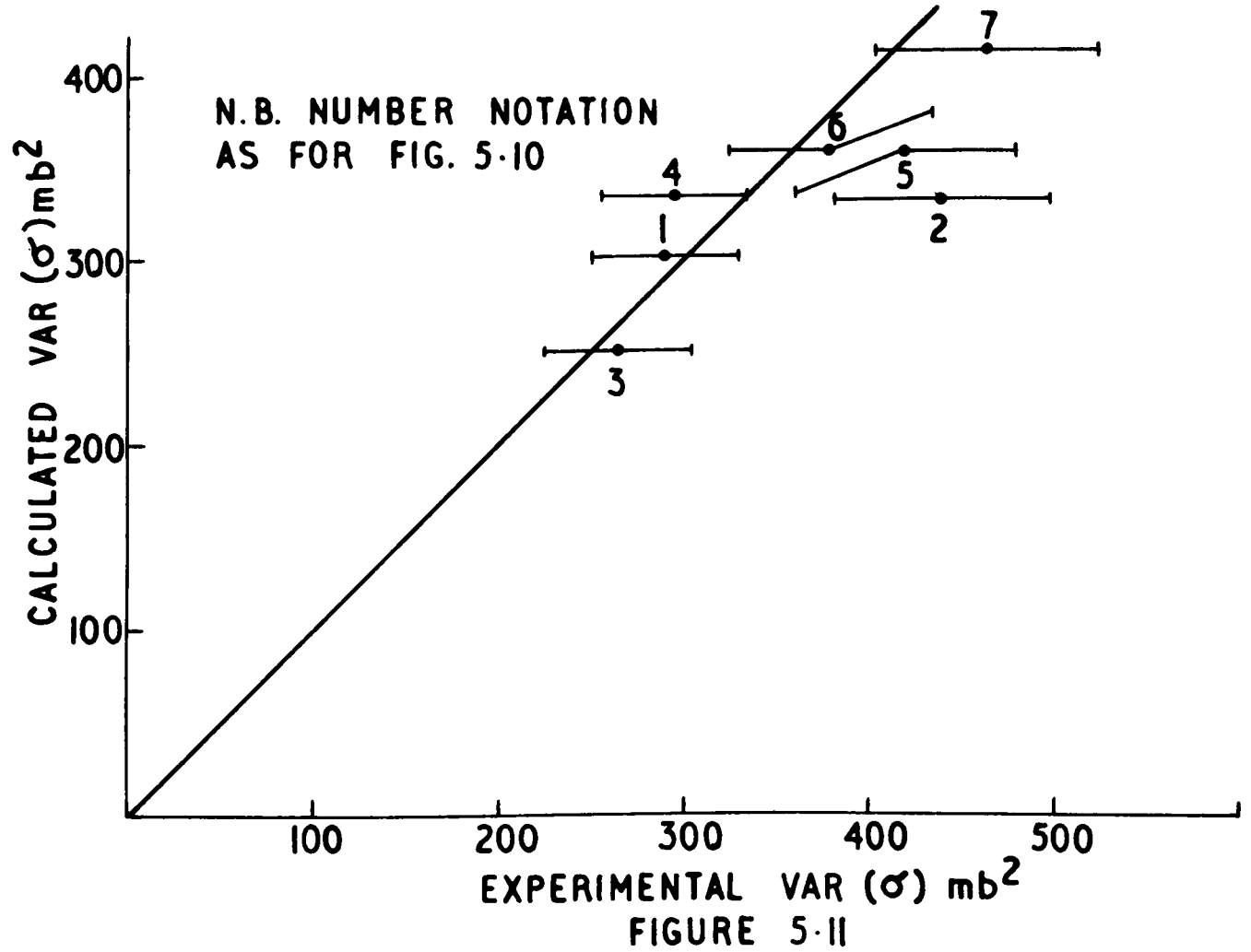

FIGURE 5·11

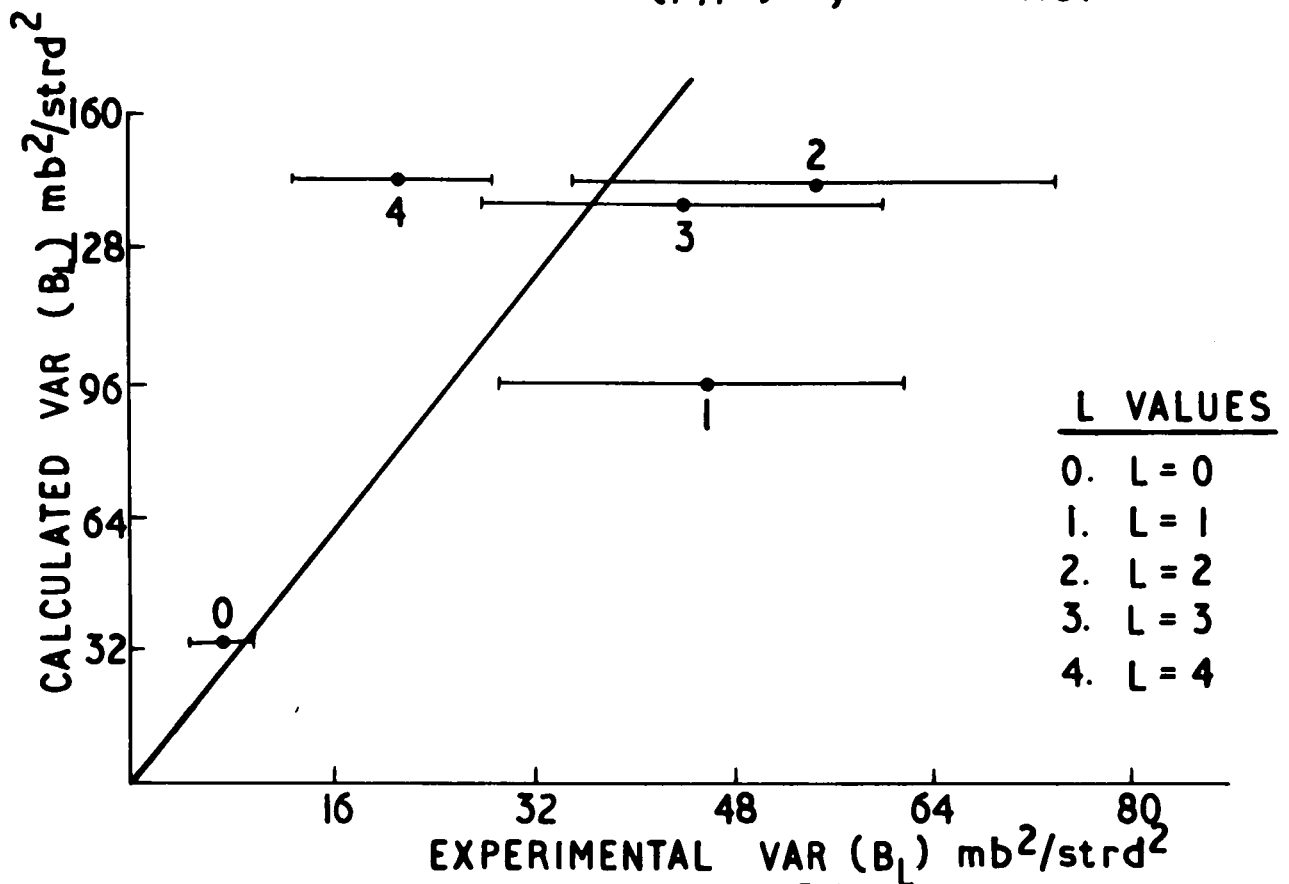

FIGURE 5·12

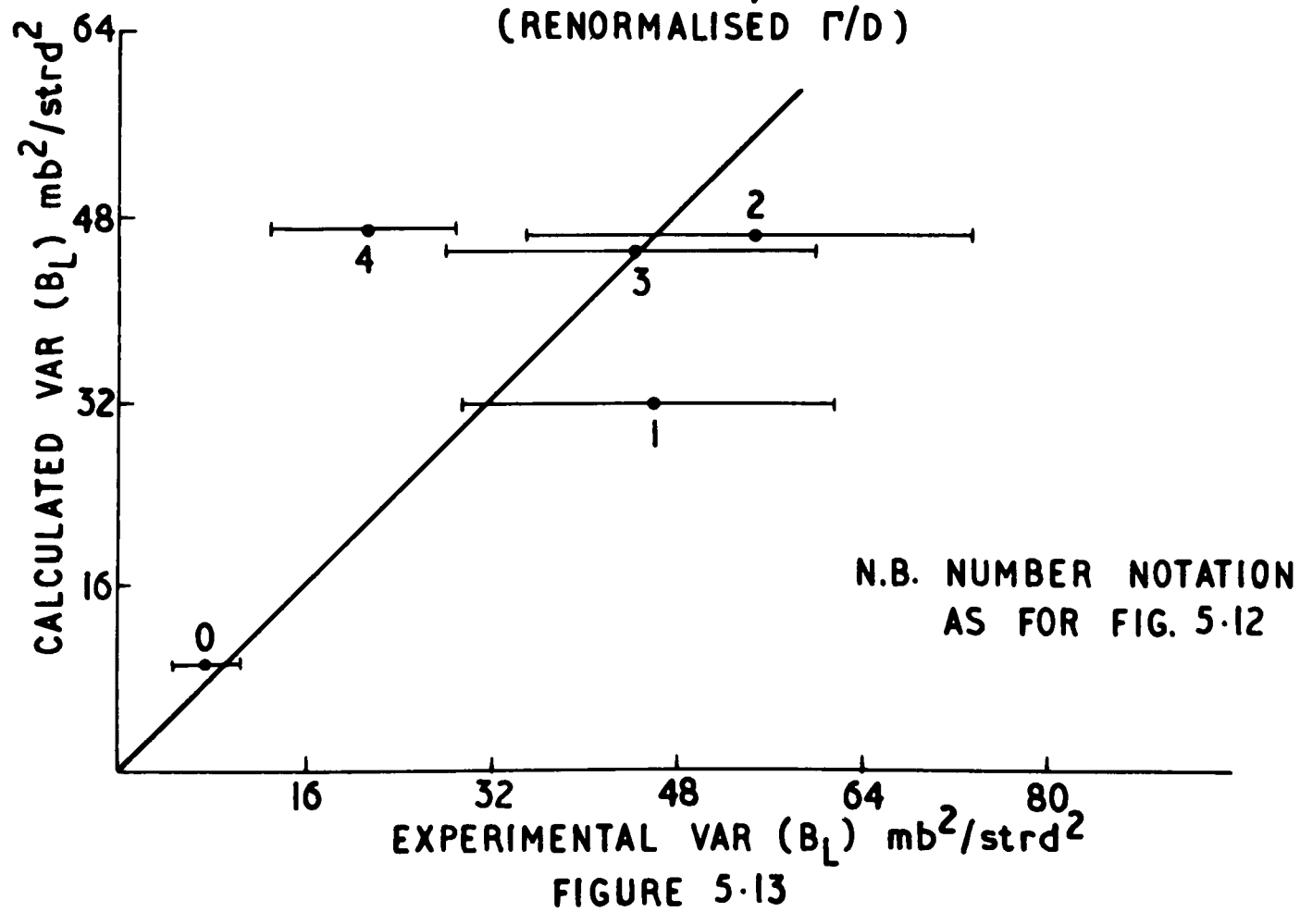

FIGURE 5·13

C H A P T E R 6

DISCUSSION AND CONCLUSION

6.1 Review of the Experimental Results

The inelastic scattering excitation functions determined by this experiment (Fig. 4.1) exhibit structure of the intermediate type. The similarity between the intermediate structure in the different excitation functions is clearly apparent although there are differences in detail; whilst intermediate-structure peaks* occur at similar energies in several of the reaction channels, a particular peak is not always conspicuous in them all. That there are common structural features in the excitation functions becomes even more evident when several of the functions are added together (Fig. 4.1). The relative fluctuations of these compounded curves appear almost as great as the individual curves - this is contrary to what would be expected if the component curves were uncorrelated.

---

* i.e., a structure "bump" with width several times greater than the fine structure coherence width.

The results of the cross-correlation analysis discussed in Section 4.4 provide further evidence that the different reaction cross-sections are correlated.

The approximate energy positions and widths of the intermediate-structure peaks are listed below.

TABLE 6.1

Energy (MeV)	Width (KeV)
12.9	300
13.4	250
13.7	200
14.1	200
14.8	200

The widths listed in this table have been estimated from the compounded cross-section excitation functions (see Fig. 4.1); it is to be noted that the widths vary between the individual excitation functions.

There is some evidence that the differential cross-section excitation functions associated with individual reaction channels are correlated. The energy variation of

the differential cross-sections associated with two reaction channels are shown in Fig. 4.7.

The angular distributions and their associated Legendre coefficients for the different reaction channels vary rapidly with incident proton energy (see Appendix 8 and Figs. 4.2, 4.3). It will be observed that in the case of inelastic scattering to the 4.97 MeV state there is correlation between the L = 2 and L = 4 coefficients and also between the L = 1 and L = 3 coefficients; a similar effect also occurs, though less marked, in some of the other reaction channels.

Inelastic proton scattering from Si^{28} has previously been studied by several workers. Brenner and Hoogenboom (1962) investigated the reaction, in the energy region 4.8 to 7.0 MeV, by measuring differential cross-sections at several scattering angles; they discovered twenty-three resonances in the energy region. Cohen and Cookson (1961) determined 90^{o} differential cross-sections over the energy region of 10 to 12.3 MeV, and discovered nine structure peaks in this region. The authors however were by no means certain that the peaks corresponded to genuine level positions in the compound nucleus; in view of the later work of Brenner and Hoogenboom this does indeed seem unlikely. Low

energy studies of the reaction in the region 2 to 5.5 MeV have been undertaken by Oda et al.(1959), Belote et al.(1961).

From the work of these authors, it is to be concluded that the intermediate-structure peaks occurring in the excitation functions determined by this experiment are unlikely to be associated with individual levels of the compound nucleus. The Ericson plot for the compound nucleus P^{29} (see Section A7.2 and Fig. A7.2) provides added support for this argument; extrapolation to the excitation energies used in the present experiment yields a value of about 900 for the number of compound nuclear levels occurring within the experimental energy range. The value derived by this method probably overestimates the actual number of levels (see Appendix 7); however, even taking this into account, the number of levels will still be much greater than the observed number of intermediate-structure peaks.

Recently discovered examples of intermediate-structure peaks in reaction excitation functions, for nuclei of the same mass region as Si^{28}, have been reported by Allardyce et al.(1964); Fink (1964); Singh et al.(1965); Allardyce et al.(1966); Elliott and Spear (1966); Lévi et al.(1966); Mehta et al.(1966); Singh et al.(1966[b]); Kroepfl et al.(1967);

Lee et al.(1967); Mehta and Divatia (1967).

6.2 The Doorway State Theory and the Experimental Results

The predictions of the doorway state theory of intermediate structure have been discussed in Chapter 1; briefly, they are the prediction of structure correlation (a) between the cross-sections associated with different reaction channels (b) between the differential cross-sections corresponding to the same reaction channel but different scattering angles. Both these characteristics are to be observed in the data collected in the course of this experiment (see Section 6.1). In the following paragraphs a brief discussion is given of the widths and spacings of the intermediate-structure peaks in relation to the doorway state theory.

The width of a doorway state resonance (see Section 1.6) is determined by its escape width to the open reaction channels and its damping width to the more complicated configurations (i.e., 3p-2h., 5p-3h. etc.). The doorway state, however, can only decay to the more complicated states which have the same spin and parity, otherwise the matrix elements determining the transition will be zero. These

conservation laws therefore place strong restrictions on the number of final states to which the doorway state can decay; this alone will cause the damping widths to vary between the different states. Specific calculations of the damping widths have been carried out by Franco and Lemmer (Feshbach et al., 1967) for the neutron mass region centring around N = 126, on the assumption that the doorway states are 2p-1h configurations, and the next reaction stage 3p-2h configurations. These calculations suggest that the damping widths for these nuclei should be roughly in the 100 KeV region, although the authors emphasise that the particular make-up of a doorway state can change this estimation by an order of magnitude in either direction. On the other hand, calculations giving results in reasonable agreement with experiment (Pfitner and Diedel, 1964; Lovas, 1966) have been made in the case of light nuclei, on the assumption that the width of the doorway state resonance is only determined by its escape width.

It has therefore been concluded (Feshbach et al., 1967[b]) that for the energy and nuclear mass region considered in this experiment the typical width of a doorway state resonance should be several hundred KeV. The experimental widths of the intermediate-structure peaks found by this

experiment are therefore not inconsistent with this estimation (see Table 6.1).

The spacing of 2p-1h states has been estimated by Le Couteur (1964) on the basis of the Fermi gas model. For the mass and energy regions used in this experiment, this model gives a value for the average spacing of between 50 and 100 KeV. In the spirit of the shell model, Lande and Block (1964) have counted the number of 2p-1h states per MeV for a range of nuclei; unfortunately P^{29} is not included in the range considered. The phenomenological model of Izumo (see Section 1.5) gives the spacing of the intermediate-structure peaks as about 500 KeV. The above estimates are to be compared with the experimental value of the spacing which is about 500 KeV (see Table 6.1).

6.3 The Statistical Theory and the Experimental Results

In Chapter 5 the experimental data were compared with the predictions of the statistical theory of the reaction mechanism. Using assumptions about the widths and energy spacings of the compound nucleus levels which enter into the theory, it was found that reasonable agreement could be obtained between the experimental and calculated variances

of the individual reaction excitation functions (see Section 5.2). It was also found that the experimental variances of compounded excitation functions* were consistently greater than the values calculated on the assumption that the individual reaction cross-sections were uncorrelated (see Section 5.4); this would seem to imply that there is structure correlation between the individual reaction cross-sections.

If the experimental data are in accord with the statistical theory, then when (Γ/D) $\gg$ 1, the individual reaction cross-sections should be uncorrelated; however, when (Γ/D) $\approx$ 1, as in this experiment, the random grouping of the compound nuclear levels begins to become a significant factor in determining the cross-section variances (see Section 5.4). Since the same compound nuclear levels are associated with each reaction channel, it is to be expected that correlation between the reaction cross-sections will become significant when (Γ/D) $\approx$ 1. This correlation will cause the variance of a compounded excitation function to be greater than it would be if the reaction cross-sections were uncorrelated.

---

* i.e., an excitation function produced by adding together several of the experimental reaction cross-sections.

For the experimental compounded excitation functions considered, the increase in variance has been estimated in each case on the assumption that the compound nuclear levels are randomly distributed in energy (see Eq. 5.9). Given this assumption, the calculated variances of the compounded excitation functions are in reasonable agreement with the experimental results (see Fig. 5.9).

Further testing of the statistical interpretation of the experimental results would involve investigation of the way in which a Wigner type level spacing distribution (Wigner, 1956) affects the theoretical estimates; further information about the level width distribution would also be required. However, in the spirit of the calculations presented in Chapter 5, it would seem that the statistical interpretation of the cross-section variance is not unreasonable.

The widths of the intermediate-structure peaks to be expected from the statistical theory when $\frac{\Gamma}{D} \gg 1$ have been considered by Singh et al. (1966[a]). The authors simulated cross-sections with parameters chosen in a random fashion from preset distributions; when the cross-sections were mathematically averaged it was found that they often exhibited structure suggestive of the intermediate type.

In fact, the authors found that, for an excitation function of interval length 25Γ, there is a 30 per cent chance of finding an intermediate-structure peak 6Γ wide, with $\sigma(\text{peak}) = 1.4\sigma(\text{average})$. (For the present experimental situation the value of $6\Gamma \approx 300$ KeV, which is approximately the same value as the observed experimental widths (see Table 6.1).) The authors however only considered large values of (Γ/D), and so it is difficult to infer what is to be expected when $(\Gamma/D) \approx 1$; nevertheless these calculations suggest that the occurrence of intermediate-structure peaks is not incompatible with the statistical theory.

It would be of interest, in connection with the present experiment, to extend this type of calculation to low values of (Γ/D), and to study, as a function of (Γ/D), the correlation between excitation functions which are generated with the same distribution of level energy positions but different level widths. If this is done, it may be found that the structure associated with the excitation functions becomes more and more correlated as (Γ/D) decreases in value.

In Chapter 5 of this thesis a study is also made of the variance of the Legendre coefficients associated with the reaction angular distributions; again it was found that the experimental results are in reasonable agreement with

the statistical theory (see Section 5.6).

6.4 Conclusion

It seems therefore from the preceding discussion that the experimental results are not inconsistent with either the statistical theory or the doorway state theory of intermediate structure. The correlation of cross-sections between the different reaction channels and also the correlation between the differential cross-sections are consistent with the predictions of the doorway state theory (see Section 6.2); this theory also offers some explanation of the experimental widths and energy spacings of the intermediate-structure peaks. On the other hand, both the variances of the experimental reaction excitation functions and the structure correlation between these functions can reasonably be explained in terms of the statistical theory.

It may be that, for the experimental situation studied, the reaction mechanisms corresponding to the theories in question each have a significant role in the reaction process. Therefore, to gain conclusive evidence that doorway states do in fact give rise to intermediate-structure peaks further experimental data are required.

One possible experiment would be cross-correlation analysis of different reaction cross-sections, as described in this thesis, but for an energy and nuclear mass region where $(\Gamma/D) \gg 1$; in this case, grouping of the statistical parameters is unlikely to be the cause of cross-correlation between the reaction cross-sections. In such an experiment it may be unprofitable to use too high an energy, otherwise the escape widths of the doorway states are likely to become so large that the associated resonant structures become indistinguishable from the background.

Another possible experiment (see Section 1.8) would be to measure elastic scattering angular distributions in some detail at energies in the proximity of an intermediate-structure peak. If the presence of the peak is due to a doorway state resonance, then analysis of the angular distributions using an S matrix of the form $S = \eta \exp(2i\delta)$ should reveal that both η and δ change smoothly through the resonance, η passing through a minimum and δ either passing through $\pi/2$ or 0 depending upon the escape width of the doorway state (see Singh et al., 1966[b]).

The experimental situation, however, may demand more than an elimination of the possibility that intermediate

structure is caused by grouping of the statistical parameters, since Moldauer (1967) has now drawn attention to another possible statistical explanation of the structure. He points out that "...in the presence of strongly absorbed channels, such intermediate resonance features are also predicted by the statistical model of highly excited nuclear states. These models specify the frequency of occurrence of the average properties of the intermediate resonances and yield properties very similar to those predicted by the dynamically more detailed doorway-state models."

APPENDICES

A P P E N D I X 1

THE KINEMATIC FRACTIONAL RATIO f

This appendix is concerned with the effect of the incident beam energy modulation on the energy of the scattered particles from the target.

If a particle of mass m_1 travelling with linear momentum P_1 and kinetic energy E is inelastically scattered from a static nucleus of mass m_2, then its scattered momentum P_1' is given by

$$P_1' = \frac{P_1}{(1+\epsilon)} \left(\cos\theta + \left(1 - \epsilon^2 \sin^2\theta - \frac{Q}{E}(1+\epsilon)\right)^{\frac{1}{2}}\right) \tag{A1.1}$$

where: $\epsilon = \frac{m_1}{m_2}$; θ = laboratory scattering angle; Q = intrinsic excitation energy of the nucleus.

Using Eq. (A1.1)

$$\frac{P_1' \, dP_1'}{P_1 \, dP_1} = \frac{(\epsilon\cos\theta + R)^2}{(1+\epsilon)^2} + Q \frac{(\epsilon\cos\theta + R)}{R(1+\epsilon)E} \tag{A1.2}$$

where: $R = \left(1 - \epsilon^2 \sin^2\theta - \frac{Q}{E}(1+\epsilon)\right)^{\frac{1}{2}}$.

For the experimental situation studied in this thesis $s = 0.035$, and so a good approximation to Eq. (A1.2) may be obtained by neglecting elements which involve terms in s^2. In this approximation Eq. (A1.2) becomes

$$\frac{P_1' \, dP_1'}{P_1 \, dP_1} = \frac{2 s \cos\theta}{(1 + 2s)} \left[\frac{r(1+s)}{2(1-r(1+s))^{\frac{1}{2}}} + (1-r(1+s))^{\frac{1}{2}} \right] + \frac{1}{(1+2s)} \qquad (A1.3)$$

where: $r = \frac{Q}{E}$.

Eq. (A1.3) may be written in the form

$$\frac{dE'}{dE} = \frac{(2 s A \cos\theta + 1)}{(1 + 2s)}$$

$$= \frac{2s (A \cos\theta - 1)}{(1 + 2s)} + 1 \qquad (A1.4)$$

$$= f(\theta, Q) + 1$$

where: A denotes that part of Eq. (A1.3) enclosed in square brackets.

The function $f(\theta, Q)$ is plotted in Fig. 2.16 for different values of θ and Q.

A P P E N D I X 2

PEAK REDUCTION RATIO

A calculation, giving the reduction in the amplitudes of the spectrum peaks caused by a finite energy spread of the incident beam, is presented in this appendix.

For this calculation it is assumed that the incident beam energy spread can be represented by a box shape resolution function of the form

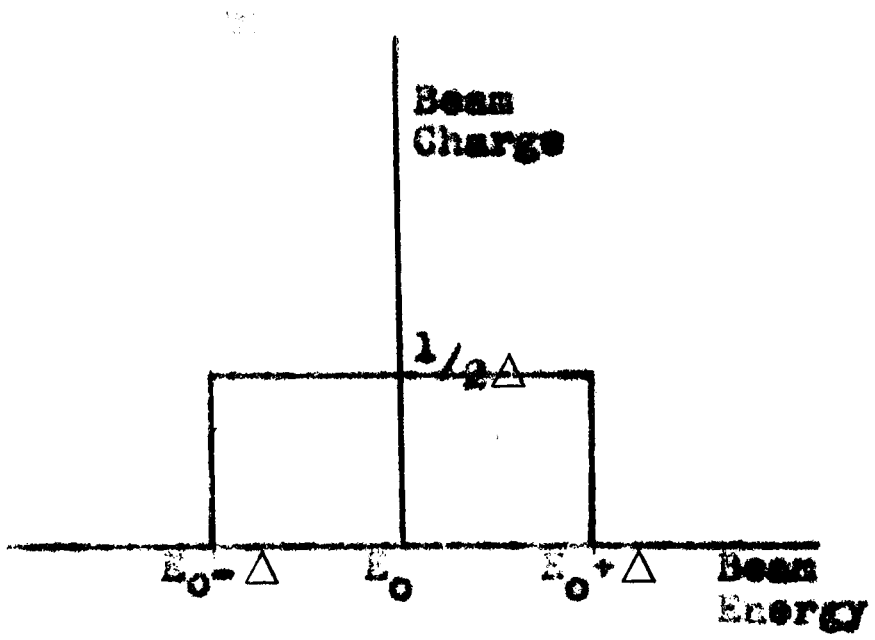

When $\Delta \rightarrow 0$, it is further assumed that the spectrum peak profiles are Gaussian, i.e.,

$$y(x) = A \exp\left(-(x-x_0)^2/w^2\right) \qquad (A2.1)$$

where: A = peak height; x_o = peak centroid; w = width of the peak.

With the above resolution function the peak amplitude at position x is given by

$$y_\Delta(x) = \frac{A}{2\Delta}\int_{-\Delta}^{+\Delta} \exp(-(x-x_o-z)^2/w^2)dz \qquad (A2.2)$$

and so the peak height is

$$y_\Delta(x_o) = \frac{A}{2\Delta}\int_{-\Delta}^{+\Delta} \exp(-z^2/w^2)dz$$

$$= A \cdot \frac{w}{2} \cdot \frac{ERF(s)}{s} \qquad (A2.3)$$

where: $s = \frac{\Delta}{w}$; ERF(s) = error function.

Using Eq. (A2.3)

$$y_\Delta(x_o) / y_{\Delta=0}(x_o) = \frac{w}{2} \cdot \frac{ERF(s)}{s}.$$

This function is plotted in Fig. 2.15.

A P P E N D I X 3

DEAD TIME CORRECTION

The formula used to estimate the counting losses (see Section 2.13) caused by the dead time of the counting electronics is derived in this appendix.

After a pulse has been received by the A.D.C. subsequent pulses are rejected if they arrive at the A.D.C. during the analogue to digital conversion time, or the waiting time of the memory buffer. Let the total dead time for a particular pulse i be denoted by t_i, and let the actual counting rate of pulses corresponding to channel c, at time T_i, be $N(c,T_i)$. Then the probability that r pulses of amplitude c arrive at the A.D.C. during the dead time t_i is given by

$$P(r,c) = \frac{(N(c,T_i)t_i)^r}{r\,!} \exp(-(N(c,T_i)t_i)) \qquad (A3.1)$$

and so the average number of pulses arriving at the A.D.C. during this time is

$$= \sum_{r=1}^{\infty} \frac{r(N(c,T_i)t_i)^r}{r!} \exp(-(N(c,T_i)t_i))$$

$$= N(c,T_i)t_i \; . \qquad (A3.2)$$

This number will be the average number of pulses of amplitude c which are lost during the dead time t_i. Denoting the actual number of pulses of amplitude c occurring during the experimental run as $\bar{N}(c)$, and the recorded number by $\bar{N}'(c)$, the relationship between these two quantities is

$$\bar{N}'(c) = \bar{N}(c) - \sum_i N(c,T_i)t_i \ . \qquad (A3.3)$$

The ratio $\frac{N(c,T_i)}{\bar{N}(c)}$ will vary if the beam intensity fluctuates, but at any time it will be independent of c. Denoting this ratio by $b(T_i)$, Eq. (A3.3) may be written

$$\frac{\bar{N}'(c)}{\bar{N}(c)} = 1 - \sum_i b(T_i)t_i \ . \qquad (A3.4)$$

If S_1 and S_2 are the number of events recorded during the experiment by the uninhibited and inhibited scalars (see Section 2.13), then

$$S_1 = \sum_{c=c_1} \bar{N}(c) \qquad (A3.5)$$

and $$S_2 = \sum_{c=c_1} (\bar{N}(c) - \sum_i \bar{N}(c,T_i)t_i) \qquad (A3.6)$$

where: c_1 = amplitude discrimination threshold for the two scalars.

Using Eqs. (A3.5), (A3.6)

$$\frac{S_2}{S_1} = 1 - \frac{\sum_{c=c_1} \sum_i N(c,T_i)\,\Delta t_i}{\sum_{c=c_1} \bar{N}(c)}$$

$$= 1 - \sum_i b(T_i)\,\Delta t_i \quad . \qquad (A3.7)$$

From Eqs. (A3.4), (A3.7)

$$\bar{N}(c) = \bar{N}'(c)\,\frac{S_1}{S_2} \quad .$$

The true channel content can therefore be determined from the ratio of the scalar events.

A P P E N D I X 4

THE VARIANCE OF CROSS-SECTIONS AND FINITE BEAM ENERGY RESOLUTION

It has been shown by Lang (1965) that the ratio of the cross-section variance measured with good energy resolution to the cross-section variance measured with an experimental energy resolution function $A(E-E_o)$ is given by

$$\frac{(\mathrm{var}(\sigma)_{\ })_{\Delta}}{(\mathrm{var}(\sigma))_{\Delta=0}} = \Gamma \int_0^{\infty} \exp(-k\Gamma)\ a(k)\ a(-k)\ dk \qquad (A4.1)$$

where: $$a(k) = \int_{-\infty}^{+\infty} \exp(ik(E-E_o))\ A(E-E_o)\ dE.$$

For a box shape resolution function similar to that shown in Appendix 2

$$a(k) = \frac{\sin(k\Delta)}{(k\Delta)} \ . \qquad (A4.2)$$

Using Eq. (A4.2) in Eq. (A4.1)

$$\frac{(\mathrm{var}(\sigma))_{\Delta}}{(\mathrm{var}(\sigma))_{\Delta=0}} = \int_0^{\infty} \exp(-k\Gamma)\ \frac{\sin^2(k\Delta)}{(k\Delta)^2}\,dk$$

$$= p\int_0^{\infty} \exp(-pt)\ \frac{\sin^2 t}{t^2}\ dt \qquad (A4.2)$$

where: $p = \frac{\Gamma}{\Delta}$.

The integral of Eq. (A4.2) is the Laplace transform of $\frac{\sin^2 t}{t^2}$, and so

$$\frac{(\mathrm{var}(\sigma))_{\Delta}}{(\mathrm{var}(\sigma))_{\Delta=0}} = p\left(\tan^{-1}\left(\frac{2}{p}\right) + \frac{p}{4}\log_e \frac{p^2}{(p^2+4)}\right) .$$

(A4.3)

This function is plotted in Fig. A4. 1.

It has also been shown by Lang (1965) that the coherence width of an experimental excitation function measured with a box shape resolution function of width 2Δ , is given by

$$\frac{\Gamma_{exp.}}{\Gamma} = \left(2.11 \cdot \frac{1}{p} + 0.62\right) \qquad (A4.4)$$

provided $p < 2$.

VARIANCE REDUCTION FUNCTION
(BOX SHAPE RESOLUTION FUNCTION)

$$R(p) = p\left(\tan^{-1}\left(\frac{2}{p}\right) + \frac{p}{4}\log_e\left(\frac{p^2}{p^2+4}\right)\right)$$

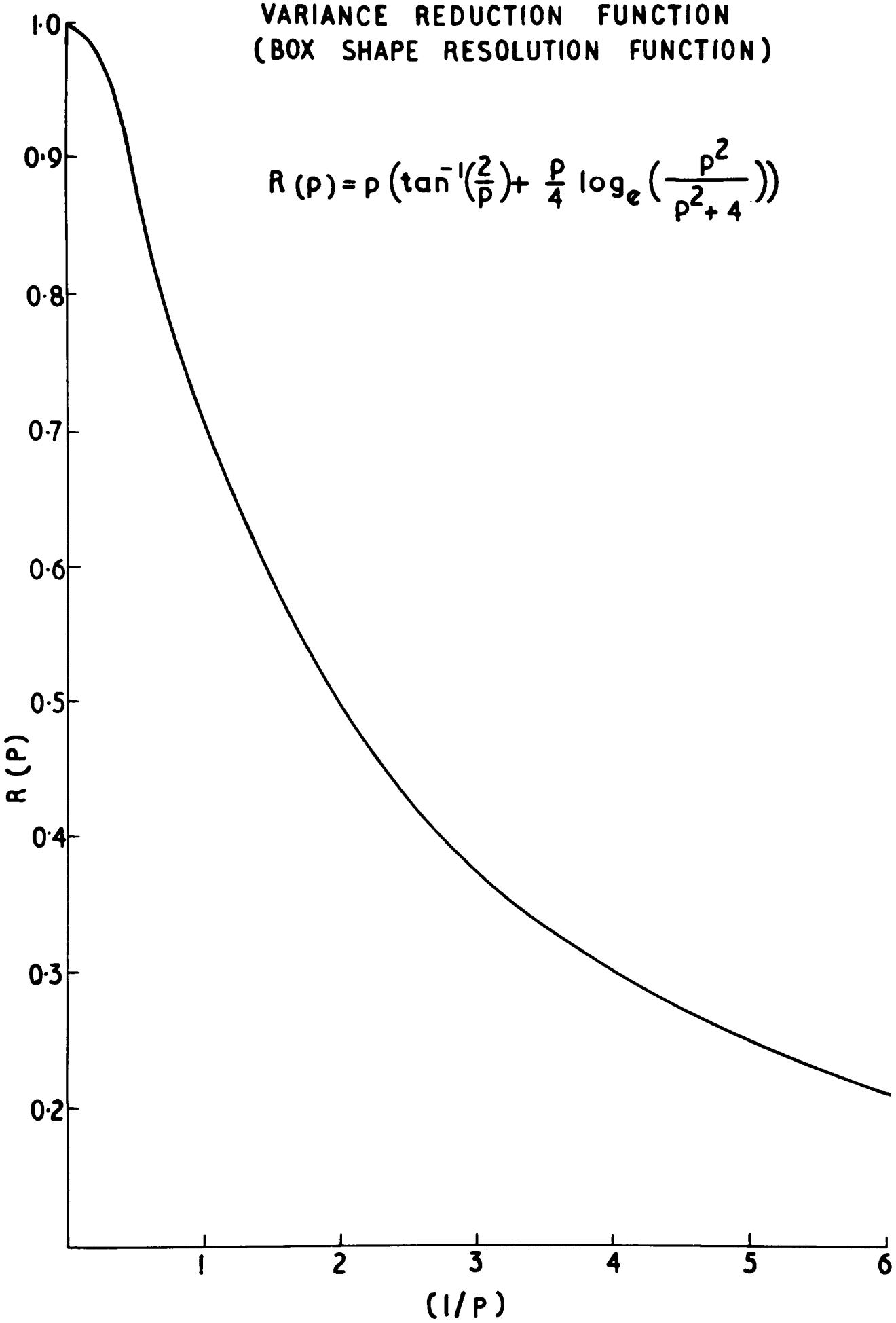

FIGURE A4·1

A P P E N D I X 5

THE VARIANCE OF REACTION CROSS-SECTIONS

A5.1 Notation

The cross-section for a reaction between two states a and a' may be written (Feshbach, 1960) in the following form :

$$\sigma(a|a') = \pi \lambda^2 \sum \frac{(2J+1)}{(2I+1)(2i+1)} |S(a\,l\,s\,|\,a'l's'\,|\,Jw)|^2 \qquad (A5.1)$$

where: $S(a\,l\,s\,|\,a'l's'\,|\,Jw)$ is the scattering matrix element describing the transition from the state a channel spin s to a state a' channel spin s', the compound system having a total angular momentum J and parity w, the incident particle an orbital angular momentum l, and the emergent particle an orbital angular momentum l'; I is the spin of the target nucleus, and i the spin of the incident particle; the sum is over the quantum numbers $(l\,l'ss'Jw)$.

It is assumed that the scattering matrix elements may be decomposed into two parts (Ericson, 1963; Feshbach, 1967[a]) -

one associated with a compound nucleus mechanism, and the other with a direct reaction mechanism, i.e.,

$$S(a\,l\,s\,|\,a'l's'|J\pi) = \sum_i \frac{a_i(aa',\beta J\pi)}{(E-E_i)} + \langle S(a\,l\,s\,|\,a'l's'\,|\,J\pi)\rangle \qquad (A5.2)$$

where: the sum extends over all nuclear compound states of particular J and π quantum numbers; $\langle S \rangle$ is the energy averaged component associated with the direct reaction; $\beta \equiv (l,s,l',s')$; $E_i = e_i - i\,\Gamma_i/2$, in which e_i and Γ_i are the energy position and width of the compound nucleus state i.

In the subsequent working it will be assumed that the real and imaginary parts of the coefficients $a_i(aa',\beta J\pi)$ belong to Gaussian distributions, and the coefficients corresponding to different sets of $(aa',\beta J\pi)$ are independent.

A5.2 One Channel Reactions

This section is concerned with the cross-section variance of reactions in which the reaction particles have zero spin, and the energy is sufficiently low so that only S-wave interactions need be considered.

The cross-section variance is defined by

$$\mathrm{var}(\sigma) = \langle (\sigma - \langle \sigma \rangle)^2 \rangle$$

$$= \langle \sigma^2 \rangle - \langle \sigma \rangle^2 \qquad \text{(A5.3)}$$

where: the angle brackets denote an average over energy.

For simplicity the direct reaction component of the scattering matrix will be taken as zero; in this case Eqs. (A5.2), (A5.3) give

$$\langle \sigma^2 \rangle = \sum_{ijmn} \left\langle \frac{a_i a_j^* a_m a_n^*}{(E-E_i)(E-E_j^*)(E-E_m)(E-E_n^*)} \right\rangle \qquad \text{(A5.4)}$$

where: the channel subscripts $(\alpha\alpha', \beta J\pi)$, since they are unique, have been omitted from the identification label of the coefficients a_i; the kinematic factor $\pi\lambda^2$ has been absorbed into the coefficients a_i.

Owing to the assumed random nature of the a_i coefficients, only terms in the summation of Eq. (A5.4) for which the 7 suffixes are pairwise equal can significantly contribute to the total sum, and so the possibilities are $(i=j, m=n, i\neq m)$; $(i=n, j=m, i\neq j)$; $(i=m, j=n, i\neq j)$ and $(i=j=m=n)$. With these terms Eq. (A5.4) becomes

$$\langle \sigma^2 \rangle = 2 \left\langle \sum_{ij} \frac{|a_i|^2 \ |a_j|^2}{|(E-E_i)|^2 \ |(E-E_j)|^2} \right\rangle_{i \neq j} + \left\langle \sum_i \frac{|a_i|^4}{|E-E_i|^4} \right\rangle$$

$$+ \left\langle \sum_{ij} \frac{(a_i)^2 \ (a_j^*)^2}{(E-E_i)^2 \ (E-E_j^*)^2} \right\rangle_{i \neq j} . \qquad \text{(A5.5)}$$

The values of the first and last terms in Eq. (A5.5) depend upon the energy spacing correlation between the neighbouring compound levels. Moldauer (1964) has argued that if the energies of the levels are randomly distributed along the real energy axis, then

$$\left\langle \sum_{ij} \frac{|a_i|^2 \ |a_j|^2}{|(E-E_i)|^2 \ |(E-E_j)|^2} \right\rangle_{i \neq j} = \langle \sigma \rangle^2 \qquad \text{(A5.6)}$$

and

$$\left\langle \sum_{ij} \frac{(a_i)^2 \ (a_j^*)^2}{(E-E_i)^2 \ (E-E_j^*)^2} \right\rangle_{i \neq j} = 0 \ . \qquad \text{(A5.7)}$$

If the spacing distribution of the levels is of the Wigner

type then the results are more complicated, but Moldauer shows that even for this distribution Eqs. (A5.6),(A5.7) are true when (Γ/D) $\gg$ 1. For the calculations in this appendix it will be assumed that Eqs. (A5.6), (A5.7) are valid. In this case Eq. (A5.5) becomes

$$\langle \sigma^2 \rangle = 2 \langle \sigma \rangle^2 + \left\langle \sum_i \frac{|a_i|^4}{|E-E_i|^4} \right\rangle \cdot \qquad (A5.8)$$

Using Eq. (A5.8) in Eq. (A5.3)

$$\mathrm{var}(\sigma) = \langle \sigma \rangle^2 + \left\langle \sum_i \frac{|a_i|^4}{|E-E_i|^4} \right\rangle \cdot \qquad (A5.9)$$

A5.3 Several Channel Reactions

This section is concerned with the cross-section variance for a reaction involving several components, β, each having the same compound system quantum numbers J,π.

The cross-section for the reaction is given by

$$\sigma = \sum_\beta \sigma(\beta)$$

$$= g(J) \sum_\beta \sum_{ij} \frac{a_i(\beta) a_j^*(\beta)}{(E-E_i)(E-E_j^*)} \qquad (A5.10)$$

where: the identification subscripts ($\alpha\alpha'$,Jw) have been omitted from the coefficients $a_i(\beta)$; $g(J) = (2J+1)/(2I+1)(2i+1)$.

From Eq. (A5.10)

$$\langle \sigma^2 \rangle = g^2(J) \sum_{\beta\beta'} \left\langle \sum_{ijmn} \frac{a_i(\beta)a_j^*(\beta)a_m(\beta')a_n^*(\beta')}{(E-E_i)(E-E_j^*)(E-E_m)(E-E_n^*)} \right\rangle . \tag{A5.11}$$

The evaluation of the terms in Eq. (A5.11) for which $\beta = \beta'$ is identical in method to that used for the one channel case considered in the previous section, and so

$$\text{sum of } (\beta=\beta') \text{ terms} = 2 \sum_\beta \langle \sigma(\beta) \rangle^2 + g^2(J) \sum_\beta \left\langle \sum_i \frac{|a_i(\beta)|^4}{|E-E_i|^4} \right\rangle , \tag{A5.12}$$

In the determination of the quantity

$$\left\langle \sum_{ijmn} \frac{a_i(\beta)a_j^*(\beta)a_m(\beta')a_n^*(\beta')}{(E-E_i)(E-E_j^*)(E-E_m)(E-E_n^*)} \right\rangle_{\beta\neq\beta'}$$

only terms need be considered for which ($i=j$, $m=n$, $i\neq m$) and ($i=j=m=n$).

In this case

$$\langle(\beta\neq\beta')\text{ term} = g^2(J)\left\langle\sum_{ij}\frac{|a_i(\beta)|^2\,|a_j(\beta')|^2}{|(E-E_i)|^2\,|(E-E_j)|^2}\right\rangle_{i\neq j}$$

$$+\,g^2(J)\left\langle\sum_{i}\frac{|a_i(\beta)|^2\,|a_i(\beta')|^2}{|(E-E_i)|^4}\right\rangle \qquad \text{(A5.13)}$$

By using arguments similar to those used in deriving Eq. (A5.8), Eq. (A5.13) becomes

$$(\beta\neq\beta')\text{ term} = \langle\sigma(\beta)\rangle\langle\sigma(\beta')\rangle + g^2(J)\left\langle\sum_{i}\frac{|a_i(\beta)|^2\,|a_i(\beta')|^2}{|(E-E_i)|^4}\right\rangle \qquad \text{(A5.14)}$$

Collecting terms for Eq. (A5.11)

$$\langle\sigma^2\rangle = \sum_{\beta}\left(2\langle\sigma(\beta)\rangle^2 + g^2(J)\left\langle\sum_{i}\frac{|a_i(\beta)|^4}{|(E-E_i)|^4}\right\rangle\right)$$

$$+\sum_{\beta\beta'}\left(\langle\sigma(\beta)\rangle\langle\sigma(\beta')\rangle + g^2(J)\left\langle\sum_{i}\frac{|a_i(\beta)|^2\,|a_i(\beta')|^2}{|E-E_i|^4}\right\rangle\right)_{\beta\neq\beta'} \qquad \text{(A5.15)}$$

The square of the averaged cross-section may be written

$$\langle \sigma \rangle^2 = \left\langle \sum_\beta \sigma(\beta) \right\rangle^2 = \sum_{\beta\beta'} \langle \sigma(\beta) \rangle \langle \sigma(\beta') \rangle \qquad (A5.16)$$

Using Eqs. (A5.15), (A5.16) in Eq. (A5.3)

$$\mathrm{var}(\sigma) = \sum_\beta \left(\langle \sigma(\beta) \rangle^2 + g^2(J) \left\langle \sum_i \frac{|a_i(\beta)|^4}{|E-E_i|^4} \right\rangle \right)$$

$$+ g^2(J) \sum_{\beta\beta'} \left\langle \sum_i \frac{|a_i(\beta)|^2 \, |a_i(\beta')|^2}{|E-E_i|^4} \right\rangle_{\beta \neq \beta'}$$

(A5.17)

To evaluate the summations occurring inside the angle brackets of Eq. (A5.17), it is assumed that the sums may be replaced by integrations

i.e., $$\left\langle \sum_i \frac{|a_i(\beta)|^4}{|(E-E_i)|^4} \right\rangle = \left\langle \frac{1}{D} \int_{-\infty}^{+\infty} \frac{|a_i(\beta)|^4}{|(E-E_i)|^4} \, de_i \right\rangle$$

(A5.18)

where: D = the average compound level spacing at energy E.

The integrand occurring in Eq. (A5.18) has a second order pole in both the upper and lower half portions of complex E plane, and therefore

$$\left\langle \frac{1}{D}\int_{-\infty}^{+\infty} \frac{|a_i(\beta)|^4}{|E-E_i|^4}\, de_i \right\rangle = \frac{4\pi}{D\Gamma^3} \langle |a_i(\beta)|^4 \rangle$$

$$= \frac{8\pi}{D\Gamma^3} \langle |a_i(\beta)|^2 \rangle^2 . \qquad (A5.19)$$

where: Γ = the average total width of the compound states.

In the last step of Eq. (A5.19) use has been made of the assumptions that the real and imaginary parts of the coefficients $a_i(\beta)$ belong to Gaussian distributions of the same dispersion.

By again replacing the summation by an integration, the averaged cross-section for the reaction component β may be written

$$\langle \sigma(\beta) \rangle = g(J) \left\langle \sum_{ij} \frac{a_i(\beta) a_j^*(\beta)}{(E-E_i)(E-E_j)^*} \right\rangle = g(J) \left\langle \sum_i \frac{|a_i(\beta)|^2}{|(E-E_i)|^2} \right\rangle$$

$$= \frac{2\pi g(J)}{\Gamma D} \langle |a_i(\beta)|^2 \rangle . \qquad (A5.20)$$

Using Eq. (A5.20), (A5.19) in Eq. (A5.18)

$$g^2(J)\left\langle \sum_i \frac{|a_i(\beta)|^4}{|(E-E_i)|^4} \right\rangle = \frac{2}{\pi} \cdot \frac{\langle \sigma(\beta) \rangle^2}{(\frac{\Gamma}{D})} \quad . \tag{A5.21}$$

By similar arguments

$$g^2(J)\left\langle \sum_i \frac{|a_i(\beta)|^2 \, |a_i(\beta')|^2}{|E-E_i|^4} \right\rangle_{\beta \neq \beta'} = \frac{1}{\pi} \frac{\langle \sigma(\beta) \rangle \langle \sigma(\beta') \rangle}{(\frac{\Gamma}{D})} \tag{A5.22}$$

The different numerical factors in Eqs. (A5.21), (A5.22) originate from the relations

$$\langle |a_i(\beta)|^4 \rangle = 2 \langle |a_i(\beta)|^2 \rangle^2 \tag{A5.23}$$

$$\langle |a_i(\beta)|^2 \, |a_i(\beta')|^2 \rangle_{\beta \neq \beta'} = \langle |a_i(\beta)|^2 \rangle \langle |a_i(\beta')|^2 \rangle \quad . \tag{A5.24}$$

Using Eqs. (A5.21), (A5.22) in Eq. (A5.17)

$$\mathrm{var}(\sigma) = \sum_\beta \langle \sigma(\beta) \rangle^2 \left(1 + \frac{1}{\pi} \cdot \frac{1}{(\Gamma/D)}\right) + \frac{\langle \sum_\beta \sigma(\beta) \rangle^2}{\pi (\Gamma/D)} \tag{A5.25}$$

It is of note that when $(\Gamma/D) \gg 1$, Eq. (A5.25) reduces to the equation

$$\mathrm{var}(\sigma) = \sum_{\beta} \langle \sigma(\beta) \rangle^2 \quad . \tag{A5.26}$$

The form of the second term in Eq. (A5.25) is determined by the fact that the different partial channels have the same random set of compound system levels. As the number of channels increases, this term becomes of increasing importance because if the number of channels is n, then

$$\frac{\langle \sum_{\beta} \sigma(\beta) \rangle^2}{\sum_{\beta} \langle \sigma(\beta) \rangle^2} \approx n \quad . \tag{A5.27}$$

A5.4 The General Compound System

In this section the formalism of the previous section is extended to include compound nucleus levels of different quantum numbers J,π.

For this case

$$\sigma = \sum_{J\pi\beta} \sigma(\beta J\pi)$$

$$= \sum_{J\pi\beta} g(J) \sum_{ij} \frac{a_i(\beta J\pi)\, a_j^*(\beta J\pi)}{(E-E_i(J\pi))(E-E_j^*(J\pi))}$$

$$\left\langle \text{in} \right.$$

(A5.28)

where: $E_i^*(J\pi)$ = the complex energy of the compound nucleus state i with quantum numbers J and π; the identification subscripts α, α' have been omitted from the coefficients $a_i(\beta J\pi)$.

From Eq. (A5.28)

$$\langle \sigma^2 \rangle = \sum_{\substack{J'\pi'\beta' \\ J\ \pi\ \beta}} g(J)\, g(J')$$

$$\cdot \left\langle \sum_{ijmn} \frac{a_i(\beta J\pi)\, a_j^*(\beta J\pi)\, a_m(\beta' J'\pi')\, a_n^*(\beta' J'\pi')}{(E-E_i(J\pi))(E-E_j^*(J\pi))(E-E_m(J'\pi'))(E-E_n^*(J'\pi'))} \right\rangle \cdot$$

(A5.29)

The evaluation of terms for which ($J'=J$, $\pi'=\pi$) is identical to the case considered in the previous section. For the terms in which one or both pairs of suffixes (J,J'), (π,π')

differ, the only significant elements in the (ijmn) summation correspond to (i=j, m=n). The sum value of these elements is given by

$$g(J)g(J') \left\langle \sum_{im} \frac{|a_i(\beta J\pi)|^2 \; |a_m(\beta' J'\pi')|^2}{|E-E_i(J\pi)|^2 \; |E-E_m(J'\pi')|^2} \right\rangle$$

$$= \langle \sigma(\beta J\pi) \rangle \langle \sigma(\beta' J'\pi') \rangle \quad . \qquad (A5.30)$$

This last result follows if it is assumed that there is zero correlation between the poles for levels of different quantum numbers J,π.

The average squared cross-section may be written

$$\langle \sigma \rangle^2 = \sum_{\substack{J'\pi'\beta' \\ J\pi\beta}} \langle \sigma(\beta J\pi) \rangle \langle \sigma(\beta' J'\pi') \rangle \qquad (A5.31)$$

and so using Eqs. (A5.31), (A5.30), (A5.25) in Eq. (A5.3)

$$\mathrm{var}(\sigma) = \sum_{J\pi\beta} \left\langle \sigma(\beta J\pi) \right\rangle^2 \left(1 + \frac{1}{\pi} \cdot \frac{1}{(\Gamma(J\pi)/D(J\pi))}\right)$$

$$+ \sum_{J\pi} \left\langle \sum_{\beta} \sigma(\beta J\pi) \right\rangle^2 / (\pi\Gamma(J\pi)/D(J\pi)) \qquad (A5.32)$$

A5.5 Scattering to Several Residual States

The cross-section for a reaction involving several residual states a_n is given by

$$\sigma = \sum_{n\beta J\pi} \sigma(\alpha a_n, \beta J\pi)$$

$$= \sum_{n\beta J\pi} g(J) \sum_{ij} \frac{a_i(\alpha a_n, \beta J\pi)\, a_j^*(\alpha a_n, \beta J\pi)}{(E-E_i)(E-E_j^*)} \quad . \qquad (A5.33)$$

By using similar methods to those used in the previous sections, the variance of the cross-section in this case is given by

$$\mathrm{var}(\sigma) = \sum_{n\beta J\pi} \left\langle \sigma(\alpha a_n, \beta J\pi) \right\rangle^2 \left(1 + \frac{1}{\pi(\Gamma(J\pi)/D(J\pi))}\right)$$

$$+ \sum_{J\pi} \left\langle \sum_{\beta n} \sigma(\alpha a_n, \beta J\pi) \right\rangle^2 / (\pi\Gamma(J\pi)/D(J\pi)) . \qquad (A5.34)$$

A P P E N D I X 6

VARIANCE OF THE LEGENDRE COEFFICIENTS

A6.1 Notation

If the angular distribution for a reaction between the states α and α' is expanded in the form

$$\frac{d\sigma(\alpha|\alpha')}{d\Omega} = \sum_L B_L(\alpha|\alpha') P_L(\cos\theta) \qquad (A6.1)$$

then in the notation of Section A.5.1 the B_L coefficients may be expressed (Feshbach, 1960) in terms of the scattering matrix in the following way :

$$B_L(\alpha|\alpha') = \frac{\chi^2}{4} \sum \frac{(-1)^{s'-s}}{(2I+1)(2i+1)} \bar{Z}(\ell_1 J_1 \ell_2 J_2; sL)\, \bar{Z}(\ell_1' J_1 \ell_2' J_2; s'L)$$

$$\cdot \mathrm{Re}\left(S^*(\alpha \ell_1 s \mid \alpha' \ell_1' s' \mid J_1 \pi_1)\, S(\alpha \ell_2 s \mid \alpha' \ell_2' s' \mid J_2 \pi_2)\right)$$

A6.2)

where: the sum extends over all possible combinations of

the quantum numbers $(\ell_1, \ell_2, \ell_1', \ell_2', s, s', J_1, J_2, \pi_1, \pi_2)$; the $\bar{Z}$ coefficients, in terms of the Racah and Clebsch-Gordan coefficients, are defined by

$$\bar{Z}(\ell_1 J_1 \ell_2 J_2; sL) = \left[(2\ell_1+1)(2J_1+1)(2\ell_2+1)(2J_2+1) \right]^{\frac{1}{2}} \cdot (\ell_1 \ell_2 00 \mid L0)\, W(\ell_1 J_1 \ell_2 J_2; sL) .$$

To later simplify the notation, a coefficient ω is introduced by the equation

$$\omega(\beta_1 J_1, \beta_2 J_2, L) = (-1)^{s'-s} \frac{\bar{Z}(\ell_1 J_1 \ell_2 J_2; sL)\, \bar{Z}(\ell_1' J_1 \ell_2' J_2; s'L)}{4\pi \sqrt{(2J_1+1)(2J_2+1)}}$$

where: $\beta_1 \equiv (\ell_1, s, \ell_1', s')$.

It is assumed, as in Appendix 5, that the scattering matrix may be decomposed into two components - one associated with a compound nucleus mechanism and the other with a direct reaction mechanism. For simplicity this latter component will be taken as zero, and so

$$S(a\,l\,s \mid a'l's' \mid Jw) = \sum_i \frac{a_i(aa',\beta Jw)}{(E-E_i)}$$

$$= \sum_i b_i(aa',\beta Jw) \qquad (A6.3)$$

where: the sum i is over compound states of given J and w;

$\beta \equiv (l,s,l',s')$; the last step in the equation defines b.

In the succeeding sections the identification labels a and a' will be omitted from the b coefficients.

A6.2 Compound System of Restricted Quantum Numbers

In this section the formalism is restricted to the case where all the compound nucleus levels have the same values of the quantum numbers J and w.

The variance of the B_L coefficient is given by

$$\mathrm{var}(B_L) = \langle (B_L - \langle B_L \rangle)^2 \rangle$$

$$= \langle B_L^2 \rangle - \langle B_L \rangle^2 \qquad (A6.5)$$

where: the angle brackets denote an average over energy.

From Eqs. (A6.2), (A6.3)

$$\langle B_L^2(a|L') \rangle_{J\pi} = \frac{1}{4} \sum_{\beta_1\beta_2\beta_1'\beta_2'} \omega(\beta_1,\beta_2,L)\, \omega(\beta_1',\beta_2',L)(2J+1)^2$$

$$\cdot\left[\sum_{ijmn} (b_i(\beta_1)b_j^*(\beta_2)+b_j(\beta_2)b_i^*(\beta_1))(b_m(\beta_1')b_n^*(\beta_2')+b_n(\beta_2')b_m^*(\beta_1'))\right]$$

(A6.6)

where: the quantum numbers J and π have been omitted from the ω and b coefficients, since, within the summation, the values of J and π are fixed; the factor $(\pi\lambda^2/(2I+1)(2I'+1))^2$ has been absorbed into the b coefficients.

The expression in square brackets in the above equation may be expanded as

$$\left[\sum_{ijmn} b_i(\beta_1)b_j^*(\beta_2)b_m(\beta_1')b_n^*(\beta_2') \right.$$

$$+ \sum_{ijmn} b_i(\beta_1)b_j^*(\beta_2)b_n(\beta_2')b_m^*(\beta_1')$$

$$+ \sum_{ijmn} b_j(\beta_2)b_i^*(\beta_1)b_m(\beta_1')b_n^*(\beta_2')$$

$$\left. + \sum_{ijmn} b_j(\beta_2)b_i^*(\beta_1)b_n(\beta_2')b_m^*(\beta_1') \right] .$$

For similar reasons given in Section A5.2, only the following

combinations of channels will give any significant contribution to the above expression:

$$\text{(a)} \quad \beta_1 \equiv \beta_2; \quad \beta_1' \equiv \beta_2'; \quad \beta_1 \neq \beta_1'$$

$$\text{(b)} \quad \beta_1 \equiv \beta_1'; \quad \beta_2 \equiv \beta_2'; \quad \beta_1 \neq \beta_2$$

$$\text{(c)} \quad \beta_1 \equiv \beta_2'; \quad \beta_2 \equiv \beta_1'; \quad \beta_1 \neq \beta_2$$

$$\text{(d)} \quad \beta_1 \equiv \beta_2 \equiv \beta_1' \equiv \beta_2' \ .$$

If, for these different possibilities, the expression in square brackets is evaluated by a method similar to that used in the evaluation of Eq. (A5.4), then Eq. (A6.6) becomes

$$\langle B_L^2(a|a') \rangle_{J\pi} = (1 + \frac{1}{\pi\Gamma(J\pi)/D(J\pi)}) \Bigg[\sum_{\beta\beta'} \Big((\omega(\beta,\beta,L)\ \omega(\beta',\beta',L) + \omega^2(\beta,\beta',L))\ \langle \sigma(\beta) \rangle \langle \sigma(\beta') \rangle \Big)_{\beta \neq \beta'} + 2 \sum_{\beta} \omega^2(\beta,\beta,L) \langle \sigma(\beta) \rangle^2 \Bigg] \ . \tag{A6.7}$$

The square of the averaged $B_L(\alpha|\alpha')$ coefficient may be written

$$\langle B_L(\alpha|\alpha')\rangle^2_{J\pi} = \left(\sum_\beta \omega(\beta,\beta,L)\langle\sigma(\beta)\rangle\right)^2$$

$$= \sum_{\beta\beta'} \omega(\beta,\beta,L)\omega(\beta',\beta',L)\langle\sigma(\beta)\rangle\langle\sigma(\beta')\rangle \qquad (A6.8)$$

Using Eqs. (A6.8), (A6.7) in Eq. (A6.5)

$$\mathrm{var}(B_L(\alpha|\alpha'))_{J\pi} = \sum_\beta \omega^2(\beta,\beta,L)\langle\sigma(\beta)\rangle^2$$

$$+ \sum_{\beta\beta'}\left(\omega^2(\beta,\beta',L)\langle\sigma(\beta)\rangle\langle\sigma(\beta')\rangle\right)_{\beta\neq\beta'}$$

$$+ \frac{1}{\pi}\frac{\Gamma(J\pi)}{D(J\pi)}\left[\sum_{\beta\beta'}\left((\omega(\beta,\beta,L)\,\omega(\beta',\beta',L) + \omega^2(\beta,\beta',L))\right.\right.$$

$$\left.\left.\cdot\langle\sigma(\beta)\rangle\langle\sigma(\beta')\rangle\right)_{\beta\neq\beta'} + 2\sum_\beta \omega^2(\beta,\beta',L)\langle\sigma(\beta)\rangle^2\right]. \qquad (A6.9)$$

This equation reduces to Eq. (A5.17) for the coefficient $B_e(\cdot|\cdot')$, as it should, since this coefficient is proportional to the total cross-section.

A6.3 The General Case

In this section the formalism of the previous section is extended to include compound nucleus levels of all J and π values.

In this case, the sum in Eq. (A6.6) must extend over all possible combinations of $\beta_1 J_1 \pi_1$, $\beta_2 J_2 \pi_2$, $\beta_1' J_1' \pi_1'$, $\beta_2' J_2' \pi_2'$. For those combinations in which $J_1 = J_2 = J_1' = J_2'$ and $\pi_1 = \pi_2 = \pi_1' = \pi_2'$ the evaluation of the corresponding term in Eq. (A6.6) is the same as in the previous section; the total sum of these combinations is therefore equal to

$$\sum_{J\pi} \left(1 + \frac{1}{\pi\Gamma(J\pi)/D(J\pi)}\right) \left[\sum_{\beta\beta'} \left(\left(\omega(\beta J,\beta J,L)\omega(\beta' J,\beta' J,L) + \omega^2(\beta J,\beta' J,L)\right) \cdot \langle \sigma(\beta J\pi)\rangle \langle \sigma(\beta' J\pi)\rangle \right)_{\beta\neq\beta'} + 2 \sum_{\beta} \omega^2(\beta J,\beta J,L) \cdot \langle \sigma(\beta J\pi)\rangle^2 \right] . \qquad (A6.10)$$

For combinations in which the angular momenta or parities differ, only those which obey the following relations will give any significant contribution to Eq. (A6.6):

$$\text{(a)} \quad c_1 \equiv c_2; \quad c_1' \equiv c_2'; \quad c_1 \neq c_1'$$

$$\text{(b)} \quad c_1 \equiv c_1'; \quad c_2 \equiv c_2'; \quad c_1 \neq c_2$$

$$\text{(c)} \quad c_1 \equiv c_2'; \quad c_2 \equiv c_1'; \quad c_1 \neq c_2$$

where: $c \equiv (\beta, J, \pi)$.

Evaluation of these terms gives

$$\sum_{c_1 c_2} \left(w(c_1, c_1, L) w(c_2, c_2, L) \; \langle \sigma(c_1) \rangle \langle \sigma(c_2) \rangle \right)_{c_1 \neq c_2}$$

$$+ \sum_{c_1 c_2} \left(w(c_1, c_2, L) w(c_2, c_1, L) \; \langle \sigma(c_1) \rangle \langle \sigma(c_2) \rangle \right)_{c_1 \neq c_2} \qquad \text{(A6.11)}$$

where: the sum over c implies the sum over β, J and π.

The square of the averaged $B_L(a|a')$ coefficient may be written

$$\langle B_L(a|a') \rangle^2 = \sum_{c_1 c_2} w(c_1, c_1, L) w(c_2, c_2, L)$$

$$\cdot \langle \sigma(c_1) \rangle \langle \sigma(c_2) \rangle \; . \qquad \text{(A6.12)}$$

Using Eqs. (A6.12), (A6.11),(A6.10) in Eq. (A6.5) gives

$$\mathrm{var}(B_L(c|a')) = \sum_{\beta J\pi} \omega^2(\beta J,\beta J,L) \langle \sigma(\beta J\pi)\rangle^2$$

$$+ \sum_{J\pi\beta\beta'} \left(\omega^2(\beta J,\beta' J,L) \langle \sigma(\beta J\pi)\rangle \langle \sigma(\beta' J\pi)\rangle \right)_{\beta\neq\beta'}$$

$$+ \sum_{\substack{\beta\ J\ \pi \\ \beta' J' \pi'}} \left(\omega^2(\beta' J',\beta J,L) \langle \sigma(\beta J\pi)\rangle \langle \sigma(\beta' J'\pi')\rangle \right)_{J\pi\neq J'\pi'}$$

$$\cdot \sum_{J\pi} \left(\frac{1}{\pi\Gamma\ (J\pi)/D(J\pi)} \right) \left[\sum_{\beta\beta'} \left(\left(\omega(\beta J,\beta J,L)\omega(\beta' J,\beta' J,L) + \omega^2(\beta J,\beta' J,L) \right) \right.\right.$$

$$\left.\left. \cdot \langle \sigma(\beta J\pi)\rangle \langle \sigma(\beta' J\pi)\rangle \right)_{\beta\neq\beta'} + 2 \sum_{\beta} \omega^2(\beta J,\beta J,L) \langle \sigma(\beta J\pi)\rangle^2 \right]$$

(A6.13)

A P P E N D I X 7

CALCULATION OF THE TOTAL WIDTH $\langle \Gamma(J\pi) \rangle$

A7.1 The Width Formula

With the proton energies used in this experiment the average excitation energy of the compound nucleus (P^{29}) was about 16 MeV; the statistical model of decay (Ericson, 1960) is therefore expected to give a fair representation of the average total width $\langle \Gamma_E(J\pi) \rangle$ (Gadioli et al., 1966). This model gives the width as

$$\langle \Gamma_E(J\pi) \rangle = \frac{\langle D_E(J\pi) \rangle}{2\pi} \sum_{rl} q(l\,J\pi) \int \rho(E_r^*) T_l(\epsilon_r) d\epsilon_r \qquad (A7.1)$$

where: $$q(l\,J\pi) = \sum_{S'=|J-l|}^{J+l} \sum_{j=|S'-I|}^{S'+I} f(j\pi).$$

In Eq. (A7.1), r denotes a particular decay mode, e.g., p, He^4; ρ is the average total density of levels for the residual nucleus at excitation energy E_r^*; $f(j\pi)$ is the spin distribution function for the residual nucleus; $T_l(\epsilon_r)$ is the transmission coefficient for an emitted particle of

spin I, decaying from the compound nucleus state j_w, with orbital angular momentum l and energy E_r.

The parameter distribution functions for the residual nucleus Si^{28} are discussed in the following section.

A7.2 The Parameter Distributions

Bethe (1936, 1937), in his original work in calculating level densities, considered a nucleus as a gas of two types of fermions; he demonstrated that this resulted in the level density approximately varying as $\exp((aE)^{\frac{1}{2}})$. At low excitation energies, however, there is significant deviation from this behaviour; it has been noted (Ericson, 1959; Gilbert and Cameron, 1965; Gilbert et al., 1965) that a linear exponential gives a better representation for this energy region. In fact, if the logarithm of the number of observed levels up to a certain energy is plotted against a linear energy scale, then for many light elements the resulting curve is linear over ten or more MeV. This suggests the relation

$$N = \exp[(E-E_0)/T] \qquad (A7.2)$$

where: N = number of levels occurring up to an excitation

energy E; E_0,T are constants.

At high excitation energies the experimental values begin to fall below this curve; this is probably partially due to levels being missed experimentally (Gilbert et al., 1965) and partly to a real deviation from the linear relation - a result not unexpected since all theories give the high energy variation as $\exp((aE)^{\frac{1}{2}})$. The question of the excitation energy at which the two formulae smoothly join has been discussed by Gilbert and Cameron (1965).

The Ericson plot for the nucleus Si^{28} is shown in Fig. A7.1; the levels have been taken from a recent survey by Endt and Van der Leun (1967). The best straight line through the plotted points has the equation

$$N(E) = \exp\left(\frac{E - 2.5}{2.3}\right) \qquad (A7.3)$$

and so $$\rho(E) = \frac{1}{2.3} \exp\left(\frac{E - 2.5}{2.3}\right) . \qquad (A7.4)$$

Gilbert and Cameron (1965) quote a value of 13 MeV for the range of validity of Eq. (A7.3), and so it was assumed that the equation was valid over the energy range considered in these calculations.

The level spin distribution has been considered by Brieson (1960); he concluded that the density of levels of given J, $\rho(E,J)$, is related to the total level density $\rho(E)$ by

$$\rho(E,J) = \rho(E) \frac{(2J+1)}{2\sigma^2} \exp\left(-(J+\tfrac{1}{2})^2/2\sigma^2\right) . \qquad (A7.5)$$

There are two difficulties in using this formula. In the first place it is based on a very general notion of random coupling of the angular momenta of individual nucleons comprising the nucleus; while this is expected to be a good model at high excitation energies, it is open to some doubt in the lower regions, since here the nucleons would be more correlated. (Unfortunately for the calculation of (Γ/D) knowledge of the spin distribution in Si^{28} was required over the whole excitation range from 0 to 14 MeV.) The second difficulty is the uncertainty in the spin parameter σ; experimental determination has come from two sources: direct observation, and determination of isomeric cross-section ratios. Ritzo (1959, 1961) determined the spins of several hundred resonances observed in neutron scattering from Na and Al, and found that a value of σ

from 1.8 to 2.2 provided the best fit to the data. It has been shown (Huizenga and Vandenbosch, 1960; Vogt, 1962; Reisch, 1963) that information on σ can be obtained from the ratios of reaction cross-sections leading to different isomers of the final nucleus; however, the experimental results tend to give unreliable values of σ because of other influences on the ratio, but some idea of the trend of σ with A is obtained: σ increases in a general way with A, being around 2 for $A \approx 25$ and 3 for $A \approx 60$.

The values of the spin parameters quoted by Gilbert and Cameron (1965), for the mass region surrounding Si^{26}, are never greater than 2.25, and so for the present calculations the spin parameter of Si^{28} was taken to be between 2.0 and 2.5.

The question of parity distribution amongst the nuclear levels has been considered by Grimes (1960) who concludes that at high enough excitation energies, essentially in the region of the neutron or proton binding energies, there is equal probability of either parity, but deviations from this behaviour are not unexpected at lower energies.

A7.3 Calculation of the ratios ($\Gamma_n(E)/\Gamma_\gamma(E)$).

In the use of Eq. (A7.1) it was assumed the compound

nucleus P^{29} could only decay by proton emission. In fact, at the energies considered, the α-particle channel is just open, but owing to the greatly reduced penetration factors in comparison with proton emission, its influence on the average width is likely to be small. The integrals occurring in Eq. (A7.1) were calculated with transmission coefficients $T_\ell(E)$ interpolated from those determined by Meldner and Linder (1964), who used the generalised optical potential coefficients of Perey (1963); the level density ρ was taken as represented by Eq. (A7.4). The calculation was carried out for a compound nucleus energy of 16 MeV, which corresponded to the mid-energy of the experimental range. The calculated values of the integrals are tabulated in Tab. A7.1, (see end of Appendix).

The factors $q_{\ell,\pi}$ were computed for two values of the Si^{28} spin parameter $\sigma = 2.0$ and 2.25. These factors are tabulated in Tab. A7.2; the factors correspond to compound states of either parity since they were calculated by assuming an equal distribution of parity amongst the levels of Si^{28}.

The values of ($\Gamma(J\pi)/D(J\pi)$), calculated with the information in Tabs. A7.1, A7.2, are shown in Fig. A7.3;

also plotted in this figure are the values corresponding to an infinite spin parameter - a value which has been used by several authors since it leads to a linear dependence between ($\Gamma(Jw)/D(Jw)$) and J, for in this case

$$\Gamma_{lJw} \propto (2l+1)(2J+1)$$

and so

$$\frac{\langle \Gamma(Jw) \rangle}{\langle D(Jw) \rangle} \propto (2J+1). \qquad (A7.6)$$

From Fig. A7.3 it is evident that eq. (A7.6) is a poor approximation for the compound nucleus P^{29}; the equation is expected to be more valid for heavier nuclei.

In these calculations of ($\Gamma(Jw)/D(Jw)$) it was considered that the main uncertainties in the values were caused by incomplete knowledge of the spin parameter σ and the parity distribution of the levels in Si^{28}. To study how the values were affected by the parity distribution, the ratios were recalculated with the assumption that the residual levels were only of positive parity; the resulting values are shown in Fig. A7.4. It is to be noted that in this case the ratio ($\Gamma(Jw)/D(Jw)$) depends upon the parity of the compound state, but the shapes of the two curves for

either parity are quite similar, and the average of the two curves is identical to the curve of Fig. A7.3 - a fact which can be understood from the associated angular momentum addition equations.

The relative dependence of $\Gamma(Jw)/D(Jw)$ with respect to J was concluded to be similar to the curves of Fig. A7.3; the absolute normalisations of the ratios, however, were regarded as somewhat uncertain.

Table A7.1

$G_\ell = \int T_\ell(E)\rho(E)dE$				
ℓ	0	1	2	3
G_ℓ	16.0	15.5	5.2	1.2

TABLE A7.2

$Q_{\ell J\pi}$ (Si^{28}, spin parameter = 2.0)					
ℓ \ J	1/2	3/2	5/2	7/2	9/2
0	0.210	0.285	0.230	0.137	0.057
1	0.495	0.725	0.652	0.424	0.194
2	0.515	0.862	0.919	0.710	0.424
3	0.367	0.709	0.919	0.919	0.709

$Q_{\ell J\pi}$ (Si^{28}, spin parameter = 2.25)					
ℓ \ J	1/2	3/2	5/2	7/2	9/2
0	0.165	0.249	0.238	0.164	0.082
1	0.414	0.652	0.651	0.484	0.246
2	0.487	0.816	0.898	0.733	0.484
3	0.402	0.733	0.898	0.898	0.733

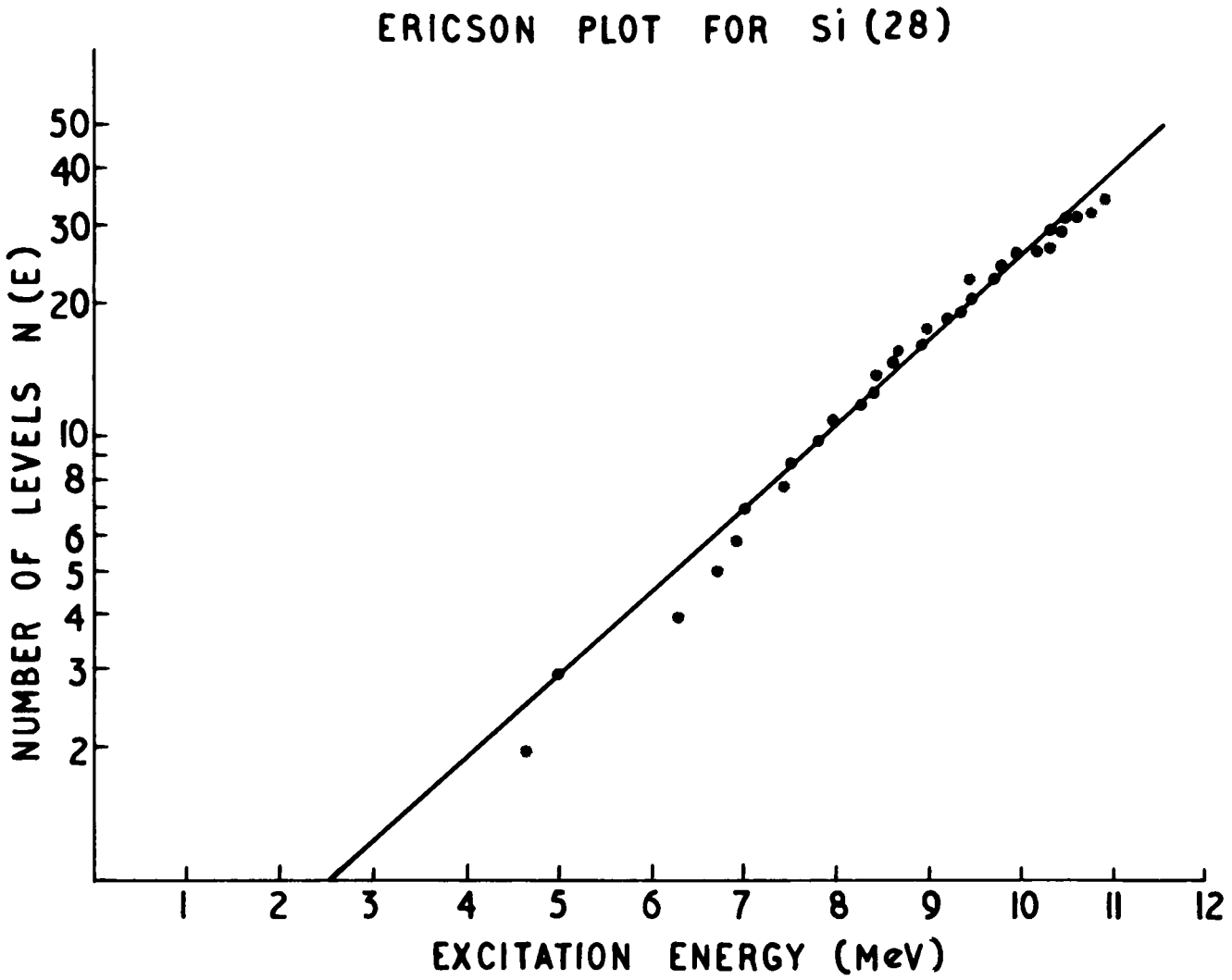

FIGURE A7·1

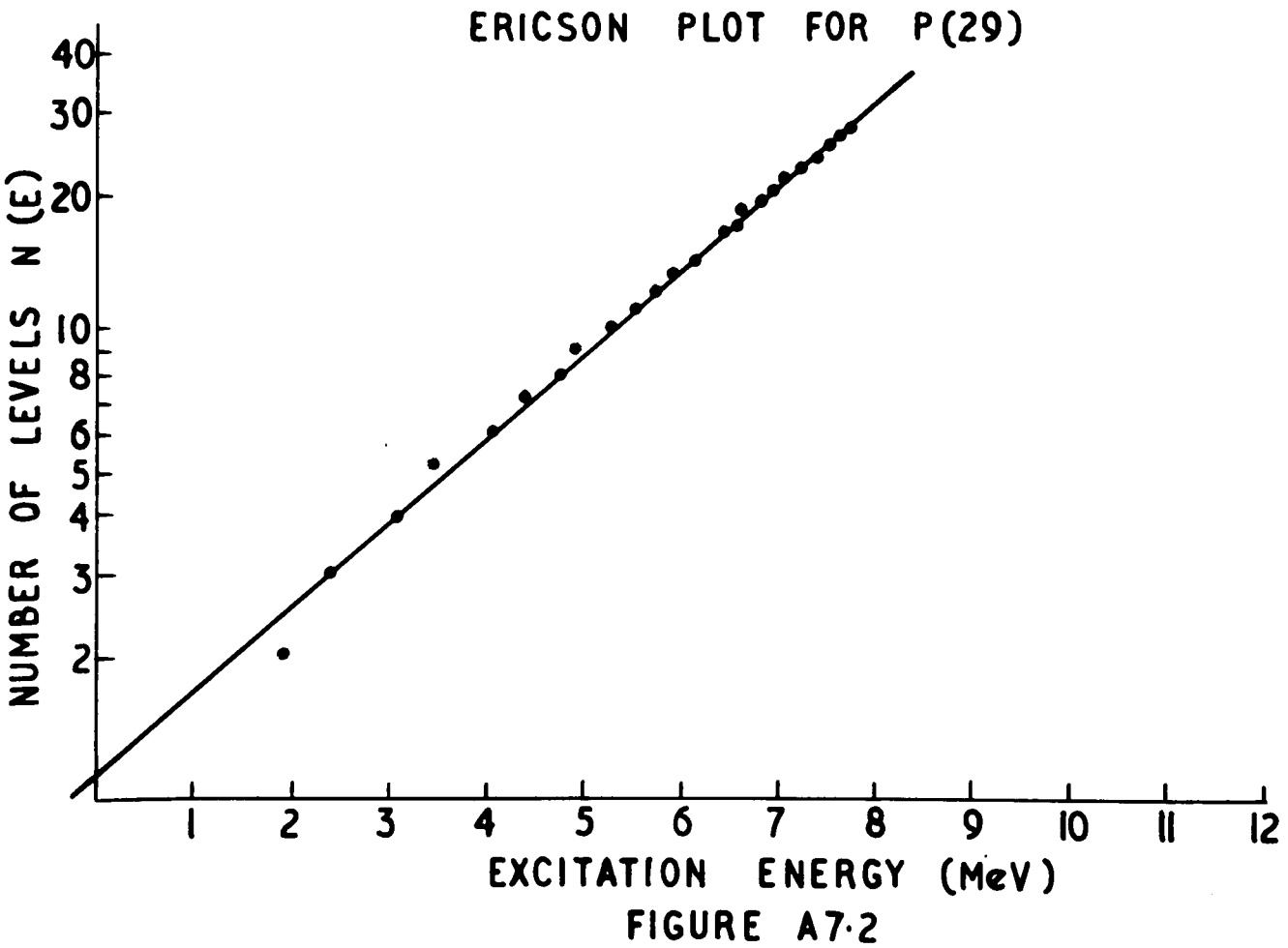

FIGURE A7·2

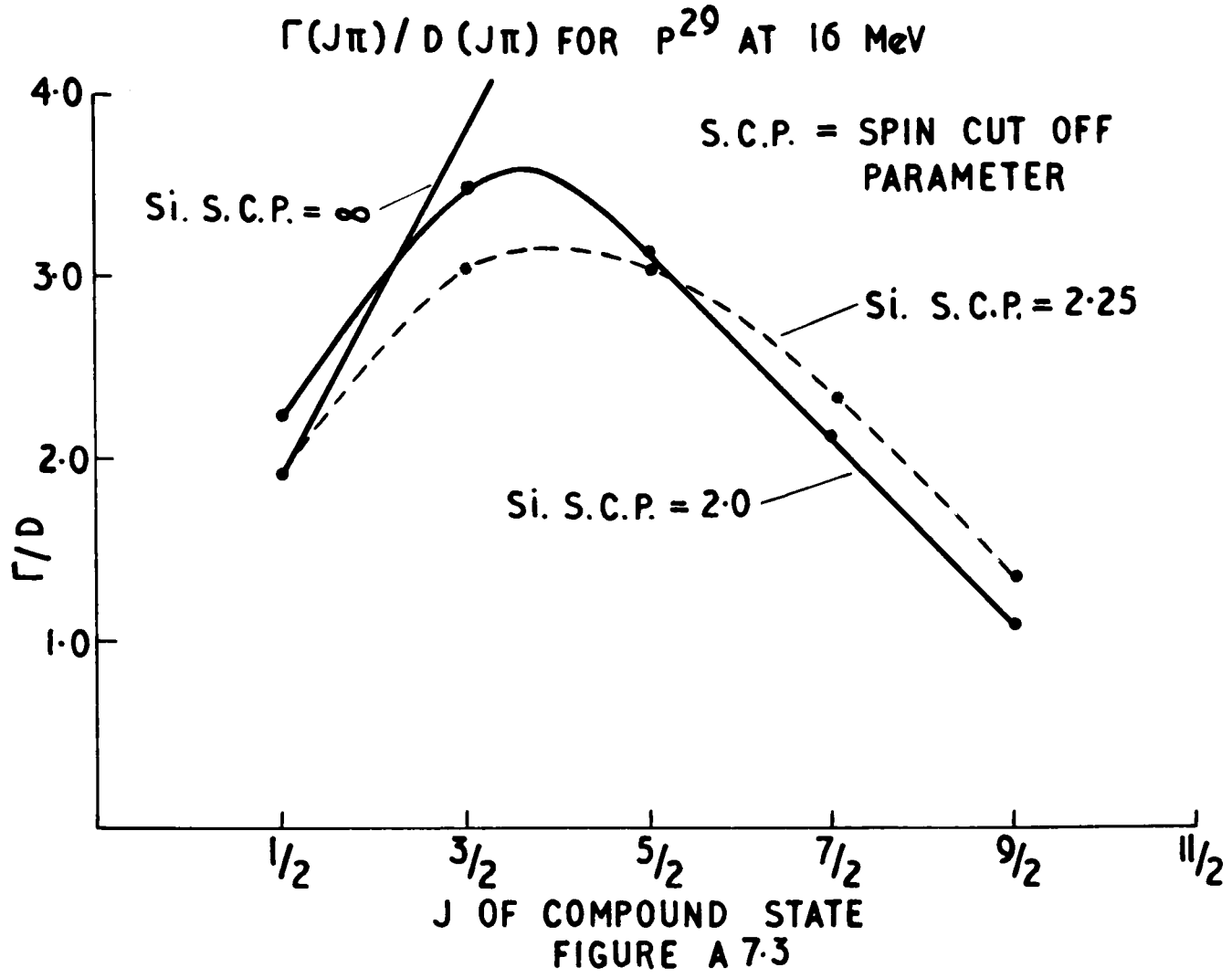

FIGURE A 7·3

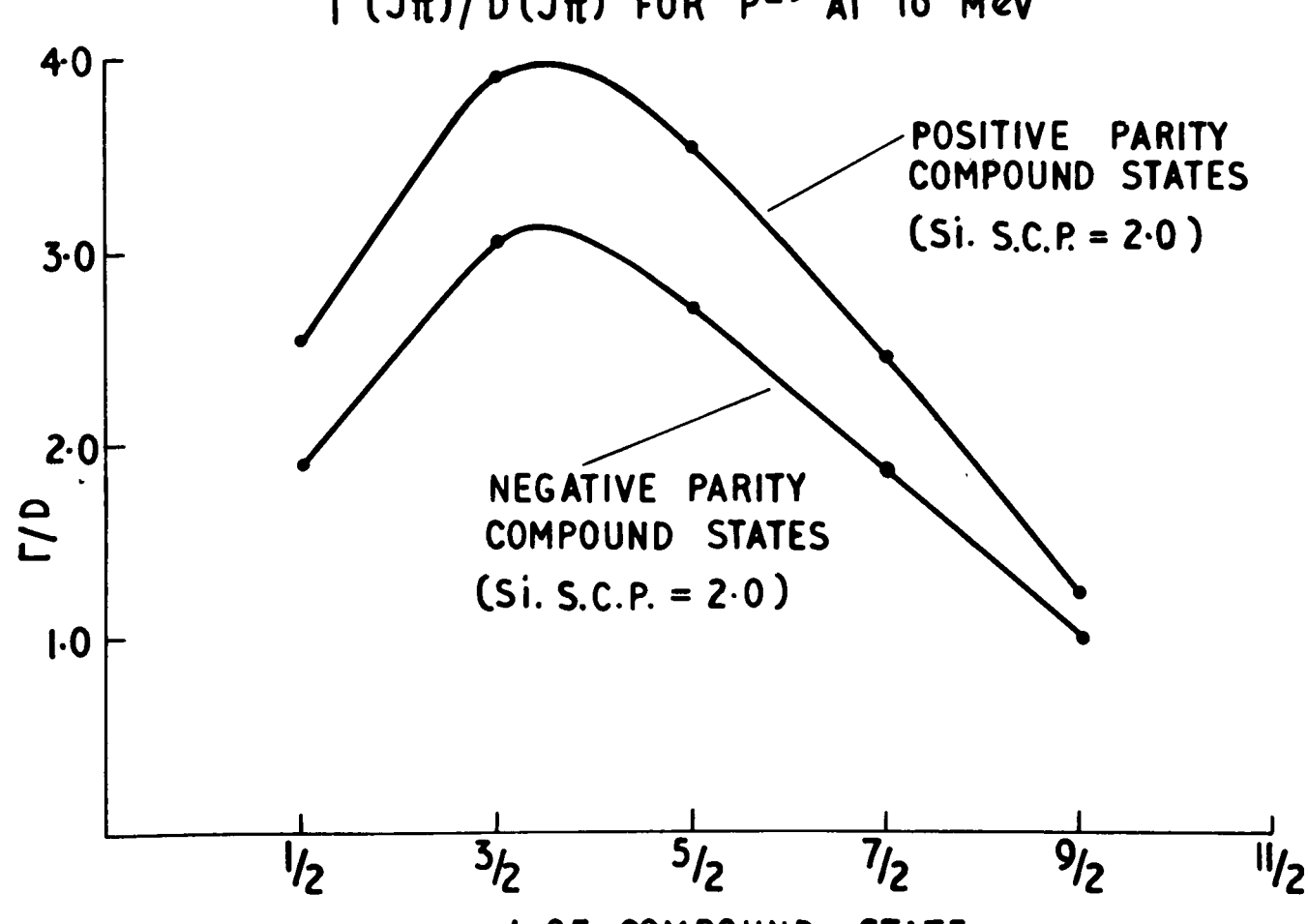

FIGURE A7·4

A P P E N D I X A

THE EXPERIMENTAL ANGULAR DISTRIBUTIONS

The angular distributions determined in the course of this experiment are displayed in the figures of this appendix.

All the angular distributions, except those corresponding to the elastic scattering reaction, are plotted on a linear scale; the elastic scattering angular distributions are plotted on a logarithmic scale. The incident proton energy (E) at which each angular distribution was measured is given, in MeV, on each graph.

The method of determining the absolute differential cross-section associated with any plotted point is described in Section 4.1; the normalization constant (B) is given on each graph. It should be noted, however, that the normalisation constants appearing in Figs. A.2, A.10 should first be multiplied by a factor of 10 before they are used in Eq. (4.1) to calculate a differential cross-section, and in using this equation to calculate an elastic scattering differential cross-section the anti-logarithm of B (base 10) should be used.

Angular distributions of the proton[4] yield from the reaction $Si^{28}(p,p)Si^{28}$ ($Q^{\dagger}$ = 0.0 MeV).

Fig. A8.1

(see following figure)

[†] In this appendix Q denotes the excitation energy of the residual nucleus Si^{28}.

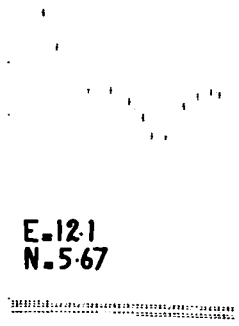

E.12·1
N.5·67

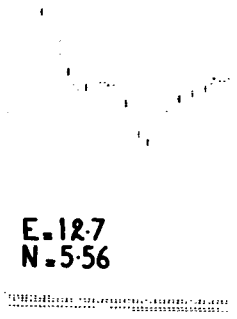

E.12·7
N.5·56

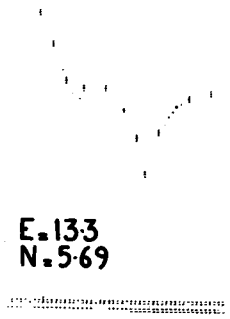

E.13·3
N.5·69

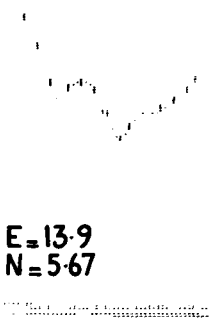

E.13·9
N.5·67

E.14·5
N.5·65

E.12·2
N.5·66

E.12·8
N.5·59

E.13·4
N.5·68

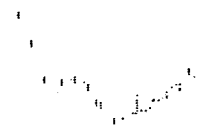

E.14·0
N.5·63

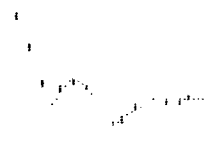

E.14·6
N.5·64

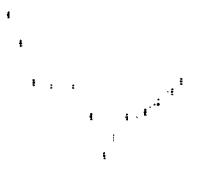

E.12·3
N.5·69

E.12·9
N.5·58

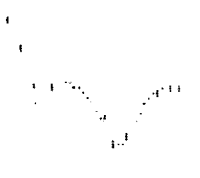

E.13·5
N.5·66

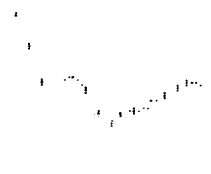

E.14·1
N.5·67

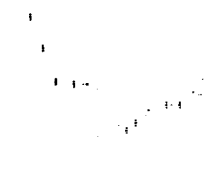

E.14·7
N.5·62

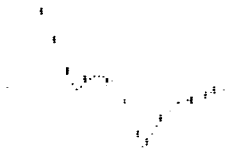

E.12·4
N.5·59

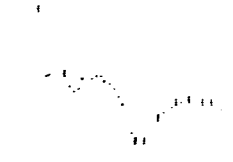

E.13·0
N.5·70

E.13·6
N.5·72

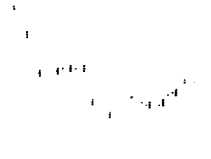

E.14·2
N.5·67

E.14·8
N.5·67

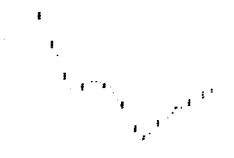

E.12·5
N.5·63

E.13·1
N.5·56

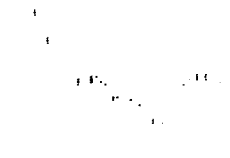

E.13·7
N.5·65

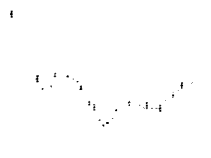

E.14·3
N.5·63

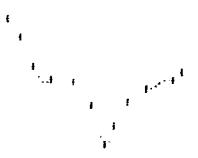

E.12·6
N.5·39

E.13·2
N.5·56

E.13·8
N.5·72

E.14·4
N.5·61

Angular distributions of the proton yield from the reaction $Si^{28}(p,p')Si^{28*}$ (Q = 1.77 MeV).

Fig. A8.2

(see following figure)

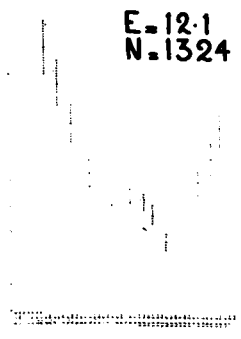
E=12·1
N=1324

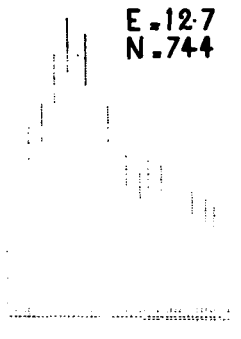
E=12·7
N=744

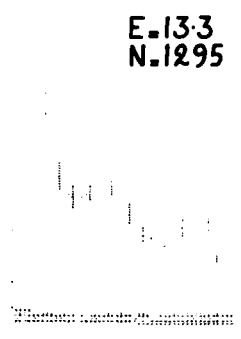
E=13·3
N=1295

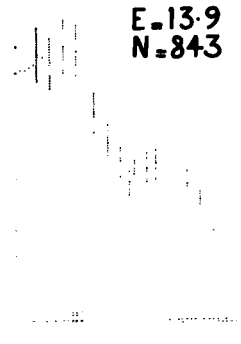
E=13·9
N=843

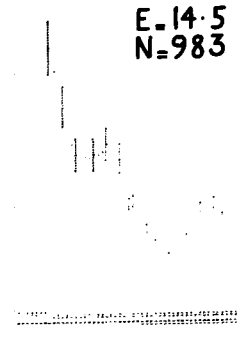
E=14·5
N=983

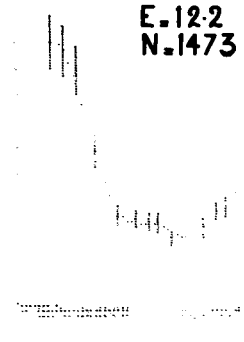
E=12·2
N=1473

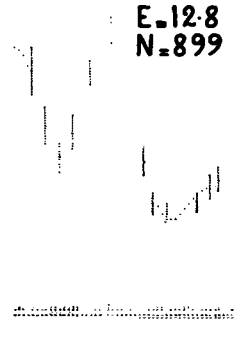
E=12·8
N=899

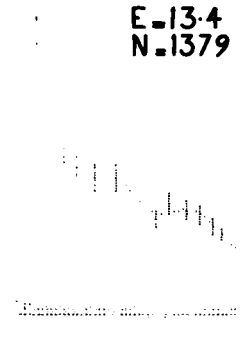
E=13·4
N=1379

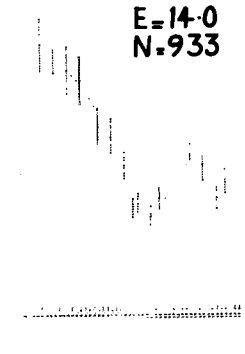
E=14·0
N=933


E=14·6
N=1474

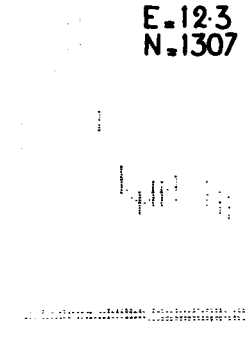
E=12·3
N=1307

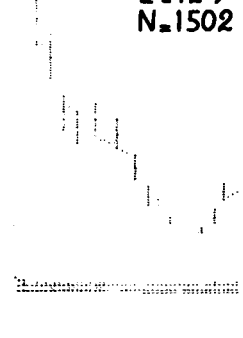
E=12·9
N=1502


E=13·5
N=977

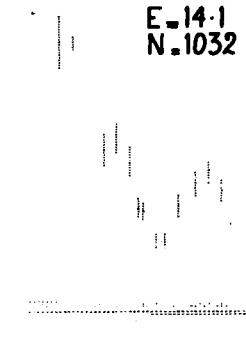
E=14·1
N=1032

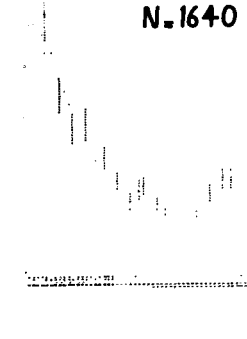
E=14·7
N=1640

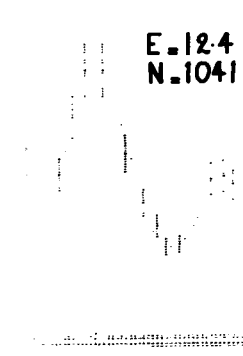
E=12·4
N=1041

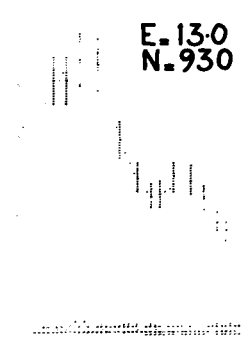
E=13·0
N=930

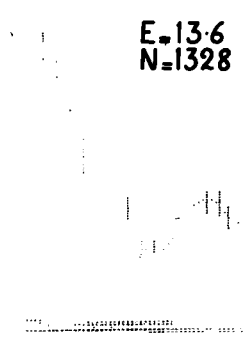
E=13·6
N=1328

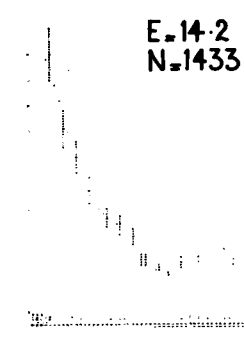
E=14·2
N=1433

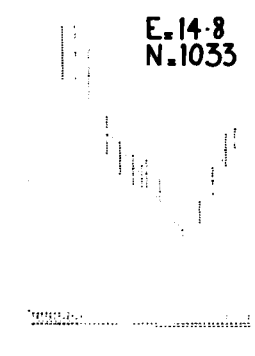
E=14·8
N=1033

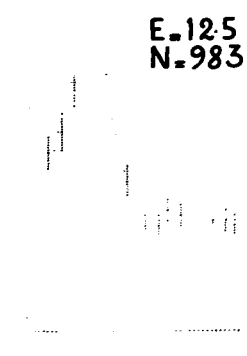
E=12·5
N=983

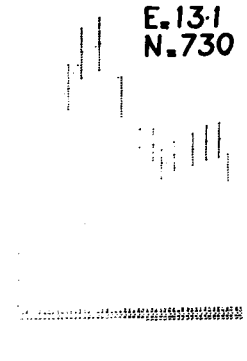
E=13·1
N=730

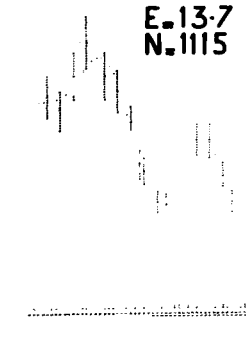
E=13·7
N=1115

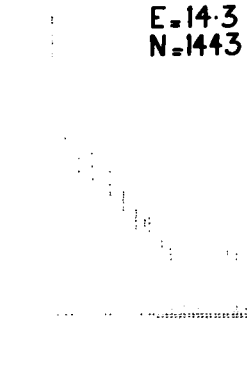
E=14·3
N=1443

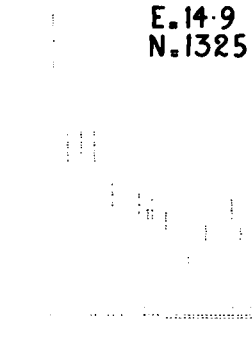
E=14·9
N=1325

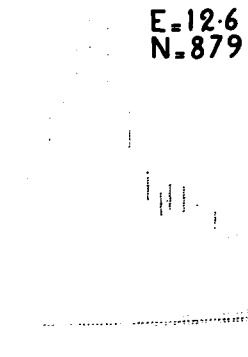
E=12·6
N=879

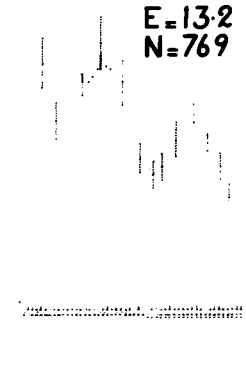
E=13·2
N=769

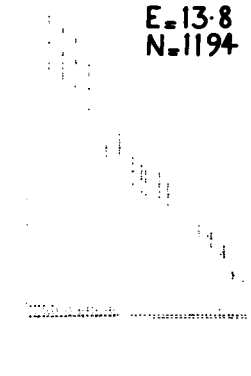
E=13·8
N=1194


E=14·4
N=1445

Angular distributions of the proton yield from the reaction $Si^{28}(p,p')Si^{28*}$ (Q = 4.61 MeV).

Fig. A8.3

(see following figure)


E.12.1
N.4436


E.12.7
N.1857

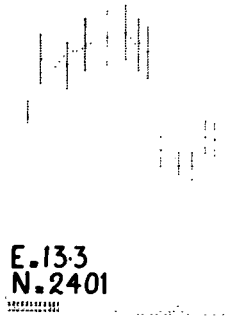
E.13.3
N.2401

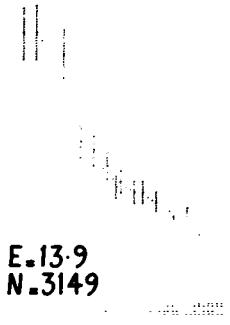
E.13.9
N.3149


E.14.5
N.2940

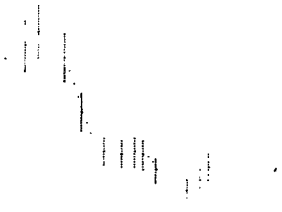
E.12.2
N.3297


E.12.8
N.2587


E.13.4
N.4006


E.14.0
N.3712

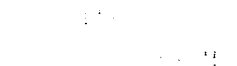
E.14.6
N.3652

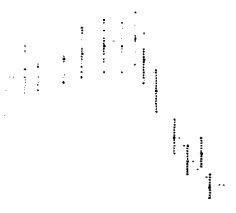
E.12.3
N.1679

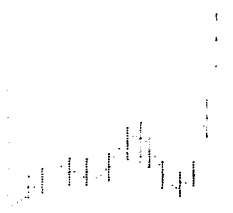
E.12.9
N.4390


E.13.5
N.7678


E.14.1
N.2337


E.14.7
N.5050

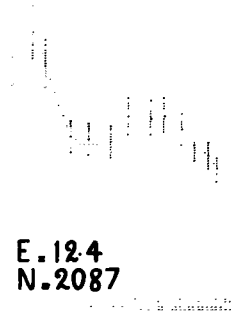
E.12.4
N.2087


E.13.0
N.2708


E.13.6
N.5890

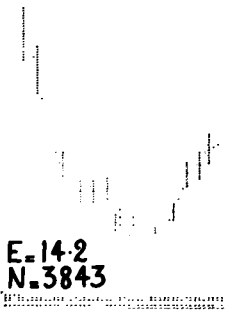
E.14.2
N.3843

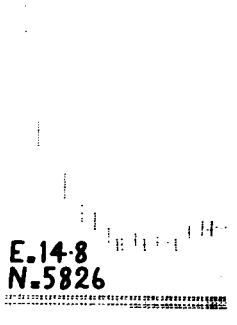
E.14.8
N.5826

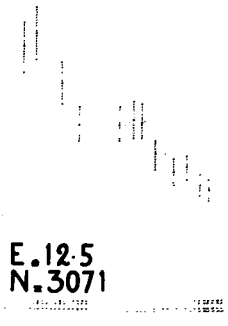
E.12.5
N.3071

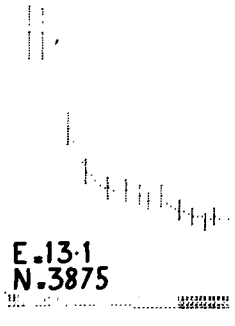
E.13.1
N.3875

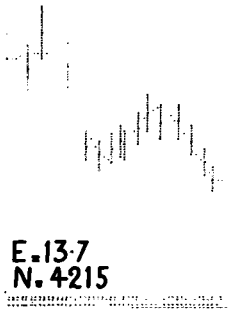
E.13.7
N.4215

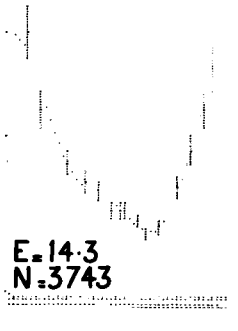
E.14.3
N.3743

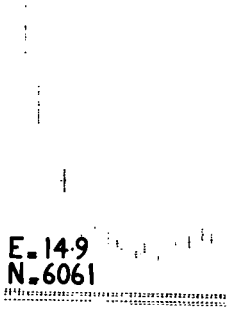
E.14.9
N.6061

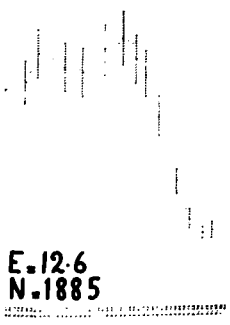
E.12.6
N.1885

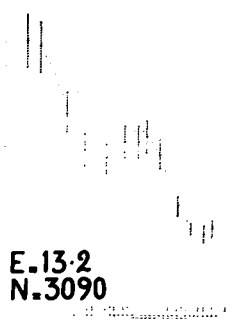
E.13.2
N.3090


E.13.8
N.3332


E.14.4
N.3945

Angular distributions of the proton yield from the reaction $Si^{28}(p,p')Si^{28*}$ (Q = 4.97 MeV).

Fig. A8.4

(see following figure)

E.12·1
N.1598

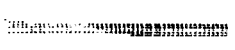

E.12·7
N.3352

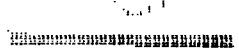

E.13·3
N.3558

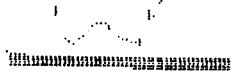

E.13·9
N.2675

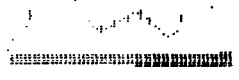

E.14·5
N.1535

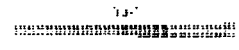

E.12·2
N.3640

E.12·8
N.1430

E.13·4
N.4093

E.14·0
N.2723

E.14·6
N.578

E.12·3
N.2092

E.12·9
N.1746

E.13·5
N.1937

E.14·1
N.1405

E.14·7
N.596

E.12·4
N.3249

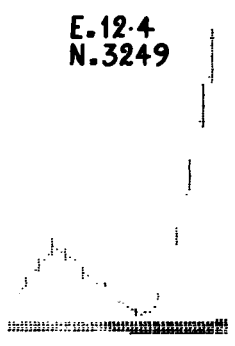

E.13·0
N.1732

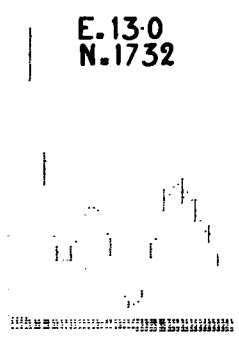

E.13·6
N.1775

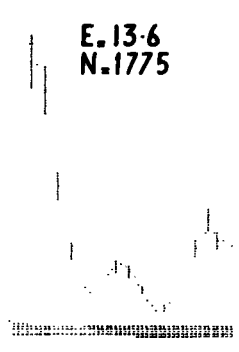

E.14·2
N.617

E.14·8
N.1516

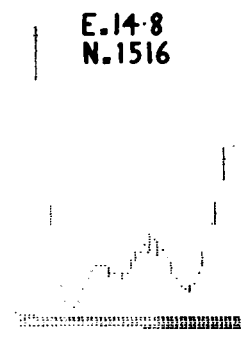

E.12·5
N.4198

E.13·1
N.1602

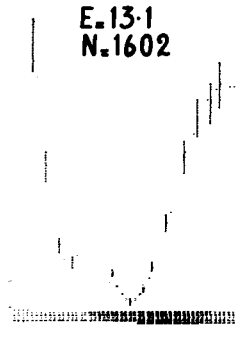

E.13·7
N.1462

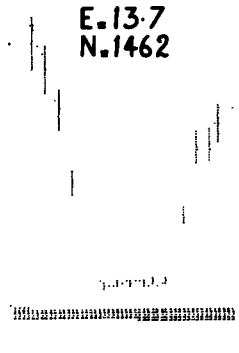

E.14·3
N.585

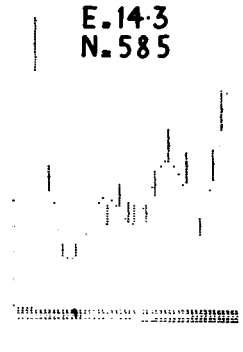

E.14·9
N.606

E.12·6
N.1816

E.13·2
N.1140

E.13·8
N.1619

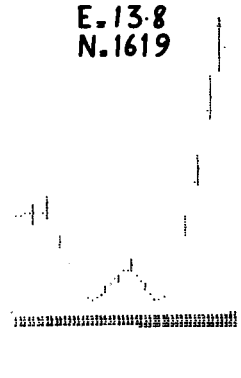

E.14·4
N.1868

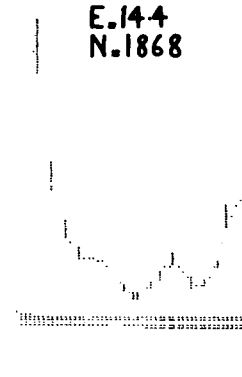

Angular distributions[29] of the proton yield from the reaction $Si^{28}(p,p')Si^{28*}$ (Q = 6.27 MeV).

Fig. A8.5

(see following figure)

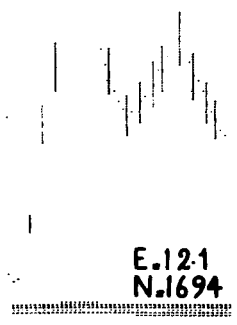
E.12·1
N.1694

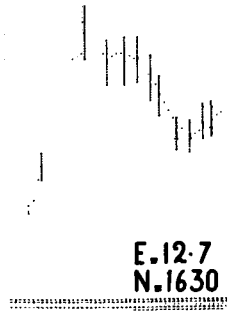
E.12·7
N.1630


E.13·3
N.1330

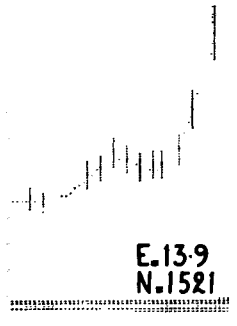
E.13·9
N.1521

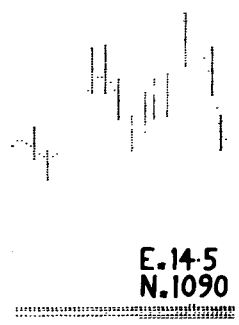
E.14·5
N.1090


E.12·2
N.1760


E.12·8
N.1747

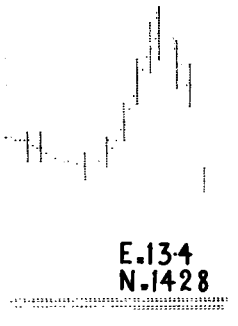
E.13·4
N.1428

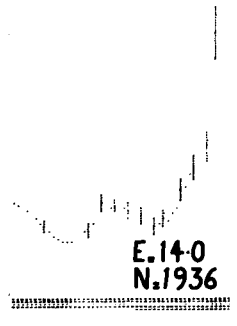
E.14·0
N.1936

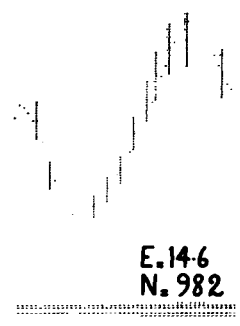
E.14·6
N. 982


E.12·3
N.2575

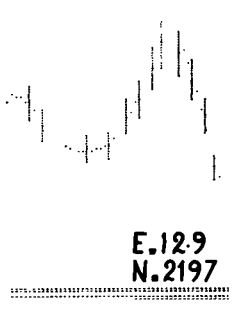
E.12·9
N.2197

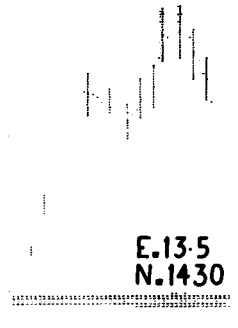
E.13·5
N.1430

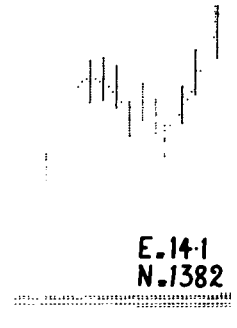
E.14·1
N.1382


E.14·7
N.1683


E.12·4
N.4410

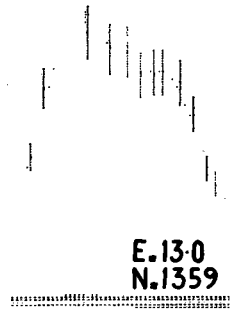
E.13·0
N.1359

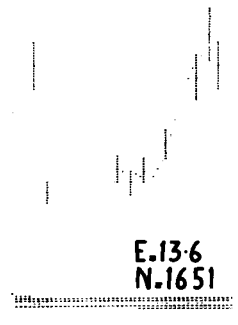
E.13·6
N.1651

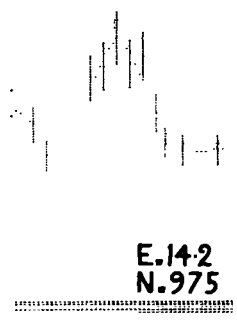
E.14·2
N.975

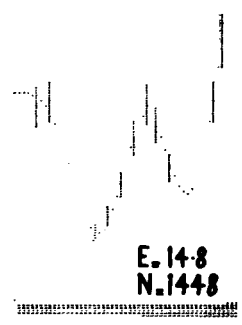
E.14·8
N.1448

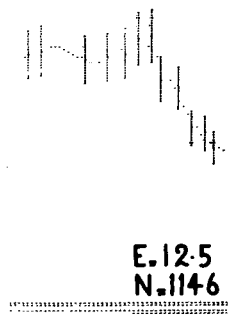
E.12·5
N.1146


E.13·1
N.1161

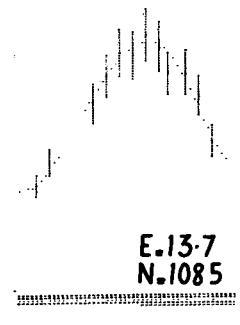
E.13·7
N.1085

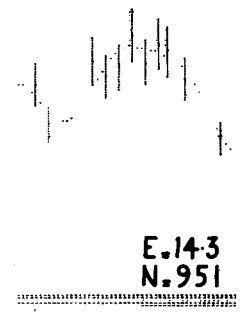
E.14·3
N.951

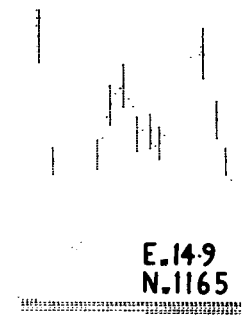
E.14·9
N.1165


E.12·6
N.1150

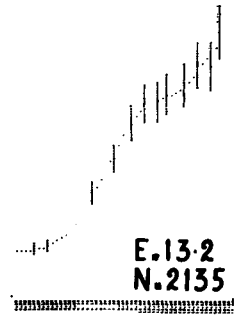
E.13·2
N.2135

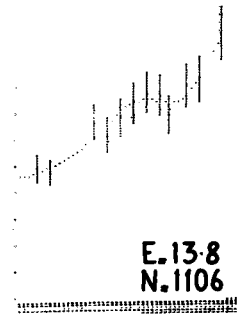
E.13·8
N.1106

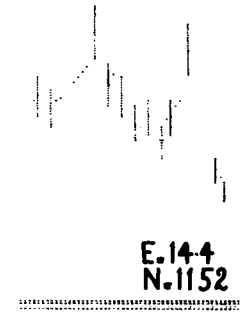
E.14·4
N.1152

Angular distributions for the sum of the proton yields from the reactions

$Si^{28}(p,p')Si^{28*}$ (Q = 6.88 MeV).

$Si^{28}(p,p')Si^{28*}$ (Q = 6.89 MeV).

Fig. A8.6

(see following figure)

E.12·1
N.3862

E.12·7
N.2905

E.13·3
N.4134

E.13·9
N.3998

E.14·5
N.4698

E.12·2
N.4289

E.12·8
N.3886

E.13·4
N.4252

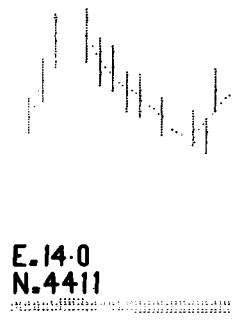

E.14·0
N.4411

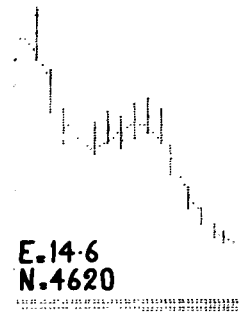

E.14·6
N.4620

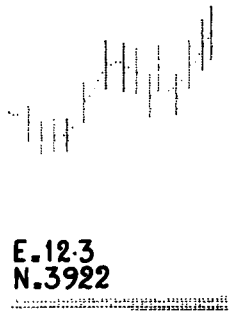

E.12·3
N.3922

E.12·9
N.5370

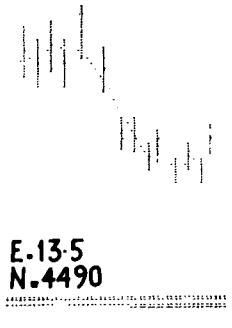

E.13·5
N.4490

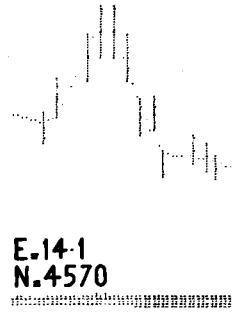

E.14·1
N.4570

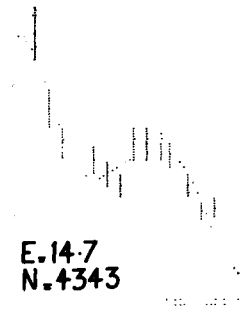

E.14·7
N.4343

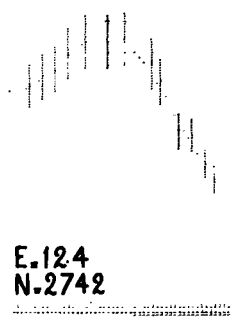

E.12·4
N.2742

E.13·0
N.3207

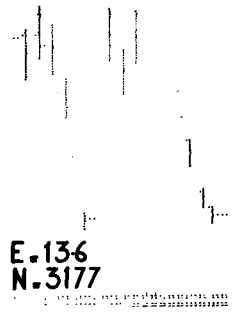

E.13·6
N.3177

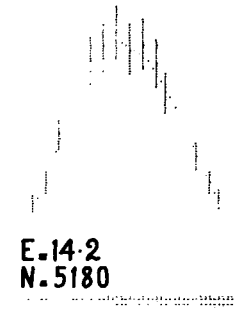

E.14·2
N.5180

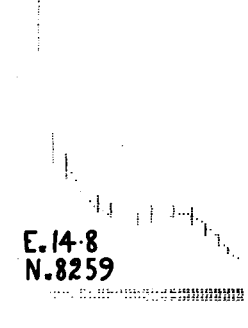

E.14·8
N.8259

E.12·5
N.3385

E.13·1
N.3207

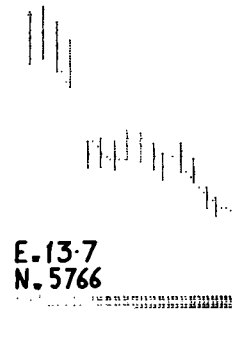

E.13·7
N.5766

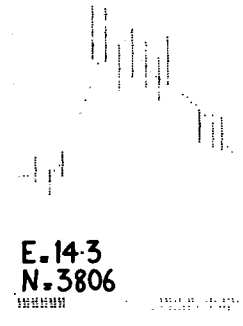

E.14·3
N.3806

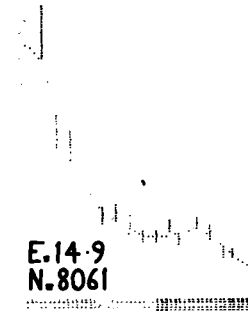

E.14·9
N.8061

E.12·6
N.3032

E.13·2
N.3125

E.13·8
N.5246

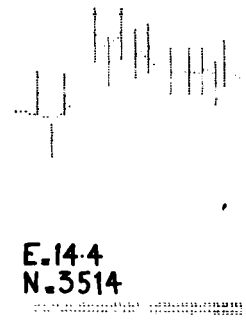

E.14·4
N.3514

Angular distributions for the sum of the proton yields from the reactions

$Si^{28}(p,p')Si^{28*}$ (Q = 7.38 MeV).

$Si^{28}(p,p')Si^{28*}$ (Q = 7.41 MeV).

Fig. A8.7

(see following page)

E.12·1
N.3432

E.12·7
N.2234

E.13·3
N.2646

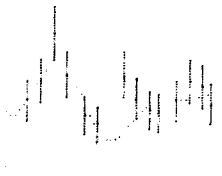

E.13·9
N.1563

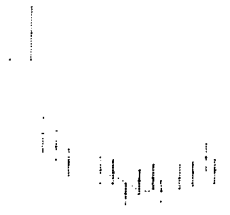

E.14·5
N.2958

E.12·2
N.3009

E.12·8
N.2711

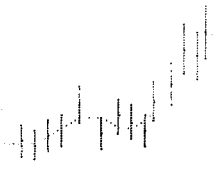

E.13·4
N.3330

E.14·0
N.2037

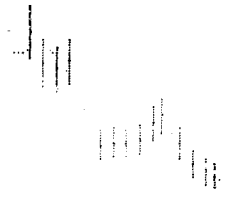

E.14·6
N.2192

E.12·3
N.2428

E.12·9
N.2104

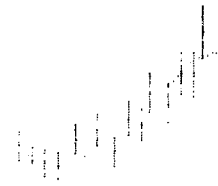

E.13·5
N.2853

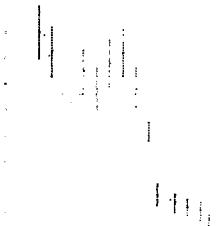

E.14·1
N.2861

E.14·7
N.3070

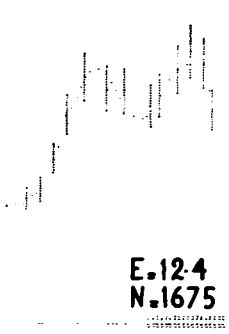

E.12·4
N.1675

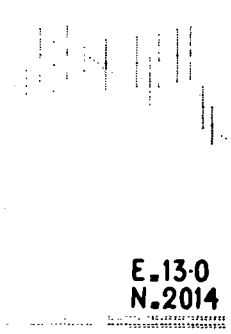

E.13·0
N.2014

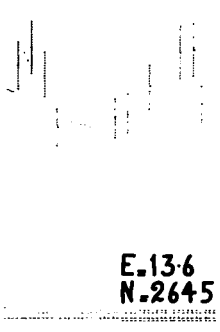

E.13·6
N.2645

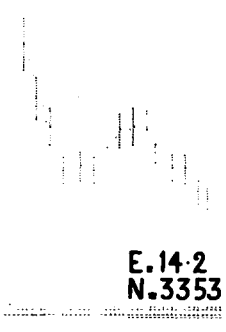

E.14·2
N.3353

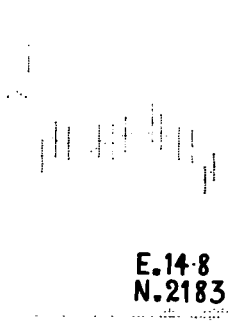

E.14·8
N.2183

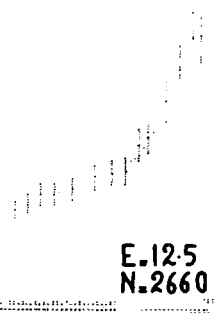

E.12·5
N.2660

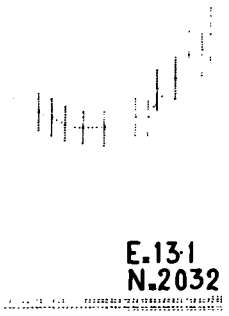

E.13·1
N.2032

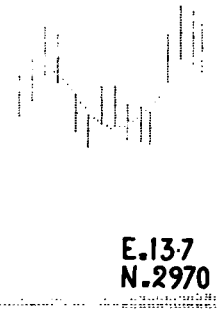

E.13·7
N.2970

E.14·3
N.2667

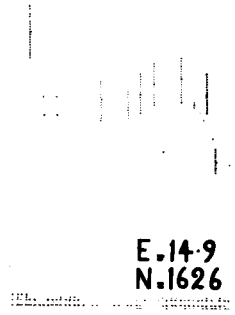

E.14·9
N.1626

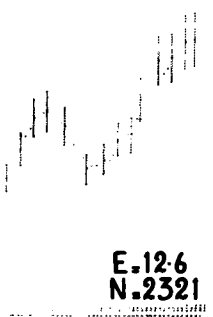

E.12·6
N.2321

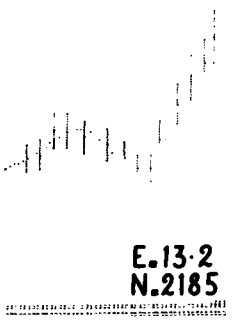

E.13·2
N.2185

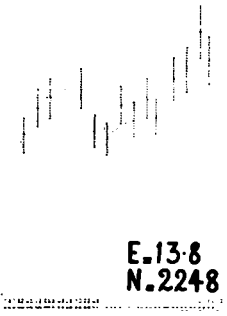

E.13·8
N.2248

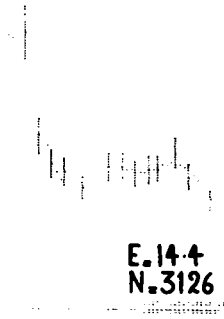

E.14·4
N.3126

Angular distributions of the proton yield from the reaction $Si^{28}(p,p')Si^{28*}$ (Q = 7.80 MeV).

Fig. A8.8

(see following figure)

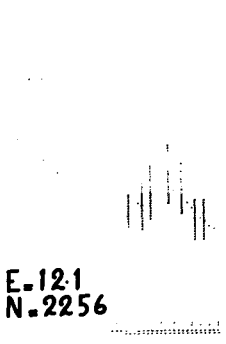
E-12·1
N-2256

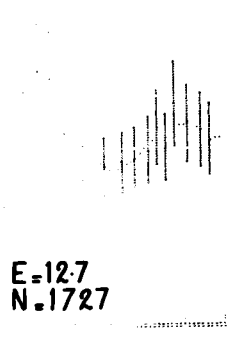
E-12·7
N-1727

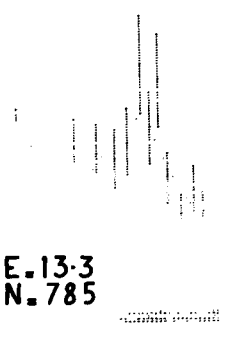
E-13·3
N-785

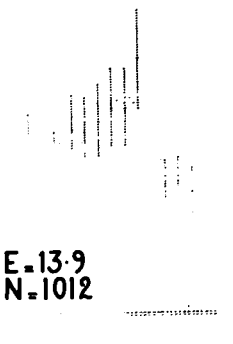
E-13·9
N-1012

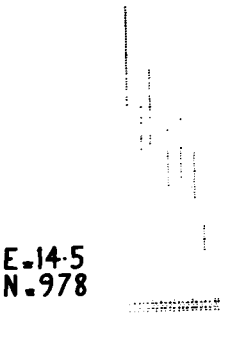
E-14·5
N-978

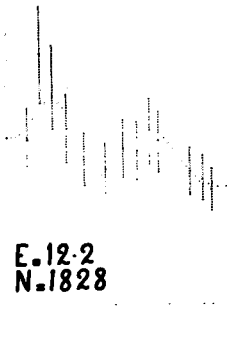
E-12·2
N-1828

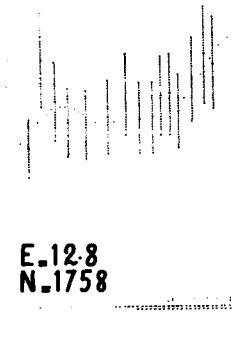
E-12·8
N-1758

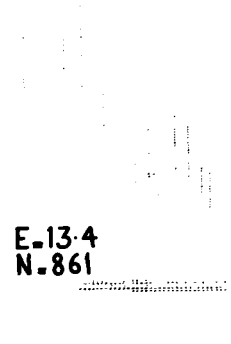
E-13·4
N-861

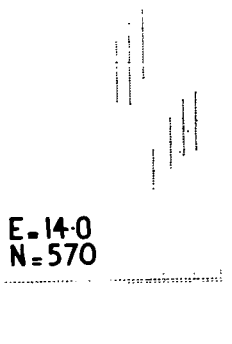
E-14·0
N-570

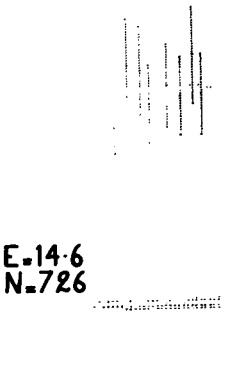
E-14·6
N-726

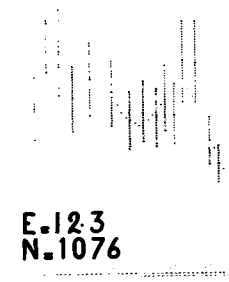
E-12·3
N-1076

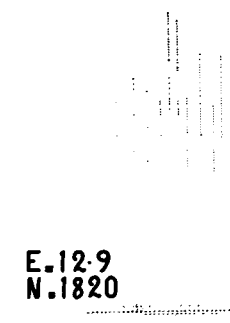
E-12·9
N-1820

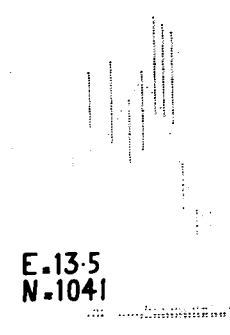
E-13·5
N-1041

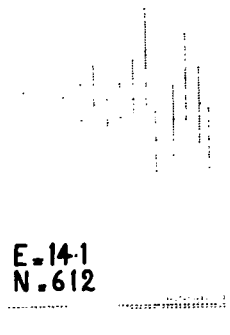
E-14·1
N-612

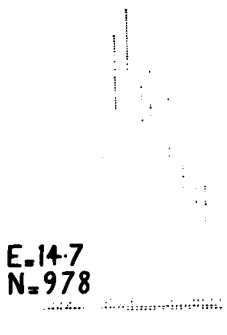
E-14·7
N-978

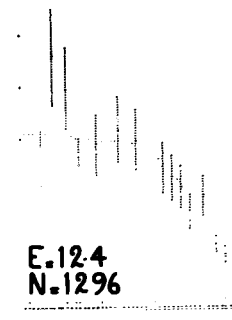
E-12·4
N-1296

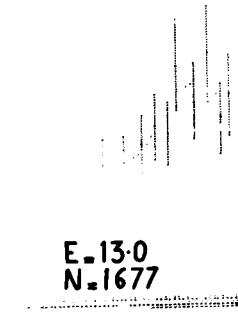
E-13·0
N-1677

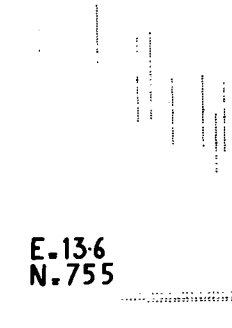
E-13·6
N-755

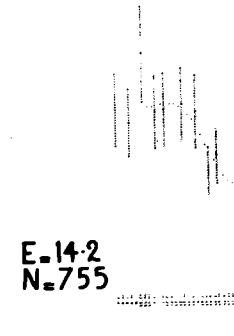
E-14·2
N-755

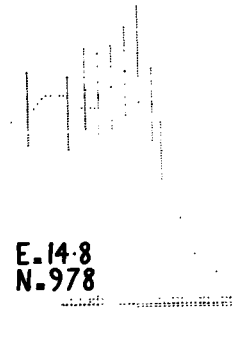
E-14·8
N-978

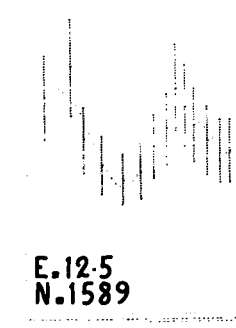
E-12·5
N-1589

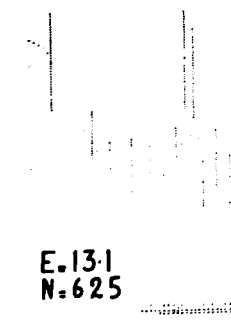
E-13·1
N-625

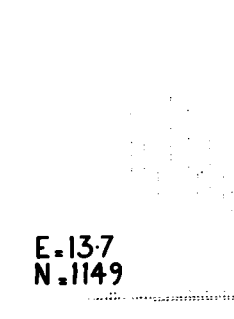
E-13·7
N-1149

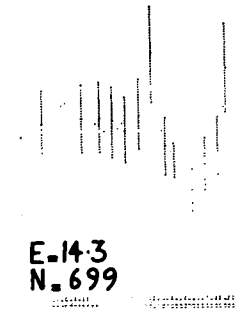
E-14·3
N-699

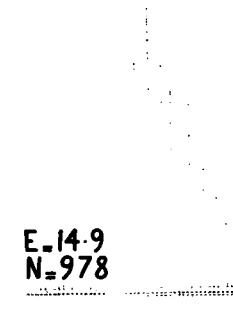
E-14·9
N-978

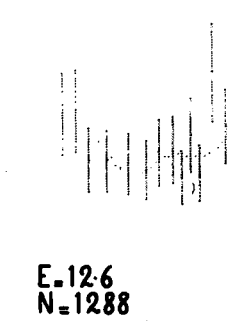
E-12·6
N-1288

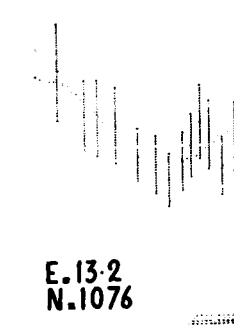
E-13·2
N-1076

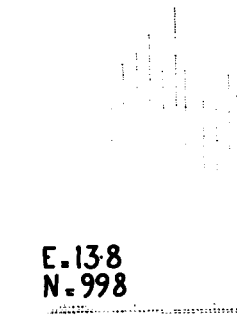
E-13·8
N-998

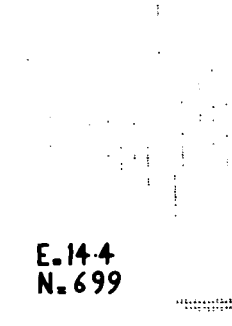
E-14·4
N-699

Angular distributions of the proton yield from the reaction $Si^{28}(p,p')Si^{28*}$ (Q = 7.93 MeV).

Fig. A8.9

(see following figure)

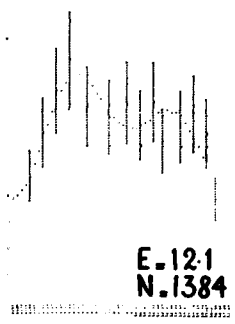
E.12·1
N.1384


E.12·7
N.2162

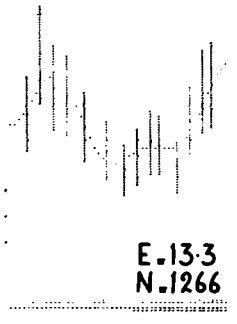
E.13·3
N.1266


E.13·9
N.1535

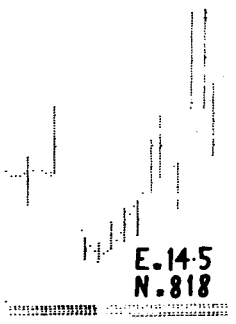
E.14·5
N.818

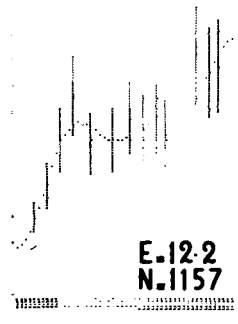
E.12·2
N.1157

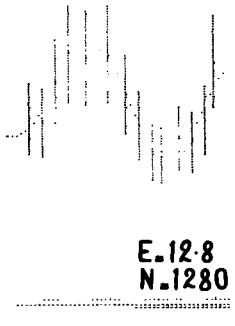
E.12·8
N.1280

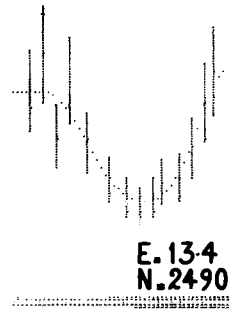
E.13·4
N.2490

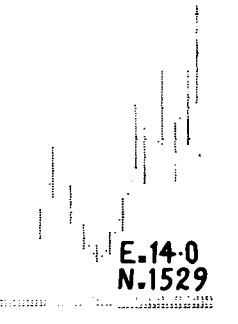
E.14·0
N.1529


E.14·6
N.750

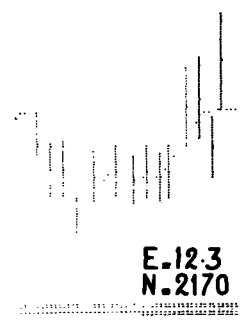
E.12·3
N.2170

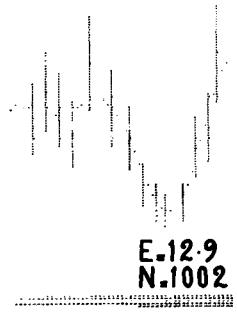
E.12·9
N.1002

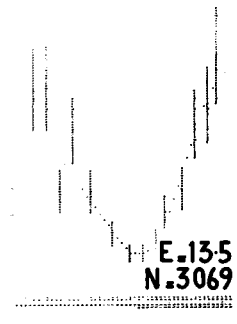
E.13·5
N.3069

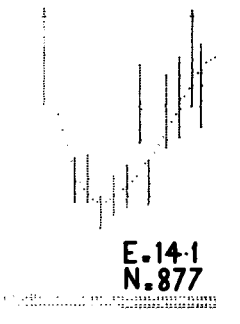
E.14·1
N.877

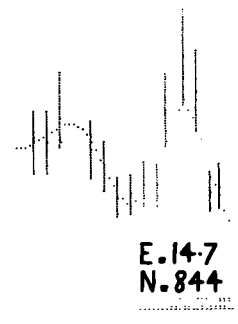
E.14·7
N.844

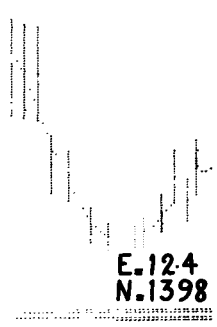
E.12·4
N.1398

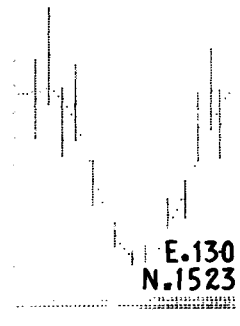
E.130
N.1523

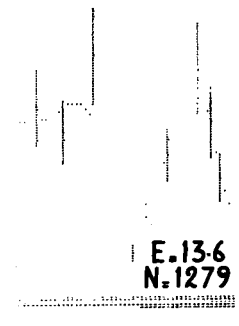
E.13·6
N.1279


E.14·2
N.687

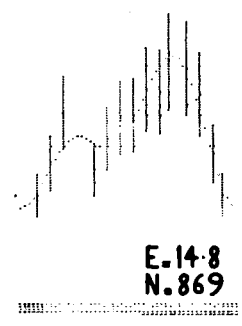
E.14·8
N.869


E.12·5
N.1547


E.13·1
N.1102


E.13·7
N.1636

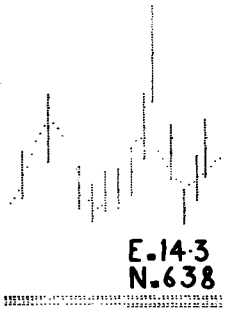
E.14·3
N.638

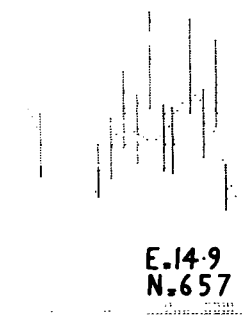
E.14·9
N.657

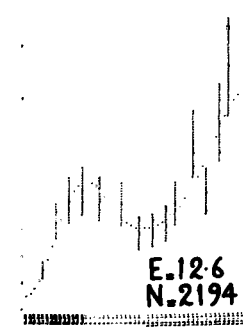
E.12·6
N.2194


E.13·2
N.663

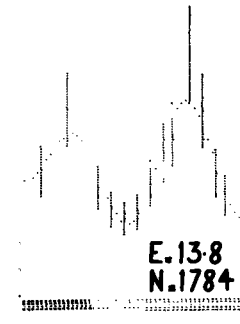
E.13·8
N.1784

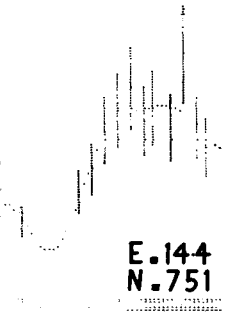
E.144
N.751

Angular distributions for the sum of the proton yields from the reactions $Si^{28}(p,p')Si^{28*}$ in which the residual nucleus is left with an excitation energy greater than 7.93 MeV.

Fig. A8.10

(see following page)

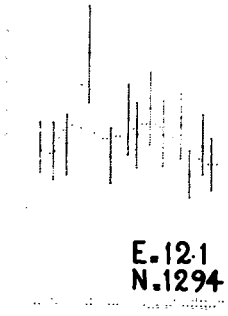

E.12·1
N.1294

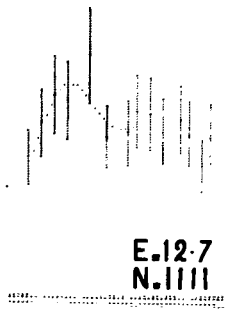

E.12·7
N.1111

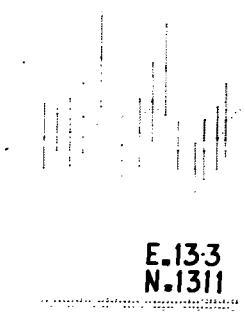

E.13·3
N.1311

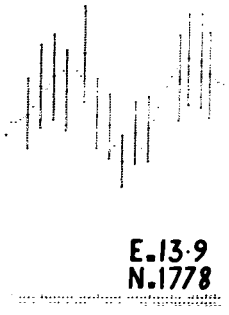

E.13·9
N.1778

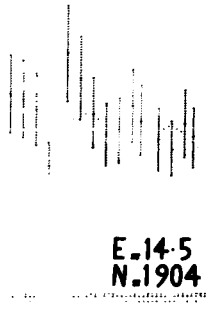

E.14·5
N.1904

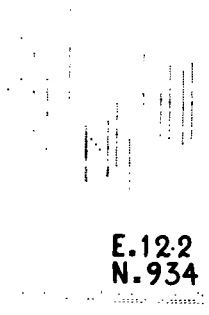

E.12·2
N.934

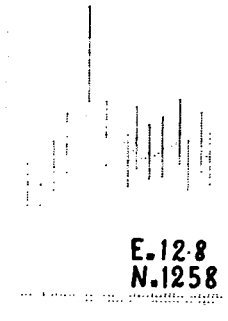

E.12·8
N.1258

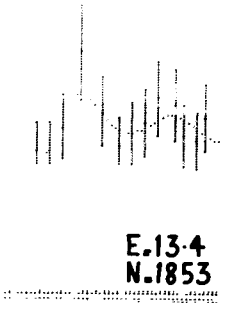

E.13·4
N.1853

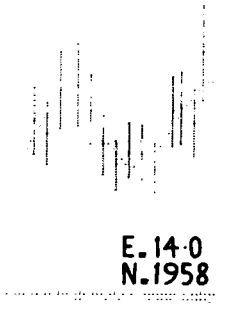

E.14·0
N.1958

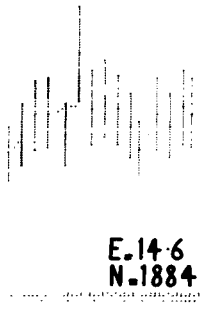

E.14·6
N.1884

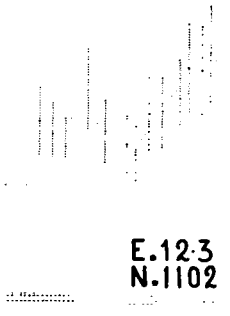

E.12·3
N.1102

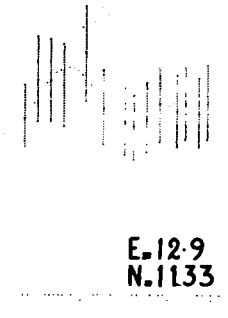

E.12·9
N.1133

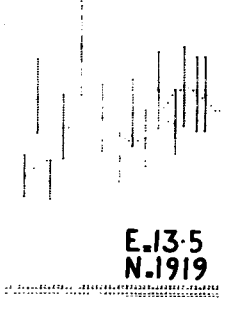

E.13·5
N.1919

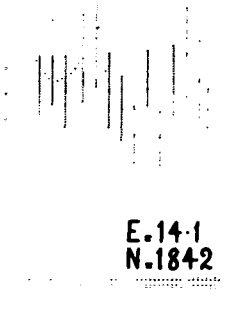

E.14·1
N.1842

E.14·7
N.2443

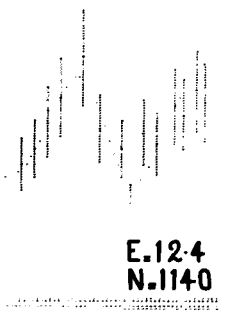

E.12·4
N.1140

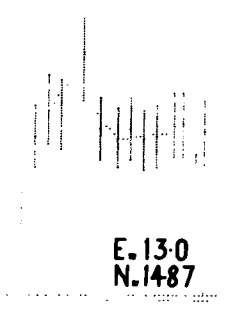

E.13·0
N.1487

E.13·6
N.2060

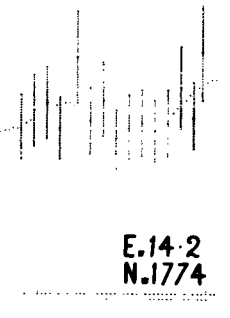

E.14·2
N.1774

E.14·8
N.2778

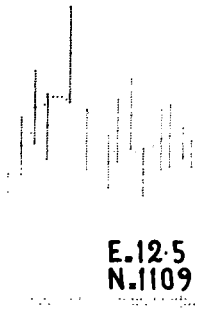

E.12·5
N.1109

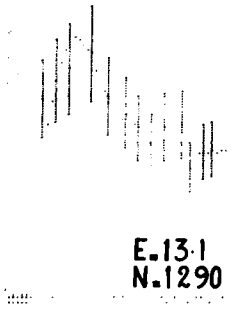

E.13·1
N.1290

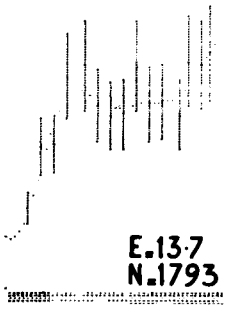

E.13·7
N.1793

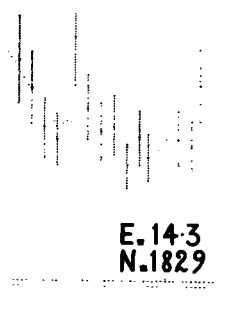

E.14·3
N.1829

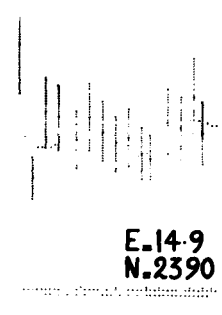

E.14·9
N.2390

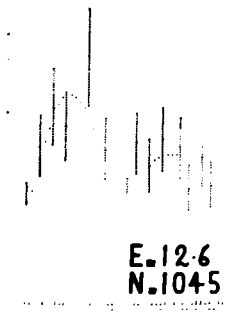

E.12·6
N.1045

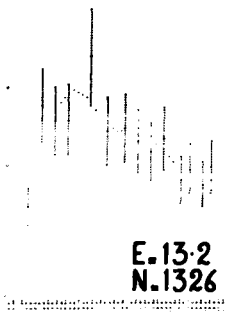

E.13·2
N.1326

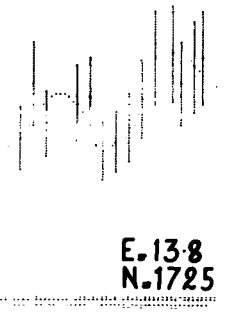

E.13·8
N.1725

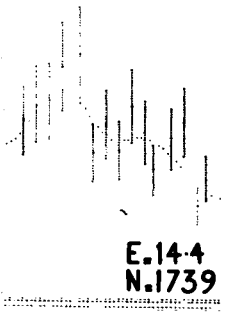

E.14·4
N.1739

BIBLIOGRAPHY

JOURNALS CONSULTED

Advances in Physics (Advan. Phys.)

Annals of Physics (Ann. Phys.)

Annual Review of Nuclear Science (Ann. Rev. Nucl. Sci.)

Bulletin of the American Physical Society (Bull. Am. Phys. Soc.)

Canadian Journal of Physics (Can. J. Phys.)

Comptes Rendus Hebdomadaires des Séances de l'Académie des Sciences (Compt. Rend. Hebd. des Séances de l'Acad. des Sci.)

Journal of the Physical Society of Japan (J. Phys. Soc. Japan)

Kongelige Danske Videnskabernes Selskab Matematisk-Fysiske Meddelelser (Mat. Fys. Med. Dan. Vid. Selsk.)

Nature

Nuovo Cimento

Nuclear Instruments and Methods (Nucl. Instruments and Methods)

Nuclear Physics (Nucl. Phys.)

Philosophical Magazine (Phil. Mag.)

Physical Review (Phys. Rev.)

Physical Review Letters (Phys. Rev. Letters)

Physics Letters (Phys. Letters)

Physics Today (Phys. Today)

Proceedings of the Physical Society (Proc. Phys. Soc.)

Proceedings of the Royal Society (Proc. Roy. Soc.)

Progress of Theoretical Physics (Prog. Theor. Phys.)

Reviews of Modern Physics (Rev. Mod. Phys.)

Ricerca Scientifica (Ricerca Sci.)

Science

Zeitschrift für Physik (Zeitschrift für Phys.)

The following list gives full details of the works consulted. Journal titles are quoted as indicated above; titles of conference reports are similarly abbreviated. The date of publication of a book or article is given, for ease of reference, following the author(s); an exception has been made in the case of papers read at conferences, where the date so shown is that of the conference; date of publication of the collected papers in these cases follows the name of the publisher.

R E F E R E N C E S

Agodi, A., Pappalardo, G., Riccamo, R. and Vinciguerra, D. (1962). Nuovo Cimento, 23, pp. 1136 ff.

Agodi, A. and Pappalardo, G. (1963). Nucl. Phys., 47, pp. 129 ff.

Allan, D.L. (1961). Nucl. Phys., 24, pp. 274 ff.

Allardyce, B.W., Graham, W.R. and Hall, I. (1964). Nucl. Phys., 52, pp. 239 ff.

Allardyce, B.W., Dallimore, P.J., Hall, I., Tanner, N.W., Richter, A., Brentano, P. and Mayer-Kuckuk, T. (1965). Phys. Letters, 18, pp. 140 ff.

Allardyce, B.W., Dallimore, P.J., Hall, I., Tanner, N.W., Richter, A., Brentano, P. and Mayer-Kuckuk, T. (1966). Nucl. Phys., 85, pp. 193 ff.

Austern, N., Butler, S.T. and McManus, H. (1953). Phys. Rev., 92, pp. 350 ff.

Belote, T.A., Kashy, E. and Risser, J. (1961). Phys. Rev., 122, pp. 920 ff.

Bethe, H.A. (1936). Phys. Rev., 50, pp. 332 ff.

Bethe, H.A. (1937). Rev. Mod. Phys., 9, pp. 69 ff.

Bizzeti, P.G., Bizzeti Sona, A.M., Boccialini, M., Di Caporiacco, G., Fazzini, T. and Mandò, M. (1964). Compt. Rend. Congr. Intern. Phys. Nucl., Paris, 2-8 Juillet 1964. Paris, Centre National de la Recherche Scientifique, 1964, vol. 2, contrib. C284, pp. 741 ff.

Blatt, J.M. and Biedenharn, L.C. (1952). Rev. Mod. Phys., 24, pp. 258 ff.

Block, B. (1963). Ann. Phys., 23, pp. 47 ff.

Blumberg, S. and Porter, C.E. (1958). Phys. Rev., 110, pp. 786 ff.

Bohr, N. (1936). Nature, 137, pp. 344 ff.

Bohr, N. and Kalckar, F. (1937). Mat. Fys. Med. Dan. Vid. Selsk., 14, no. 10, pp. 1 ff.

Bolsterli, M., Gibbs, W.R., Kerman, A.K. and Young, J.E. (1966). Phys. Rev. Letters, 17, pp.878 ff.

Breit, G. and Wigner, E. (1936). Phys. Rev., 49, pp. 519 ff.

Breit, G. (1959). Encyclopedia of Physics, ed. S. Flügge. Berlin etc., Springer-Verlag, vol. XLI/I, pp. 194, 270.

Brenner, M.W. and Hoogenboom, A.M. (1962). Phys. Rev., 127, pp. 947 ff.

Brink, D.M. and Stephen, R.O. (1963). Phys. Letters, 5, pp. 77 ff.

Brink, D.M., Stephen, R.O. and Tanner, N.W. (1964).
Nucl. Phys., 54, pp. 577 ff.

Brueckner, K.A. (1954[a]). Phys. Rev., 96, pp. 508 ff.

Brueckner, K.A., Levinson, C.A. and Mahmoud, H.M. (1954[b]).
Phys. Rev., 95, pp. 217 ff.

Brueckner, K.A. (1955[a]). Phys. Rev., 100, pp. 36 ff.

Brueckner, K.A., Eden, R.J. and Francis, N.C. (1955[b]).
Phys. Rev., 100, pp. 891 ff.

Brueckner, K.A., Gammel, J.L. and Kubis, J.T. (1960).
Phys. Rev., 118, pp. 1438 ff.

Budd, I.F., Poate, J.M. and Spear, R.H. (1965).
Nucl. Phys., 65, pp. 655 ff.

Butler, S.T. (1951). Proc. Roy. Soc., A208, pp. 559 ff.

Carlson, A.D. and Barschall, H.H. (1965). Proc. Intern.
Conf. Stu. Nucl. Str. Neu., 19-23 July 1965, Antwerp.
Amsterdam, North Holland Pub. Co., 1966, contrib. 101,
p. 537.

Cassagnou, Y., Iori, I., Lévi, C., Mayer-Kuckuk, T.,
Mermaz, M. and Papineau, L. (1963). Phys. Letters,
6, pp. 209 ff.

Cohen, A.V. and Cookson, J.A. (1961).
Nucl. Phys., 24, pp. 529 ff.

Cohen, B.L., Mead, J.B., Price, H.E., Kulsenberry, K.S. and Hartz, C. (1960). Phys. Rev., 118, pp. 499 ff.

Colli, L., Facchini, U., Iori, I., Marcazzan, G.M., Milazzo, M. and Tonolini, F. (1962[a]). Phys. Letters, 1, pp. 120 ff.

Colli, L., Iori, I., Marcazzan, G.M. and Milazzo, M. (1962[b]). Proc. Conf. Direct Interactions and Nucl. Reaction Mechanisms, 3-8 September 1962. New York and London, Gordon and Breach, 1963, pp. 387 ff.

Cook, L.J. and Macmillan, E. (1949). Phys. Rev., 75, pp. 7 ff.

Dallimore, P.J. and Hall, I. (1965). Phys. Letters, 18, pp. 138 ff.

Dearnaley, G., Gibbs, W.R., Leachman, R.B. and Rogers, F.C. (1965). Phys. Rev., B139, pp. 1170 ff.

Dunning, J.R., Pegram, G.B., Fink, G.A. and Mitchell, J.P. (1935). Phys. Rev., 48, pp. 265 ff.

Egelstaff, P.A. (1956). Oak Ridge National Laboratory Report. ORNL-2309, p. 124.

Elliott, R.V. and Spear, R.H. (1966). Nucl. Phys., 84, pp. 209 ff.

Endt, P.M. and Van der Leun, C. (1967). Nucl. Phys., A105, pp. 1 ff.

Erba, E., Facchini, U. and Saetta Menichella, E. (1961). Nuovo Cimento, 22, pp. 1237 ff.

Ericson, T. (1959). Nucl. Phys., 11, pp. 481 ff.

Ericson, T. (1960). Advan. Phys., 9, pp. 425 ff.

Ericson, T. (1963). Ann. Phys., 23, pp. 390 ff.

Ericson, T. and Mayer-Kuckuk, T. (1966). Ann. Rev. Nucl. Sci., 16, pp. 183 ff.

Facchini, U., Saetta Menichella, E. and Tonolini, F. (1962). Phys. Letters, 1, pp. 209 ff.

Fano, U. (1961). Phys. Rev., 124, pp. 1866 ff.

Fasoli, U., Toniolo, D., Zago, G. and Fabiani, F. (1966). Nuovo Cimento, 44B, pp. 455 ff.

Fermi, E. and Amaldi, E. (1935). Ricerca Sci., 6, pp. 544 ff.

Fernbach, S., Serber, R. and Taylor, T.B. (1949). Phys. Rev., 75, pp. 1352 ff.

Feshbach, H., Peaslee, D.C. and Weisskopf, V.F. (1947). Phys. Rev., 71, pp. 145 ff.

Feshbach, H. and Weisskopf, V.F. (1949). Phys. Rev., 76, pp. 1550 ff.

Feshbach, H., Porter, C.E. and Weisskopf, V.F. (1953).
Phys. Rev., 90, pp. 166 ff.

Feshbach, H., Porter, C.E. and Weisskopf, V.F. (1954).
Phys. Rev., 96, pp. 448 ff.

Feshbach, H. (1958). Ann. Phys., 5, pp. 357 ff.

Feshbach, H. (1960). Nuclear Spectroscopy, ed. F.Ajzenberg-Selove. New York and London, Academic Press, part B.

Feshbach, H. (1962). Ann. Phys., 19, pp. 287 ff.

Feshbach, H. (1965). Proc. Intern. Conf. Stu. Nucl. Str. Neu., 19-23 July 1965, Antwerp. Amsterdam, North Holland Pub. Co., 1966, pp. 257 ff.

Feshbach, H. (1967[a]). Ann. Phys., 43, pp. 410 ff.

Feshbach, H., Kerman, A.K. and Lemmer, R.H. (1967[b]).
Ann. Phys., 41, pp. 230 ff.

Fields, T., Russell, B., Sachs, D. and Wattenberg, A. (1947).
Phys. Rev., 71, pp. 508 ff.

Firk, F.W.K. (1964). Nucl. Phys., 52, pp. 437 ff.

Fischer, C.F., Fischer, V.K., Hemler, E.A. and Tatcher, M.D. (1958). Phys. Rev., 110, pp. 286 ff.

Fox, J.D., Moore, C.F. and Robson, D. (1964).
Phys. Rev. Letters, 12, pp. 198 ff.

Frisch, O.R., Harvey, G. and McKay, H.A.C. (1936).
Nature, 137, p. 149.

Gadioli, E., Marcazzan, G.M. and Pappalardo, G. (1964). Phys. Letters, 11, pp. 13[illegible] ff.

Gadioli, E., Iori, I., Marini, A. and Sansoni, M. (1966). Nuovo Cimento, 44B, pp. 338 ff.

Gibbs, W.R. (1965[a]). Los Alamos Scientific Laboratory Report. Los Alamos, LA. 3266.

Gibbs, W.R. (1965[b]). Phys. Rev., B139, pp. 1185 ff.

Gilbert, A. and Cameron, A.G.W. (1965). Can. J. Phys., 43, pp. 1446 ff.

Gilbert, A., Chen, F.C. and Cameron, A.G.W. (1965). Can. J. Phys., 43, pp. 1248 ff.

Gillet, V., Melanoff, M.A. and Raynal, J. (1967). Nucl. Phys., A97, pp. 631 ff.

Goldhammer, P. (1963). Rev. Mod. Phys., 35, pp. 40 ff.

Goodman, C.D. and Ball, J.B. (1960). Phys. Rev., 118, pp. 1062 ff.

Griffin, J.J. (1966). Phys. Rev. Letters, 17, pp. 478 ff.

Halban, H.V. and Preiswerk, P. (1936). Compt. Rend. Hebd. des Séances de l'Acad. des Sci., 202, pp. 133 ff.

Halbert, M. and Böhning, M. (1965). Bull. Am. Phys. Soc., 10, p. 120.

Hall, I. (1964). Phys. Letters, 10, pp. 199 ff.

Harkins, W.D. and Gans, D. (1934). Phys. Rev., 46, pp. 397 ff.

Häusser, O., Richter, A., Brentano, P. and Mayer-Kuckuk, T. (1964). Compt. Rend. Congr. Interm. Phys. Nucl., Paris, 2-8 Juillet 1964. Paris, Centre National de la Recherche Scientifique, 1964, vol. 2. contrib. C256, pp. 728 ff.

Hauser, W. and Feshbach, H. (1952). Phys. Rev., 87, pp. 366 ff.

Haxel, O., Jensen, J.H.D. and Suess, H.E. (1949). Phys. Rev., 75, pp. 1766 ff.

Haxel, O., Jensen, J.H.D. and Suess, H.E. (1950). Zeitschrift für Phys., 128, pp. 295 ff.

Hibdon, C.T. (1959). Phys. Rev., 114, pp. 179 ff.

Hibdon, C.T. (1961). Phys. Rev., 124, pp. 500 ff.

Huby, R. (1954). Proc. Phys. Soc., A67, pp. 1103 ff.

Huizenga, J.R. and Vandenbosch, R. (1960). Phys. Rev., 120, pp. 1305 ff.

Ikegami, H. and Emery, G.T. (1964). Phys. Rev. Letters, 13, pp. 26 ff.

Izumo, K. (1961). Prog. Theor. Phys., 26, pp. 807 ff.

Kapur, P.L. and Peierls, R.E. (1938). Proc. Roy. Soc., A166, pp. 277 ff.

Keisch, B. (1963). Phys. Rev., 129, pp. 769 ff.

Kimura, M., Shoda, K., Mutsuro, N., Tohei, T., Sato, K. and Kuroda, K. (1961). Nucl. Phys., 23, pp. 338 ff.

Kroepfl, J.J., Marvin, T.P., Watson, B.A. and Singh, P.P. (1967). Contribs. [to] Intern. Conf. on Nucl. Str., Sept. 7-13, 1967, Tokyo, Japan. Tokyo, University of Tokyo, [1967], contrib. 8. 119, p. 347.

Lande, A. and Block, B. (1964). Phys. Rev. Letters, 12, pp. 334 ff.

Lane, A.M., Thomas, R.G. and Wigner, E.P. (1955). Phys. Rev., 98, pp. 693.

Lang, D.W. (1965). Nucl. Phys., 72, pp. 461 ff.

Le Couteur, K.J. (1964). Phys. Letters, 11, pp. 53 ff.

Lee, S.M., Hiratate, Y., Miura, K., Kato, S. and Morita, S. (1967). Contribs. [to] Intern. Conf. on Nucl. Str., Sept. 7-13, 1967, Tokyo, Japan. Tokyo, University of Tokyo, [1967], contrib. 8. 115, p. 343.

Lemmer, R.H. and Shakin, C.M. (1964). Ann. Phys., 27, pp. 13 ff.

Lévesque, R.J.A., Ollerhead, R.W., Blackmore, E.W. and Kuehner, J.A. (1966). Can.J. Phys., 44, pp. 1087 ff.

Lévi, C., Nemaz, N. and Papineau, L. (1966).
Phys. Letters, 22, pp. 483 ff.

Lovas, I. (1966). Nucl. Phys., 81, pp. 353 ff.

McCracken, D. and Dorn, W. (1964). Numerical Methods of Fortran Programming. New York, etc., John Wiley, p. 273.

Mohanus, P. and Sharp, W.T. (1952). Phys. Rev., 87, p. 188.

Mayer, M.G. (1949). Phys. Rev., 75, pp. 1969 ff.

Mayer, M.G. (1950). Phys. Rev., 78, pp. 16 ff.

Mayer-Kuckuk, T. (1964). 9th Yugoslav Summer Meeting of Physicists, Herceg-Novi, Yugoslavia. Heidelberg, Max Planck Institut für Kernphysik, unpublished.

Meadday, D.F., Fisher, F.S., Kalmykov, A., Nikolaev, F.A. and Clegg, A.B. (1963). Nucl. Phys., 45, pp. 98 ff.

Mehta, M.K., John, J., Kerekatte, S.S. and Divatia, A.S. (1966). Nucl. Phys., 89, pp. 22 ff.

Mehta, M.K. and Divatia, A.S. (1967). Contribs. [to] Intern. Conf. on Nucl. Str., Sept. 7-13, 1967, Tokyo, Japan. Tokyo, University of Tokyo, [1967], contrib. B. 118, p. 346.

Meldner, H. and Linder, A. (1964). Zeitschrift für Phys., 180, pp. 362 ff.

Messiah, A. (1966). Quantum Mechanics. Amsterdam, North Holland Pub. Co., vol. 2, p. 839.

Miller, D.W., Fields, A.E. and Bockelman, C.K. (1952). Phys. Rev., 85, p. 704.

Moldauer, P.A. (1964). Phys. Letters, 8, pp. 70 ff.

Moldauer, P.A. (1967). Phys. Rev. Letters, 18, pp. 249 ff.

Monahan, J.E. (1966). Bull. Am. Phys. Soc., 11, p. 451.

Monahan, J.E. and Llwyn, A.J. (1967). Nucl. Phys., A93, pp. 683 ff.

Murray, J.L. and Macefield, B.E.F. (1967). Nucl. Instruments and Methods, 51, pp. 229 ff.

Naqib, I.M., Gleyvod, R. and Heydenberg, N.P. (1965). Nucl. Phys., 66, pp. 129 ff.

National Institute for Research in Nuclear Science. See Rutherford Laboratory.

Oda, Y., Takeda, M., Hu, C. and Kato, S. (1959). J. Phys. Soc. Japan, 14, pp. 1255 ff.

Ogata, H. (1959). J. Phys. Soc. Japan, 14, pp. 707 ff.

Ogata, H., Itoh, K., Kasuda, Y., Takamatsu, K., Kawashima, K., Masaika, A. and Kumabe, I. (1960). J. Phys. Soc. Japan, 15, pp. 1719 ff.

Perey, F.G. (1963). Phys. Rev., 131, pp. 745 ff.

Pfitner, A. and Riedel, C. (1964). Nucl. Phys., 60, pp. 672 ff.

Porter, C.E. and Thomas, R.G. (1956). Phys. Rev., 104, pp. 483 ff.

Preston, M.A. (1962). Physics of the Nucleus. Reading, Mass. and London, Addison-Wesley, p. 509.

Ralston, A. (1965). A First Course in Numerical Analysis. New York, etc., McGraw-Hill, p. 235.

Rateliff, K.F. (1964). Technical Report. University of Pittsburgh.

Rauch, F. and Rössle, E. (1964). Phys. Letters, 12, pp. 217 ff.

Rimmer, E.M. and Fisher, F.S. (1964). Compt. Rend. Conf. Intern. Phys. Nucl., Paris, 2-8 Juillet 1964. Paris, Centre National de la Recherche Scientifique, 1964, vol. 2, contrib. C130, pp. 375 ff; also in Nucl. Phys., A108, pp. 561 ff. and pp. 567 ff.

Rodberg, L.S. (1961). Phys. Rev., 124, pp. 210 ff.

Roman, P. (1965). Advanced Quantum Theory. Reading, Mass. and London, Addison-Wesley, p. 286.

Rössle, E. (1965). Habilitationsschrift. University of Frankfurt.

Rotenberg, M., Bivins, R., Metropolis, N. and Wooten, J.K. (1959). The 3-j and 6-j Symbols. London, Crosby Lockwood.

Rutherford Laboratory (1962). Electrostatic Generator Group Final Report. Chilton, Rutherford High Energy Lab., NIRL/R/23.

Rutherford Laboratory (1966). Electrostatic Generator Group Progress Report. Chilton, Rutherford High Energy Lab., RHEL/R/120.

Scott, D.K., Fisher, R.B. and Chant, N.S. (1967). Nucl. Phys., A99, pp. 177 ff.

Scott, G.M.C. (1954). Phil. Mag., 45, pp. 1322 ff.

Segnal, M.L. (1962). Phys. Rev., 128, pp. 761 ff.

Seward, F.D. (1959). Phys. Rev., 114, pp. 514 ff.

Shakin, C. (1963). Ann. Phys., 22, pp. 373 ff.

Shaw, G.L. (1959). Ann. Phys., 8, pp. 509 ff.

Singh, P.P., Segal, R.A., Meyer-Schützmeister, L., Hanna, S.S. and Allas, R.G. (1965). Nucl. Phys., 65, pp. 577 ff.

Singh, P.P., Hoffman-Pinther, P. and Lang, D.W. (1966[a]). Phys. Letters, 23, pp. 255 ff.

Singh, P.P., Watson, R.A., Kroepfl, J.J. and Marvin, T.F. (1966[b]). Phys. Rev. Letters, 17, pp. 968 ff.

Stephen, R.O. (1963). Clarendon Laboratory Report. Oxford, Clarendon Laboratory.

Szilard, L. (1935). Nature, 136, pp. 950 ff.

Temmer, G.M. (1964). Phys. Rev. Letters, 12, pp. 330 ff.

Tillman, J.A. and Moon, P.B. (1935). Nature, 136, pp. 66 ff.

Tsukada, K. and Tanaka, O. (1963). J. Phys. Soc. Japan, 18, pp. 610 ff.

Van der Woude, A. (1966). Nucl. Phys., 80, pp. 14 ff.

Weisskopf, V.F. (1937). Phys. Rev., 52, pp. 295 ff.

Weisskopf, V.F. (1952). Bull. Am. Phys. Soc., 27, no.1, p.7.

Weisskopf, V.F. (1961). Phys. Today, 14, no.7, pp. 18 ff.

Wigner, E.P. (1946). Phys. Rev., 70, pp. 15 ff. and pp. 606 ff.

Wigner, E.P. and Eisenbud, L. (1947). Phys. Rev., 72, pp. 29 ff.

Wigner, E.P. (1954). Science, 120, p. 790.

Wigner, E.P. (1956). Oak Ridge National Laboratory Report. ORNL-2309, p. 59.

Wilks, S.S. (1962). Mathematical Statistics. New York,etc., John Wiley.

Wood, R.M., Borchers, H.R. and Marshall, H.H. (1965). Nucl. Phys., 71, pp. 529 ff.